A GRASP ON GFAP IN GLIOMA

From tumour cell invasion to nuclear fragmentation

UMC Utrecht Brain Center

Jessy van Asperen

A grasp on GFAP in Glioma

From tumour cell invasion to nuclear fragmentation

Jessy Valerie van Asperen

COLOFON

PhD thesis, Utrecht University, The Netherlands

Author: Jessy V. van Asperen
Cover & Layout: Jessy V. van Asperen
Printing: proefschriften.nl
ISBN: 978-90-393-7467-2

About the cover:

During my PhD I have repeatedly been hypnotized by the beautiful structures that are formed within tissues and cells. From the maze of blood vessels in the brain, to the web of intermediate filaments within the cell. On the front cover, the part of the research that was performed at tissue level scale is depicted. It shows individual glioma cells escaping the tumour (blue) and invading the brain tissue along the blood vessels (gold) of the brain. On the back cover, the structures continue into a representation of the work performed on cell level scale, where the GFAP fibers (gold) are swirling around the nucleus of the cell (blue).

The studies presented in this thesis were funded by the Dutch Cancer Society (KWF 101123). Printing of this thesis was financially supported by the UMC Utrecht Brain Center.

A grasp on GFAP in Glioma

From tumour cell invasion to nuclear fragmentation

Een grip op GFAP in Gliomen

Van tumorcelinvasie tot celkernfragmentatie

(met een samenvatting in het Nederlands)

Proefschrift

ter verkrijging van de graad van doctor aan de
Universiteit Utrecht
op gezag van de
rector magnificus, prof. dr. H.R.B.M. Kummeling,
ingevolge het besluit van het college voor promoties
in het openbaar te verdedigen op

donderdag 19 mei 2022 des middags te 12.15

door

Jessy Valerie van Asperen

geboren op 15 mei 1993
te Westerbork

Promotoren:

Prof. dr. E.M. Hol

Prof. dr. P.A.J.T. Robe

Table of contents

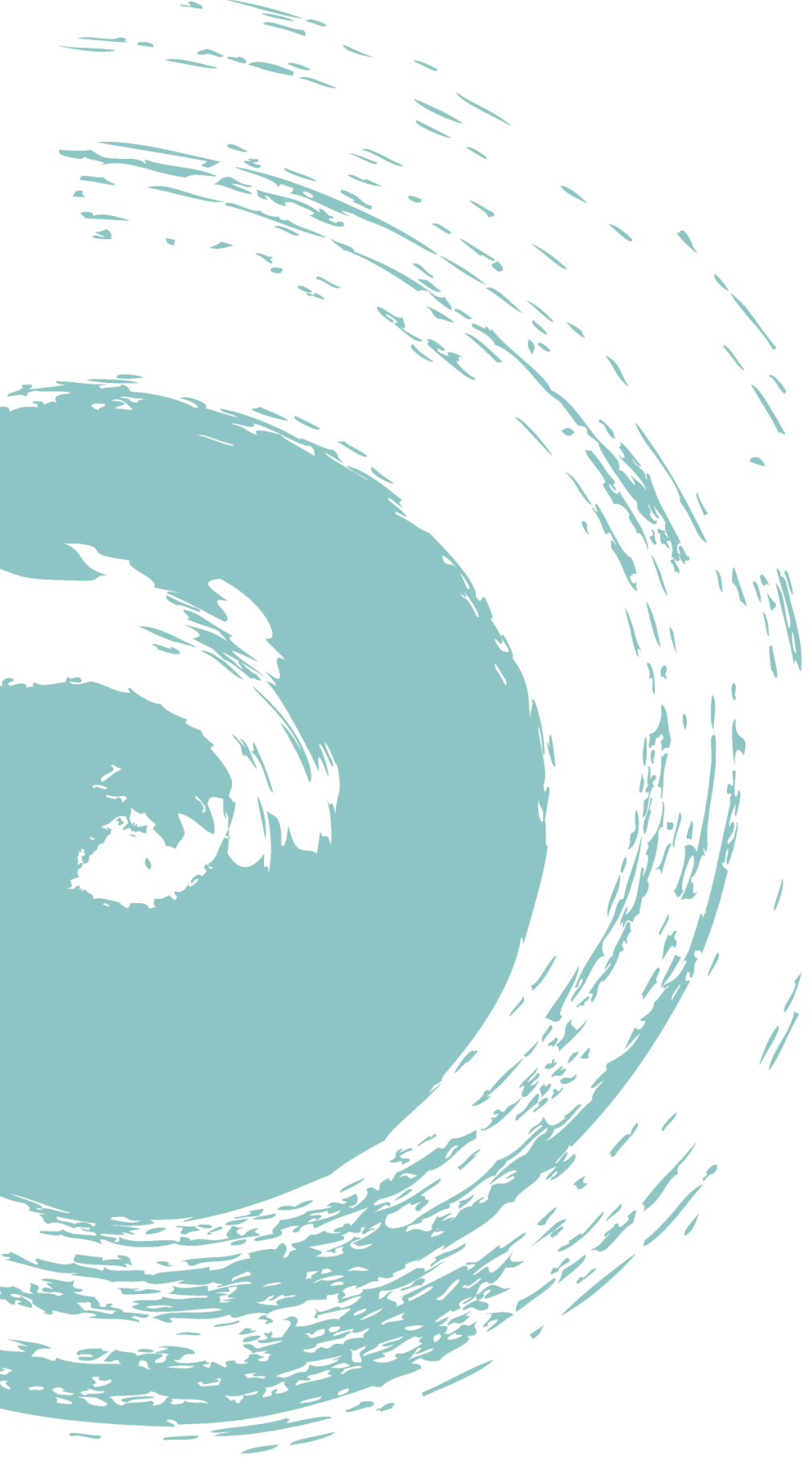

General Introduction

& Aim and Outline

Manuscript in revision

1. Diffuse gliomas
    1.1. Classification of diffuse gliomas
    1.2. Clinicopathology of diffuse gliomas
    1.3. Molecular subtypes and heterogeneity
    1.4. Glioma invasion and diffuse growth
2. GFAP and the intermediate filament network
    2.1. Classification and assembly of intermediate filaments
    2.2. GFAP and GFAP isoforms
    2.3. Regulation of *GFAPa* and *GFAPδ* isoform expression and localisation
    2.4. GFAPα and GFAPδ protein characteristics and dynamics
3. Characteristics of the GFAP IF network in diffuse gliomas
    3.1. The IF network composition in diffuse gliomas
    3.2. Expression of GFAP in relation to clinical outcome
    3.3. GFAP isoform expression in diffuse gliomas
4. The functional role GFAP in glioma cell behaviour
    4.1. Tumorigenesis, cell proliferation and growth
    4.2. Cellular stress and survival
    4.3. Cell motility and migration
5. Adding the third dimension: the role of GFAP in cell invasion

1. Diffuse gliomas

Cell division is a rare event in the fully developed central nervous system (CNS) and only occurs in specialised neurogenic niches of the human brain (Bergmann, Spalding, and Frisén 2015). Nevertheless, upon an accumulation of mutations in CNS cells, uncontrollable cell division leads to the formation of CNS tumours. Tumours in the CNS commonly arise from glial cells in the brain, and this group of neoplasms is classified as gliomas. Within this group, the most prevalent form of malignancies in adults are diffuse gliomas, malignant brain tumours characterised by infiltrative growth into the CNS parenchyma (Louis et al. 2016). Both adult and paediatric forms of glioma exist, but throughout this thesis, the term 'gliomas' refers to the adult form of diffuse gliomas.

1.1 Classification of diffuse gliomas

Classically, diffuse gliomas were subdivided into different subgroups based on histopathological features, namely astrocytomas, oligodendrogliomas, and tumours with mixed astrocytic and oligodendroglial phenotypes. This sub-distinction can be made based on the nuclear shape, with uniformly rounded nuclei generally considered to be

oligodendrogliomas whereas nuclear irregularities and hyperchromasia point towards astrocytomas (Perry and Wesseling 2016). In addition, the presence or absence of atypic nuclei, mitotic activity, microvascular proliferation, and necrosis are used to assign the tumour to a malignancy grade II, III, or IV, of which the latter is also referred to as glioblastoma multiforme (GBM) (Louis et al. 2016; Wesseling and Capper 2018). This histological classification: i.e. astrocytoma, oligodendroglioma (grade II/III), and GBM is still used. However, in the most recent update of the World Health Organization (WHO) classification of CNS tumours, the molecular genetic features of the tumour play a more prominent role (Louis et al. 2021). The main driver mutations used for diffuse glioma classification are point mutations in the isocitrate dehydrogenase 1 and 2 (IDH1 and IDH2) genes, and mutations in these genes are associated with a more favourable prognosis (Sanson et al. 2009; Hartmann et al. 2011). In accordance, the majority of diffuse gliomas that present as grade IV at first diagnosis (primary GBM) are IDH wild-type (WT), whereas IDH1/IDH2 mutated grade IV gliomas more frequently develop from lower-grade tumours (secondary GBM) (Louis et al. 2016). In lower grade IDH1/IDH2 mutated gliomas, two additional molecular subgroups can be identified. IDH1/IDH2 mutations in combination with 1p/19q codeletion and TERT promoter mutation coincide with histological features of oligodendrogliomas, whereas IDH1/IDH2 mutations in combination with ATRX mutations and frequent TP53 mutations correspond to astrocytomas. With the integration of these molecular markers in the diagnosis of low-grade gliomas (LGGs), the use of mixed oligoastrocytoma can be avoided as most LGGs fall within one of the molecular categories. Nevertheless, the terminology is still used for gliomas when molecular genetic features are not specified, and these gliomas are classified into the 'not otherwise specified' (NOS) category (Wesseling and Capper 2018).

1.2 Clinicopathology of diffuse gliomas

With an average of about 5.9/6.0 patients per 100,000 in the Netherlands and the USA respectively, glioma is a relatively rare disease (Ho et al. 2014; Ostrom et al. 2018). Nevertheless, the aggressiveness of the disease, particularly grade IV glioma, and the absence of a curative treatment makes glioma a serious health burden. Besides being the most severe form, GBMs are also the most prevalent form of diffuse gliomas, representing 52.9% of the cases (Ostrom et al. 2018). The most recent therapeutic progress in the treatment of grade IV glioma has been the Stupp-protocol, which has become the standard of care for grade IV glioma treatment since the publication of the protocol in 2005 (Stupp et al. 2005). The treatment protocol comprises surgical resection of the tumour followed by radiotherapy of 2 Gy per day up to a total of 60 Gy over 6 weeks, in combination with temozolomide treatment during and post-

radiotherapy (Stupp et al. 2005). Although this protocol advances median survival from 12.1 to 14.6 months after diagnosis, tumour recurrence in grade IV glioma is common (Stupp et al., 2005). Treatment options for LGGs are less standardised, but can also include total resection, radiotherapy, and chemotherapy, of which total resection was reported to have the largest effect on patient survival (Brown et al. 2019). Although LGGs present with slower tumour growth, over time LGGs frequently develop into GBMs and this makes also this tumour type not fully curable (Louis et al. 2016). The incurability of both low- and high-grade gliomas can be largely attributed to two clinical challenges in the treatment of the disease: heterogeneity and the invasive growth of tumour cells. Both challenges will be discussed below.

1.3 Molecular subtypes and heterogeneity

Similar to many other cancers, gliomas are not a homogeneous population of cells, but rather consist of a heterogeneous bulk with many different subpopulations (Patel et al. 2014). Heterogeneity is one of the major challenges in developing novel curative treatments for the disease. The cellular heterogeneity within gliomas is a result of the molecular evolution in which genetic drift, hijacking of developmental programs, and environmental factors play an important role (Turajlic et al. 2019). Based on the current state of knowledge, the initial events leading to glioma are thought to arise when either mutations in the TERT promoter (pathway 1) or IDH1/IDH2, G-CIMP, CDKN2A/CDKN2B (pathways 2) occur in glial (stem) cells (Fig. 1), although the exact cell-type or origin is still uncertain (Molinaro et al. 2019; Sottoriva et al. 2013). Further progression drives the formation of different glioma molecular subtypes, first described by Verhaak and colleagues in grade IV gliomas (Verhaak et al. 2010). Although initially four subtypes of GBMs were discovered (Verhaak et al. 2010), later this was corrected to three as the fourth subtype was likely to arise from contamination with tumour-associated non-malignant cells (Wang et al. 2017). The remaining three subtypes are the classical, mesenchymal, and proneural subtypes that correspond to aberrant expression of EGFR (classical subtype), NF1 (mesenchymal subtype), and PDGFRA/IDH1 (proneural subtype). Bulk categorisation into the proneural subtype is associated with a more favourable survival outcome, whereas the mesenchymal subtype is associated with a worse prognosis (Verhaak et al. 2010; Wang et al. 2017).

Single-cell analysis data revealed that tumours can contain transcriptional signatures of multiple subtypes, highlighting the inter-tumour heterogeneity and plasticity of GBMs (Patel et al. 2014; Neftel et al. 2019). Neftel and colleagues described the existence of four dynamic cellular states that overlap in transcriptional signatures with non-malignant neuronal cell types, identified as mesenchymal-like, astrocyte-like, oligodendrocyte progenitor cell (OPC)-like, and neural progenitor cell (NPC)-like (Neftel et al. 2019). The different cellular states and transitions in-between states are thought

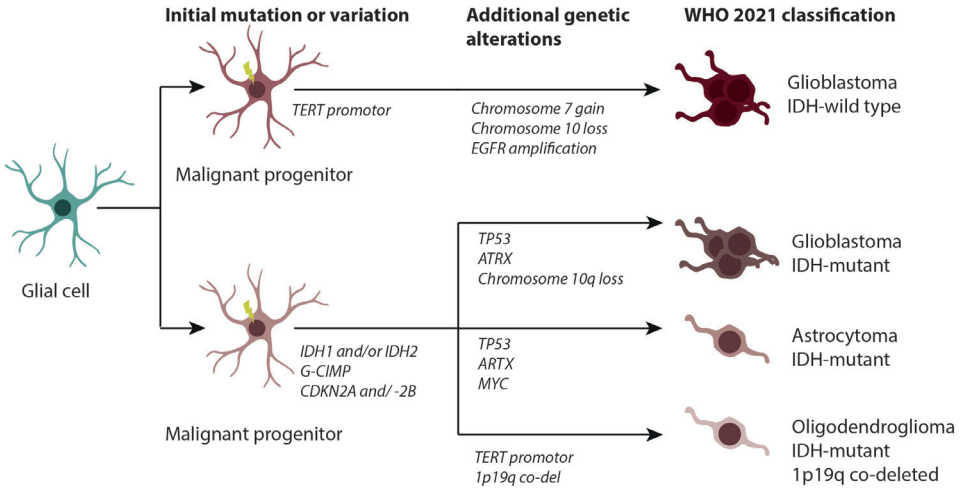

Figure 1. Hypothesised pathways leading to the different types of diffuse gliomas of the WHO 2021 classification. The sequence of mutations and genetic alterations is based on Molinaro et al., 2019

to reflect neurodevelopmental hierarchies. Reinitiation of developmental programs and neural stem cell hierarchies also contribute to different lineages in LGG (Venteicher et al. 2017) and are thought to contribute to glioma heterogeneity. Also, the composition of the tumour microenvironment (TME) affects the gene expression signatures of single cells in LGG and GBM, as transcriptomics are affected by environmental factors like hypoxia and the presence of immune cells (Venteicher et al. 2017; Neftel et al. 2019).

Altogether, the interplay between genetic alterations, genetic subclones, conservation of developmental programs, and interaction with the TME drive glioma heterogeneity. This heterogeneity of the tumour is a major problem in the treatment of gliomas due to multiple reasons. First of all, heterogeneity can lead to an adaptive response of specific subsets of cells to existing treatment regimes, leading to treatment evasion (Wang et al. 2016). This is illustrated by the fact that recurrent tumours frequently have a different transcriptional signature in comparison to the primary tumour, due to the positive selection of resistant clones. This is sometimes even associated with a switch in key driver gene alterations (Wang et al. 2016). Secondly, treatment can lead to alterations of the TME, which due to its effect on glioma heterogeneity can lead to increased malignancy of the non-targeted cells. As an example, tumour resection and biopsies can stimulate proliferation and migration of the non-resected tumour cells, explained by the inflammatory response associated with the treatment (Alieva et al. 2017). Lastly, glioma heterogeneity hampers the development of novel treatments. Treatments targeting specific oncogenic pathways are unsuccessful due to diversity in pathway activation within the tumour and due to the counteracting effect of compensatory pathways (Pearson and Regad 2017).

1.4 Glioma invasion and diffuse growth

In addition to the heterogeneity of the tumour, one other major challenge in the treatment of gliomas is their infiltrative growth pattern. This diffuse growth of gliomas was already recognised over 70 years ago by neuropathologist Hans-Joachim Scherer, who examined brain sections of glioma patients and studied the morphological characteristics of the tumour cells (Scherer 1940; Peiffer 1999). In his work, he described the existence of 'secondary structures', patterns of glioma growth which contrary to primary structures do not reflect the intrinsic biology of the tumour (e.g. rosette-like structures), but rather are dependent on pre-existing characteristics of the brain tissue (Scherer 1940). Examples of secondary structures, now frequently called Scherer's structures, are perineuronal growth, subpial growth, perivascular growth, and intrafascicular (white matter) growth of gliomas and reflect the tendency of glioma cells to migrate along the pre-existing structures in the brain (Fig. 2, Cuddapah et al. 2014). Whole-brain immunohistochemical analysis of IDH1 mutations in post-mortem tissue of glioma patients showed that single malignant cells can be found in most areas of the brain, including regions that appeared unaffected (Sahm et al. 2012). This highlights the complication in targeted treatment of gliomas, as current imaging techniques do not allow visualisation of these single invaded cells. Therefore, whole tumour resection and radiotherapy will unavoidably miss some of the malignant cells. Treatment of glioma has

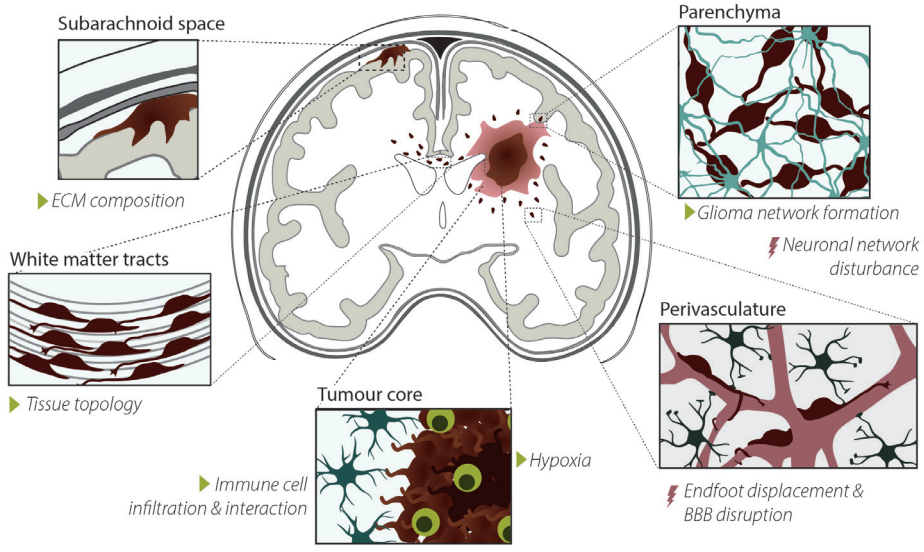

Figure 2. Characteristics, drivers and consequences of glioma cell invasion. Glioma cell invasion typically occurs along pre-existing structures in the brain, including the subarachnoid space, along the perivasculature and white-matter tracks. Glioma invasion is influenced by different factors (indicated with the green triangles) and negatively impacts brain physiology (indicated with the red lightning bolts).

fittingly been compared to fighting a guerrilla war in a review from Claes and colleagues. Like guerrilla warriors, glioma cells infiltrate foreign territory abusing the pre-existing infrastructure, and individual or small group movements make detection of the invasive front problematic (Claes, Idema, and Wesseling 2007).

With the advancements in *in vivo* and *ex vivo* imaging techniques, the real-time dynamic growth patterns of glioma cells can now be captured. Glioma cells *in vivo* adapt a unipolar morphology extending a thin leading process that frequently follows the lining of blood vessels. This leading process is highly dynamic as it extends, retracts, and branches while the cell scans its environment (Farin et al. 2006; Beadle et al. 2008). Also, glioma cells in patient-derived xenograft models show characteristic cell protrusions, which are frequently called tumour microtubes (TMs), since the introduction of this term by Osswald and colleagues in 2015 (Osswald et al. 2015). TMs underlie the formation of a highly dynamic interconnected network of different glioma cells that are mainly associated with astrocytomas and GBMs, but less with oligodendrogliomas (Osswald et al. 2015). The TM-connected glioma cells have stem-cell-like characteristics and have increased resistance to radiotherapy (Xie et al. 2020). Cellular protrusions of glioma cells also form a leading track for translocation of the soma, both during mitosis and migration. Translocation of the soma occurs in saltatory movement fashion, characterised by bursts of movements in which the soma jumps forward followed by immobile periods (Farin et al 2006; Beadle et al. 2008), resembling the migration patterns of neural progenitors during embryonic development (Tsai, Bremner, and Vallee 2007). Both in glioma- and neural progenitor cells, somal translocation is occasionally associated with an hourglass-like deformation of the nucleus, due to confinement of the surrounding tissue environment (Beadle et al. 2008; Tsai, Bremner, and Vallee 2007). Also, proliferation patterns of glioma cells share resemblances with neurodevelopmental phenomena. During mitosis, glioma cells can undergo mitotic somal translocation, where the cell soma translocates 50-100 μm prior to cytokinesis, similarly to outer radial glia cells during development (Bhaduri et al. 2020). Proliferation frequently occurs around vascular branch points (Farin et al. 2006), although relatively quiescent cells can also be found in the perivascular niche (Osswald et al. 2015).

Glioma cell invasion is not only problematic because it hampers treatment, but also because it interferes with normal brain functioning. During perivascular migration, electron microscopy images show that glioma cells squeeze themselves between the vasculature and astrocyte endfeet leading to endfeet displacement (Nagano et al. 1993; Zagzag et al. 2000; Watkins et al. 2014). This displacement can lead to loss of the integrity of the blood-brain barrier (BBB) and BBB leakiness (Watkins et al. 2014). In addition, two independent lines of research have recently discovered the presence of functional synapses terminating on TMs of glioma cells (Venkataramani et al.

2019; Venkatesh et al. 2019). Synaptic transmission can lead to calcium transients and potassium waves that are further conducted through the glioma network through gap junctions and lead to glioma progression (Venkataramani et al. 2019; Venkatesh et al. 2017). Also, adherent junctions play a role in the formation of these multicellular networks of glioma cells in a p120-catenin dependent fashion (Gritsenko et al. 2020). The interplay between neural- and glioma-networks could be a potential underlying mechanism for the pathophysiological hallmark of neuronal hyperexcitability and epilepsy, occurring in about 40-80% of glioma patients (Venkataramani et al. 2020). Also, cognitive impairments are frequently reported in glioma patients (van Kessel et al. 2017), potentially as a result of the hijacked neural network.

Altogether, the diffuse growth pattern of gliomas is a major challenge for curative treatment and is likely an important contributor to the neuropathological hallmarks of the disease. A better understanding of the molecular- and cellular mechanisms driving and facilitating glioma invasion is needed for the development of novel treatment targets. In the next section, the intermediate filament network and its link to glioma invasion will be introduced.

2. The GFAP Intermediate filaments network

2.1 Classification and assembly of intermediate filaments

The intermediate filament (IF) family is a large group of proteins that give rise to one of the three cytoskeletal networks in the cell. With a diameter of 10 nm, the filaments were originally distinguished by their intermediate size in comparison to microtubules (24 nm) and actin filaments (7 nm), the other two cytoskeletal components in the cell (Herrmann and Aebi 2016). With around 70 genes encoding for different IF proteins, the expression pattern of IFs is very cell type- and differentiation state-specific, a characteristic that sets it apart from the more ubiquitously expressed isoforms of actin and tubulin (Hesse, Magin, and Weber 2001). All IF proteins share a secondary structure consisting of an α-helical 'rod' domain flanked by a flexible N-terminal 'head' and a C-terminal 'tail' domain. Based on homology in sequence and assembly properties, the IF proteins are further classified into six subtypes (Fig. 3a). Although most subtypes contain proteins that form a network in the cytoplasm of the cell, the lamins of subtype V form a separate network on the inside of the nuclear envelope, also termed the nuclear lamina (Etienne-Manneville 2018). GFAP is a type III IF protein that is most abundantly expressed in the brain, where it is classically used as a marker for astrocytes. However, its expression can also be found in several cell types outside the CNS, including liver stellate cells, fibroblasts, myoepithelial cells, chondrocytes, and lymphocytes (Messing and Brenner 2020). Although GFAP is the most characteristic IF in glial cells, glial cells can express a combination of IF proteins, including vimentin,

a

Class	Proteins	Localization
I	Keratins 9-20 (acidic)	epithelial cells
II	Keratins 1-8 (basic)	epithelial cells
III	GFAP Vimentin Desmin Peripherin	glial cells mesenchymal cells muscle cells neurons
IV	NF-L, NF-M, NF-H Nestin Synemin	neurons stem cells glial cells
V	Lamins	nucleus
VI	Filensin Phakinin	lens cells

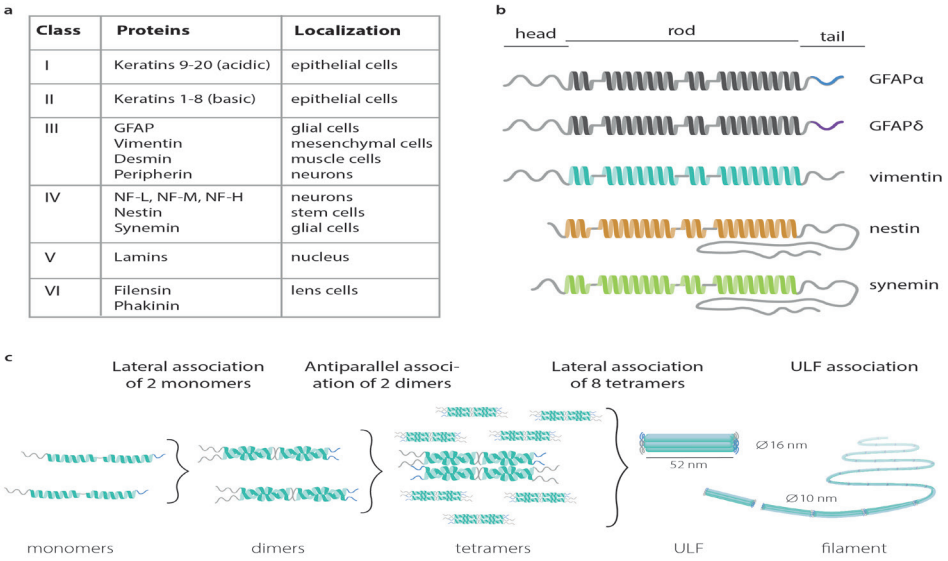

Figure 3. Intermediate filaments classification and assembly. (a) Classification of intermediate filament proteins. (b) The IF proteins that are expressed by glial cells and their malignant analogues. (c) The multi-assembly steps from intermediate protein monomers to filaments.

nestin, and synemin (Fig. 3b, Hol and Pekny 2015).

Assembly of IF proteins into the IF network is a multistep process (Fig. 3c) that occurs in the absence of cofactors and nucleotides (Leduc and Etienne-Manneville 2017). The first step in this process is the lateral association of monomers to form a dimer. Whereas most IF proteins (including GFAP) can form homodimers, heterodimer formation is a distinctive feature of class I and II keratins, where heterodimers are composed out of one acidic (class I) and one basic (class II) chain (Guzenko, Chernyatina, and Strelkov 2017). In the next step of IF network assembly, dimers bind in an antiparallel fashion to form tetramers, which then laterally associate into octamers forming structures called unit-length filaments (ULFs). Subsequent association of ULFs in a non-polar fashion leads to the formation of a filament, which then undergoes radial compaction leading to the final diameter of 10 nm. The intrinsic capacity of IFs to spontaneously form dimers and tetramers, which is mainly dependent on the rod domain of the IF protein, has made it challenging to unravel the 3D structure of IFs. Depolymerizing IFs into soluble subunits, necessary for crystallography, is virtually impossible (Chernyatina, Guzenko, and Strelkov 2015; Guzenko, Chernyatina, and Strelkov 2017). Because of this extreme stability, IF networks were long thought to be stagnant structures, but live-cell imaging has revealed that the IF network is in fact very dynamic and has a continuous turnover (Leduc and Manneville 2017).

2.1 GFAP and GFAP isoforms

Glial fibrillary acidic protein (GFAP) has recently celebrated its 50th birthday after being first described by Lawrence Eng in a publication called 'An acidic protein isolated from fibrous astrocytes' published on May 7th 1971 (Helman et al. 2020; Eng et al. 1971). After its discovery in 1971 and official naming in 1972 (Uyeda, Eng, and Bignami 1972), GFAP was classified as a type III IF protein along with vimentin, desmin, and peripherin based on homology in sequence (Geisler and Weber 1983). Unique to GFAP in comparison to the other type III IFs is the regulation of the *GFAP* pre-mRNA transcript by alternative splicing and alternative polyadenylation. Since the discovery of canonical isoform GFAPα, seven murine and eleven human splice-isoforms have been described (Middeldorp and Hol 2011), of which the isoforms GFAPλ and GFAPμ were only discovered recently (Helman et al. 2020; van Bodegraven et al. 2021). In this thesis, the focus will be on two of the most highly expressed isoforms: the canonical GFAPα and the alternative GFAPδ isoforms, which differ in their last 41/42 amino-acid of their tail-region (Fig. 4).

2.2 Regulation of *GFAPα* and *GFAPδ* isoform expression and localisation

The human *GFAP* gene is located on chromosome 17q21 and spans over 10 kb of DNA (Bongcam-Rudloff et al. 1991). The promoter region of the human *GFAP* gene extends from -2162 to +47 and contains consensus sequences and binding sites for a dozen transcription factors, as extensively discussed in Brenner and Messing 2021. Of the different transcription factors, AP-1, NF1, and STAT3 are considered most evidently involved in *GFAP* expression (Brenner and Messing 2021). Both the *GFAPa* and *GFAPδ* splice variants share their RNA start site, and their pre-mRNA consists out of nine exons, eight introns, four alternative exons, and two alternative introns (Middeldorp and Hol, 2011). Canonical splicing of the pre-mRNA leads to the inclusion of nine exons and results in the mRNA transcript of *GFAPa*. Upon an alternative splice event, the last two exons are replaced by an alternative exon 7a, which encodes for the tail region of the GFAPδ protein (Fig. 4). In addition to a difference in the last 123/126 nucleotides of the coding region of the mRNA, the transcript of *GFAPδ* has an alternative 3 prime untranslated region (3' UTR) and polyadenylation site. The 3' UTR of *GFAPδ* is shared with another isoform of *GFAP, GFAPκ*, where the intron 7 is retained (Blechingberg et al. 2007). A study by Blechingberg and colleagues showed that the activity of the polyadenylation signal rather than the 3'-splice site usage was the primary determent for processing into the *GFAPa* or *GFAPδ/κ* mRNA (Blechingberg et al. 2007). Nevertheless, manipulation of splice enhancers and the polyadenylation signal in exon 7a within the minigene system used in this study also hinted towards an interplay between splicing and polyadenylation regulation, indicating a role for both

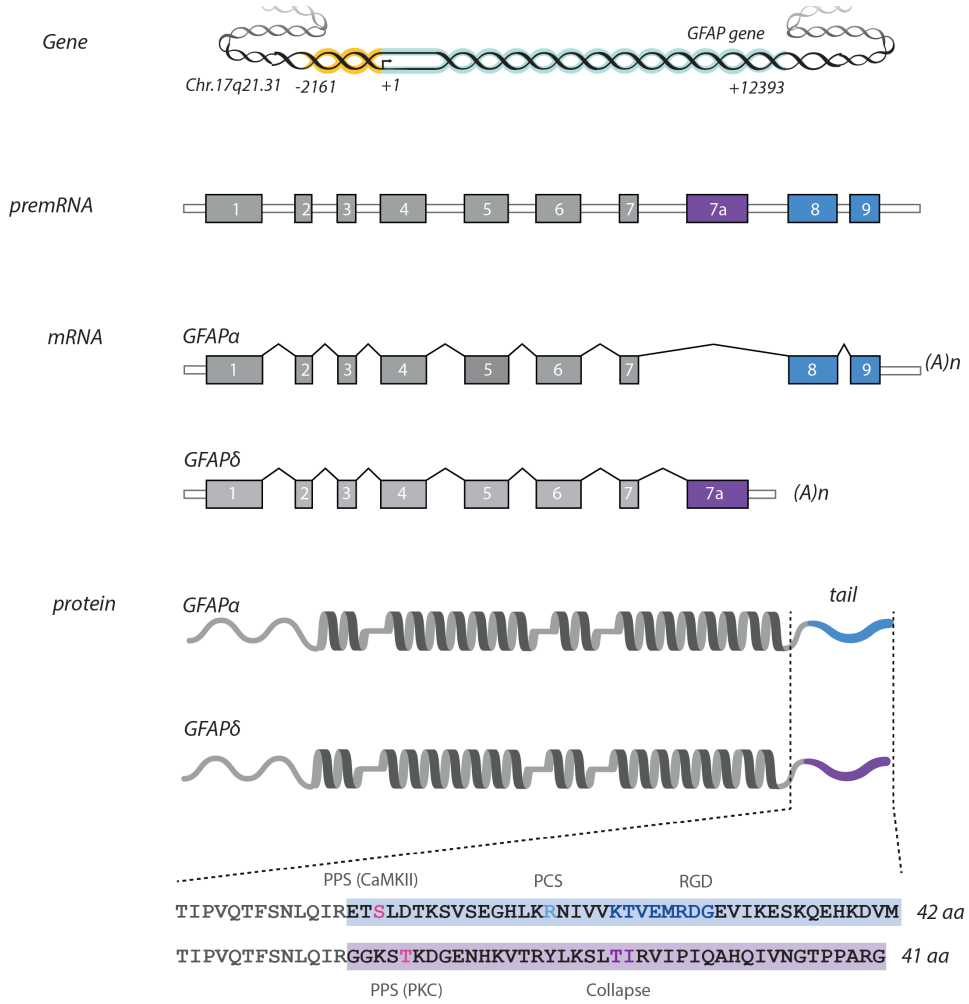

Figure 4. GFAPα and GFAPδ, from gene to protein. The promoter region of GFAP is marked in yellow, the coding region in light blue. Large squares represent exons, small white squares introns. Dark blue represent the exons and tail region specific for the GFAPα transcript/ protein, purple for GFAPδ. Unique features in the tail regions are marked. GFAPα contains an additional citrullination site (Jin et al. 2013) and a conserved RDG sequence (Chen and Liem 1994). Both tail regions have different predicted phosphorylation sites (Boyd et al. 2012). Collapse of GFAPδ has been assigned to T411 and T412 (Nielsen and Jørgensen 2004). Abbreviations: aa= amino acids, PCS = predicted citrullination site, PPS = predicted phosphorylation site.

machineries in the modulation of levels of *GFAPa* and *GFAPδ* isoforms (Blechingberg et al. 2007). The effect of the transcriptional rate of the *GFAP* gene on isoforms balance has also been studied, although findings are inconclusive. Studies with the *GFAP* minigene with different promotors did not indicate an effect of transcriptional

rate on polyadenylation site selection (Blechingberg et al. 2007). On the other hand, inhibition of histone deacetylases activity in glioma cells and primary astrocytes was linked to decreased expression of *GFAP* and a shift in balance from the *GFAPa* to the *GFAPδ* isoform, a process modulated by splicing factor SR6 (Kanski et al. 2014). Although this suggests that lower transcriptional rates lead to increased alternative splicing and polyadenylation site usage, increased transcriptional rates have also been linked to higher levels of *GFAPδ*. In a transgenic mouse model carrying several copies of the human *GFAP* transgene, disproportionally increased levels of *GFAPδ* and also isoform *GFAPλ* were found (Lin et al. 2021).

Another level of post-transcriptional regulation of *GFAP* isoforms can come from microRNAs (miRNA). miRNAs are small non-coding RNAs that affect mRNA translation and stability. Upon association with the Argonaute protein, the seed sequence of the miRNA can bind to a complementary sequence of the mRNA, leading to mRNA cleavage or silencing (Matsuyama and Suzuki 2020). Since miRNAs usually target the 3' UTR of a transcript, and *GFAPa* and *GFAPδ* have different 3' UTRs, their transcripts can be targeted by different miRNAs. A number of studies have investigated the effect of miRNAs on *GFAP* expression in mouse models and human cell lines. However, direct regulation of specific miRNA of human *GFAP* transcripts has thus far not been proven, as aptly discussed by Brenner and Messing 2021.

Besides regulation of *GFAP* mRNA isoform expression, also the localisation of the different *GFAP* mRNAs within the cell has been investigated. Two independent studies made similar observations regarding distinct subcellular localisation patterns of the *GFAPa* and *GFAPδ* transcripts within astrocytes in culture (Thomsen et al. 2013) and in mouse brain tissue (Oudart 2012). Whereas *GFAPδ* localisation is mainly restricted to the soma of the cell, *GFAPa* mRNA is particularly enriched within the fine processes of the astrocyte (Thomsen et al. 2013; Oudart 2012).

2.3 GFAPα and GFAPδ protein characteristics and dynamics

The human canonical GFAPα protein consists out of 432 amino acids with a molecular weight of 55 kDa. As a result of the alternative exon usage, the last 42 amino acids of the tail region of the GFAPα isoform are replaced by 41 alternative amino acids in the GFAPδ isoform (Fig. 4). Despite the similarity in length, the tail sequences of GFAPα and GFAPδ share no homology and have different isoelectric points (Boyd et al. 2012). Also on a phylogenetic level, the two isoforms are different. Most of the GFAP protein, including the tail-region of the GFAPα isoform, is highly conserved between species and shows more than 90% homology to mouse, rat, and pig GFAP and even 67% to the protein in zebrafish (Nielsen and Jørgensen 2004). In contrast, the C-terminus of GFAPδ varies considerably between species, and is only conserved

among higher primates, but not among other mammals (Singh et al. 2003). Since many of the non-conserved sequence changes in primates also alter the amino acid sequence of the C-terminus, it has been suggested that this change may have led to a positive selection of a novel function of the protein in higher primates. What this potential novel function is, remains to be investigated (Singh et al. 2003; Messing and Brenner 2020).

On a functional level, the difference between the GFAPα and GFAPδ isoforms is best illustrated by the assembly properties of the proteins. Whereas GFAPα can self-assemble into a filamentous network, expression of solely GFAPδ leads to the formation of perinuclear aggregates (Nielsen and Jørgensen 2004; Roelofs et al. 2005; Perng et al. 2009). Despite the incapacity of GFAPδ to form filaments by itself, the isoform can be incorporated into the IF network by forming heterodimers with GFAPα or vimentin. Nevertheless, only low amounts of GFAPδ are tolerated within the GFAPα/vimentin network and abundance of GFAPδ of more than 10% of all GFAPs leads to a collapse of the entire IF network (Nielsen and Jørgensen 2004; Moeton et al. 2016). The lack of the highly conserved RGD-motif (KTXEMRDG, Fig. 4) in the C-terminus of GFAPδ was hypothesised to play a role in this incapacity to self-assemble into networks, as mutations in this motif in vimentin were associated with aberrant filament assembly (McCormick et al. 1993). Nevertheless, it is unlikely that the lack of filament-forming efficiency can be solely explained by the absence of this region, as the RGD-motif is not essential for homodimer formation of GFAPα (Chen and Liem 1994). In addition, GFAP lacking the entire tail-domain can still dimerise and does not fully aggregate like GFAPδ. The inhibitory effect of the C-terminus of GFAPδ can likely be explained by its capacity to bind the coiled-coil 2B domain of the GFAP protein, pinpointed to the residues 411 and 412 of the sequence (Fig. 4, Nielsen and Jørgensen 2004). The presence of GFAPδ within the network can also lead to altered exchange dynamics. Fluorescence after photobleaching experiments showed that GFAPδ incorporates and dissociates slower from an IF network than GFAPα, and that collapse of the network slows down both isoforms even more (Moeton et al. 2016).

In addition to distinct assembly properties and dynamics, the difference in the tail region between the GFAPα and GFAPδ isoforms can also lead to altered protein interactions. In a yeast two-hybrid screen it was shown that GFAPδ has decreased affinity for other IFs, like NFL, peripherin and internexin, but also non-IF proteins like periplakin and envoplakin, both focal adhesion proteins (Nielsen and Jørgensen 2004). Presenilin, on the other hand, a protein that is part of the γ-secretase complex involved in the cleavage of amyloid precursor protein and notch, was identified as a protein that specifically binds to GFAPδ, but not GFAPα (Nielsen et al. 2002). In another unpublished screen, SOX2 was identified as a binding partner of specifically GFAPδ, and Sox2-GFAPδ complexes were found within the nucleus of glioma cell lines (Ruther,

Senner, personal communication). In addition to protein-protein interactions, GFAPα and GFAPδ also have different predicted kinase binding sites and phosphorylation residues (Fig. 4, Boyd et al. 2012). Whether the predicted phosphorylation sites can indeed be phosphorylated and what the functional consequences are for the protein, remains to be investigated.

3. Characteristics of the GFAP IF network in diffuse gliomas

Shortly after the discovery of GFAP, high expression levels of the protein were discovered in the tissue of primary tumour patients, where GFAP was found in gliomas with astrocyte-like characteristics (Uyeda, Eng, and Bignami 1972). Since then, GFAP has been widely studied in the context of brain tumours, both to study the relevance as a biomarker, and to understand its function as a potential therapeutical target. After the discovery of GFAPδ in adult neural stem cells (Roelofs et al. 2005), also GFAP isoform research extended to the field of glioma biology, where glioma stem cells are hypothesised to play a major role in the biology of the disease (Bradshaw et al. 2016). In the next part, we describe the IF network composition and GFAP expression patterns in diffuse gliomas and the clinical relevance hereof.

3.1 The IF network composition in diffuse gliomas

The IF network of glioma cells resembles the expression patterns of their non-malignant analogues (Fig. 3). Gliomas with astrocytic characteristics, like astrocytomas and also GBMs, can express a combination of cytosolic IF proteins that are also found in immature, mature, and reactive astrocytes and neural stem cells. These IF proteins include GFAP, vimentin, nestin, and synemin (Hol and Pekny 2015). Like the earlier described GFAP, vimentin is a class III IF that is similar in amino acid length and also has the property to self-assemble into networks. Nestin and synemin on the other hand are class IV IF proteins that cannot homodimerise and are characterised by an 8 to 10 times larger C-terminus (Hol and Pekny 2015). Heteropolymerisation of GFAP and vimentin was already discovered in glioma cell lines and surgical biopsies over 30 years ago with immunoelectron microscopy and more recently also nestin was observed to be part of the GFAP/vimentin-positive filaments in astrocytes (Wang, Cairncross, and Liem 1984; Paulus and Roggendorf 1988; Leduc and Manneville 2017). Depletion of either GFAP or vimentin leads to different IF network structures in astrocytes, with GFAP dominant networks being more compact and dense and vimentin dominant networks more dispersed (Lepekhin et al. 2001; Menet et al. 2001). Although the effects of nestin and synemin and different isoforms of GFAP on the ultrastructure of IF networks have not yet been described in glia- and glioma cells, these findings show that

different IF components within the same filament can have distinct contributions to the filament characteristics. In addition to cytosolic IF proteins, gliomas also express class IV IF proteins that make up the nuclear lamina. Of the four different lamins/ lamin isoforms, lamin B1 is the dominant protein expressed in glioma cells, and lamin A levels are relatively low in comparison to other cell types (Swift et al. 2013). In addition, lamin B1 but not lamin A depletion affects the organisation of the cytosolic IF network in astrocytes (Dupin, Sakamoto, and Etienne-Manneville 2011). Although this thesis will mainly focus on the cytosolic IF network, this and other finding suggest that the nuclear- and cytosolic IF network interact and should not be regarded as two entirely separate entities.

3.2 Expression of GFAP in relation to diffuse glioma clinical outcome

The organisation and general expression patterns of GFAP and other IF proteins have been determined in relation to glioma malignancy and overall survival. Based on semiquantitative immunohistochemical evaluation of vimentin, nestin, GFAP, and synemin expression in glioma tissue, Skalli and colleagues identified three subtypes of glioma: one group with high expression levels of all four IFs, one with low expression levels of all, and one group with strong nestin expression but low vimentin, GFAP, and, synemin (Skalli et al. 2013). No correlation between staining patterns and survival was found in this study, and patient numbers were limited. The expression of GFAP is often regarded as a differentiation marker and is therefore associated with a less malignant tumour. Nevertheless, a recent systematic review on GFAP expression levels in different malignancy grades performed by our group found that GFAP is heterogeneously expressed, and is not consistently associated with more differentiated tumours (van Bodegraven et al. 2019b). A more recent study investigated the correlation between the percentage of GFAP staining in GBM tissue sections and overall survival and found that high levels of GFAP correlate with poorer survival estimates (Ahmadipour et al. 2020). Also, the presence of GFAP in serum has been repeatedly associated with high-grade glioma (van Bodegraven et al. 2019b). Together these studies highlight that GFAP protein levels are frequently altered in gliomas, but heterogeneity between patients and inconsistent findings between studies makes the use of pan GFAP levels as a biomarker uncertain.

3.3 GFAP isoform expression in diffuse glioma

In addition to general GFAP levels, multiple studies, including research performed in our group, have looked into the expression patterns of GFAP isoforms in tissue sections of gliomas. In healthy adults, GFAPδ expression is limited to a subgroup of

astrocytes located in the subpial zone of the cerebral cortex, the subgranular zone of the hippocampus, the subventricular zone, the rostral migratory stream, and the olfactory bulb (Roelofs et al. 2005; van den Berge et al. 2010). In accordance, whereas GFAPδ positive cells are absent in cortical sections of control autopsy brains, GFAPδ positive cells are present in tissue sections of gliomas of different grades in the brain (Choi et al. 2009; Andreiuolo et al. 2009), and in the spinal cord (Heo et al. 2012). In contrast to general GFAP levels, multiple studies report an increase in GFAPδ levels in high- versus low-grade tumours (Choi et al. 2009; Andreiuolo et al. 2009; Brehar et al. 2015; reviewed in van Bodegraven et al. 2019b). Brehar and colleagues compared the GFAPδ and nestin immunopositive staining of tissue biopsies to the macroscopic invasive properties of the tumour based on neuroimaging. They reported that neuroimaging features of highly invasive tumours correlate to a higher percentage of GFAPδ and nestin-positive cells in the corresponding tumour biopsy (Brehar et al. 2015). Since the biopsies were taken from the tumour core and areas of the tumour with the highest IF staining were selected, it remains to be investigated whether different regions of the tumour, like the invasive front, show the same increase in GFAPδ and nestin-expressing cells. In addition to immunohistochemical analysis of gliomas, *GFAP* isoform expression patterns have also been investigated at the RNA level. Analysis of *GFAP* isoform expression in bulk RNA sequencing data of 165 high grade- and 168 low-grade gliomas, derived from the Cancer Genome Atlas (TCGA), showed that canonical isoform *GFAPa* is significantly lower in grade IV versus grade II and III tumours. *GFAPδ* on the other hand remains constant over the different malignancy grades. This results in a shift in ratios, with high *GFAPδ/a* ratios in high-grade tumours and a low *GFAPδ/a* ratio in lower grade tumours (Stassen et al. 2017).

Although multiple research groups report changes in GFAPδ/α ratios in the different malignancy grades of glioma, it is important to note the high heterogeneity when it comes to GFAPδ expression. Unpublished data from our group on tissue microarray (TMA) section of 220 patients showed a large variety in GFAPδ/α levels in high- and low-grade tumours, indicating heterogeneity both between tumours and also even between different areas from the same tumour (van Bodegraven et al., 2019a). Also, Andreiuoli and colleagues reported a large variation in GFAPδ staining levels, with strongly positive and negative foci in tumour tissue of grade IV glioma patients (Andreiuolo et al. 2009). Despite the high heterogeneity, some basal observations on the characteristics of the GFAPδ and GFAPα/pan positive cells were reported. First of all, Andreiuoli and colleagues described a high extent of overlap between GFAPδ and vimentin immunostaining in grade II and grade IV, although this observation has not been systematically quantified (Andreiuolo et al. 2009). Also, observations on morphological differences have been described. Choi and colleagues found a correlation between GFAPδ levels and the number of primary processes of the cell. In this study,

increased levels of GFAPδ was associated with fewer primary processes and rounder cell morphology (Choi et al. 2009). Similar observations have been made in the GFAPδ and GFAPα positive cells in the TMA study performed by our group. Cells with high levels of GFAPδ often show more rounded morphology with a single thick process and GFAPδ localisation around the nuclear membrane. GFAPα expressing cells on the other hand frequently have multiple processes, both short and thick, as well as long and thin processes forming a meshwork of fibres (van Bodegraven et al., 2019a). Also in pediatric diffuse intrinsic pontine glioma (DIPG) GFAPδ-positive cells with distinctive morphologies are found, although no morphological characterisation has been performed in this context (Caretti et al. 2014). The morphological analysis of GFAPα and GFAPδ expressing cells is performed in tissue biopsies that are frequently taken from areas of the tumour with high malignant cell densities. Whether similar morphological characteristics are found in cells that have invaded the brain parenchyma remains to be investigated.

4. The functional role GFAP in glioma cell behaviour

GFAP and GFAP isoforms have not only been studied as potential (bio)markers but their function has also been investigated. GFAP plays a role in a broad range of cellular processes, including but not limited to vesicle trafficking, localisation of organelles, and autophagy (Middeldorp and Hol 2011). In the next paragraph, we will discuss some of the functions that have been discovered for GFAP in cell biological domains that are relevant to glioma malignancy, with a focus on GFAP isoforms where possible (Fig. 5).

4.1 Tumorigenesis, cell proliferation and growth

Uncontrolled cell division is a key hallmark of cancer. Several studies have investigated the link between manipulation of GFAP expression and tumorigenesis, cell proliferation, and cell cycle progression, however, the findings are contradictory. An early study investigated the effect of the presence of GFAP on spontaneous astrocytoma development in p53-negative mice exposed to carcinogen ethyl nitrosourea. When comparing GFAP wild-type mice to GFAP-null mice, tumour incidence, histological characteristics and tumour progression were similar (Wilhelmsson et al. 2003). This is in contrast to a study performed by Toda and colleagues, where C6 rat glioma cells transfected with murine GFAP formed smaller tumours in athymic mice (Toda et al. 1999). Also, studies using *in vitro* models are inconclusive. Most studies associate high levels of GFAP with decreased cell proliferation (Toda et al. 1999; Rutka et al. 1994; Elobeid et al. 2000) or find no effect (Weinstein, Shelanski, and Liem 1991a; Murphy, Hatton, and Hoi 1998). However, one study described that a subpopulation of glioma

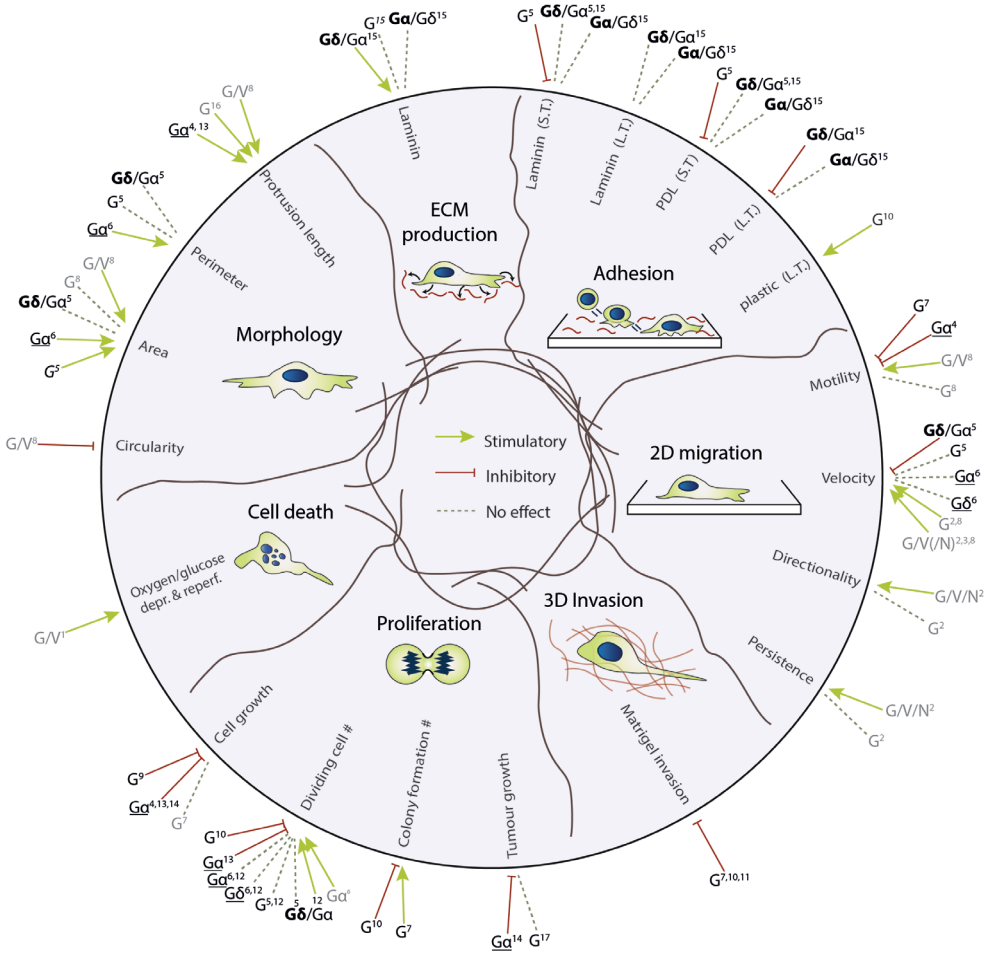

Figure 5. The effect of modifications of the GFAP intermediate filament network on different biological domains relevant for glioma biology. The studies based on overexpression experiments are underlined, the other studies are based on endogenous expression levels, knock-down or knock-out experiments. All studies in grey are based on experiments with (primary) astrocytes, the studies in black on studies with glioma cell lines. G=GFAP, Gδ/α = High GFAPδ/α-ratio cells, Gα/δ = Low GFAPδ/α-ratio cells, G/V/N = GFAP, vimentin, nestin. (1) De Pablo et al. 2013; (2) De Pascalis et al. 2018; (3) Dupin, Sakamoto, and Etienne-Manneville 2011; (4) Elobeid et al. 2000; (5) Moeton et al. 2014; (6) Moeton et al. 2016; (7) Murphy et al. 1998; (8) Lepekhin et al. 2001; (9) Pekny et al. 1998; (10) Rutka et al. 1994; (11) Rutka et al. 1998; (12) Stassen et al. 2017; (13) Toda et al. 1994; (14) Toda et al. 1999; (15) van Bodegraven et al. 2019b; (16) Weinstein et al 1991; (17) Wilhelmsson et al. 2003.

cells with high GFAP expression generated more and larger colonies in a soft-agar colony formation assay in comparison to the GFAP low population (Murphy, Hatton, and Hoi 1998). Previous studies from our lab have investigated the effect of the GFAP isoforms on proliferation, but also here findings are somewhat contradictory. Whereas

overexpression of GFAPα and GFAPδ does not affect proliferation based on BrdU incorporation, MTT assays, and PHP3 positivity (Moeton et al. 2016; Stassen et al. 2017), a higher fraction of BrdU positive cells was described in GFAPα vs GFAPpan depleted cells (Stassen et al. 2017). However, in these knockdown (KD) cells, proliferation was not affected based on Ki67 positivity or number of cells in the G2/M/S phase of the cell cycle (Moeton et al. 2014).

GFAP has also been studied in the context of tumour suppressor gene regulation. The head domain of GFAP, and also vimentin, can bind to tumour suppressor protein menin, and colocalises with menin during the S and early G2 phase of the cell cycle (Lopez-Egido et al. 2002). The authors suggest that the GFAP IF network is involved in sequestering menin during the S-G2 phase of the cell cycle, thereby regulating the activity of menin (Lopez-Egido et al. 2002). Whether these interactions are involved in glioma malignancy, remains to be investigated.

4.2 Cellular stress and survival

GFAP and other IF proteins are frequently linked to the cellular response to stress, and regulators of apoptosis and cell death (Toivola et al. 2010). GFAP interacts with Heat Shock Protein 27 (HSP27) and protein chaperone αB-crystallin (CRYAB), and integration of these proteins into the network prevents aggregation of GFAP (Perng et al. 2006). GFAP is also identified as an interactor of c-Jun N-terminal Kinases (JNK) JNK1α1 and JNK3α1 in a yeast two-hybrid screen, linking GFAP to a major signalling pathway of apoptosis (Chen, Yeap, and Bogoyevitch 2014). In addition, another yeast two-hybrid screen linked GFAP to caspase-activated DNAse/DNA Fragmentation Factor 45 (DFF45), a protein involved in the execution of apoptosis. The binding of GFAP to DFF45 prevents cleavage of the DFF45 protein by caspase-3, therewith preventing nuclease activity of the catalytic subunit DFF40 (Hanus, Kalinowska-Herok, and Widlak 2010). Many IF proteins, including GFAP and vimentin, also contain caspase 3 and 6 cleavage sites, showing that IFs are also targets of the apoptotic pathway (Byun et al. 2001; Zhang et al. 2014; Messing and Brenner 2020).

Although the effect of GFAP on cell survival has not been investigated in detail in glioma, in astrocytes GFAP was found to protect against cell death in response to cellular stress. In astrocytes challenged with oxygen-glucose deprivation, cell death was observed more frequently in GFAP/vimentin-null mice in comparison to astrocytes where the IF network remained intact (De Pablo et al. 2013). High-grade gliomas are frequently associated with hypoxia (Gérard et al. 2019; Jensen et al. 2014), therefore whether GFAP has a protective role in hypoxia-induced cell death in glioma is an interesting topic for further investigation.

4.3 Cell motility and migration

Several studies have investigated the role of GFAP in glial- and glioma cell motility and migration, however, the effect of GFAP on motility and migratory behaviour is not straightforward. Early studies linked downregulation of GFAP with antisense oligonucleotides to increased velocity and motility of cell migration, suggesting an inhibitory effect of GFAP on migration (Rutka et al. 1994; Rutka et al. 1998; Murphy, Hatton, and Hoi 1998). However, in astrocytes isolated from mice lacking GFAP and vimentin, depletion of GFAP or vimentin alone led to a small defect in cell migration, but when both IFs were targeted a larger reduction in cell migration was observed (Lepekhin et al. 2001). Similar observations were made in primary astrocytes treated with siRNAs targeting GFAP, nestin, and/or vimentin, where the lack of all three IFs together leads to a stronger decrease in velocity, directionality, and persistence in comparison to depletion of individual IFs (Dupin, Sakamoto, and Etienne-Manneville 2011; De Pascalis et al. 2018). When only GFAP was targeted in these cells, a reduction in velocity was observed, although no changes were seen in the directionality and persistence of the migration (De Pascalis et al. 2018). The role of GFAP isoforms has also been studied in the context of migration and motility. In glioma cells, shRNAs specifically targeting GFAPα reduced motility of glioma cells, whereas targeting all GFAP isoforms did not affect this (Moeton et al. 2014). Overexpression of GFAPα or GFAPδ in these cells on the other hand does not affect cell motility and migration (Moeton et al. 2016).

The cell migration machinery is a complex system that depends on many dynamic processes in the cell. In several of these processes the IF network has been proven the play a role. One of the first steps in directional migration is cell polarisation (Petrie, Doyle, and Yamada 2009). In migrating astrocytes, cell polarisation is characterised by translocation of the nucleus to the rear of the cell, termed nucleus off-centring. Loss of GFAP, nestin, and vimentin in primary astrocytes leads to aberrant nucleus off-centring during cell polarisation (Dupin, Sakamoto, and Etienne-Manneville 2011). In contrast to nucleus off-centring, centrosome positioning during cell polarisation is not dependent on the presence of GFAP but is regulated by nestin (Dupin, Sakamoto, and Etienne-Manneville 2011). After the polarisation of the cells, the next step in the process of glioma cell migration is the formation of focal adhesions through integrin-extracellular matrix (ECM) binding. The role of vimentin in the regulation of integrin- and focal adhesion dynamics is well established (Ivaska et al. 2007; Leube, Moch, and Windoffer 2015), and over the years the role of GFAP is becoming more apparent as well. The size of focal adhesions is affected by GFAP isoform expression, as both overexpression of GFAPα and GFAPδ leads to a smaller focal adhesion size (Moeton et al. 2016). GFAP can interact with FAs through binding to vinculin and talin (De

Pascalis et al. 2018), but whether this interaction directly affects FA size remains to be investigated. After the formation of adhesions, forces can be loaded on the integrin-ECM complexes by actomyosin contractility, facilitating cellular movement (Case and Waterman 2015). Knockdown of vimentin, nestin, and GFAP in migrating astrocytes leads to stronger traction forces and a loss of force distribution in leader versus follower cells in collectively migrating astrocytes (De Pascalis et al. 2018). Also cell-cell interactions are altered under these conditions, as the flow of N-cadherins at cell-cell adherent junctions is diminished. Interestingly, the morphology of the adherent junctions is also affected when GFAP is targeted alone, indicating a direct involvement of GFAP in the regulation of adherent junctions (De Pascalis et al. 2018).

5. Adding the third dimension: the role of GFAP in cell invasion

Although the role of GFAP and other IFs has been frequently investigated in two-dimensional (2D) cell culture conditions, fewer studies have investigated the role of GFAP in glioma invasion within three-dimensional (3D) environments. Current knowledge is limited to Matrigel invasion studies. Low levels of GFAP or depletion of GFAP in glioma cells leads to higher invasiveness into Matrigel (Rutka et al. 1994; Murphy, Hatton, and Hoi 1998; Rutka et al. 1998; 1999). Although Matrigel experiments help to understand how glioma cells migrate through 3D environments, not all aspects of glioma infiltration of the brain parenchyma are recapitulated. During tissue invasion, cells encounter ECM matrices with different topologies, ligand densities/distributions, and the presence of other malignant and non-malignant cells in all directions (Charras and Sahai 2014). This requires cells to constantly sense the chemical- and physical characteristics of their environment, integrate these signals and adjust the behavioural response to it. That depletion of IFs can have different effects within 2D and 3D environments recently became clear from a study with mouse embryonic fibroblasts. Whereas expression of vimentin in these cells is associated with higher migration speed on flat surfaces, when the same cells migrate in 3D collagen matrices or confined microchannels, the cells are slowed down by the presence of vimentin (Patteson et al. 2019). Therefore, to fully understand the role of GFAP and GFAP isoforms in glioma cell invasion, it is important to investigate the protein within a cellular context that recapitulates the environmental conditions that glioma cells normally encounter.

Aim and outline

In this thesis, we aim to unravel the versatile role of the GFAP intermediate filament (IF) network in glioma cell invasion. Due to altered expression patterns of *GFAPα* and *GFAPδ* in high- and low-grade gliomas and the strong association between the GFAPδ/α ratio and extracellular matrix regulatory genes, we hypothesise that GFAP splice variants are differentially involved in regulating invasion of glioma cells. Our main approach to address our aim, is to regulate the expression levels of GFAP and the GFAPδ/α ratio by genetically modifying glioma cell lines and to investigate the effects of these manipulations on cell behaviour within different three-dimensional invasion assays. This approach is complemented by a literature study on IFs in cell invasion and by a meta-analysis on GFAP as a serum biomarker in glioma patients.

In **Chapter 1** we regulate GFAP alternative splicing using CRISPR-Cas9 technology and describe how manipulation of the GFAPδ/α ratio affects cell signalling pathways that regulate cell-extracellular matrix interactions. We discover DUSP4, a gene that correlates with glioma malignancy and patient survival, as a central player in the GFAP isoform induced changes on cell-environment interactions.

In **Chapter 2** we review the literature to investigate what is currently known about the role of the IF family in cell migration and invasion within a three-dimensional (3D) context. We focus on how IF proteins contribute to mechanoreciprocity and mechanical resilience during cell invasion.

In **Chapter 3**, we describe a method to systematically study the invasive and proliferative capacities of glioma cells within a native-like brain environment. In a novel approach, we combine an *ex vivo* organotypic brain slice invasion model with whole-mount immunofluorescence and tissue clearing to visualise and reconstruct the three-dimensional invasion patterns of glioma cells.

In **Chapter 4**, we apply the *ex vivo* organotypic brain slice invasion assay to the GFAPδ/α ratio modulated cells to investigate how GFAPδ and GFAPα modulate the invasive capacities of glioma cells. In addition, we use intravital imaging to follow the migration patterns of the GFAP isoform modulated cells *in vivo*. We show that GFAPδ/α ratio modulated cells differentially affect the migration dynamics and tumour growth patterns of glioma cells.

In **Chapter 5**, we discover that exposure to physical constraints during glioma cell invasion can lead to nuclear fragmentation and cell death. We show that this

phenotype is exacerbated by a full loss of GFAP, but not specific GFAP isoforms or vimentin, and is associated with diminished nuclear envelope integrity.

In **Chapter 6,** we perform a systematic search and meta-analysis on the presence of GFAP and other IF proteins in body fluids of glioma patients to investigate the usefulness of GFAP as a biomarker. We describe that the presence of GFAP in serum (sGFAP) is specifically detected and elevated in grade IV glioma patients and further explore the utility of GFAP in body fluids as a biomarker in diffuse glioma.

At last, in the General Discussion, we give an overview of the main findings described in this thesis, discuss open questions, reflect on the methodological approaches used, and discuss the clinical implications and future considerations.

References

Ahmadipour, Y., O. Gembruch, D. Pierscianek, U. Sure, and R. Jabbarli. 2020. "Does the Expression of Glial Fibrillary Acid Protein (GFAP) Stain in Glioblastoma Tissue Have a Prognostic Impact on Survival?" Neurochirurgie 66 (3): 150–54. https://doi.org/10.1016/j.neuchi.2019.12.012.

Alieva, Maria, Andreia S. Margarido, Tamara Wieles, Erik R. Abels, Burcin Colak, Carla Boquetale, Herke Jan Noordmans, Tom J. Snijders, Marike L. Broekman, and Jacco van Rheenen. 2017. "Preventing Inflammation Inhibits Biopsy-Mediated Changes in Tumor Cell Behavior." *Scientific Reports* 7 (1): 7529. https://doi.org/10.1038/s41598-017-07660-4.

Andreiuolo, Felipe, Marie Pierre Junier, Elly M. Hol, Catherine Miquel, Leila Chimelli, Nadine Leonard, Hervé Chneiweiss, Catherine Daumas-Duport, and Pascale Varlet. 2009. "GFAPδ Immunostaining Improves Visualization of Normal and Pathologic Astrocytic Heterogeneity." *Neuropathology* 29 (1): 31–39. https://doi.org/10.1111/j.1440-1789.2008.00936.x.

Beadle, Christopher, Marcela C. Assanah, Pascale Monzo, Richard Vallee, Steven S. Rosenfeld, and Peter Canoll. 2010. "The Role of Myosin II in Glioma Invasion of the Brain." *Molecular Biology of the Cell* 19 (8): 327–31. https://doi.org/10.1091/mbc.E08.

Berge, Simone A. van den, Jinte Middeldorp, C. Eleana Zhang, Maurice A. Curtis, Brian W. Leonard, Diego Mastroeni, Pieter Voorn, Wilma D J van de Berg, Inge Huitinga, and Elly M. Hol. 2010. "Longterm Quiescent Cells in the Aged Human Subventricular Neurogenic System Specifically Express GFAP-δ." *Aging Cell* 9 (3): 313–26. https://doi.org/10.1111/j.1474-9726.2010.00556.x.

Bergmann, Olaf, Kirsty L. Spalding, and Jonas Frisén. 2015. "Adult Neurogenesis in Humans." *Cold Spring Harbor Perspectives in Medicine* 5 (7): 1–12. https://doi.org/10.1101/cshperspect.a018994.

Bhaduri, Aparna, Elizabeth Di Lullo, Diane Jung, Sören Müller, Elizabeth Erin Crouch, Carmen Sandoval Espinosa, Tomoko Ozawa, et al. 2020. "Outer Radial Glia-like Cancer Stem Cells Contribute to Heterogeneity of Glioblastoma." *Cell Stem Cell* 26 (1): 48-63.e6. https://doi.org/10.1016/j.stem.2019.11.015.

Blechingberg, Jenny, Holm, Ida E., Nielsen, Karsten B., Jensen, Torben H., Jørgensen, Arne L., Nielsen, Anders L. 2007. "Identification and Characterization of GFAPj, a Novel Glial Fibrillary Acidic Protein Isoform." *Glia* 55: 487-507. https://doi.org/10.1002/glia.

Blechingberg, Jenny, Søren Lykke-andersen, Torben Heick Jensen, Arne Lund Jørgensen, and Anders Lade Nielsen. 2007. "Regulatory Mechanisms for 3'-End Alternative Splicing and Polyadenylation of the Glial Fibrillary Acidic Protein, GFAP, Transcript." *Nucleic Acids Research* 35 (22): 7636–50. https://doi.org/10.1093/nar/gkm931.

Bodegraven, Emma J. van. 2019a. "GFAP revisited - From biomarker to an isoform-specific function in glioma malignancy." PhD thesis. Utrecht University.

Bodegraven, Emma J. van, Jessy V. van Asperen, Pierre A.J. Robe, and Elly M. Hol. 2019b. "Importance of GFAP Isoform-Specific Analyses in Astrocytoma." *Glia* 67 (8): 1417–33. https://doi.org/10.1002/glia.23594.

Bodegraven, Emma J. van, Jacqueline A. Sluijs, A. Katherine Tan, Pierre A.J.T. Robe, and Elly M. Hol. 2021. "New GFAP Splice Isoform (GFAPμ) Differentially Expressed in Glioma Translates into 21 KDa N-Terminal GFAP Protein." *FASEB Journal* 35 (3). https://doi.org/10.1096/fj.202001767R.

Boyd, Sarah E., Betina Nair, Sze Woei Ng, Jonathan M. Keith, and Jacqueline M. Orian. 2012. "Computational Characterization of 3' Splice Variants in the GFAP Isoform Family." *PLoS ONE* 7 (3): 36–41. https://doi.org/10.1371/journal.pone.0033565.

Bradshaw, Amy, Agadha Wickremsekera, Swee T. Tan, Lifeng Peng, Paul F. Davis, and Tinte Itinteang. 2016. "Cancer Stem Cell Hierarchy in Glioblastoma Multiforme." *Frontiers in Surgery* 3 (April): 1–15. https://doi.org/10.3389/fsurg.2016.00021.

Brehar, Felix Mircea, Dorel Arsene, Lacramioara Aurelia Brinduse, and Mircea Radu Gorgan. 2015. "Immunohistochemical Analysis of GFAP-δ And Nestin in Cerebral Astrocytomas." *Brain Tumor Pathology* 32 (2): 90–98. https://doi.org/10.1007/s10014-014-0199-8.

Brenner, Michael, and Albee Messing. 2021. "Regulation of GFAP Expression". *ASN Neuro*. Vol. 13. https://doi.org/10.1177/1759091420981206.

Brown, Timothy J., Daniela A. Bota, Martin J. Van Den Bent, Paul D. Brown, Elizabeth Maher, Dawit Aregawi, Linda M. Liau, et al. 2019. "Management of Low-Grade Glioma: A Systematic Review and Meta-Analysis." *Neuro-Oncology Practice* 6 (4): 249–58. https://doi.org/10.1093/nop/npy034.

Byun, Y., F. Chen, R. Chang, M. Trivedi, K. J. Green, and V. L. Cryns. 2001. "Caspase Cleavage of Vimentin Disrupts Intermediate Filaments and Promotes Apoptosis." *Cell Death and Differentiation* 8 (5): 443–50. https://doi.org/10.1038/sj.cdd.4400840.

Caretti, Viola, Marianna Bugiani, Morgan Freret, Pepijn Schellen, Marc Jansen, Dannis van Vuurden, Gertjan Kaspers, et al. 2014. "Subventricular Spread of Diffuse Intrinsic Pontine Glioma." *Acta Neuropathologica* 128 (4): 605–7. https://doi.org/10.1007/s00401-014-1307-x.

Case, Lindsay B., and Clare M. Waterman. 2015. "Integration of Actin Dynamics and Cell Adhesion by a Three-Dimensional, Mechanosensitive Molecular Clutch." *Nature Cell Biology* 17 (8): 955–63. https://doi.org/10.1038/ncb3191.

Charras, Guillaume, and Erik Sahai. 2014. "Physical Influences of the Extracellular Environment on Cell Migration." *Nature Reviews Molecular Cell Biology* 15 (12): 813–24. https://doi.org/10.1038/nrm3897.

Chen, Wan Jui, and Ronald K.H. Liem. 1994. "The Endless Story of the Glial Fibrillary Acidic Protein." *Journal of Cell Science* 107 (8): 2299–2311. https://doi.org/10.1242/jcs.107.8.2299.

Chen, Wei Kai, Yvonne Y.C. Yeap, and Marie A. Bogoyevitch. 2014. "The JNK1/JNK3 Interactome - Contributions by the JNK3 Unique N-Terminus and JNK Common Docking Site Residues." *Biochemical and Biophysical Research Communications* 453 (3): 576–81. https://doi.org/10.1016/j.bbrc.2014.09.122.

Chernyatina, Anastasia A., Dmytro Guzenko, and Sergei V. Strelkov. 2015. "Intermediate Filament Structure: The Bottom-up Approach." *Current Opinion in Cell Biology* 32 (Box 1): 65–72. https://doi.org/10.1016/j.ceb.2014.12.007.

Choi, Kyung-Chan, Sung-Eun Kwak, Ji-Eun Kim, Seung Hun Sheen, and Tae-Cheon Kang. 2009. "Enhanced Glial Fibrillary Acidic Protein-δ Expression in Human Astrocytic Tumor." *Neuroscience Letters* 463 (3): 182–87. https://doi.org/10.1016/j.neulet.2009.07.076.

Claes, An, Albert J. Idema, and Pieter Wesseling. 2007. "Diffuse Glioma Growth: A Guerilla War." *Acta Neuropathologica* 114 (5): 443–58. https://doi.org/10.1007/s00401-007-0293-7.

Cuddapah, Vishnu Anand, Stefanie Robel, Stacey Watkins, and Harald Sontheimer. 2014. "A Neurocentric Perspective on Glioma Invasion." *Nature Reviews. Neuroscience* 15 (7): 455–65. https://doi.org/10.1038/nrn3765.

Doyle, Andrew D., Nicole Carvajal, Albert Jin, Kazue Matsumoto, and Kenneth M. Yamada. 2015. "Local 3D Matrix Microenvironment Regulates Cell Migration through Spatiotemporal Dynamics of Contractility-Dependent Adhesions." *Nature Communications* 6. https://doi.org/10.1038/ncomms9720.

Dupin, Isabelle, Yasuhisa Sakamoto, and Sandrine Etienne-Manneville. 2011. "Cytoplasmic Intermediate Filaments Mediate Actin-Driven Positioning of the Nucleus." *Journal of Cell Science* 124 (Pt 6): 865–72. https://doi.org/10.1242/jcs.076356.

Elobeid, A., E. Bongcam-Rudloff, B. Westermark, and M. Nistér. 2000. "Effects of Inducible Glial Fibrillary Acidic Protein on Glioma Cell Motility and Proliferation." *Journal of Neuroscience Research* 60 (2): 245–56. https://doi.org/10.1002/(SICI)1097-4547(20000415)60:2

Eng, L. F., J. J. Vanderhaeghen, A. Bignami, and B. Gerstl. 1971. "An Acidic Protein Isolated from Fibrous Astrocytes." *Brain Research* 28 (2): 351–54. https://doi.org/10.1016/0006-8993(71)90668-8.

Etienne-Manneville, Sandrine. 2018. "Cytoplasmic Intermediate Filaments in Cell Biology." *Annual Review of Cell and Developmental Biology* 34 (1): annurev-cellbio-100617-062534. https://doi.org/10.1146/annurev-cellbio-100617-062534.

Farin A, Suzuki SO, Weiker M, Goldman JE, Bruce JN, Canoll P. 1994. "Transplanted Glioma Cells Migrate and Proliferate on Host Brain Vasculature: A Dynamic Analysis." *American Journal of Tropical Medicine and Hygiene* 51 (5): 523–32. https://doi.org/10.1002/glia.

Geisler, N., and K. Weber. 1983. "Amino Acid Sequence Data on Glial Fibrillary Acidic Protein (GFA); Implications for the Subdivision of Intermediate Filaments into Epithelial and Non-Epithelial Members." *The EMBO Journal* 2 (11): 2059–63. https://doi.org/10.1002/j.1460-2075.1983.tb01700.x.

Gérard, Michael, Aurélien Corroyer-Dulmont, Paul Lesueur, Solène Collet, Michel Chérel, Mickael Bourgeois, Dinu Stefan, et al. 2019. "Hypoxia Imaging and Adaptive Radiotherapy: A State-of-the-Art Approach in the Management of Glioma." *Frontiers in Medicine* 6 (June). https://doi.org/10.3389/fmed.2019.00117.

Gritsenko, Pavlo G., Nader Atlasy, Cindy E.J. Dieteren, Anna C. Navis, Jan Hendrik Venhuizen, Cornelia Veelken, Dirk Schubert, et al. 2020. "P120-Catenin-Dependent Collective Brain Infiltration By Glioma Cell Networks." *Nature Cell Biology* 22 (1): 97–107. https://doi.org/10.1038/s41556-019-0443-x.

Guzenko, Dmytro, Anastasia A. Chernyatina, and Sergei V. Strelkov. 2017. "Crystallographic Studies of Intermediate Filament Proteins." *Sub-Cellular Biochemistry* 82 (January): 151–70. https://doi.org/10.1007/978-3-319-49674-0_6.

Hanus, Jakub, Magdalena Kalinowska-Herok, and Piotr Widlak. 2010. "Identification of Novel Putative Regulators of the Major Apoptotic Nuclease DNA Fragmentation Factor." *Acta Biochimica Polonica* 57 (4): 521–27. https://doi.org/10.18388/abp.2010_2438.

Hartmann, Christian, Bettina Hentschel, Marcos Tatagiba, Johannes Schramm, Oliver Schnell, Clemens Seidel, Robert Stein, et al. 2011. "Molecular Markers in Low-Grade Gliomas: Predictive or Prognostic?" *Clinical Cancer Research* 17 (13): 4588–99. https://doi.org/10.1158/1078-0432.CCR-10-3194.

Helman, Guy, Asako Takanohashi, Tracy L. Hagemann, Ming D. Perng, Marzena Walkiewicz, Sarah Woidill, Sunetra Sase, et al. 2020. "Type II Alexander Disease Caused by Splicing Errors and Aberrant Overexpression of an Uncharacterized GFAP Isoform." *Human Mutation* 41 (6): 1131–37. https://doi.org/10.1002/humu.24008.

Heo, Dong Hwa, Se Hoon Kim, Kyung-Moo Yang, Yong Jun Cho, Keung Nyun Kim, Do Heum Yoon, and Tae-Cheon Kang. 2012. "A Histopathological Diagnostic Marker for Human Spinal Astrocytoma: Expression of Glial Fibrillary Acidic Protein-δ." *Journal of Neuro-Oncology* 108 (1): 45–52. https://doi.org/10.1007/s11060-012-0801-z.

Herrmann, Harald, and Ueli Aebi. 2016. "Intermediate Filaments: Structure and Assembly." *Cold Spring Harbor Perspectives in Biology* 8 (11). https://doi.org/10.1101/cshperspect.a018242.

Hesse, M., T. M. Magin, and K. Weber. 2001. "Genes for Intermediate Filament Proteins and the Draft Sequence of the Human Genome: Novel Keratin Genes and a Suprisingly High Number of Pseudogenes Related to Keratin Genes 8 and 18." *Journal of Cell Science* 114 (14): 2569–75.

Ho, Vincent K.Y., Jaap C. Reijneveld, Roelien H. Enting, Henri P. Bienfait, Pierre Robe, Brigitta G. Baumert, and Otto Visser. 2014. "Changing Incidence and Improved Survival of Gliomas." *European Journal of Cancer* 50 (13): 2309–18. https://doi.org/10.1016/j.ejca.2014.05.019.

Hol, Elly M., and Milos Pekny. 2015. "Glial Fibrillary Acidic Protein (GFAP) and the Astrocyte Intermediate Filament System in Diseases of the Central Nervous System." *Current Opinion in Cell Biology* 32: 121–30. https://doi.org/10.1016/j.ceb.2015.02.004.

Huebner, Kay, Carlo M. Croce, Christer Betsholtz, Jia Lun Wang, and Bengt Westermark. 1991. "Human Glial Fibrillary Acidic Protein: Complementary DNA Cloning, Chromosome Localization, and Messenger RNA Expression in Human Glioma Cell Lines of Various Phenotypes." *Cancer Research* 51 (5): 1553–60.

Ivaska, Johanna, Hanna Mari Pallari, Jonna Nevo, and John E. Eriksson. 2007. "Novel Functions of Vimentin in Cell Adhesion, Migration, and Signaling." *Experimental Cell Research* 313 (10): 2050–62. https://doi.org/10.1016/j.yexcr.2007.03.040.

Jensen, Randy L., Michael L. Mumert, David L. Gillespie, Anita Y. Kinney, Matthias C. Schabel, and Karen L. Salzman. 2014. "Preoperative Dynamic Contrast-Enhanced MRI Correlates with Molecular Markers of Hypoxia and Vascularity in Specific Areas of Intratumoral Microenvironment and Is Predictive of Patient Outcome." *Neuro-Oncology* 16 (2): 280–91. https://doi.org/10.1093/neuonc/not148.

Jin, Zhicheng, Zongming Fu, Jun Yang, Juan Troncosco, Allen D. Everett, and Jennifer E. Van Eyk. 2013. "Identification and Characterization of Citrulline-Modified Brain Proteins by Combining HCD and CID Fragmentation." *Proteomics* 13 (17): 2682–91. https://doi.org/10.1002/pmic.201300064.

Kanski, Regina, Marjolein A M Sneeboer, Emma J van Bodegraven, Jacqueline A Sluijs, Wietske Kropff, Marit W Vermunt, Menno P Creyghton, et al. 2014. "Histone Acetylation in Astrocytes Suppresses GFAP and Stimulates a Reorganization of the Intermediate Filament Network." *Journal of Cell Science* 127 (Pt 20): 4368–80. https://doi.org/10.1242/jcs.145912.

Kessel, Emma van, Anniek E. Baumfalk, Martine J.E. van Zandvoort, Pierre A. Robe, and Tom J. Snijders. 2017. "Tumor-Related Neurocognitive Dysfunction in Patients with Diffuse Glioma: A Systematic Review of Neurocognitive Functioning Prior to Anti-Tumor Treatment." *Journal of Neuro-Oncology* 134 (1): 9–18. https://doi.org/10.1007/s11060-017-2503-z.

Leduc, Cécile, and Sandrine Etienne-Manneville. 2017. "Intermediate Filaments Join the Action." *Cell Cycle* 16 (15): 1389–90. https://doi.org/10.1080/15384101.2017.1345230.

Leduc, Cécile, and Sandrine Etienne Manneville. 2017. "Regulation of Microtubule-Associated Motors Drives Intermediate Filament Network Polarization" 216 (6): 1689–1704. https://doi.org/10.1083/jcb.201607045.

Lepekhin, Eugene A., Camilla Eliasson, Claes Henric Berthold, Vladimir Berezin, Elisabeth Bock, and Milos Pekny. 2001. "Intermediate Filaments Regulate Astrocyte Motility." *Journal of Neurochemistry* 79 (3): 617–25. https://doi.org/10.1046/j.1471-4159.2001.00595.x.

Leube, Rudolf E., Marcin Moch, and Reinhard Windoffer. 2015. "Intermediate Filaments and the

Regulation of Focal Adhesion." *Current Opinion in Cell Biology* 32: 13–20. https://doi.org/10.1016/j.ceb.2014.09.011.

Lin, Ni Hsuan, Ai Wen Yang, Chih Hsuan Chang, and Ming Der Perng. 2021. "Elevated GFAP Isoform Expression Promotes Protein Aggregation and Compromises Astrocyte Function." *FASEB Journal* 35 (5). https://doi.org/10.1096/fj.202100087R.

Lopez-Egido, Juan R., Janet Cunningham, Mikael Berg, Kjell Oberg, Erik Bongcam-Rudloff, and Anders E. Gobl. 2002. "Menin's Interaction with Glial Fibrillary Acidic Protein and Vimentin Suggests a Role for the Intermediate Filament Network in Regulating Menin Activity." *Experimental Cell Research* 278 (2): 175–83. https://doi.org/10.1006/excr.2002.5575.

Louis, David N., Arie Perry, Guido Reifenberger, Andreas von Deimling, Dominique Figarella-Branger, Webster K. Cavenee, Hiroko Ohgaki, Otmar D. Wiestler, Paul Kleihues, and David W. Ellison. 2016. "The 2016 World Health Organization Classification of Tumors of the Central Nervous System: A Summary." *Acta Neuropathologica* 131 (6): 803–20. https://doi.org/10.1007/s00401-016-1545-1.

Louis, David N, Arie Perry, Pieter Wesseling, Daniel J Brat, Ian A Cree, Dominique Figarella-Branger, Cynthia Hawkins, et al. 2021. "The 2021 WHO Classification of Tumors of the Central Nervous System: A Summary." *Neuro-Oncology* 23 (8): 1231–51. https://doi.org/10.1093/neuonc/noab106.

Matsuyama, Hironori, and Hiroshi I. Suzuki. 2020. "Systems and Synthetic MicroRNA Biology: From Biogenesis to Disease Pathogenesis." *International Journal of Molecular Sciences* 21 (1): 1–23. https://doi.org/10.3390/ijms21010132.

McCormick, M. B., P. Kouklis, A. Syder, and E. Fuchs. 1993. "The Roles of the Rod End and the Tail in Vimentin IF Assembly and IF Network Formation." *Journal of Cell Biology* 122 (2): 395–407. https://doi.org/10.1083/jcb.122.2.395.

Menet, Véronique, Minerva Giménez Y Ribotta, Norbert Chauvet, Marie Jeanne Drian, Julie Lannoy, Emma Colucci-Guyon, and Alain Privat. 2001. "Inactivation of the Glial Fibrillary Acidic Protein Gene, but Not That of Vimentin, Improves Neuronal Survival and Neurite Growth by Modifying Adhesion Molecule Expression." *Journal of Neuroscience* 21 (16): 6147–58. https://doi.org/10.1523/jneurosci.21-16-06147.2001.

Messing, Albee, and Michael Brenner. 2020. "GFAP at 50." *ASN Neuro* 12. https://doi.org/10.1177/1759091420949680.

Middeldorp, J., and E. M. Hol. 2011. "GFAP in Health and Disease." *Progress in Neurobiology* 93 (3): 421–43. https://doi.org/10.1016/j.pneurobio.2011.01.005.

Moeton, Martina, Regina Kanski, Oscar M J A Stassen, Jacqueline A. Sluijs, Dirk Geerts, Paula Van Tijn, Gerhard Wiche, Miriam E. Van Strien, and Elly M. Hol. 2014. "Silencing GFAP Isoforms in Astrocytoma Cells Disturbs Laminin-Dependent Motility and Cell Adhesion." *FASEB Journal* 28 (7): 2942–54. https://doi.org/10.1096/fj.13-245837.

Moeton, Martina, Oscar M J A Stassen, Jacqueline A. Sluijs, Vincent W N van der Meer, Liselot J. Kluivers, Hedde van Hoorn, Thomas Schmidt, Eric A J Reits, Miriam E. van Strien, and Elly M. Hol. 2016. "GFAP Isoforms Control Intermediate Filament Network Dynamics, Cell Morphology, and Focal Adhesions." *Cellular and Molecular Life Sciences* 73 (21): 4101–20. https://doi.org/10.1007/s00018-016-2239-5.

Molinaro, Annette M., Jennie W. Taylor, John K. Wiencke, and Margaret R. Wrensch. 2019. "Genetic and Molecular Epidemiology of Adult Diffuse Glioma." *Nature Reviews Neurology* 15 (7): 405–17. https://doi.org/10.1038/s41582-019-0220-2.

Murphy, Katrina G., James D. Hatton, and Sang H. Hoi. 1998. "Role of Glial Fibrillary Acidic Protein Expression in the Biology of Human Glioblastoma U-373MG Cells." *Journal of Neurosurgery* 89 (6): 997–1006. https://doi.org/10.3171/jns.1998.89.6.0997.

Nagano, N, H Sasaki, M Aoyagi, and K Hirakawa. 1993. "Invasion of Experimental Rat Brain Tumor: Early

Morphological Changes Following Microinjection of C6 Glioma Cells." *Acta Neuropathologica* 86 (2): 117–25. https://doi.org/10.1007/BF00334878.

Neftel, C., J. Laffy, Mariella G. Filbin, Toshiro Hara, Marni E. Shore, Gilbert J. Rahme, Alyssa R. Richman, et al. 2019. "An Integrative Model of Cellular States, Plasticity, and Genetics for Glioblastoma." *Cell* 178 (4): 835-849.e21. https://doi.org/10.1016/j.cell.2019.06.024.

Nielsen, Anders Lade, Ida E. Holm, Marianne Johansen, Bjarne Bonven, Poul Jørgensen, and Arne Lund Jørgensen. 2002. "A New Splice Variant of Glial Fibrillary Acidic Protein, GFAP Epsilon, Interacts with the Presenilin Proteins." *Journal of Biological Chemistry* 277 (33): 29983–91. https://doi.org/10.1074/jbc.M112121200.

Nielsen, Anders Lade, and Arne Lund Jørgensen. 2004. "Self-Assembly of the Cytoskeletal Glial Fibrillary Acidic Protein Is Inhibited by an Isoform-Specific C Terminus." *Journal of Biological Chemistry* 279 (40): 41537–45. https://doi.org/10.1074/jbc.M406601200.

Osswald, Matthias, Erik Jung, Felix Sahm, Gergely Solecki, Varun Venkataramani, Jonas Blaes, Sophie Weil, et al. 2015. "Brain Tumour Cells Interconnect to a Functional and Resistant Network." *Nature* 528 (7580): 93–98. https://doi.org/10.1038/nature16071.

Ostrom, Quinn T., David J. Cote, Mustafa Ascha, Carol Kruchko, and Jill S. Barnholtz-Sloan. 2018. "Adult Glioma Incidence and Survival by Race or Ethnicity in the United States from 2000 to 2014." *JAMA Oncology* 4 (9): 1254–62. https://doi.org/10.1001/jamaoncol.2018.1789.

Oudart, Marc. 2012. "AstroDot – a New Method for Studying the Spatial Distribution of MRNA in Astrocytes." *Stem Cells*, no. February.

Pablo, Yolanda De, Michael Nilsson, Marcela Pekna, and Milos Pekny. 2013. "Intermediate Filaments Are Important for Astrocyte Response to Oxidative Stress Induced by Oxygen-Glucose Deprivation and Reperfusion." *Histochemistry and Cell Biology* 140 (1): 81–91. https://doi.org/10.1007/s00418-013-1110-0.

Pascalis, Chiara De, Carlos Pérez-González, Shailaja Seetharaman, Batiste Boëda, Benoit Vianay, Mithila Burute, Cécile Leduc, Nicolas Borghi, Xavier Trepat, and Sandrine Etienne-Manneville. 2018. "Intermediate Filaments Control Collective Migration by Restricting Traction Forces and Sustaining Cell–Cell Contacts." *The Journal of Cell Biology*, jcb.201801162. https://doi.org/10.1083/jcb.201801162.

Patel, Anoop P., Itay Tirosh, John J. Trombetta, Alex K. Shalek, Shawn M. Gillespie, Hiroaki Wakimoto, Daniel P. Cahill, et al. 2014. "Single-Cell RNA-Seq Highlights Intratumoral Heterogeneity in Primary Glioblastoma." *Science* 344 (6190): 1396–1401. https://doi.org/10.1126/science.1254257.

Patteson, Alison E., Katarzyna Pogoda, Fitzroy J. Byfield, Kalpana Mandal, Zofia Ostrowska-Podhorodecka, Elisabeth E. Charrier, Peter A. Galie, et al. 2019. "Loss of Vimentin Enhances Cell Motility through Small Confining Spaces." *Small* 1903180: 1–10. https://doi.org/10.1002/smll.201903180.

Paulus, Werner, and Wolfgang Roggendorf. 1988. "Vimentin and Glial Fibrillary Acidic Protein Are Codistributed in the Same Intermediate Filament System of Malignant Glioma Cells in Vivo - A Double-Labeling Immunoelectron-Microscopical Study." *Virchows Archiv B Cell Pathology Including Molecular Pathology* 56 (1): 67–70. https://doi.org/10.1007/BF02890003.

Pearson, Joshua R.D., and Tarik Regad. 2017. "Targeting Cellular Pathways in Glioblastoma Multiforme." *Signal Transduction and Targeted Therapy* 2 (May): 1–11. https://doi.org/10.1038/sigtrans.2017.40.

Peiffer, Jürgen. 1999. "Hans-Joachim Scherer (1906-1945), Pioneer in Glioma Research." *Brain Pathology* 9 (2): 241–45. https://doi.org/10.1111/j.1750-3639.1999.tb00222.x.

Pekny, Milos, Camilla Eliasson, Chung Liang Chien, Lars Gunnar Kindblom, Ronald Liem, Anders Hamberger, and Christer Betsholtz. 1998. "GFAP-Deficient Astrocytes Are Capable of Stellation in Vitro When Cocultured with Neurons and Exhibit a Reduced Amount of Intermediate Filaments and an Increased Cell Saturation Density." *Experimental Cell Research* 239 (2): 332–43. https://doi.

org/10.1006/excr.1997.3922.

Perng, M., Shu-Fang Wen, Terry Gibbon,Jinte Middeldorp, Jacqueline Sluijs, and and Roy A. Quinlan Elly M. Hol. 2008. "Glial Fibrillary Acidic Protein Filaments Can Tolerate the Incorporation of Assembly-Compromised GFAP-δ, but with Consequences for Filament Organization and αB-Crystallin Association." *Molecular Biology of the Cell* 82 (4): 327–31. https://doi.org/10.1091/mbc.E08.

Perng, Ming Der, Mu Su, Shu Fang Wen, Rong Li, Terry Gibbon, Alan R. Prescott, Michael Brenner, and Roy A. Quinlan. 2006. "The Alexander Disease-Causing Glial Fibrillary Acidic Protein Mutant, R416W, Accumulates into Rosenthal Fibers by a Pathway That Involves Filament Aggregation and the Association of αB-Crystallin and HSP27." *American Journal of Human Genetics* 79 (2): 197–213. https://doi.org/10.1086/504411.

Perry, Arie, and Pieter Wesseling. 2016. *Histologic Classification of Gliomas*. *Handbook of Clinical Neurology*. 1st ed. Vol. 134. Elsevier B.V. https://doi.org/10.1016/B978-0-12-802997-8.00005-0.

Petrie, Ryan J., Andrew D. Doyle, and Kenneth M. Yamada. 2009. "Random versus Directionally Persistent Cell Migration." *Nature Reviews Molecular Cell Biology* 10 (8): 538–49. https://doi.org/10.1038/nrm2729.

Roelofs, Reinko F., David F. Fischer, Simone H. Houtman, Jacqueline A. Sluijs, Wendy Van Haren, Fred W. Van Leeuwen, and Elly M. Hol. 2005. "Adult Human Subventricular, Subgranular, and Subpial Zones Contain Astrocytes with a Specialized Intermediate Filament Cytoskeleton." *Glia* 52 (4): 289–300. https://doi.org/10.1002/glia.20243.

Rutka, J T, S L Hubbard, K Fukuyama, K Matsuzawa, P B Dirks, and L E Becker. 1994. "Effects of Antisense Glial Fibrillary Acidic Protein Complementary DNA on the Growth, Invasion, and Adhesion of Human Astrocytoma Cells." *Cancer Res.* 54 (0008-5472 (Print)): 3267–72.

Rutka, James T., Cameron Ackerley, Sherri Lynn Hubbard, Aina Tilup, Peter B. Dirks, Shin Jung, Stacey Ivanchuk, Masanori Kurimoto, Atsushi Tsugu, and Laurence E. Becker. 1998. "Characterization of Glial Filament-Cytoskeletal Interactions in Human Astrocytomas: An Immuno-Ultrastructural Analysis." *European Journal of Cell Biology* 76 (4): 279–87. https://doi.org/10.1016/S0171-9335(98)80006-X.

Rutka, James T., Stacey Ivanchuk, Soma Mondal, Michael Taylor, Keiichi Sakai, Peter Dirks, Peter Jun, Shin Jung, Laurence E. Becker, and Cameron Ackerley. 1999. "Co-Expression of Nestin and Vimentin Intermediate Filaments in Invasive Human Astrocytoma Cells." *International Journal of Developmental Neuroscience* 17 (5–6): 503–15. https://doi.org/10.1016/S0736-5748(99)00049-0.

Sahm, Felix, David Capper, Astrid Jeibmann, Antje Habel, Werner Paulus, Dirk Troost, and Andreas Von Deimling. 2012. "Addressing Diffuse Glioma as a Systemic Brain Disease with Single-Cell Analysis." *Archives of Neurology* 69 (4): 523–26. https://doi.org/10.1001/archneurol.2011.2910.

Sanson, Marc, Yannick Marie, Sophie Paris, Ahmed Idbaih, Julien Laffaire, François Ducray, Soufiane El Hallani, et al. 2009. "Isocitrate Dehydrogenase 1 Codon 132 Mutation Is an Important Prognostic Biomarker in Gliomas." *Journal of Clinical Oncology* 27 (25): 4150–54. https://doi.org/10.1200/JCO.2009.21.9832.

Scherer, H.J. 1940. "Cerebral Astrocytomas And Their Derivatives". *The American Journal of Cancer* 40 (2): 1–15.

Singh, Ripudaman, Anders L. Nielsen, Marianne G. Johansen, and Arne L. Jørgensen. 2003. "Genetic Polymorphism and Sequence Evolution of an Alternatively Spliced Exon of the Glial Fibrillary Acidic Protein Gene, GFAP." *Genomics* 82 (2): 185–93. https://doi.org/10.1016/S0888-7543(03)00106-X.

Skalli, Omar, Ulrika Wilhelmsson, Charlotte Örndahl, Boglarka Fekete, Kristina Malmgren, Bertil Rydenhag, and Milos Pekny. 2013. "Astrocytoma Grade IV (Glioblastoma Multiforme) Displays 3 Subtypes with Unique Expression Profiles of Intermediate Filament Proteins." *Human Pathology* 44 (10): 2081–88. https://doi.org/10.1016/j.humpath.2013.03.013.

Stassen, Oscar M.J.A., Emma J. van Bodegraven, Fabrizio Giuliani, Martina Moeton, Regina Kanski, Jacqueline A. Sluijs, Miriam E. van Strien, Willem Kamphuis, Pierre A.J. Robe, and Elly M. Hol. 2017. "GFAPδ/GFAPα Ratio Directs Astrocytoma Gene Expression towards a More Malignant Profile." *Oncotarget* 8 (50): 88104–21. https://doi.org/10.18632/oncotarget.21540.

Stupp, Roger, Ricardo J. Komotar, Marc L. Otten, Gaetan Moise, and E. Sander Connolly. 2005. "Radiotherapy plus Concomitant and Adjuvant Temozolomide for Glioblastoma—A Critical Review." *The New England Journal of Medicine* 2: 421–22. https://doi.org/10.4137/cmo.s390.

Swift, Joe, Irena L. Ivanovska, Amnon Buxboim, Takamasa Harada, P. C.Dave P. Dingal, Joel Pinter, J. David Pajerowski, et al. 2013. "Nuclear Lamin-A Scales with Tissue Stiffness and Enhances Matrix-Directed Differentiation." *Science* 341 (6149). https://doi.org/10.1126/science.1240104.

Thomsen, Rune, Tina F. Daugaard, Ida E. Holm, and Anders Lade Nielsen. 2013. "Alternative MRNA Splicing from the Glial Fibrillary Acidic Protein (GFAP) Gene Generates Isoforms with Distinct Subcellular MRNA Localization Patterns in Astrocytes." *PLoS ONE* 8 (8). https://doi.org/10.1371/journal.pone.0072110.

Toda, Masahiro, Masayuki Miura, Hiroaki Asou, Ichiro Sugiyama, Takeshi Kawase, and Keiichi Uyemura. 1999. "Suppression of Glial Tumor Growth by Expression of Glial Fibrillary Acidic Protein." *Neurochemical Research* 24 (2): 339–43. https://doi.org/10.1023/A:1022538810581.

Toivola, D. M., P. Strnad, A. Habtezion, and M. B. Omary. 2010. "Intermediate Filaments Take the Heat as Stress Proteins." *Trends in Cell Biology* 20 (2): 79–91. https://doi.org/10.1016/j.tcb.2009.11.004.

Tsai, Jin Wu, K. Helen Bremner, and Richard B. Vallee. 2007. "Dual Subcellular Roles for LIS1 and Dynein in Radial Neuronal Migration in Live Brain Tissue." *Nature Neuroscience* 10 (8): 970–79. https://doi.org/10.1038/nn1934.

Turajlic, Samra, Andrea Sottoriva, Trevor Graham, and Charles Swanton. 2019. "Resolving Genetic Heterogeneity in Cancer." *Nature Reviews Genetics* 20 (7): 404–16. https://doi.org/10.1038/s41576-019-0114-6.

Uyeda, C. T., L. F. Eng, and A. Bignami. 1972. "Immunological Study of the Glial Fibrillary Acidic Protein." *Brain Research* 37 (1): 81–89. https://doi.org/10.1016/0006-8993(72)90347-2.

Venkataramani, Varun, Dimitar Ivanov Tanev, Thomas Kuner, Wolfgang Wick, and Frank Winkler. 2020. "Synaptic Input to Brain Tumors: Clinical Implications." *Neuro-Oncology*, no. July: 1–11. https://doi.org/10.1093/neuonc/noaa158.

Venkataramani, Varun, Dimitar Ivanov Tanev, Christopher Strahle, Alexander Studier-Fischer, Laura Fankhauser, Tobias Kessler, Christoph Körber, et al. 2019. "Glutamatergic Synaptic Input to Glioma Cells Drives Brain Tumour Progression." *Nature* 573 (7775): 532–38. https://doi.org/10.1038/s41586-019-1564-x.

Venkatesh, Humsa S., Wade Morishita, Anna C. Geraghty, Dana Silverbush, Shawn M. Gillespie, Marlene Arzt, Lydia T. Tam, et al. 2019. "Electrical and Synaptic Integration of Glioma into Neural Circuits." *Nature* 573 (7775): 539–45. https://doi.org/10.1038/s41586-019-1563-y.

Venkatesh, Humsa S., Lydia T. Tam, Pamelyn J. Woo, James Lennon, Surya Nagaraja, Shawn M. Gillespie, Jing Ni, et al. 2017. "Targeting Neuronal Activity-Regulated Neuroligin-3 Dependency in High-Grade Glioma." *Nature*. https://doi.org/10.1038/nature24014.

Venteicher, Andrew S., Itay Tirosh, Christine Hebert, Keren Yizhak, Cyril Neftel, Mariella G. Filbin, Volker Hovestadt, et al. 2017. "Decoupling Genetics, Lineages, and Microenvironment in IDH-Mutant Gliomas by Single-Cell RNA-Seq." *Science* 355 (6332): eaai8478. https://doi.org/10.1126/science.aai8478.

Verhaak, Roel G.W., Katherine A. Hoadley, Elizabeth Purdom, Victoria Wang, Yuan Qi, Matthew D. Wilkerson, C. Ryan Miller, et al. 2010. "Integrated Genomic Analysis Identifies Clinically Relevant Subtypes of Glioblastoma Characterized by Abnormalities in PDGFRA, IDH1, EGFR, and NF1."

Cancer Cell 17 (1): 98–110. https://doi.org/10.1016/j.ccr.2009.12.020.

Wang, E., J. G. Cairncross, and R. K.H. Liem. 1984. "Identification of Glial Filament Protein and Vimentin in the Same Intermediate Filament System in Human Glioma Cells." *Proceedings of the National Academy of Sciences of the United States of America* 81 (7 I): 2102–6. https://doi.org/10.1073/pnas.81.7.2102.

Wang, Jiguang, Emanuela Cazzato, Erik Ladewig, Veronique Frattini, Daniel I.S. Rosenbloom, Sakellarios Zairis, Francesco Abate, et al. 2016. "Clonal Evolution of Glioblastoma under Therapy." *Nature Genetics* 48 (7): 768–76. https://doi.org/10.1038/ng.3590.

Wang, Qianghu, Baoli Hu, Xin Hu, Hoon Kim, Massimo Squatrito, Lisa Scarpace, Ana C. deCarvalho, et al. 2017. "Tumor Evolution of Glioma-Intrinsic Gene Expression Subtypes Associates with Immunological Changes in the Microenvironment." *Cancer Cell* 32 (1): 42-56.e6. https://doi.org/10.1016/j.ccell.2017.06.003.

Watkins, Stacey, Stefanie Robel, Ian F. Kimbrough, Stephanie M. Robert, Graham Ellis-Davies, and Harald Sontheimer. 2014. "Disruption of Astrocyte-Vascular Coupling and the Blood-Brain Barrier by Invading Glioma Cells." *Nature Communications* 5 (May): 1–15. https://doi.org/10.1038/ncomms5196.

Weinstein, D. E., M. L. Shelanski, and R. K.H. Liem. 1991a. "Suppression by Antisense MRNA Demonstrates a Requirement for the Glial Fibrillary Acidic Protein in the Formation of Stable Astrocytic Processes in Response to Neurons." *Journal of Cell Biology* 112 (6): 1205–13. https://doi.org/10.1083/jcb.112.6.1205.

Wesseling, P., and D. Capper. 2018. "WHO 2016 Classification of Gliomas." *Neuropathology and Applied Neurobiology* 44 (2): 139–50. https://doi.org/10.1111/nan.12432.

Wilhelmsson, Ulrika, Camilla Eliasson, Rolf Bjerkvig, and Milos Pekny. 2003. "Loss of GFAP Expression in High-Grade Astrocytomas Does Not Contribute to Tumor Development or Progression." *Oncogene* 22 (22): 3407–11. https://doi.org/10.1038/sj.onc.1206372.

Xie, Ruifan, Tobias Kessler, Julia Grosch, Wolfgang Wick, and Frank Winkler. 2020. "Tumor Cell Network Integration in Glioma Represents a Stemness Feature." *The Journals of Gerontology Series A: Biological Sciences and Medical Sciences* 0813 (April): 1–11.

Yamada, Kenneth M., and Michael Sixt. 2019. "Mechanisms of 3D Cell Migration." *Nature Reviews Molecular Cell Biology*, no. Box 1. https://doi.org/10.1038/s41580-019-0172-9.

Zagzag, David, Ramin Amirnovin, M. Alba Greco, Herman Yee, Jocelyn Holash, Stanley J. Wiegand, Stephanie Zabski, George D. Yancopoulos, and Martin Grumet. 2000. "Vascular Apoptosis and Involution in Gliomas Precede Neovascularization: A Novel Concept for Glioma Growth and Angiogenesis." *Laboratory Investigation* 80 (6): 837–49. https://doi.org/10.1038/labinvest.3780088.

Zhang, Zhiqun, J. Susie Zoltewicz, Stefania Mondello, Kimberly J. Newsom, Zhihui Yang, Boxuan Yang, Firas Kobeissy, et al. 2014. "Human Traumatic Brain Injury Induces Autoantibody Response against Glial Fibrillary Acidic Protein and Its Breakdown Products." *PLoS ONE* 9 (3): 1–16. https://doi.org/10.1371/journal.pone.0092698.


1

CHAPTER 1

GFAP alternative splicing regulates glioma cell-ECM interaction in a DUSP4 dependent manner

Emma J. van Bodegraven[1], Jessy V. van Asperen[1], Jacqueline A. Sluijs[1], Coen B. J. van Deursen[1], Miriam E. van Strien[1], Oscar M.J.A. Stassen[2,3], Pierre A.J.T. Robe[4†], Elly M. Hol[1†]

[1] Department of Translational Neurosciences, UMC Utrecht Brain Center, University Medical Center Utrecht, Utrecht University, 3584 CG Utrecht, The Netherlands
[2] Faculty of Science and Engineering, Biosciences, Åbo Akademi University, Turku, Finland
[3] Centre for Biotechnology, Åbo Akademi University and University of Turku, Turku, Finland
[4] Department of Neurology and Neurosurgery, University Medical Center Utrecht Brain Center, Utrecht University, 3584 CG Utrecht, The Netherlands

[†]These authors jointly supervised this work

FASEB J. 2019 Nov; 33(11):12941-12959.
doi: 10.1096/fj.201900916R

Abstract

Gliomas are the most common primary brain tumours. Their highly invasive character and the heterogeneity of active oncogenic pathways within single tumours complicate the development of curative therapies and cause poor patient prognosis. Glioma cells express the intermediate filament protein glial fibrillary acidic protein (GFAP), and the level of its alternative splice variant *GFAPδ*, relative to its canonical splice variant *GFAPa*, is higher in grade IV compared to lower grade and lower malignant glioma. In this study we show that a high GFAPδ/α ratio induces the expression of the dual specificity phosphatase 4 (DUSP4) in focal adhesions. By focussing on pathways up- and down-stream of DUSP4 that are involved in the cell-extracellular matrix interaction we show that a high GFAPδ/α ratio equips glioma cells to better invade the brain. This study supports the hypothesis that glioma cells with a high GFAPδ/α ratio are highly invasive and more malignant cells, thus making GFAP alternative splicing a potential therapeutic target.

Introduction

Tumours of glial cells, called glioma, form a heterogenous group of primary brain tumours. Glioblastoma multiforme (GBM), also known as glioma or astrocytoma grade IV, is the most common and most malignant form of glioma with a very poor prognosis for patients (Ho et al., 2014). Currently, despite resection surgery, radio-, and chemotherapy, the median survival time after diagnosis is between 4 and 20 months (Ho et al., 2014). The highly invasive nature and intra-tumour heterogeneity are key factors in the poor response to treatment (Claes et al., 2007; Patel et al., 2014). Invasive tumour cells migrate away from the tumour core, evade treatment, and initiate recurrence (Claes et al., 2007). Due to the heterogeneity and the compensatory oncogenic signalling activity, most single molecule targeting therapies so far have failed in clinical trials (Pearson and Regad, 2017). To improve treatment strategies, more knowledge on how tumour cells integrate signalling information and interact with their cellular and proteinaceous environment is essential.

A central player in the integration of intra- and extracellular signals is the cell's cytoskeleton that consists of actin, microtubules, and intermediate filament (IF) proteins (Coulombe and Wong, 2004). In tumour diagnostics, IF proteins are valuable markers as they help to identify tumour subtypes, due to their cell- and tissue-specific expression (Velasco et al., 1980). Recently, the functional role of IF network dynamics in regulating tumour malignancy has gained more attention. Up- or downregulation of different IF proteins changes the composition of the network and alters the malignant behaviour of tumour cells (Cheung et al., 2013; Havel et al., 2015; Ivaska et al., 2007;

Mendez et al., 2010; Moeton et al., 2016, 2014; Sankar et al., 2013; Stassen et al., 2017; Thiery et al., 2009; Virtakoivu et al., 2015). For example, vimentin regulates cellular changes that characterise the epithelial to mesenchymal transition (Mendez et al., 2010) and keratin 14 plays a pivotal role in breast cancer cell invasion (Cheung et al., 2013).

The IF network in astrocytoma is composed of GFAP, vimentin, synemin, and nestin. Changes in the expression of individual IF proteins, post-translational protein modifications, and mechanisms of alternative splicing create IF protein diversity and modulate the composition and function of the network (Godsel et al., 2008; Perng et al., 2008; Snider and Omary, 2014). Alternative splicing of GFAP largely contributes to IF protein diversity as at least 10 different splice-isoforms are known to be expressed in the central and peripheral nervous system (Clairembault et al., 2014; Middeldorp and Hol, 2011). The canonical GFAPα isoform is widely expressed in mature astrocytes of the healthy brain and in glioma of astrocytic origin. In addition, the alternative splice variant GFAPδ that is specifically expressed in subventricular neurogenic astrocytes (Roelofs et al., 2005; van den Berge et al., 2010), cells that have the capacity to convert into glioma (Jiang et al., 2017; Lee et al., 2018), was found to be expressed in glioma (Brehar et al., 2014; Choi et al., 2009; Stassen et al., 2017). We have shown that GFAPδ overexpression at high levels leads to IF aggregation and a collapse of the entire IF network of glioma cells, but when expressed at lower endogenous levels, GFAPδ can incorporate into the network and modulate interactions with cytoplasmic proteins, such as αB-crystallin (Perng et al., 2008; Roelofs et al., 2005)

In grade IV astrocytoma, higher levels of *GFAPδ* relative to *GFAPa* are expressed compared to low grade (grade II and III) astrocytoma (Stassen et al., 2017). In our previous studies we have shown that mimicking this increase in the GFAPδ/α ratio *in vitro* changes glioma malignant cell behaviour that mostly involves a changed interaction of the cell with its extracellular environment (Moeton et al., 2016, 2014; Stassen et al., 2017). Moreover, the comparison of patient and *in vitro* genome-wide transcriptional data shows that a high GFAPδ/α ratio directs astrocytoma gene expression to a more malignant profile making GFAP alternative splicing a potential therapeutic target that needs further exploration (Stassen et al., 2017). In this study we further investigate how a high GFAPδ/α ratio contributes to a more malignant glioma phenotype.

One of the strongest responders to an increased GFAPδ/α ratio *in vitro*, is the dual-specificity phosphatase 4 (DUSP4) (Stassen et al., 2017). In glioma of patients, *DUSP4* expression correlates to the GFAPδ/α ratio, and high expression is associated with a worse prognosis (Stassen et al., 2017). DUSP4, also known as Mitogen-Activated Protein Kinase Phosphatase 2 (MKP-2), is a nuclear phosphatase that mainly targets phosphoserine/threonine and phosphotyrosine residues of mitogen-activated protein kinases (MAPK) signalling pathway players. The MAPK-signalling pathway is an

integrator of extra- and intracellular signalling and regulates various tumour malignancy related processes. Mutations in MAPK pathway players (Brennan et al., 2013; Cancer Genome Atlas Research Network, 2008; Ciriello et al., 2013; Jeuken et al., 2007; Pandey et al., 2016) and constitutive activation of the DUSP4-targets extracellular signal-regulated kinase (ERK) and c-Jun N-terminal kinase (JNK) (Antonyak et al., 2002; Bhaskara et al., 2005; Li et al., 2008; Lopez-Gines et al., 2008; Pandey et al., 2016; Tsuiki et al., 2003) are frequent in glioma. DUSP4 activity affects cell migration (Lin et al., 2017), invasion (Lin et al., 2017; Zhang et al., 2017), proliferation (Lawan et al., 2011; Zhang et al., 2017), extracellular matrix (ECM) degradation (Paumelle et al., 2000), and (chemotherapy-induced) cytotoxicity (Al-Mutairi et al., 2010; Balko et al., 2012; Barajas-Espinosa et al., 2015; Cadalbert et al., 2005; Lawan et al., 2011; Schmid et al., 2015; Watson et al., 2007).

The current study focuses on DUSP4 regulation by the GFAPδ/α ratio and DUSP4 up- and downstream pathways that are involved in the cell's interaction with its extracellular environment. We used CRISPR/Cas9 technology to direct GFAP alternative splicing and provide evidence for a GFAPδ/α ratio-induced change in the cell's interaction with the ECM, which is associated with a more malignant phenotype and is dependent on, and possibly enhanced by, the expression of DUSP4.

Results

The GFAPδ/α ratio modulates DUSP4 expression levels in glioma cells

First, we confirmed our earlier obtained microarray data in which we found significant alterations in *DUSP4* gene expression upon modulation of the GFAPδ/α ratio (Stassen et al., 2017). We determined *DUSP4* expression levels by qPCR analysis in GFAP modulated U251 malignant glioma (U251-MG) cell models (for cell line characterization see Stassen *et al.*, 2017). In accordance with our previous findings, we found that *DUSP4* expression was significantly increased in GFAPα knockdown cells (GFAPα^{-}) compared to non-targeted control (NTC) or all GFAP isoform knockdown (panGFAP^{-}) cells (Fig. 1a). In these GFAPα^{-} cells, GFAPα is specifically knocked down which results in an increase in the GFAPδ/α ratio. In an alternative approach to change the GFAPδ/α ratio by recombinant expression of GFAPδ or GFAPα, *DUSP4* expression did not differ from control cells (Fig. 1b). These results indicate that *DUSP4* expression most prominently responds to a GFAPα induced increase in the GFAPδ/α ratio. This is supported by a significant positive correlation, determined by linear regression analysis within GFAPα^{-}, panGFAP^{-}, and NTC cells, of *DUSP4* to the GFAPδ/α ratio (Fig. 1c) but not to *pan GFAP* levels (Fig. 1d).

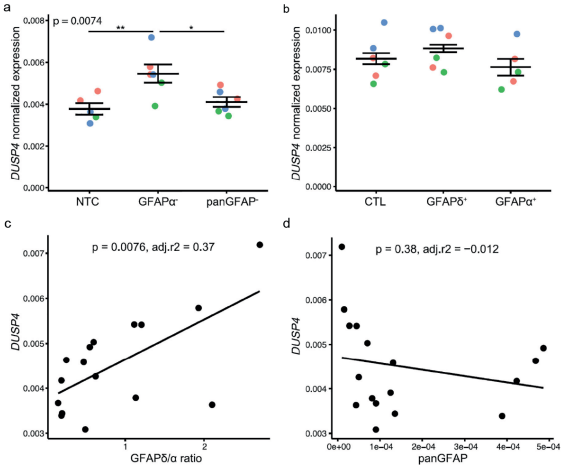

Figure 1. GFAP modulation in glioma cells regulates DUSP4 expression. DUSP4 expression levels normalized to reference genes in GFAP modulated U251-MG glioma cells determined by qPCR analysis. (a) GFAPα knockdown cells (GFAPα^{-}) and all GFAP isoform knockdown cells (panGFAP^{-}) were generated using shRNA targeting a GFAPα specific sequence or a sequence present in all GFAP isoforms, respectively. Non-targeting shRNA was used as a control (NTC) (n = 3, colours indicate experimental duplicates). The p-value results from a one-way ANOVA. (b) Overexpression lines were generated by recombinant expression of GFAPδ (GFAPδ^{+}) and GFAPα (GFAPα^{+}). GFAPδ^{+} and GFAPα^{+} cells expressed mCherry and GFP, respectively. Control cells expressed mCherry (CTL) (n = 3, colours indicate experimental duplicates). (c,d) Linear regression analysis for the correlation between DUSP4 and GFAPδ/α ratio (c) and pan GFAP (d) in shRNA GFAP modulated glioma cell lines (NTC, panGFAP^{-} and GFAPα^{-}). p < 0.05 *, p < 0.01 **, p < 0.001 ***, p < 0.0001 ****, p < 1.e-05 *****.

Steering GFAP splicing using CRISPR Cas9 leads to controlled GFAPδ/α ratios.

We generated clonal cell lines with a low, intermediate, and high GFAPδ/α ratio by deleting the *GFAPδ* specific exon 7a (Fig. 2a) or the *GFAPa* specific exons 8 and 9 (Fig. 2b). Using two guide RNAs (gRNAs) surrounding exon 7a or exon 8 and 9, Cas9 generated cuts that led to the deletion of the DNA region encoding these regions. To generate clonal cell lines, targeted cells were single cell sorted using Fluorescence Activated Cell sorting (FACS). Two control clonal cell lines were generated by transfection of a Cas9 construct without targeting guide RNAs (ctl 1 and ctl 2). Two GFAPδ knockout (GFAPδ-KO 1, GFAPδ-KO 2) and two GFAPα knockout (GFAPα-KO 1, GFAPα-KO 2) clonal lines were selected for further characterization. Fig. 2c and d show that the expected DNA regions were deleted which indicated that GFAPδ-KO lines consisted of a homozygous deletion of exon 7a, and GFAPα-KO lines of a heterozygous deletion of exon 8 and 9. Fig. 2e shows that deletion of exon 7a (GFAPδ-KO) led to a significant decrease in *GFAPδ* mRNA levels compared to control (ctl) and GFAPα-KO cell lines. *GFAPδ* mRNA was mostly undetectable in GFAPδ-KO cells after 40 PCR cycles. Deletion of exon 8 and 9 (GFAPα-KO) significantly decreased

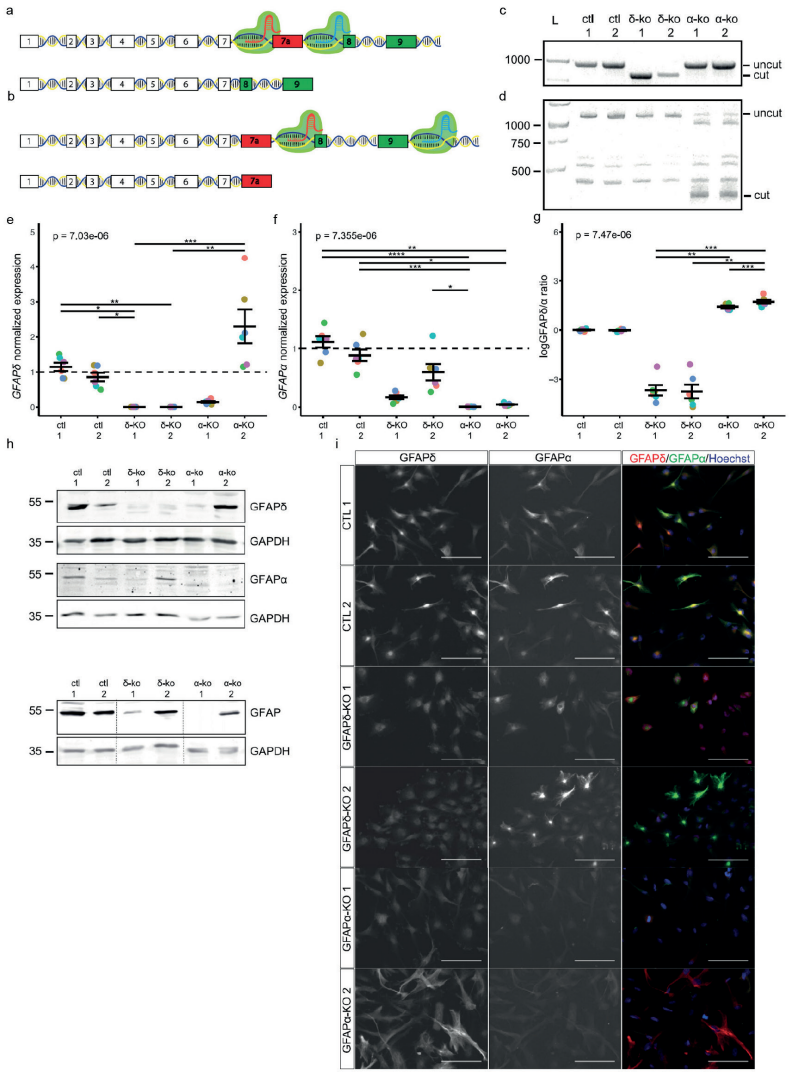

Figure 2. Clonal glioma cell lines with different level of the GFAPδ/α ratio generated with CRISPR Cas9 technology. (a,b) Illustration of GFAP DNA with the Cas9 targeted locations to generate GFAP isoform knockouts. To generate a GFAPδ knockout cell line (GFAPδ-KO), two guide RNAs were designed (Supp. Table 1) targeting the intronic regions surrounding the GFAPδ specific exon 7a resulting in a deletion of exon 7a in the GFAP gene (a). GFAPα-KO cell lines were generated in the same way with two guide RNAs designed to guide Cas9 to intronic regions just outside exon 8 and exon 9 (b). After Cas9 targeting of the above described regions, clonal cell lines were generated by single cell FACS sorting and selection of clones. Two control, two GFAPδ-KO and two GFAPα-KO cell lines were selected for further characterization. (c,d) Gel electrophoresis images of PCR products generated using primers up- and downstream of the targeted area. PCR amplification of DNA of GFAPδ-KO cells using primers up- and downstream exon 7a results in a 140 bp shorter fragment compared to ctl and GFAPα-KO cells. This fragment corresponds to the size that was expected to be deleted. Thus, GFAPδ-KO cells consist of a homozygous deletion of exon 7a (c). PCR amplification of DNA of GFAPα-KO cells using primers up-

GFAPa mRNA levels compared to ctl and GFAPδ-KO cells (Fig. 2f). In addition, clonal differences were observed between GFAPα-KO lines and GFAPδ-KO lines. GFAPα-KO 1 cells showed a clear trend for decreased *GFAPδ* expression, whereas *GFAPa* levels in GFAPα-KO 2 cells showed a trend for a compensatory increased *GFAPδ* expression. Similarly, a trend for decreased *GFAPa* levels was seen in GFAPδ-KO 1 cells whereas in GFAPδ-KO 2 cells *GFAPa* levels were comparable to ctl cells. These changes in *GFAP* isoform expression levels led to strong differences in the GFAPδ/α ratio between cell lines (Fig. 2g). Table 1 shows the wide range of the GFAPδ/α ratio that was created using this method. A significant downregulation of *pan GFAP* levels was only observed in GFAPδ-KO 1 and GFAPα-KO 1 lines due to the compensatory downregulation of *GFAPa* and the lack of *GFAPδ* upregulation (Supp. Fig. 1a), respectively.

Western blot analysis showed that GFAP isoform protein expression was similarly affected by the genetic modifications as mRNA expression levels were (Fig. 2h). The compensatory down-regulation of GFAPα in GFAPδ-KO 1 cells and up-regulation of GFAPδ in GFAPα-KO 2 cells and the effect on pan GFAP levels is shown at protein level as well (see Supp. Fig. 1b for the complete blot). Differences were present in both the soluble and insoluble protein pool (Supp. Fig. 1c,d). Furthermore, the GFAP protein expression alterations led to changes in the GFAP network composition (Fig. 2i). There was decreased GFAPδ incorporation in the network of GFAPδ-KO cells with more GFAPα present in GFAPδ-KO 2 cells. Similarly, GFAPα network incorporation was decreased in GFAPα-KO cells with increased GFAPδ in GFAPα-KO 2 cells and decreased in GFAPα-KO 1 cells. Clear filamentous structures of IF assembly incompetent GFAPδ were observed in GFAPα-KO 2 cells, explained by the presence of IF assembly competent vimentin (Supp. Fig. 1e). These results indicate that we successfully generated cell lines with different levels of the GFAPδ/α ratio using CRISPR Cas9 that consist of a different GFAP network.

and downstream of exon 8 and 9 results in the amplification of both an 884 shorter fragment compared to ctl and GFAPδ-KO cells and a 1273 bp long fragment similar to ctl and GFAPδ-KO cells. The short fragment corresponds to the size that was expected to be deleted. The long fragment is a product of DNA that includes exon 8 and 9. This indicates that GFAPα-KO cells consist of a heterozygous deletion of exon 8 and 9 (d). E, F, G qPCR analysis of ctl, GFAPδ-KO (δ-KO) and GFAPα-KO (α-KO) clonal cell lines (n = 6). Expression values for each gene were normalized to reference gene expression values. Each dot shows the expression value after normalization to the average of the ctl cell lines (ctl 1, ctl 2). Colours represent each individual experiment. GFAPδ (e) GFAPα (f) and the GFAPδ/α ratio (here shown as log 10 of normalized expression values) (g) were significantly different between clonal cell lines. The p-values all result from Kruskal-Wallis tests. (h) Western blot analysis of proteins isolated from whole lysates of ctl, GFAPδ-KO and GFAPα-KO clonal cell lines. Blots were stained with antibodies specific for GFAPδ and GFAPα (left panel), a pan GFAP antibody (right panel) and GAPDH as a loading control. (i) Immunostainings of clonal cell lines for GFAPδ (left), GFAPα (middle) and Hoechst to counterstain the nuclei. The right panel shows the overlay of images. Scale bar = 100 μm. $p < 0.05$ *, $p < 0.01$ **, $p < 0.001$ ***, $p < 0.0001$ ****, $p < 1.e\text{-}05$ *****

Table 1. Primers used for quantitative PCR

Clonal cell line	GFAPδ/α ratio* *(average)*	SEM
GFAPδ-KO 1	8.8e-05	9.77e-04
GFAPδ-KO 2	1.13e-04	1.30e-03
ctl 2	0.11	1.55e-02
ctl 1	0.12	2.84e-02
GFAPα-KO 1	3.18	0.98
GFAPα-KO 2	5.55	1.18

*calculated from normalized expression levels of GFAPδ and GFAPα to reference genes, SEM = standard error of the mean

A high GFAPδ/α ratio induces DUSP4 expression, DUSP4 localization in focal adhesions, and a polarized cell morphology

DUSP4 mRNA expression was strongly increased in cells with high GFAPδ/α ratio levels (Fig. 3a). Compared to ctl cells, *DUSP4* expression showed a 10.9- and 7.7-fold increase in GFAPα-KO 1 and GFAPα-KO 2 lines, respectively. Linear regression analysis showed that within all cell lines, *DUSP4* expression levels strongly correlated to the GFAPδ/α ratio whereas the correlation to *pan GFAP* levels was not significant (Fig. 3b,c). Interestingly, DUSP4 protein expression in GFAPα-KO cells was specifically induced in focal adhesions of these cells, instead of the expected increase in the nucleus of this nuclear phosphatase (Fig. 3d,e). This coincided with an overall increase in DUSP4 protein levels in GFAPα-KO cells, although steady state levels of DUSP4 were low in our cell lines, and treatment with a proteasome inhibitor epoxomicin was needed to prevent DUSP4 degradation and visualize DUSP4 on western blot (Supp. Fig. 1d,e). The DUSP4 increase in focal adhesions was accompanied with cell polarization and clear visible actin stress fibres shown as long filamentous bundles connecting focal adhesions on one end of the cells the other end (Fig. 3d, two right images) which were less pronounced in ctl and GFAPδ-KO cells (Fig. 3d, left images). Fig. 3e shows DUSP4 protein localization in GFAPα-KO cells actin-rich focal adhesions that sometimes extended beyond labelled actin (Fig. 3e, left image). DUSP4 protein in ctl and GFAPδ-KO cells rarely localized to focal adhesions and was present at very low levels (Fig. 3d, left images). A clear difference in morphology to GFAPα-KO cells was observed as GFAPδ-KO cell morphology was flat and polyhedral (Fig. 3d, lower left images). Ctl cells consisted of a morphology intermediate to the polarized and spindle shaped GFAPα-KO cells and the flat polyhedral GFAPδ-KO cells (Fig. 3d, upper left images).

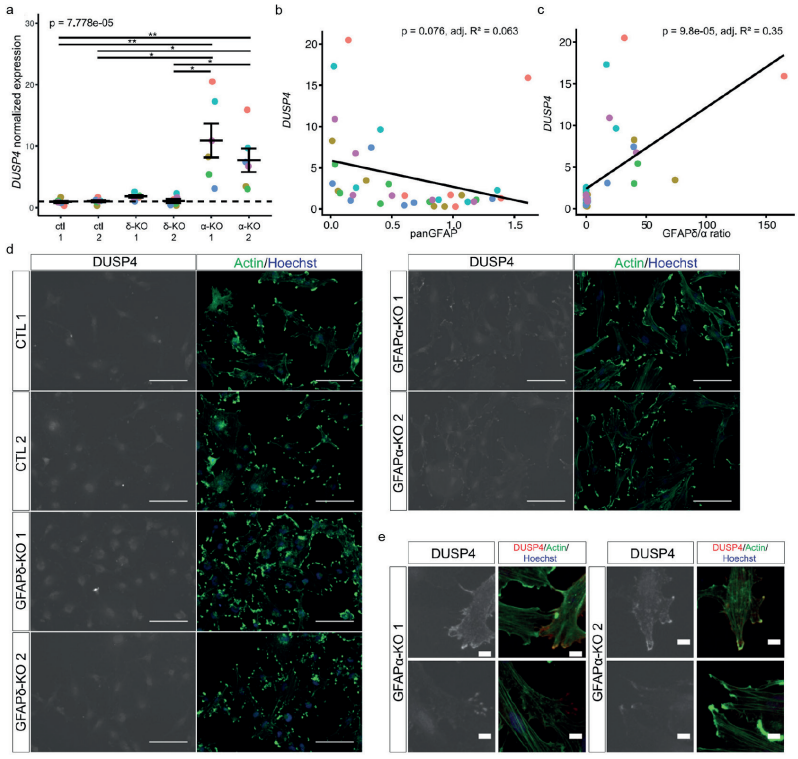

Figure 3. DUSP4 expression levels in GFAP modulated glioma clonal cell lines. (a) DUSP4 mRNA expression levels in ctl, GFAPδ-KO (δ-KO) and GFAPα-KO (α-KO) clonal cell lines (n = 6). Expression values for each gene were normalized to reference gene expression values. Each dot shows the expression value after normalization to the average of the ctl cell lines (ctl 1, ctl 2). Colours represent an individual experiment. DUSP4 expression is significantly increased in GFAPα-KO cells. The p-value results from a Kruskal-Wallis test. (b,c) Linear regression analysis for the correlation between pan GFAP and DUSP4 (b) and the GFAPδ/α ratio and DUSP4 (c) within ctl, GFAPδ-KO and GFAPα-KO clonal cell lines. DUSP4 and pan GFAP did not significantly fit a linear model. The GFAPδ/α ratio and DUSP4 levels show a significant positive correlation within the clonal cell lines. Colours represent an individual experiment and correspond to colours in (a). (d) Co-immunostainings of ctl, GFAPδ-KO and GFAPα-KO cells for DUSP4 (left) and phalloidin that labels the actin cytoskeleton and visualizes cell morphology (right) (scale bar = 100 μm). (e) Co-localization of DUSP4 and actin in focal adhesions of GFAPα-KO cells (scale bar = 5 μm). $p < 0.05$ *, $p < 0.01$ **, $p < 0.001$ ***, $p < 0.0001$ ****, $p <$ 1.e-05 *****

A high GFAPδ/α ratio increases the level of DUSP4 target pJNK

The main targets of DUSP4 phosphatase activity are the MAPK-pathway players phosphorylated ERK and phosphorylated JNK (pJNK). Western blot analysis of protein isolated from ctl, GFAPδ-KO cells and GFAPα-KO cells shows that only general levels of ERK were affected by GFAP isoform modulation (data not shown), but that pJNK levels were significantly different between our cell lines with increased levels in GFAPα-KO cells (Fig. 4).

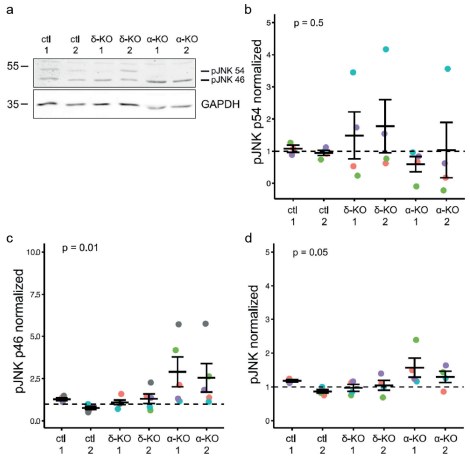

Figure 4. Western blot analysis of the DUSP4 target pJNK. Western blot analysis of proteins isolated from ctl, GFAPδ-KO and GFAPα-KO whole cell lysates. (a) Western blot stained for phosphorylated JNK (pJNK) and GAPDH as a loading control. (b-d) Quantification of pJNK 54 kDa bands (pJNK n = 4), pJNK 46 kDa bands (pJNK n = 5) and average pJNK (n = 4) from western blots stained for pJNK. pJNK 46 kDa expression was always higher. Bands were normalized to GAPDH. Each dot in the graph represents an individual experiment and all values are normalized to the average of the ctl lines (ctl 1, ctl 2) per experiment. P-values of Kruskal-Wallis tests are shown in each graph.

The GFAPδ/α ratio regulates laminin-111 expression, secretion, expression of its integrin receptors, and downstream effectors

We then continued to analyse upstream regulators of the MAPK-signalling pathway that have been linked to tumour cell malignant behaviour and regulate the cell's interaction with the ECM (Campos et al., 2004; Givant-Horwitz et al., 2004; Hynes, 2002; Mruthyunjaya et al., 2010; Reich et al., 1995; Turck et al., 2006; Vehlow et al., 2017; Velpula et al., 2012; Vial et al., 2003), and previously shown to be regulated by changes in the GFAP network (Moeton et al., 2014; Stassen et al., 2017): laminin-111 and its integrin receptors. *LAMA1*, that encodes the laminin α1 chain, forms the ECM molecule laminin-111 together with the β1 and γ1 chain of laminin (Fig. 5a). In agreement with our previous studies (Moeton et al., 2014; Stassen et al., 2017), *LAMA1* was significantly increased in cells with a high GFAPδ/α ratio (Fig. 5b). Compared to ctl and GFAPδ-KO cells, a strong increase in mRNA expression of 15,000-fold on average was observed in GFAPα-KO cells (Fig. 5b). Cell-derived extracellular matrices were generated of both the shRNA modulated cell lines and the ctl 1, GFAPδ-KO 2 and GFAPα-KO 2 clonal cells and immunostaining for laminin was performed. This showed that an increase in the GFAPδ/α ratio induces laminin secretion and polymerization into the ECM generated by these cells as well (Fig. 5c and d). Interestingly, mRNA expression of *integrin β1* (*ITGB1*), *integrin a6* (*ITGA6*), and *a7* (*ITGA7*) (Fig. 5e), encoding laminin-111 receptor components, were significantly increased in cells with a high GFAPδ/α ratio as well (Fig. 5f-h). Previous experiments showed an effect of the GFAPδ/α ratio on a downstream effector of laminin-signalling activity, metalloproteinase 2 (MMP2) (Reich et al., 1995; Stassen et al., 2017). MMP2 is secreted by the cell, degrades the ECM, induces cell invasion (Gialeli et al., 2011; Nakagawa et al., 1996), and is associated with glioma malignancy (Ramachandran et al., 2017). Fig. 5i shows that *MMP2* is differentially expressed between our GFAP-modulated cell lines as well and was significantly increased in one of the GFAPα-KO clonal lines with a high GFAPδ/α ratio (Fig. 5i). In addition, in both of the GFAPα-KO clonal lines expression of

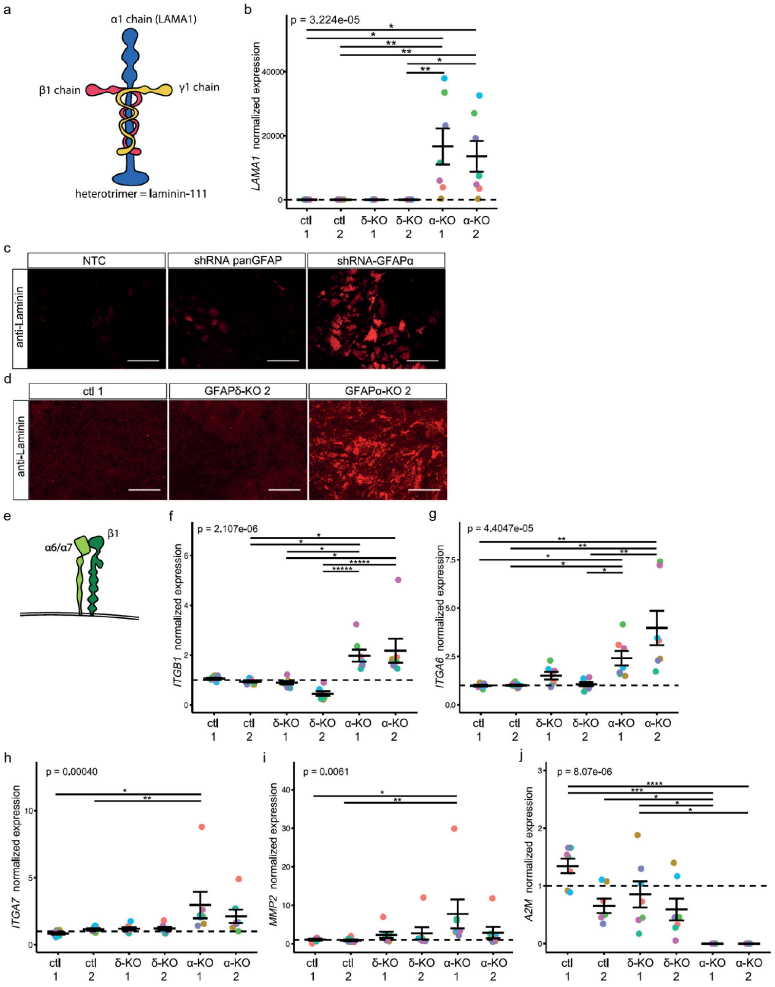

Figure 5. LAMA1 expression, laminin secretion and expression of laminin signalling components in GFAP modulated glioma cell lines. (a) Schematic overview of laminin-111. (b) mRNA expression level of LAMA1 in ctl, GFAPδ-KO and GFAPα-KO cell lines determined by qPCR analysis. Dots represent expression levels normalized to the average of ctl lines (ctl 1, ctl 2) for each experiment. Colours represent individual experiments (n = 7). The p-value results from a Kruskal-Wallis test. (c,d) Immunostaining for Laminin (red) of cell-derived matrices. Cell derived matrices were generated by NTC, panGFAP^{-}, or GFAPα^{-} shRNA modulated cells (c), and ctl 1, GFAPδ-KO 2, or GFAPα-KO 2 cell lines (d). Scale bar is 100 µm. E Schematic overview integrin-β1 that heterodimerizes with integrin-α6 or integrin-α7 and form a laminin-111 receptor. (f-h) mRNA expression levels of ITGB1 (f), ITGA6 (g), and ITGA7 (h) analysed by qPCR in ctl, GFAPδ-KO and GFAPα-KO cell lines. Dots represent expression levels normalized to the average of ctl lines (ctl 1, ctl 2) for each experiment. Colours represent individual experiments (n = 7). The expression of the receptor components was significantly different between cell lines. The p-values results from Kruskal-Wallis tests. (i) mRNA expression level of MMP2 in ctl, GFAPδ-KO and GFAPα-KO cell lines determined by qPCR analysis. Dots represent expression levels normalized to the average of ctl lines (ctl. 1, ctl 2) for each experiment. Colours represent individual experiments (n = 7). The p-value results from a Kruskal-Wallis test. (j) mRNA expression level of A2M in ctl, GFAPδ-KO and GFAPα-KO cell

lines determined by qPCR analysis. Dots represent expression levels normalized to the average of ctl lines (ctl 1, ctl 2) for each experiment. Colours represent individual experiments (n = 7). The p-value results from a Kruskal-Wallis test.p < 0.05 *, p < 0.01 **, p < 0.001 ***, p < 0.0001 ****, p < 1.e-05 *****

alpha-2-macroglobulin (*A2M*) that binds and inhibits the active form of MMP2 (Kim et al., 2018) was strongly decreased and expression was even mostly below detection (Fig. 5j).

A high GFAPδ/α ratio causes laminin-dependent cell adhesion

As laminin-111 expression, secretion, and receptor expression were increased in cells with a high GFAPδ/α ratio, we determined the strength of the interaction of the cells to laminin and non-laminin substrates in an adhesion assay. Fig. 6 shows that after both 2 and 24 hours of adherence, lower numbers of GFAPα-KO cells were adhered to glass and poly-D lysine (PDL), compared to ctl and GFAPδ-KO cells (Fig. 6a,b,d,e). In contrast, the same number of GFAPα-KO cells, with a trend for an increase, adhered to a laminin-coated surface both after 2 and 24 hours (Fig. 6c,f). This data suggests that cells with a high GFAPδ/α ratio depend on laminin within the ECM for strong surface adherence.

The expression of laminin signalling components is dependent on DUSP4

To determine how DUSP4 is involved in the laminin-111 signalling pathway, DUSP4 knockdown U251-MG cell lines were created using CRISPR/Cas9. Fig. 7a shows the expression of *DUSP4* in two different DUSP4 knockdown (DUSP4-KO) cell lines and a control clonal line (DUSP4-CTL). DUSP4-KO line 1 (DUSP4-KO 1) showed a stronger decrease of *DUSP4* mRNA analysed compared to DUSP4-KO cell line 2 (DUSP4-KO 2). To visualize DUSP4 at the protein level, cells were treated with epoxomicin to prevent DUSP4 degradation. Fig. 7b shows that the protein level reflects the observations at the mRNA level with a stronger knockdown of DUSP4 in DUSP4-KO line 1 compared to DUSP4-KO line 2. In the DUSP4-KO cells, a strong decrease to often undetectable levels of *LAMA1* mRNA was observed as well as a significant decrease of *ITGB1* mRNA (Fig. 7c,d). The expression of *ITGA6* did not decrease upon DUSP4 knockdown (Fig. 7e). However, *ITGA7* and *MMP2* expression showed a trend for decreased expression in DUSP4-KO cells compared to DUSP4-CTL cells as well (Fig. 7f,g) and the MMP2 inhibitor *A2M* was strongly increased (Fig. 7h). In addition, DUSP4-KO cells showed a flatter, polyhedral and more round morphology compared to DUSP4-CTL cells (Fig. 7i). These results show that DUSP4 depletion induced an opposite effect to what is observed in high GFAPδ/α ratio cells that express high DUSP4 levels. This suggests that the effect on cell-ECM interaction components seen in high GFAPδ/α ratio cells is dependent on DUSP4 expression.

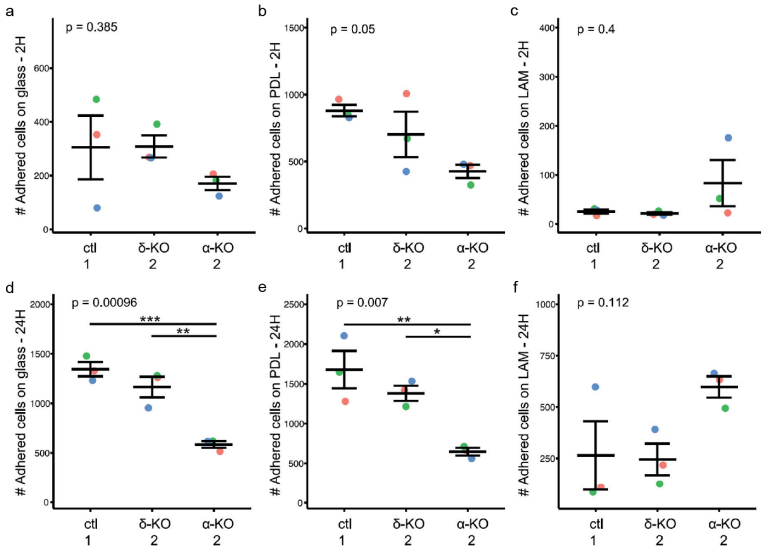

Figure 6. Adhesive capacity of GFAP modulated cells on different surfaces. Adhesive capacity of different cell lines determined in an adhesion assay. Cells were plated at a density of 50,000 cells per well of a 24 well plate and washed off after 2 and 24 hours. Hoechst positive nuclei were counted to determine the number of adhered cells. A, B, C The number of adhered ctl 1.2, GFAPδ-KO 7, and GFAPα-KO 3.3 cells after 2 hours on glass cover slips (a), poly-D lysine coated cover slips (b), and laminin-coated cover slips (c). The p-values in (a) and (b) result from one-way ANOVA tests and in (c) from a Kruskal-Wallis test. (d-f) The number of adhered ctl 1.2, GFAPδ-KO 7, and GFAPα-KO 3.3 cells after 24 hours on glass cover slips (a), poly-D lysine coated cover slips (b), and laminin-coated cover slips (c). The p-values in d-f result from one-way ANOVA tests. $p < 0.05$ *, $p < 0.01$ **, $p < 0.001$ ***, $p < 0.0001$ ****, $p <$ 1.e-05 *****

GFAP expression is dependent on DUSP4

Interestingly mRNA and protein expression of the different *GFAP* isoforms were significantly decreased upon a knockdown of DUSP4. *GFAPa* (Fig. 7j), *GFAPδ* (Fig. 7k), and *pan GFAP* (Fig. 7l) mRNA levels were significantly decreased in DUSP4-KO 1 cells. Decreased *GFAPa*, *GFAPδ*, and *pan GFAP* expression in DUSP4-KO 2 was less pronounced but significant for both *GFAPδ* and *pan GFAP* compared to the DUSP4-CTL cells. This corresponds to the intermediate DUSP4 expression levels in DUSP4-KO 2 compared to DUSP4-KO 1 and DUSP4-CTL cells. The GFAPδ/α ratio did not change in DUSP4-KO cells compared to DUSP4-CTL cells (data not shown). Protein expression of GFAPα, GFAPδ, and pan GFAP was also decreased upon knocking down DUSP4 (Fig. 7m), with the strongest downregulation of GFAP again in the DUSP4-KO 1 cells. GFAP isoform expression levels did not change upon overexpression of DUSP4 (data not shown). These results show that GFAP expression is dependent on DUSP4 as well.

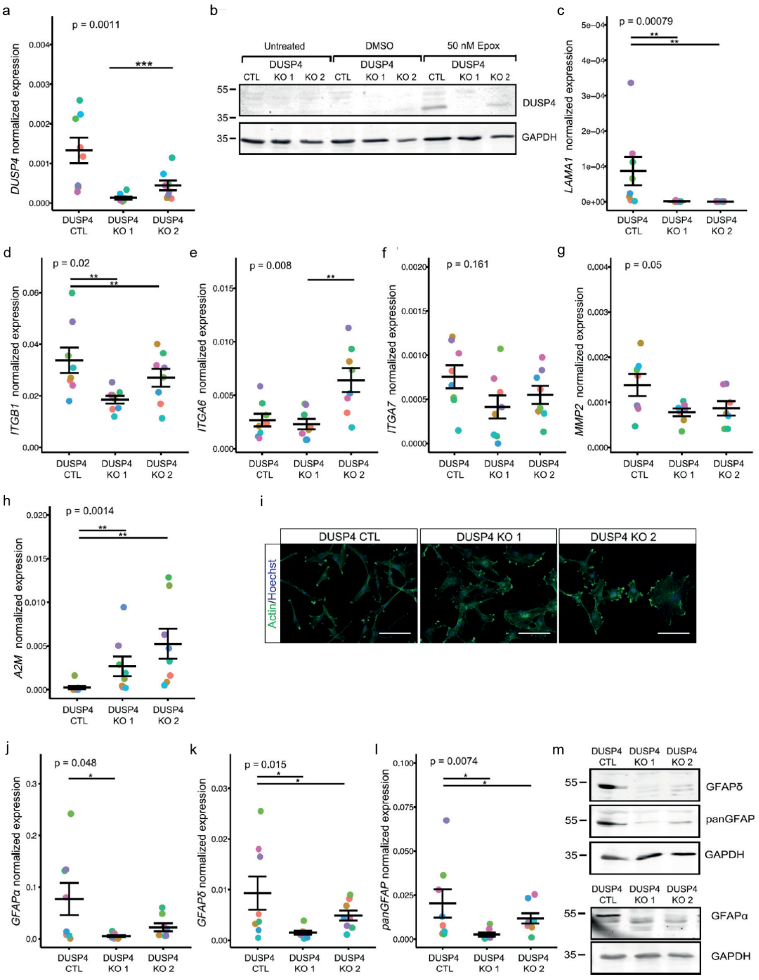

Figure 7. Expression of laminin signalling components and GFAP isoforms in DUSP4 knockdown cells. CRISPR Cas9 was used to generate DUSP4 knockdown cell lines (DUSP4-KO) from U251-MG glioma cells. (a) DUSP4 mRNA expression levels normalized to reference gene expression determined by qPCR. Colours represent individual experiments (n = 8). The p-value results from a Kruskal-Wallis test. (b) Western blot analysis for DUSP4 expression in untreated, DMSO-treated or 50 nM epoxomicin-treated DUSP4-KO and DUSP4-CTL cells. (c-h) mRNA expression levels of LAMA1, ITGB1, ITGA6, ITGA7, MMP2, and A2M in DUSP4-KO and ctl cells. Expression values were normalized to reference genes. Colours represent individual experiments (n = 8, MMP2 n = 7). The p-value results from Kruskal-Wallis test (c,e,g,h) or one-way ANOVA tests (d,f). I Phalloidin and Hoechst labelling of DUSP4-KO and DUSP4-CTL cells to visualize the cell morphology. (j-l) mRNA expression levels determined by qPCR of GFAPα (j), GFAPδ (k) and pan GFAP (l) for DUSP4-KO and DUSP4-CTL cells. Expression values were normalized to reference gene expression and colours represent individual experiments (n = 8). The p-values result from a Kruskal-Wallis tests. M Western blot analysis for GFAPδ, pan GFAP and GFAPα of DUSP4-KO and ctl cells. GAPDH protein levels were used as a loading control. $p < 0.05$ *, $p < 0.01$ **, $p < 0.001$ ***, $p < 0.0001$ ****, $p < 1.e\text{-}05$ *****

High DUSP4 levels correlate to a more malignant glioma subtype

We previously showed that *DUSP4* expression levels are increased in higher grade astrocytoma and are of prognostic value for astrocytoma grade III patients (World Health Organization classification of 2007 (WHO 2007)) (Stassen et al., 2017). Recently, a new classification system for glioma has been developed. This system includes both histological assessment and genetic information of the tumour. Therefore, we investigated the expression of *DUSP4* in the newly defined glioma subtypes (Fig. 8a). Increased *DUSP4* expression was observed in grade IV compared to most, but not all, low grade glioma subtypes (Fig. 8a). In addition, we assessed the prognostic value of *DUSP4* in the different glioma subtypes and found a strong trend for a worse survival probability and a worse progression free survival probability for patients with grade III glioma with an isocitrate dehydrogenase 1 (IDH1) mutation without a co-deletion of chromosomal arms 1q and 19p (IDHmut non-codel) and above median levels of *DUSP4* (Fig. 8b,c). This patient group mostly consists of the WHO 2007 defined grade III astrocytoma (Supplementary Table 4). Within all low grade IDHmut non-codel glioma patients, a trend for a worse survival probability ($p = 0.092$) and a significant worse progression free survival probability ($p = 0.0372$) for patients with above median *DUSP4* expression levels was found (data not shown).

Discussion

The high invasive character of malignant glioma and the heterogeneity of active oncogenic signalling pathways within single tumour cells cause an insufficient response to treatment, tumour recurrence and poor prognosis for glioma patients (Claes et al., 2007; Patel et al., 2014). In this study we show that a specific part of the cytoskeleton, the intermediate filament system, is involved in glioma malignancy. The cell's cytoskeleton plays a central role in the integration of extra- and intracellular signalling and is essential for cell invasion (Coulombe and Wong, 2004). Several studies show the involvement of the IF network in regulating the malignancy of different types of tumours including glioma (Cheung et al., 2013; Havel et al., 2015; Ivaska et al., 2007; Mendez et al., 2010; Moeton et al., 2016, 2014; Sankar et al., 2013; Stassen et al., 2017; Thiery et al., 2009; Virtakoivu et al., 2015). In the current study we provide more evidence that modulating the IF network, by changing the relative expression level of the GFAP alternative splice variant GFAPδ to the expression of the canonical splice variant GFAPα, contributes to glioma malignancy characteristics. We here show that increasing the GFAPδ/α ratio in glioma cells, as observed in grade IV compared to lower grade glioma (Stassen et al., 2017), changes the cell's interaction with the ECM in a DUSP4 dependent manner (Fig. 9). The observed molecular changes in high GFAPδ/α ratio cells provide them with the appropriate equipment to invade the brain and therefore contribute to a more malignant glioma phenotype.

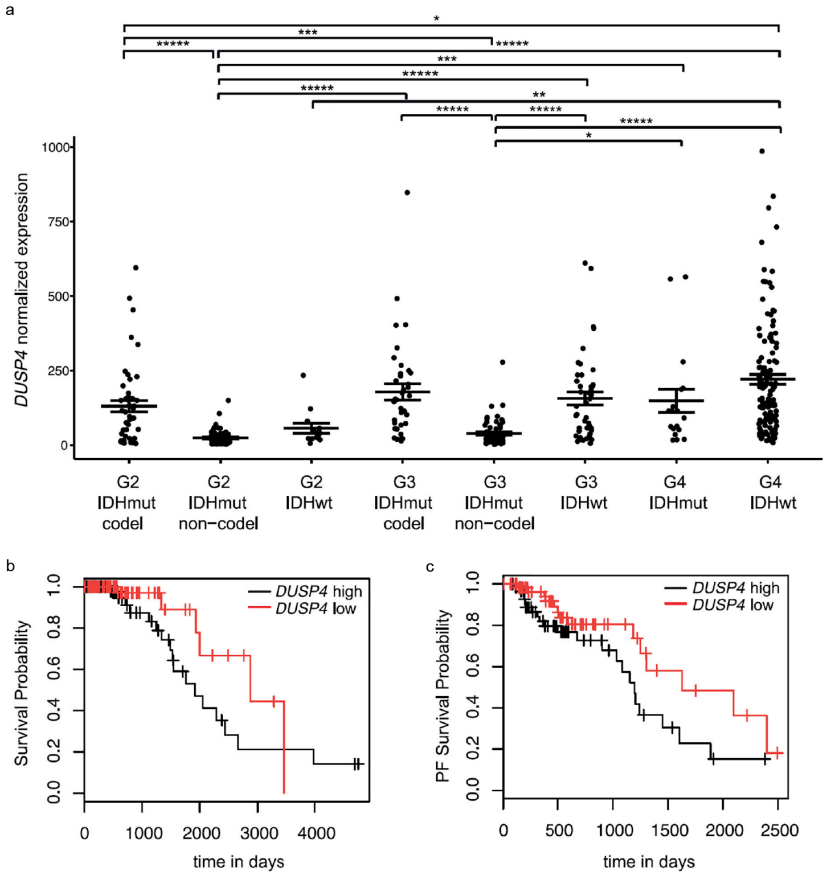

Figure 8. DUSP4 expression in glioma subtypes and correlation to survival and progression free survival of patients. Analysis of The Cancer Genome Atlas RNA sequencing (upper quartile normalized RNA-Seq by Expectation Maximization count estimates) and survival data to determine DUSP4 expression levels and prognostic value in different glioma subtypes. (a) DUSP4 expression levels in different WHO2016 glioma subtypes. Kruskal-Wallis test p = 2.2E-16. (b, c) Kaplan Meier survival analysis (log-rank) for low grade III IDHmut non-codel glioma patients. A strong trend for a worse survival (p = 0.0871) and progression free survival probability (p = 0.0745) was found for patients with above median levels of DUSP4. G2 = grade II glioma, G3 = grade III glioma, G4 = grade IV glioma, IDHmut = IDH1 mutated, IDHwt = IDH1 wild type, codel = 1q19p co-deleted, non-codel = 1q19p wild type.p < 0.05 *, p < 0.01 **, p < 0.001 ***, p < 0.0001 ****, p < 1.e-05 *****

High GFAPδ/α ratio cells are more malignant and invasive, glioma cells

For successful invasion a glioma cell needs to rearrange its cytoskeleton and find or create a scaffold to migrate on. It requires tools to interact with and adhere to the extracellular environment. In addition, it needs to remove obstacles from the extracellular environment that block its migratory path, and to release its interactions to the scaffold at the cell's rear end when it is moving forward (Claes et al., 2007). Fig.

9 gives an overview of the molecular characteristics induced in glioma cells with a high GFAPδ/α ratio that provide these tools. First of all, actin cytoskeleton rearrangements were observed. Clear actin stress fibres that connect the front of the cell to its rear end were present in high GFAPδ/α ratio cells which obtained a more spindle-shaped and polarized morphology compared to the polyhedral shaped low GFAPδ/α ratio cells (Fig. 9a). Expression of *LAMA1* and secretion of laminin was increased which the cells need for proper adherence (Fig. 9b). Increased levels of *ITGB1*, *ITGA6* and *ITGA7* (Fig. 9c) provided tools to adhere to the glioma cell-generated laminin-rich scaffold (Fig. 9b), and to induce a signalling response in the cell that could result in the observed increased levels of pJNK (Fig. 9d), DUSP4 (Fig. 9e), and *MMP2* (Fig. 9f). Increased levels of *MMP2* and a strong decrease in its inhibitor *A2M* (Fig. 5j) can be responsible for the degradation of the ECM in front and rear of the cell. Together these changes prepare the cells for proper invasion.

Increased *LAMA1* expression, laminin secretion into the glioma-cell generated ECM, laminin-dependent adhesion, and high expression levels of the laminin-111 receptors integrin α6β1 and integrin α7β1 in cells with a high GFAPδ/α ratio could contribute to glioma malignancy and invasiveness in different ways. First, as laminin is mainly present in the basal lamina of blood vessels of the adult human brain (Ferrer et al., 2018), cells with a high GFAPδ/α ratio might be better equipped to migrate alongside the brain vasculature, which is one of the preferred routes of glioma cell invasion (Winkler et al., 2009). Second, as glioma cells can create their own preferred microenvironment to invade the brain by the deposition of ECM proteins (Claes et al., 2007; Zamecnik, 2005), cells with a high GFAPδ/α ratio could create a migratory path by deposition of laminin in the absence of laminin containing vasculature. Interestingly, laminin deposits have been found near GFAP positive glioma cells in patient material (Tysnes et al., 1999) and in the area that borders migrating glioma cells and healthy brain tissue in a glioma animal model (Pedersen et al., 1993). Finally, soluble laminin-111 can activate signalling pathways by binding receptors on the secreting cell and/or its neighbours. Indeed, several studies support that laminin-111 activation of integrin β1 signalling can induce the changes observed in cells with a high GFAPδ/α ratio (Fig. 9), i.e. increased β1 integrin clustering (Ichikawa et al., 2009), MAPK signalling activity (Givant-Horwitz et al., 2004; Mruthyunjaya et al., 2010), and MMP2 expression and activity (Reich et al., 1995), that promote glioma invasion (Chou et al., 2015; Pereira et al., 2011; Tong et al., 2012). Thus, both the generation of a laminin scaffold as well as increased signalling provide tools for high GFAPδ/α ratio cells to invade the brain.

High GFAPδ/α, not the lack of GFAPα or general GFAP levels, induces a more malignant phenotype

As expression levels of the canonical GFAPα isoform are much higher in comparison

to GFAPδ, one could argue that the observed effects attributed to the increase in the GFAPδ/α ratio are a result of a general decrease in GFAP expression. However, different lines of evidence support a GFAPδ/α ratio specific effect. First, in our current study pan GFAP levels were decreased in both GFAPδ-KO 1 and GFAPα-KO1 clonal cell lines (Supp. Fig. 1A). As the described characteristics of cells with a high GFAPδ/α were not observed in GFAPδ-KO 1 cells, they cannot result from a decrease in pan GFAP alone. Moreover, there was no significant decrease in pan GFAP expression in GFAPα-KO 2 cells, but a clear high GFAPδ/α ratio related phenotype was observed. Second, DUSP4-KO cells in which a strong decrease in pan GFAP was observed did not consist of high GFAPδ/α ratio related characteristics and even contain characteristics of cells with a lower GFAPδ/α ratio (ctl and GFAPδ-KO cells). Third, in experiments in which shRNAs were used to modulate GFAP, different effects for a GFAPα knockdown and a pan GFAP knockdown were observed compared to control cells. For example, the increase in *DUSP4, LAMA1,* and *MMP2* was not observed in pan GFAP knockdown cells, and often an opposite direction of change of pan GFAP and GFAPα knockdown in comparison to control cells was seen (Moeton et al., 2014; Stassen et al., 2017). Therefore, we attribute the observed malignant phenotype of cells in this study specifically to an increase in the GFAPδ/α ratio. Whether the observed phenotype is a consequence of a relative increase in soluble GFAPδ protein, GFAPδ protein within the IF network, or both remains to be determined in future studies. We observed both filamentous and soluble GFAPδ protein in the GFAPα-KO cells. However, the lack of IF depolymerizing agents complicates the investigation of this matter.

DUSP4 plays a central role in the malignant phenotype of high GFAPδ/α ratio glioma cells

The results obtained in this study provide evidence for a central role of DUSP4 in the regulation of malignant characteristics in high GFAPδ/α ratio cells. We show that DUSP4 is both induced by a high GFAPδ/α ratio (Fig. 9e), and essential to the observed molecular alterations in these cells (Fig. 9, green letters). Indeed, DUSP4 has already been associated with many malignancy related biological processes in different types of cells (Al-Mutairi et al., 2010; Balko et al., 2012; Barajas-Espinosa et al., 2015; Cadalbert et al., 2005; Lawan et al., 2011; Lin et al., 2017; Schmid et al., 2015; Watson et al., 2007; Zhang et al., 2017) and with a worse prognosis for low grade astrocytoma patients (Stassen et al., 2017). We here show that high DUSP4 expression levels are specifically detrimental to the glioma subgroup of patients with low grade IDH1 mutated tumours without a 1q19p co-deletion (WHO2016), as a significant lower progression free survival is associated with high levels of DUSP4. Thus, we here confirm that DUSP4 is associated with a more malignant glioma phenotype.

In cells with a high GFAPδ/α ratio, DUSP4 protein is specifically increased

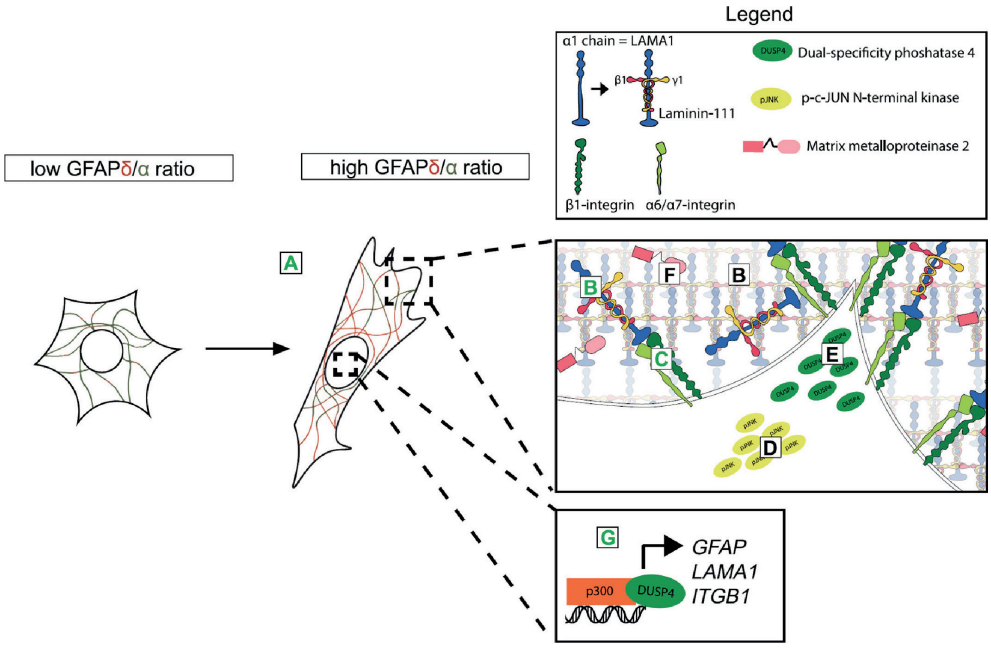

Figure 9. Observed changes in high GFAPδ/α ratio glioma cells. Overview of molecular and cellular alterations in cells with a high GFAPδ/α ratio compared to cells with a low GFAPδ/α ratio reported in this study. Green letters indicate molecular or cellular characteristics that were affected by a knockdown of DUSP4 as well. (A) Clear differences in cell morphology between cells with a low and a high GFAPδ/α ratio were observed. Low GFAPδ/α ratio cells consisted of a round, polyhedral shape whereas high GFAPδ/α ratio cells were spindle-shaped and more polarized. Upon DUSP4 depletion cells obtained a round and polyhedral shape again. (B) LAMA1 expression and laminin content in the extracellular matrix was increased in high GFAPδ/α ratio cells. (C-F) ITGB1, ITGA6, ITGA7, MMP2, DUSP4 gene expression levels and pJNK and DUSP4 protein levels were increased in high GFAPδ/α ratio cells. Local differences in pJNK protein levels were not determined and the cytoplasmic localization as depicted here is hypothetical (D). DUSP4 protein levels were specifically increased in focal adhesions (E). (G) GFAP, LAMA1 and ITGB1 expression is decreased in DUSP4-KO cells. A hypothetical localization of DUSP4 to DNA in the nucleus of high GFAPδ/α ratio cells is depicted here where it can bind histone acetyltransferase p300 and regulate gene expression as has previously been reported (Boulding et al., 2016).

in focal adhesions (Fig. 9e). As DUSP4 is known to be a nuclear phosphatase and expression in focal adhesions has not been previously reported, its function in this cellular compartment is unknown. As balanced phosphorylation in focal adhesions, of for example focal adhesion kinase, is essential for cell invasion (Claes et al., 2007), DUSP4 phosphatase activity in this area might be of great functional relevance.

Contradictory to the known function of DUSP4 as a nuclear phosphatase of pJNK, pJNK levels were increased in cells with a high GFAPδ/α ratio cells (Fig. 9d). Increased pJNK levels in glioma cells that overexpress GFAPδ have been previously reported (Perng et al., 2008). Our current data on the changes in DUSP4 localization

together with increased integrin β1 signalling, that increases JNK phosphorylation (Pereira et al., 2011; Snider et al., 2008), in cells with a high GFAPδ/α ratio can explain these observations. Interestingly, although pJNK localizes to the nucleus in most glioma cells (Mangiola et al., 2007), pJNK sequestration in the cytoplasm has been associated with increased glioma migration (Alapati et al., 2014). Location specific pJNK alterations were beyond the scope of this research, but sequestration of signalling molecules by changes in the IF network of glioma cells has been previously reported (Klotzsche et al., 1998; Pitre et al., 2012; Sembritzki et al., 2002), and might therefore be of interest for future studies.

The DUSP4 knockdown experiments in this study imply an essential role for DUSP4 in maintaining the malignant phenotype of cells with a high GFAPδ/α ratio (Fig. 9, green letters). The lack of DUSP4 decreases the expression of genes and alters cell morphology that both are characteristic of high GFAPδ/α ratio cells. This is accompanied with a strong decrease in GFAP expression suggesting that the alterations could be mediated by an overall absence of GFAP. However, compared to control cells, decreased *LAMA1* or *ITGB1* expression was neither observed in GFAPδ-KO nor in GFAPα-KO clonal cell lines, favouring a direct effect of decreased DUSP4. Moreover, we hypothesize that in addition to a cytoplasmic function in focal adhesions, DUSP4 promotes glioma malignancy by directly regulating gene expression via its interaction with the histone acetyltransferase p300 at gene promoters (Fig. 9g) (Boulding et al., 2016; Panicker et al., 2010; Zou et al., 2010).

Conclusion

Steering GFAP alternative splicing towards an increase in the GFAPδ/α ratio induced a more malignant glioma cell phenotype by activating signalling pathways up- and downstream of DUSP4 that changed the cell's interaction with the ECM and equipped the cell for invasion and possibly therapy evasion. Our data highlight an important role for GFAP alternative splicing in the functional diversity of the GFAP positive cell population of glioma and direct futures studies towards this cell population and GFAP alternative splicing as a therapeutic target.

Material and methods

Cell lines and culture

In this study two sub-clones of the human glioma U251-MG cell line, for which cell identity was confirmed by short terminal repeat analysis (Eurofins, Luxembourg), were used. One of the subclones expressed high levels of GFAP and was used in all GFAP isoform knockdown, DUSP4 knockdown and DUSP4 overexpression experiments

(obtained from Lars Ruether, Muenster, Germany). The second subclone expressed low levels of GFAP and was used to overexpress GFAP isoforms (obtained from Annemarie van Dam, Vrije Universiteit Amsterdam, The Netherlands). All cell lines were maintained in DMEM high glucose: Ham's F10 nutrient mix, supplemented with 100 U/ml penicillin, 100µg/ml streptomycin (1% p/s) and 10% (v/v) Fetal Bovine Serum (FBS) (Invitrogen, Carlsblad, CA, USA) at 37°C in a humidified incubator with 5% CO_2.

Generation of GFAP isoform and DUSP4 modulated cell lines

Stable cell lines expressing recombinant human GFAPα-IRES-eGFP (referred to as 'GFAPα$^+$'), recombinant human GFAPδ-IRES-mCherry (referred to as 'GFAPδ$^+$'), and control lines expressing recombinant mCherry were generated using lentiviral vectors as described before (Moeton et al., 2016; Stassen et al., 2017). To knock down GFAP isoforms lentiviral vector transductions containing shRNA targeting GFAPα (referred to as 'GFAPα$^-$'), GFAPpan (referred to as 'panGFAP$^-$') and non-targeting shRNA (referred to as 'NTC') were performed to generate stable GFAP modulated glioma cell lines as previously described (Moeton et al., 2016; Stassen et al., 2017).

For the generation of GFAP isoform knockouts, the U251-MG glioma cell genome was engineered using CRISPR Cas9. To modify GFAP isoform gene expression we designed gRNAs targeting sequences up- and downstream of the to-be-deleted exon (Fig. 2a,b) using the Broad Institute gRNA design tool (Hsu et al., 2013)(http://tools.genome-engineering.org/). Target sequences as near as possible to the start and end of the to-be-deleted exonic regions were chosen in order to prevent deletion of regulatory sequences within intronic regions. To knockout DUSP4, a gRNA was designed to target the first coding exon after the ATG start-codon. Guide RNA templates were generated by annealing specifically designed complementary oligonucleotides (cooling down from 100 °C to room temperature: 2 µM oligo 1, 2 µM oligo 2, 10 mM Tris pH 8.0, 1 mM EDTA, 50 mM NaCl). Oligonucleotide sequences were designed to generate specific overhangs (Supplementary Table 1) that were compatible for ligation (~20 ng plasmid, ~0.2 nM gRNA template, T4 DNA ligase and T4 DNA ligase Buffer (Roche, Basel, Switzerland) overnight at room temperature) into pSpCas9(BB)-2A-Puro (Addgene, Cambridge, MA, USA; (Ran et al., 2013) after digestion (3 hours at 37 °C) using BbsI (50 U/µl, Thermo Fisher Scientific, Waltham, MA, USA). The correct sequence was verified by sequencing (Macrogen, Amsterdam). To generate glioma cell lines containing the desired genetic modifications, U251-MG cells were seeded at a density of 120,000 cells/well in a 6 well plate. 24 hours after seeding, cell medium was depleted of penicillin and streptomycin for 16 hours and pSpCas9(BB)-2A-Puro plasmids (1 µg total DNA) containing gRNA up- and downstream of the to be deleted region were co-transfected using PEI (166 ng/ml final concentration). To generate the DUSP4 knockout (DUSP4-

KO) line, a single plasmid containing the gRNA was transfected into U251-MG cells. Uncut and empty pSpCas9(BB)-2A-Puro was transfected and used as a control. Transfection reagents were washed out after 16 hours, and 24 hours after transfection cells were treated with 1 μg/ml puromycin for 96 hours to select for transfected cells. After cells reached ~90% density they were transferred to T75 flasks and culturing was maintained. To generate clonal cell lines, FACS (BD Biosciences FACSAria II Cell Sorter, San Jose, CA, USA) was used to plate 1 cell/well of a 96 well plate from a cell suspension labelled with 7-Aminoactinomycin D (BD Biosciences, Franklin Lakes, NJ, USA) to exclude dead cells. After cells reached a density of 80% the cells were passaged to 24 well plates. 100% dense 24 wells were subsequently split in half to both continue culturing of the cells and to isolate DNA and/or RNA for clone selection. Using this method, GFAPδ knockout (referred to as 'GFAPδ-KO'), GFAPα knockout (referred to as 'GFAPα-KO') and control (referred to as 'ctl') clonal cell lines and DUSP4 knockout (referred to as 'DUSP4-KO') and control (referred to as 'DUSP4-CTL)' clonal cell lines were generated.

Overexpression of DUSP4 in glioma cells

DUSP4 plasmid (R777-E039 Hs.DUSP4, Addgene #70323) was used as a template to clone DUSP4 cDNA into the pcDNA3.1 plasmid. Primers with linkers were used to create Bam-HI and HindIII restriction sites. These restrictions enzymes were used to digest pcDNA3.1 and the PCR products and generate pcDNA3.1-DUSP4 expression plasmid by ligation of the digested products. The correct sequence was verified by sequencing (Macrogen, Amsterdam). The pcDNA3.1-DUSP4 overexpression was subsequently used to transfect U251-MG glioma cells using polyethylenimine that were seeded at a 1 x 10^4 density 24 hours before transfection. Empty pcDNA3.1 was transfected as a control. 5 days post-transfection cells were harvested and processed for RNA isolation.

DNA isolation and PCR

To determine the genotype of the CRISPR Cas9 modulated glioma cell lines, DNA was isolated from cell pellets. Cells were lysed in 5 mM Tris HCl pH 8.8 at 95°C for 10 min., cooled down on ice and treated with 10 μg/ml proteinase K by incubation at 56°C for 30 min. Proteinase K was subsequently deactivated for 5 min. at 95°C. 10 ng of DNA was used in a 20 μl PCR reaction mix containing 1 μl primer mix (0.5 μM forward and reverse primer, Supplementary Table 2), 4 μl of 7.5 or 12.5 μg MgCl2 FIREPol PCR Master mix (Solis BioDyne, Tartu, Estonia) and milliQ. The PCR reaction was performed in a T100 thermal cycler (Hercules, CA, USA): 95°C for 3 min. followed by 34 cycles of 95°C for 30 sec., 54.4°C (exon 8&9 amplification) or 51.4°C (exon 7a amplification) for 30 sec. and 72°C for 1.25 min. (exon 8&9 amplification) or 1.10 min.

(exon 7a amplification), and a final step of 72°C for 10 min. afterwards. PCR products were separated on a 1% agarose gel containing SYBR Safe DNA Gel Stain (Invitrogen, Carlsblad, CA, USA) and gels were imaged using an E-Gel Imager System with Blue Light Base (Life Technologies, Carlsblad, CA, USA).

RNA isolation

For RNA isolation of cell lines, cells were seeded at a 4 x 10^4 cell density in a 24 well plate on poly-D lysine (PDL) coated wells (20 μg/ml). After 3 days of culture, cells were washed in PBS and lysed using TRIzol (Ambion by Thermo Scientific, Waltham, MA, USA). To extract RNA chloroform (EMD Millipore Inc., Darmstadt, Germany) was added to the lysate and RNA was separated from proteins and lipids by centrifugation for 15 min. at 12,000 g at 7°C. RNA was subsequently precipitated in 2-propanol (EMD Millipore Inc., Darmstadt, Germany) at -20°C overnight and pelleted by centrifugation at 16,000 g at 4°C for 45 min. Pellets were washed twice with 75% cold ethanol and dissolved in MilliQ. RNA concentrations and purity were measured using the Varioskan Flash (Thermo Scientific, Waltham, MA, USA).

cDNA synthesis and real time quantitative PCR

The Quantitect Reverse Transcription kit (Qiagen, Hilden, Germany) was used to generate cDNA according to the manufacturer's protocol. 200 ng to 500 ng of RNA was treated with DNAse (gDNA wipe out buffer, Qiagen) for 2 min. at 42°C and subsequently converted to cDNA in a 10 μl reaction mix containing reverse transcriptase (RT), RT buffer and a mix of oligo-dT (Qiagen) for 30 min. at 42°C. RT was inactivated at 95°C for 3 min. For real-time quantitative PCR (qPCR) cDNA was diluted 20x in MilliQ and 1 μl was added to the qPCR reaction mix containing 1 μl primers mix (final concentration of 0.1 μM for forward and reverse primer), 5 μl FastStart Universal SYBR Green Master mix (ROX) (Roche, Basel, Switzerland) and 3 μl MilliQ. The reaction mix was added to a 96 or 384 plate and amplification of the product was measured after incubation steps at 50°C for 2 min. and 95°C for 10 min., during 40 PCR cycles (95°C for 15 sec. and 60°C for 1 min.) using a QuantStudio 6 Flex Real-Time PCR System (Applied Biosystems, Foster City, CA, USA). A dissociation curve was generated afterwards by ramping the temperature from 60°C to 95°C. Amplification curves were analysed using QuantStudio 6 and 7 Flex Real-Time PCR System Software (version 1.1, Applied Biosystems, Foster City, CA, USA) with a standard threshold of 0.2, according to the log linear part of the amplification curve. Correction of baseline fluorescence was automatically determined and corrected for by the systems software. Expression values were calculated by transforming Ct values (2^-Ct) and were normalized to the mean value of the transformed Ct values of reference genes (*GAPDH, Alu-J*). If the fluorescent threshold was not reached after 40 PCR cycles, a Ct value of 40 was used

in the analyses. Outlier analysis was performed on normalized gene expression values and experiments with values above and below 1.5 times the inter quartile ranges were excluded from further analysis. Supplementary Table 2 shows primer pair sequences used in this study.

Western blot analysis

For protein isolation 1.2 x 10^5 cells or 6.0 x 10^5 cells were plated in 6 wells or 15 cm dishes respectively. Cells were washed in PBS and scraped in suspension buffer (0.1 M NaCl, 0.01 M Tris-HCl pH 7.6, 0.001 M EDTA, complete EDTA-free protease inhibitor cocktail (Roche, Basel, Switzerland). Cells were lysed by 2 times 10 sec. ultrasonic bath treatment in suspension buffer. The soluble protein pool (supernatant) was separated from the insoluble pool (pellet) by centrifugation at 15,000 rpm for 1 min. Pellets were dissolved in 1x SDS loading buffer (50 mM Tris pH 6.8, 2% SDS, 10% glycerol, 2.5% 2-mercaptoethanol, bromophenol blue) and 2x SDS loading buffer (100 mM Tris pH 6.8, 4% SDS, 20% glycerol, 5% 2-mercaptoethanol, bromophenol blue) was added to the supernatant. Samples were heated at 95°C for 5 min. after which the DNA in the pellet fraction was broken up by running it through a 25-gauge needle. Both supernatant and pellet samples were then loaded on a 10% SDS-PAGE gel and proteins were separated by electrophoresis. Proteins were blotted on a 0.45 mM pore size nitrocellulose membrane (GE Healthcare, Chicago, IL, USA) using a Transblot SD semi-dry transfer system (Bio-Rad, Hercules, CA, USA) system for 1 hour. Blots were incubated in blocking buffer (50 mM Tris pH 7.4, 150 mM NaCl, 0.25% (w/v) gelatine, and 0.5% triton X-100) and incubated in primary antibody in blocking buffer at 4°C overnight. Blots were washed 3 times in TBS-T (100 mM Tris-HCl pH 7.4, 150 mM NaCl and 0.2% Tween-20) and incubated in secondary AB in blocking buffer for 1 hour at room temperature. Blots were washed 3 times in TBS-T and once in milliQ before blots were scanned using the Odyssey CLx Western Blot Detection System (LI-COR Biosciences, Lincoln, NE, USA). Supplementary Table 3 shows a list of primary and secondary antibodies used in this study.

Immunocytochemistry

For immunocytochemistry, cells were plated on PDL coated cover slips (20 μg/ml) at a density of 2 x 10^4 cells/well in a 24 well plate. After 3 days cells were washed in PBS and fixed in 4% (w/v) paraformaldehyde (4% PFA) dissolved in phosphate buffer saline, pH 7.4 (PBS) for 30 min. Cells were washed with PBS and incubated in blocking buffer (50 mM Tris pH 7.4, 150 mM NaCl, 0.25% (w/v) gelatine, and 0.5% triton X-100) for 15 min.at room temperature. Cells were subsequently incubated overnight in primary antibody in blocking buffer at 4°C. Cells were washed 3 times in PBS and incubated in blocking buffer with secondary antibody and Hoechst (1:1,000, 33528,

Thermo Fisher Scientific, Waltham, MA, USA) to counterstain the nuclei for 1 hour at room temperature. To label the actin cytoskeleton, fluorescently labelled phalloidin (Alexa Fluor 488, Thermo Fisher Scientific, Waltham, MA, USA) was added to the solution (1:1,000). Cells were washed 3 times in PBS and mounted in Mowiol (0.1 M tris-HCl pH 8.5, 25% glycerol, 10% Mowiol (Calbiochem, Merck Millipore, Darmstadt, Germany)). Immunofluorescent images were taken using a Zeiss Axioscope.A1 microscope (Oberkochen, Germany). Confocal images were taken using an Olympus Fluoview FV100 (Olympus Corporation, Tokio, Japan).

Generation of cell-derived matrices

Cells seeded at a density of 7.5 x 10^4 cells per PDL coated coverslip (20 μg/mL) in a 24 well plate. After 96 hours, when cells reached confluence, the medium was changed daily. After 7 days, medium was removed, and cells were washed with PBS. Cells were subsequently denuded from the cell-derived matrices (CDM) by incubation in sterile extraction buffer (20 mM NH_4OH, 0.5% Triton X-100 (Roche, Basel, Switzerland)) at 37 °C and 75 rpm for 15 min. CDMs were washed four times in PBS and used for immunostaining.

Adhesion assay

Cells were seeded on glass (uncoated) coverslips, PDL (20 μg/mL) coated coverslips, or laminin (10 μg/mL, derived from Engelbreth-Holm-Swarm murine sarcoma basement membrane, Sigma) coated coverslips at a density of 5.0 x 10^4 cells in a 24 well plate. After 2 or 24 hours cells were washed three times in PBS to remove unadhered cells. Adhered cells were fixed in 4% PFA in PBS, nuclei were stained using Hoechst (1:1,000, 33528, Thermo Fisher Scientific, Waltham, MA, USA) and after mounting of the coverslips, immunofluorescent images were taken using a Zeiss Axioscope.A1 microscope (Oberkochen, Germany) at three different areas per coverslip. Cell number was determined using ImageJ Software (version 1.52e, http://imagej.nih.gov.ij/).

Survival analysis using RNA sequencing data available from TCGA

Level 3 released RNA sequencing data (downloaded June 2015) from The Cancer Genome Atlas (TCGA) of 165 grade IV and 306 low grade glioma was used to determine DUSP4 expression levels within glioma subtypes (WHO 2016). Patient characteristics are shown in Supplementary Table 4. Expression levels were extracted as upper quartile normalized RNA-Seq by Expectation Maximization (RSEM) count estimates (normalized counts). Recurrent tumours were excluded, and normalized counts of duplicate tumour samples were averaged. For grade IV glioma patients, relevant mutation and expression data was downloaded from the UCSC Cancer Browser

(June 2015) and 144 grade IV patients could be classified according to the WHO 2016 classification system (Supplementary Table 4). For low grade glioma, data on relevant mutations was extracted from the TCGA network publication of 2015 (The Cancer Genome Atlas Research Network, 2015) and was available for 282 low grade glioma (Supplementary Table 4). Survival and progression free survival data was available for 422 glioma patients (downloaded from TCGA January 2016). The prognostic value of DUSP4 expression was determined in a Kaplan Meier survival analysis by comparing the survival curves of patients with below and above median expression of DUSP4 using the Survival package (version 2.41-3) in R software (version 3.4.3). Survival curves were compared using a log-rank regression analysis.

Statistical analysis

All statistical analyses were performed using R software (version 3.4.3). To test for significant differences between groups, the data was first tested for a normal distribution and normality of variances using the Shapiro Wilk test and Levene's test, respectively, using the PMCMR package (version 4.3). If these conditions for parametric testing were met a one-way ANOVA was performed followed by a Tukey's honestly significant difference (HSD) post-hoc test. If the conditions were not met, the non-parametric Kruskal-Wallis test was performed followed by a Nemenyi test. To test for a significant correlation between two variables, a linear regression analysis was performed. All graphs were generated using the ggplot2 package (3.0.0).

Acknowledgements

The results shown here are in part based upon data generated by the TCGA Research Network: http://cancergenome.nih.gov/. This work was supported by the research program of the Foundation for Fundamental Research on Matter [FOM; grant 09MMC06], the Netherlands Organization for Scientific Research [NWO; VICI grant 865.09.003], the T&P Bohnenn fund, and the Dutch Cancer Society [KWF 10123].

Authors contributions

E.J. van Bodegraven: conceptualization, formal analysis, investigation, methodology, visualization, writing – original draft; J.V. van Asperen: conceptualization, investigation, methodology, visualization, writing – review & editing; J.A. Sluijs: investigation, methodology, writing – review & editing ; C.B.J. van Deursen: investigation, writing – review & editing ; M.E. van Strien: conceptualization, supervision, writing – review & editing; O.M.J.A. Stassen: conceptualization, investigation, methodology, writing – review & editing; P.A.J. Robe: conceptualization, methodology, project administration,

supervision, writing – review & editing; E.M. Hol: conceptualization, funding acquisition, methodology, project administration, supervision, writing – review & editing.

References

Al-Mutairi, Mashael, Sameer Al-Harthi, Laurence Cadalbert, and Robin Plevin. 2010. "Over-Expression of Mitogen-Activated Protein Kinase Phosphatase-2 Enhances Adhesion Molecule Expression and Protects against Apoptosis in Human Endothelial Cells." *British Journal of Pharmacology* 161 (4): 782–98. https://doi.org/10.1111/j.1476-5381.2010.00952.x.

Alapati, Kiranmai, Divya Kesanakurti, Jasti S. Rao, and Venkata Ramesh Dasari. 2014. "UPAR and Cathepsin B-Mediated Compartmentalization of JNK Regulates the Migration of Glioma-Initiating Cells." *Stem Cell Research* 12 (3): 716–29. https://doi.org/10.1016/j.scr.2014.02.008.

Antonyak, Marc A, Lawrence C Kenyon, Andrew K Godwin, David C James, David R Emlet, Isamu Okamoto, Mehdi Tnani, Marina Holgado-Madruga, David K Moscatello, and Albert J Wong. 2002. "Elevated JNK Activation Contributes to the Pathogenesis of Human Brain Tumors." *Oncogene* 21 (33): 5038–46. https://doi.org/10.1038/sj.onc.1205593.

Balko, Justin M, Rebecca S Cook, David B Vaught, María G Kuba, Todd W Miller, Neil E Bhola, Melinda E Sanders, et al. 2012. "Profiling of Residual Breast Cancers after Neoadjuvant Chemotherapy Identifies DUSP4 Deficiency as a Mechanism of Drug Resistance." *Nature Medicine* 18 (7): 1052–59. https://doi.org/10.1038/nm.2795.

Barajas-Espinosa, Alma, Ariel Basye, Mark G. Angelos, and Chun-An Chen. 2015. "Modulation of P38 Kinase by DUSP4 Is Important in Regulating Cardiovascular Function under Oxidative Stress." *Free Radical Biology and Medicine* 89 (December): 170–81. https://doi.org/10.1016/j.freeradbiomed.2015.07.013.

Berge, Simone A. van den, Jinte Middeldorp, C. Eleana Zhang, Maurice A. Curtis, Brian W. Leonard, Diego Mastroeni, Pieter Voorn, Wilma D.J. van de Berg, Inge Huitinga, and Elly M. Hol. 2010. "Longterm Quiescent Cells in the Aged Human Subventricular Neurogenic System Specifically Express GFAP-δ." *Aging Cell* 9 (3): 313–26. https://doi.org/10.1111/j.1474-9726.2010.00556.x.

Bhaskara, Vasanth Kumar, Manas Panigrahi, Sundaram Challa, and Phanithi Prakash Babu. 2005. "Comparative Status of Activated ERK1/2 and PARP Cleavage in Human Gliomas." *Neuropathology* 25 (1): 48–53. https://doi.org/10.1111/j.1440-1789.2004.00585.x.

Boulding, Tara, Fan Wu, Robert McCuaig, Jennifer Dunn, Christopher R. Sutton, Kristine Hardy, Wenjuan Tu, et al. 2016. "Differential Roles for DUSP Family Members in Epithelial-to-Mesenchymal Transition and Cancer Stem Cell Regulation in Breast Cancer." Edited by Aamir Ahmad. *PLOS ONE* 11 (2): e0148065. https://doi.org/10.1371/journal.pone.0148065.

Brehar, Felix Mircea, Dorel Arsene, Lacramioara Aurelia Brinduse, and Mircea Radu Gorgan. 2015. "Immunohistochemical Analysis of GFAP-δ And Nestin in Cerebral Astrocytomas." *Brain Tumor Pathology* 32 (2): 90–98. https://doi.org/10.1007/s10014-014-0199-8.

Brennan, Cameron W., Roel G.W. Verhaak, Aaron McKenna, Benito Campos, Houtan Noushmehr, Sofie R. Salama, Siyuan Zheng, et al. 2013. "The Somatic Genomic Landscape of Glioblastoma." *Cell* 155 (2): 462–77. https://doi.org/10.1016/j.cell.2013.09.034.

Cadalbert, Laurence, Callum M. Sloss, Pamela Cameron, and Robin Plevin. 2005. "Conditional Expression of MAP Kinase Phosphatase-2 Protects against Genotoxic Stress-Induced Apoptosis by Binding and Selective Dephosphorylation of Nuclear Activated c-Jun N-Terminal Kinase." *Cellular Signalling* 17 (10): 1254–64. https://doi.org/10.1016/j.cellsig.2005.01.003.

Campos, Lia S., Dino P. Leone, Joao B. Relvas, Cord Brakebusch, Reinhard Fässler, Ueli Suter, and Charles Ffrench-Constant. 2004. "B1 Integrins Activate a MAPK Signalling Pathway in Neural Stem Cells That Contributes to Their Maintenance." *Development* 131 (14): 3433–44. https://doi.org/10.1242/

dev.01199.

Cancer Genome Atlas Research Network. 2008. "Comprehensive Genomic Characterization Defines Human Glioblastoma Genes and Core Pathways." *Nature* 455 (7216): 1061–68. https://doi.org/10.1038/nature07385.

Cancer Genome Atlas Research Network 2015. "Comprehensive, Integrative Genomic Analysis of Diffuse Lower-Grade Gliomas." *New England Journal of Medicine* 372 (26): 2481–98. https://doi.org/10.1056/NEJMoa1402121.

Cheung, Kevin J., Edward Gabrielson, Zena Werb, and Andrew J. Ewald. 2013. "Collective Invasion in Breast Cancer Requires a Conserved Basal Epithelial Program." *Cell* 155 (7): 1639–51. https://doi.org/10.1016/j.cell.2013.11.029.

Choi, Kyung-Chan, Sung-Eun Kwak, Ji-Eun Kim, Seung Hun Sheen, and Tae-Cheon Kang. 2009. "Enhanced Glial Fibrillary Acidic Protein-δ Expression in Human Astrocytic Tumor." *Neuroscience Letters* 463 (3): 182–87. https://doi.org/10.1016/j.neulet.2009.07.076.

Chou, Yu-Cheng, Meng-Ya Chang, Mei-Jen Wang, Fu-Shun Yu, Hsin-Chung Liu, Tomor Harnod, Chih-Huang Hung, Hsu-Tung Lee, and Jing-Gung Chung. 2015. "PEITC Inhibits Human Brain Glioblastoma GBM 8401 Cell Migration and Invasion through the Inhibition of UPA, Rho A, and Ras with Inhibition of MMP-2, -7 and -9 Gene Expression." *Oncology Reports* 34 (5): 2489–96. https://doi.org/10.3892/or.2015.4260.

Ciriello, Giovanni, Martin L Miller, Bülent Arman Aksoy, Yasin Senbabaoglu, Nikolaus Schultz, and Chris Sander. 2013. "Emerging Landscape of Oncogenic Signatures across Human Cancers." *Nature Genetics* 45 (10): 1127–33. https://doi.org/10.1038/ng.2762.

Claes, An, Albert J. Idema, and Pieter Wesseling. 2007. "Diffuse Glioma Growth: A Guerilla War." *Acta Neuropathologica* 114 (5): 443–58. https://doi.org/10.1007/s00401-007-0293-7.

Clairembault, Thomas, Willem Kamphuis, Laurène Leclair-Visonneau, Malvyne Rolli-Derkinderen, Emmanuel Coron, Michel Neunlist, Elly M. Hol, and Pascal Derkinderen. 2014. "Enteric GFAP Expression and Phosphorylation in Parkinson's Disease." *Journal of Neurochemistry* 130 (6): 805–15. https://doi.org/10.1111/jnc.12742.

Coulombe, Pierre A., and Pauline Wong. 2004. "Cytoplasmic Intermediate Filaments Revealed as Dynamic and Multipurpose Scaffolds." *Nature Cell Biology* 6 (8): 699–706. https://doi.org/10.1038/ncb0804-699.

Ferrer, Valéria Pereira, Vivaldo Moura Neto, and Rolf Mentlein. 2018. "Glioma Infiltration and Extracellular Matrix: Key Players and Modulators." *Glia* 66 (8): 1542–65. https://doi.org/10.1002/glia.23309.

Gialeli, Chrisostomi, Achilleas D. Theocharis, and Nikos K. Karamanos. 2011. "Roles of Matrix Metalloproteinases in Cancer Progression and Their Pharmacological Targeting." *FEBS Journal* 278 (1): 16–27. https://doi.org/10.1111/j.1742-4658.2010.07919.x.

Givant-Horwitz, Vered, Ben Davidson, and Reuven Reich. 2005. "Laminin-Induced Signaling in Tumor Cells." *Cancer Letters* 223 (1): 1–10. https://doi.org/10.1016/j.canlet.2004.08.030.

Godsel, Lisa M., Ryan P. Hobbs, and Kathleen J. Green. 2008. "Intermediate Filament Assembly: Dynamics to Disease." *Trends in Cell Biology* 18 (1): 28–37. https://doi.org/10.1016/j.tcb.2007.11.004.

Havel, L S, E R Kline, A M Salgueiro, and A I Marcus. 2015. "Vimentin Regulates Lung Cancer Cell Adhesion through a VAV2–Rac1 Pathway to Control Focal Adhesion Kinase Activity." *Oncogene* 34 (15): 1979–90. https://doi.org/10.1038/onc.2014.123.

Ho, Vincent K.Y., Jaap C. Reijneveld, Roelien H. Enting, Henri P. Bienfait, Pierre Robe, Brigitta G. Baumert, and Otto Visser. 2014. "Changing Incidence and Improved Survival of Gliomas." *European Journal of Cancer* 50 (13): 2309–18. https://doi.org/10.1016/j.ejca.2014.05.019.

Hsu, Patrick D, David A Scott, Joshua A Weinstein, F Ann Ran, Silvana Konermann, Vineeta Agarwala, Yinqing Li, et al. 2013. "DNA Targeting Specificity of RNA-Guided Cas9 Nucleases." *Nature*

Biotechnology 31 (9): 827–32. https://doi.org/10.1038/nbt.2647.

Hynes, Richard O. 2002. "Integrins." *Cell* 110 (6): 673–87. https://doi.org/10.1016/S0092-8674(02)00971-6.

Ichikawa, Naoki, Kazuhisa Iwabuchi, Hidetake Kurihara, Kumiko Ishii, Toshihide Kobayashi, Takako Sasaki, Nobutaka Hattori, et al. 2009. "Binding of Laminin-1 to Monosialoganglioside GM1 in Lipid Rafts Is Crucial for Neurite Outgrowth." *Journal of Cell Science* 122 (2): 289–99. https://doi.org/10.1242/jcs.030338.

Ivaska, Johanna, Hanna Mari Pallari, Jonna Nevo, and John E. Eriksson. 2007. "Novel Functions of Vimentin in Cell Adhesion, Migration, and Signaling." *Experimental Cell Research* 313 (10): 2050–62. https://doi.org/10.1016/j.yexcr.2007.03.040.

Jeuken, Judith, Caroline van den Broecke, Sabine Gijsen, Sandra Boots-Sprenger, and Pieter Wesseling. 2007. "RAS/RAF Pathway Activation in Gliomas: The Result of Copy Number Gains Rather than Activating Mutations." *Acta Neuropathologica* 114 (2): 121–33. https://doi.org/10.1007/s00401-007-0239-0.

Jiang, Yiwen, Voichita Dana Marinescu, Yuan Xie, Malin Jarvius, Naga Prathyusha Maturi, Caroline Haglund, Sara Olofsson, et al. 2017. "Glioblastoma Cell Malignancy and Drug Sensitivity Are Affected by the Cell of Origin." *Cell Reports* 18 (4): 977–90. https://doi.org/10.1016/j.celrep.2017.01.003.

Kim, Kyung Mok, Ki Wung Chung, Hyeong Oh Jeong, Bonggi Lee, Dae Hyun Kim, June Whoun Park, Seong Min Kim, Byung Pal Yu, and Hae Young Chung. 2018. "MMP2-A2M Interaction Increases ECM Accumulation in Aged Rat Kidney and Its Modulation by Calorie Restriction." *Oncotarget* 9 (5): 5588–99. https://doi.org/10.18632/oncotarget.23652.

Klotzsche, Oliver, Dörte Etzrodt, Heinz Hohenberg, Wolfgang Bohn, and Wolfgang Deppert. 1998. "Cytoplasmic Retention of Mutant Tsp53 Is Dependent on an Intermediate Filament Protein (Vimentin) Scaffold." *Oncogene* 16 (26): 3423–34. https://doi.org/10.1038/sj.onc.1202155.

Lawan, Ahmed, Sameer Al-Harthi, Laurence Cadalbert, Anthony G. McCluskey, Muhannad Shweash, Gianluca Grassia, Anne Grant, Marie Boyd, Susan Currie, and Robin Plevin. 2011. "Deletion of the Dual Specific Phosphatase-4 (DUSP-4) Gene Reveals an Essential Non-Redundant Role for MAP Kinase Phosphatase-2 (MKP-2) in Proliferation and Cell Survival." *Journal of Biological Chemistry* 286 (15): 12933–43. https://doi.org/10.1074/jbc.M110.181370.

Lee, Joo Ho, Jeong Eun Lee, Jee Ye Kahng, Se Hoon Kim, Jun Sung Park, Seon Jin Yoon, Ji Yong Um, et al. 2018. "Human Glioblastoma Arises from Subventricular Zone Cells with Low-Level Driver Mutations." *Nature* 560 (7717): 243–47. https://doi.org/10.1038/s41586-018-0389-3.

Li, Jian Yi, Hua Wang, Stephen May, Xianzhou Song, Juan Fueyo, Gregory N. Fuller, and Huamin Wang. 2008. "Constitutive Activation of C-Jun N-Terminal Kinase Correlates with Histologic Grade and EGFR Expression in Diffuse Gliomas." *Journal of Neuro-Oncology* 88 (1): 11–17. https://doi.org/10.1007/s11060-008-9529-1.

Lin, Hua, Shiyang Qiu, Lihua Xie, Chun Liu, and Shenghua Sun. 2017. "Nimbolide Suppresses Non-Small Cell Lung Cancer Cell Invasion and Migration via Manipulation of DUSP4 Expression and ERK1/2 Signaling." *Biomedicine & Pharmacotherapy* 92 (August): 340–46. https://doi.org/10.1016/j.biopha.2017.05.072.

Lopez-Gines, Concha, Rosario Gil-Benso, Rafa Benito, Manolo Mata, Javier Pereda, Juan Sastre, Pedro Roldan, Jose Gonzalez-Darder, and Miguel Cerdá-Nicolás. 2008. "The Activation of ERK1/2 MAP Kinases in Glioblastoma Pathobiology and Its Relationship with EGFR Amplification." *Neuropathology* 28 (5): 507–15. https://doi.org/10.1111/j.1440-1789.2008.00911.x.

Mangiola, Annunziato, Gina Lama, Cecilia Giannitelli, Pasquale De Bonis, Carmelo Anile, Libero Lauriola, Giuseppe La Torre, et al. 2007. "Stem Cell Marker Nestin and C-Jun NH 2 -Terminal Kinases in Tumor and Peritumor Areas of Glioblastoma Multiforme: Possible Prognostic Implications." *Clinical Cancer Research* 13 (23): 6970–77. https://doi.org/10.1158/1078-0432.CCR-07-1229.

Mendez, Melissa G, Shin-Ichiro Kojima, and Robert D Goldman. 2010. "Vimentin Induces Changes in Cell Shape, Motility, and Adhesion during the Epithelial to Mesenchymal Transition." *FASEB Journal : Official Publication of the Federation of American Societies for Experimental Biology* 24 (6): 1838–51. https://doi.org/10.1096/fj.09-151639.

Middeldorp, J., and E. M. Hol. 2011. "GFAP in Health and Disease." *Progress in Neurobiology* 93 (3): 421–43. https://doi.org/10.1016/j.pneurobio.2011.01.005.

Moeton, Martina, Regina Kanski, Oscar M J A Stassen, Jacqueline A. Sluijs, Dirk Geerts, Paula Van Tijn, Gerhard Wiche, Miriam E. Van Strien, and Elly M. Hol. 2014. "Silencing GFAP Isoforms in Astrocytoma Cells Disturbs Laminin-Dependent Motility and Cell Adhesion." *FASEB Journal* 28 (7): 2942–54. https://doi.org/10.1096/fj.13-245837.

Moeton, Martina, Oscar M J A Stassen, Jacqueline A. Sluijs, Vincent W N van der Meer, Liselot J. Kluivers, Hedde van Hoorn, Thomas Schmidt, Eric A J Reits, Miriam E. van Strien, and Elly M. Hol. 2016. "GFAP Isoforms Control Intermediate Filament Network Dynamics, Cell Morphology, and Focal Adhesions." *Cellular and Molecular Life Sciences* 73 (21): 4101–20. https://doi.org/10.1007/s00018-016-2239-5.

Mruthyunjaya, S., Rumma Manchanda, Ravibhushan Godbole, Radha Pujari, Anjali Shiras, and Padma Shastry. 2010. "Laminin-1 Induces Neurite Outgrowth in Human Mesenchymal Stem Cells in Serum/Differentiation Factors-Free Conditions through Activation of FAK–MEK/ERK Signaling Pathways." *Biochemical and Biophysical Research Communications* 391 (1): 43–48. https://doi.org/10.1016/j.bbrc.2009.10.158.

Nakagawa, Takao, Toshihiko Kubota, Masanori Kabuto, Noboru Fujimoto, and Yasunori Okada. 1996. "Secretion of Matrix Metalloproteinase-2 (72 KD Gelatinase/Type IV Collagenase = Gelatinase A) by Malignant Human Glioma Cell Lines: Implications for the Growth and Cellular Invasion of the Extracellular Matrix." *Journal of Neuro-Oncology* 28 (1): 13–24. https://doi.org/10.1007/BF00300442.

Paal-Henning, Pedersen, Kirsten Marienhagen, Sverre Mork, and Rolf Bjerkvig. 1993. "Migratory Pattern of Fetal Rat Brain Cells and Human Glioma Cells in the Adult Rat Brain." *Cancer Research* 53 (21): 5158–65.

Pandey, Vimal, Vasantha Kumar Bhaskara, and Phanithi Prakash Babu. 2016. "Implications of Mitogen-Activated Protein Kinase Signaling in Glioma." *Journal of Neuroscience Research* 94 (2): 114–27. https://doi.org/10.1002/jnr.23687.

Panicker, Sreejith P., Baisakhi Raychaudhuri, Pankaj Sharma, Russell Tipps, Tapati Mazumdar, Asoke K. Mal, Juan M. Palomo, Michael A. Vogelbaum, and Saikh Jaharul Haque. 2010. "P300- and Myc-Mediated Regulation of Glioblastoma Multiforme Cell Differentiation." *Oncotarget* 1 (4): 289–303. https://doi.org/10.18632/oncotarget.139.

Patel, A P, I Tirosh, J J Trombetta, A K Shalek, S M Gillespie, H Wakimoto, D P Cahill, et al. 2014. "Single-Cell RNA-Seq Highlights Intratumoral Heterogeneity in Primary Glioblastoma." *Science* 344 (6190): 1396–1401. https://doi.org/10.1126/science.1254257.

Paumelle, Réjane, David Tulasne, Catherine Leroy, Jean Coll, Bernard Vandenbunder, and Véronique Fafeur. 2000. "Sequential Activation of ERK and Repression of JNK by Scatter Factor/Hepatocyte Growth Factor in Madin-Darby Canine Kidney Epithelial Cells." Edited by Marc Mumby. *Molecular Biology of the Cell* 11 (11): 3751–63. https://doi.org/10.1091/mbc.11.11.3751.

Pearson, Joshua R.D., and Tarik Regad. 2017. "Targeting Cellular Pathways in Glioblastoma Multiforme." *Signal Transduction and Targeted Therapy* 2 (May): 1–11. https://doi.org/10.1038/sigtrans.2017.40.

Pereira, Andrea Maria, Cicerone Tudor, Johannes S. Kanger, Vinod Subramaniam, and Enrique Martin-Blanco. 2011. "Integrin-Dependent Activation of the JNK Signaling Pathway by Mechanical Stress." Edited by Maddy Parsons. *PLoS ONE* 6 (12): e26182. https://doi.org/10.1371/journal.pone.0026182.

Perng, Ming-Der, Shu-Fang Wen, Terry Gibbon, Jinte Middeldorp, Jacqueline Sluijs, Elly M. Hol, and

Roy A. Quinlan. 2008. "Glial Fibrillary Acidic Protein Filaments Can Tolerate the Incorporation of Assembly-Compromised GFAP-δ, but with Consequences for Filament Organization and AB-Crystallin Association." Edited by Thomas D. Pollard. *Molecular Biology of the Cell* 19 (10): 4521–33. https://doi.org/10.1091/mbc.e08-03-0284.

Pitre, Aaron, Nathan Davis, Madhumita Paul, A Wayne Orr, and Omar Skalli. 2012. "Synemin Promotes AKT-Dependent Glioblastoma Cell Proliferation by Antagonizing PP2A." *Molecular Biology of the Cell* 23 (7): 1243–53. https://doi.org/10.1091/mbc.e11-08-0685.

Ramachandran, Rahimsan K., Mia D. Sørensen, Charlotte Aaberg-Jessen, Simon K. Hermansen, and Bjarne W. Kristensen. 2017. "Expression and Prognostic Impact of Matrix Metalloproteinase-2 (MMP-2) in Astrocytomas." Edited by Ilya Ulasov. *PLOS ONE* 12 (2): e0172234. https://doi.org/10.1371/journal.pone.0172234.

Ran, F Ann, Patrick D Hsu, Jason Wright, Vineeta Agarwala, David A Scott, and Feng Zhang. 2013. "Genome Engineering Using the CRISPR-Cas9 System." *Nature Protocols* 8 (11): 2281–2308. https://doi.org/10.1038/nprot.2013.143.

Reich, Reuven, Michal Blumenthal, and Mordechai Liscovitch. 1995. "Role of Phospholipase D in Laminin-Induced Production of Gelatinase A (MMP-2) in Metastatic Cells." *Clinical & Experimental Metastasis* 13 (2): 134–40. https://doi.org/10.1007/BF00133618.

Roelofs, Reinko F., David F. Fischer, Simone H. Houtman, Jacqueline A. Sluijs, Wendy Van Haren, Fred W. Van Leeuwen, and Elly M. Hol. 2005. "Adult Human Subventricular, Subgranular, and Subpial Zones Contain Astrocytes with a Specialized Intermediate Filament Cytoskeleton." *Glia* 52 (4): 289–300. https://doi.org/10.1002/glia.20243.

Sankar, Savita, Jason M. Tanner, Russell Bell, Aashi Chaturvedi, R. Lor Randall, Mary C. Beckerle, and Stephen L. Lessnick. 2013. "A Novel Role for Keratin 17 in Coordinating Oncogenic Transformation and Cellular Adhesion in Ewing Sarcoma." *Molecular and Cellular Biology* 33 (22): 4448–60. https://doi.org/10.1128/MCB.00241-13.

Schmid, Corina A., Mark D. Robinson, Nicole A. Scheifinger, Sebastian Müller, Sergio Cogliatti, Alexandar Tzankov, and Anne Müller. 2015. "DUSP4 Deficiency Caused by Promoter Hypermethylation Drives JNK Signaling and Tumor Cell Survival in Diffuse Large B Cell Lymphoma." *Journal of Experimental Medicine* 212 (5): 775–92. https://doi.org/10.1084/jem.20141957.

Sembritzki, Olivier, Christian Hagel, Katrin Lamszus, Wolfgang Deppert, and Wolfgang Bohn. 2002. "Cytoplasmic Localization of Wild-Type P53 in Glioblastomas Correlates with Expression of Vimentin and Glial Fibrillary Acidic Protein." *Neuro-Oncology* 4 (3): 171–78. https://doi.org/10.1093/neuonc/4.3.17

Snider, Jared L., Cody Allison, Bryan H. Bellaire, Richard L. Ferrero, and James A. Cardelli. 2008. "The B1 Integrin Activates JNK Independent of CagA, and JNK Activation Is Required for Helicobacter Pylori CagA+-Induced Motility of Gastric Cancer Cells." *Journal of Biological Chemistry* 283 (20): 13952–63. https://doi.org/10.1074/jbc.M800289200.

Snider, Natasha T., and M. Bishr Omary. 2014. "Post-Translational Modifications of Intermediate Filament Proteins: Mechanisms and Functions." *Nature Reviews Molecular Cell Biology* 15 (3): 163–77. https://doi.org/10.1038/nrm3753.

Stassen, Oscar M J A, Emma J van Bodegraven, Fabrizio Giuliani, Martina Moeton, Regina Kanski, Jacqueline A Sluijs, Miriam E van Strien, Willem Kamphuis, Pierre A J Robe, and Elly M Hol. 2017. "GFAPδ/GFAPα Ratio Directs Astrocytoma Gene Expression towards a More Malignant Profile." *Oncotarget* 8 (50): 88104–21. https://doi.org/10.18632/oncotarget.21540.

Thiery, Jean Paul, Hervé Acloque, Ruby Y.J. Huang, and M. Angela Nieto. 2009. "Epithelial-Mesenchymal Transitions in Development and Disease." *Cell* 139 (5): 871–90. https://doi.org/10.1016/j.cell.2009.11.007.

Tong, Jiao Jian, Zhang Yan, Ren Jian, Huang Tao, Ouyang Tao Hui, and Chen Jian. 2012. "RhoA Regulates

Invasion of Glioma Cells via the C-Jun NH2-Terminal Kinase Pathway under Hypoxia." *Oncology Letters* 4 (3): 495–500. https://doi.org/10.3892/ol.2012.777.

Tsuiki, Hiromasa, Mehdi Tnani, Isamu Okamoto, Lawrence C Kenyon, David R Emlet, Marina Holgado-Madruga, Irene S Lanham, Christopher J Joynes, Kim T Vo, and Albert J Wong. 2003. "Constitutively Active Forms of C-Jun NH2-Terminal Kinase Are Expressed in Primary Glial Tumors." *Cancer Research* 63 (1): 250–55. http://www.ncbi.nlm.nih.gov/pubmed/12517805.

Turck, Natacha, Olivier Lefebvre, Isabelle Gross, Patrick Gendry, Michèle Kedinger, Patricia Simon-Assmann, and Jean-François Launay. 2006. "Effect of Laminin-1 on Intestinal Cell Differentiation Involves Inhibition of Nuclear Nucleolin." *Journal of Cellular Physiology* 206 (2): 545–55. https://doi.org/10.1002/jcp.20501.

Tysnes, Berit BØlge, Rupavathana Mahesparan, Frits Thorsen, Hans Kristian Haugland, Torsten Porwol, Per Øyvind Enger, Morten Lund Johansen, and Rolf Bjerkvig. 1999. "Laminin Expression by Glial Fibrillary Acidic Protein Positive Cells in Human Gliomas." *International Journal of Developmental Neuroscience* 17 (5–6): 531–39. https://doi.org/10.1016/S0736-5748(99)00055-6.

Vehlow, Anne, Erik Klapproth, Katja Storch, Ellen Dickreuter, Michael Seifert, Antje Dietrich, Rebecca Bütof, Achim Temme, and Nils Cordes. 2017. "Adhesion- and Stress-Related Adaptation of Glioma Radiochemoresistance Is Circumvented by B1 Integrin/JNK Co-Targeting." *Oncotarget* 8 (30): 49224–37. https://doi.org/10.18632/oncotarget.17480.

Velasco, Manuel E., Doris Dahl, Uros Roessmann, and Pierluigi Gambetti. 1980. "Immunohistochemical Localization of Glial Fibrillary Acidic Protein in Human Glial Neoplasms." *Cancer* 45 (3): 484–94. https://doi.org/10.1002/1097-0142(19800201)45:3<484::AID-CNCR2820450312>3.0.CO;2-9.

Velpula, Kiran Kumar, Azeem A. Rehman, Bharath Chelluboina, Venkata Ramesh Dasari, Christopher S. Gondi, Jasti S. Rao, and Krishna Kumar Veeravalli. 2012. "Glioma Stem Cell Invasion through Regulation of the Interconnected ERK, Integrin A6 and N-Cadherin Signaling Pathway." *Cellular Signalling* 24 (11): 2076–84. https://doi.org/10.1016/j.cellsig.2012.07.002.

Vial, Emmanuel, Erik Sahai, and Christopher J. Marshall. 2003. "ERK-MAPK Signaling Coordinately Regulates Activity of Rac1 and RhoA for Tumor Cell Motility." *Cancer Cell* 4 (1): 67–79. https://doi.org/10.1016/S1535-6108(03)00162-4.

Virtakoivu, Reetta, Anja Mai, Elina Mattila, Nicola De Franceschi, Susumu Y. Imanishi, Garry Corthals, Riina Kaukonen, et al. 2015. "Vimentin–ERK Signaling Uncouples Slug Gene Regulatory Function." *Cancer Research* 75 (11): 2349–62. https://doi.org/10.1158/0008-5472.CAN-14-2842.

Watson, Mark B., Michael J. Lind, Laura Smith, Philip J. Drew, and Lynn Cawkwell. 2007. "Expression Microarray Analysis Reveals Genes Associated with in Vitro Resistance to Cisplatin in a Cell Line Model." *Acta Oncologica* 46 (5): 651–58. https://doi.org/10.1080/02841860601156157.

Winkler, Frank, Yvonne Kienast, Martin Fuhrmann, Louisa Von Baumgarten, Steffen Burgold, Gerda Mitteregger, Hans Kretzschmar, and Jochen Herms. 2009. "Imaging Glioma Cell Invasion in Vivo Reveals Mechanisms of Dissemination and Peritumoral Angiogenesis." *Glia* 57 (12): 1306–15. https://doi.org/10.1002/glia.20850.

Zamecnik, Josef. 2005. "The Extracellular Space and Matrix of Gliomas." *Acta Neuropathologica* 110 (5): 435–42. https://doi.org/10.1007/s00401-005-1078-5.

Zhang, Rui, Ge Wang, Peng-Fei Zhang, Jing Zhang, Yan-Xia Huang, Yun-Min Lu, Wei Da, Qun Sun, and Jin-Shui Zhu. 2017. "Sanguinarine Inhibits Growth and Invasion of Gastric Cancer Cells via Regulation of the DUSP4/ERK Pathway." *Journal of Cellular and Molecular Medicine* 21 (6): 1117–27. https://doi.org/10.1111/jcmm.13043.

Zou, Wei, Zhenyuan Wang, Ying Liu, Yan Fan, Betty Y. Zhou, X. Frank Yang, and Johnny J. He. 2010. "Involvement of P300 in Constitutive and HIV-1 Tat-Activated Expression of Glial Fibrillary Acidic Protein in Astrocytes." *Glia* 58 (13): 1640–48. https://doi.org/10.1002/glia.21038.

Supplementary Data

Supplementary Figures

Supp. Fig. 1. GFAP expression in GFAP modulated glioma clonal cell lines

Supplementary Tables

Supp. Table 1. Cas9 guide RNA target information and materials

Supp. Table 2. Primer pairs used for PCR and qPCR analysis

Supp. Table 3. List of antibodies

Supp. Table 4. Patient characteristics


2

CHAPTER 2

Intermediate filaments in three-dimensional cell migration and glioma invasion– a tailored fit to the mechanical needs of the cell

Jessy V. van Asperen[1], Pierre A.J.T. Robe[2], Elly M. Hol[1]

[1] Department of Translational Neurosciences, UMC Utrecht Brain Center, University Medical Center Utrecht, Utrecht University, 3584 CG Utrecht, The Netherlands
[2] Department of Neurology and Neurosurgery, University Medical Center Utrecht Brain Center, Utrecht University, 3584 CG Utrecht, The Netherlands

Manuscript in preparation

Abstract

Cell migration through tissues requires cells to continuously sense the mechanical and molecular characteristics of the environment and adapt to these multiplex stimuli accordingly. This adaptive response involves dynamic switching between migration modes and level of force generation but also involves molecular adaptations to protect cellular organelles against migration induced mechanical damage. In this review, we explore the function of intermediate filaments (IFs) in the adaptive response of cells during three-dimensional migration. We start by describing how the composition and organisation of IFs are responsive to the characteristics of the environment and how IFs reversely affect tissue mechanics. We continue with outlining what is currently known about the contribution of IFs to mesenchymal, ameboid and lobopodial migration modes. Three-dimensional migration entails exposure to mechanical stress due to the compact and confined nature of tissues. In the last part of the review, we review how IFs are essential in providing mechanical resilience to the migrating cell. We conclude with the concept that IF expression and composition is tailor-fit to the mechanical needs of a migrating cell within a specific tissue environment.

Introduction

Cell migration is an essential process throughout the lifetime of multicellular organisms. During development, cells travel large distances to form the different tissue in the body and also postnatally, cell migration is essential to maintain homeostasis (Trepat, Chen, and Jacobson 2012). Cell migration can also be pathological, with metastasis and local invasion of tumour cells as the most infamous examples (Friedl and Alexander 2011). During migration through three-dimensional (3D) tissues, cells are surrounded by a complex environment of extracellular matrix (ECM) proteins with different organizational structures, rigidities, and chemical characteristics (Yamada and Sixt 2019). To effectively migrate through these heterogeneous landscapes, cells have to constantly sense the chemical and physical characteristics of the environment, integrate the signals within the cell and adjust the behavioural response to it. This adjustment can subsequently lead to remodelling of the cellular environment, illustrating the continues crosstalk between the cell and its environment, also defined as mechanoreciprocity (van Helvert, Storm, and Friedl 2018). In addition to cellular adaptation to facilitate the displacement, cells also have to adapt to the mechanical stress that is associated with migration through 3D environments. Cells migrating through tissues are frequently confined by ECM and densely packed cells, and movement through these constricted spaces requires the cell to actively deform the plasma membrane and cellular organelles, including the nucleus (McGregor, Hsia, and Lammerding 2016). Therefore, not only mechanoreciprocity but also mechanical resilience plays an important role during

migration through 3D environments.

Intermediate filaments (IFs) are important players in the regulation of cell migration in 2D conditions (Chung, Rotty, and Coulombe 2013; Leduc and Etienne-Manneville 2015). Proteins of the IF family are encoded by 70 genes in the human genome and are subdivided into 6 groups based on homology in sequence and assembly properties (Szeverenyi et al. 2008). All IFs share a secondary structure consisting of an alpha-helical rod domain flanked by an N-terminal 'head' domain and a C-terminal 'tail'-domain that can self-assemble into ~ 10 nm networks independently of cofactors and nucleotides (Herrmann and Aebi 2016). Despite their similarity in secondary structure, IF proteins have pronounced heterogeneity in amino acid sequence, length, and molecular mass (Block et al. 2015). More remarkably, the expression patterns of the different IF genes are highly tissue- and differentiation state-dependent, and therefore combinations of specific IF proteins are often used as biomarkers to identify the origin of cells in healthy tissues or tumours, or IF-associated diseases (Omary 2009). Moreover, given the heterogeneity in the effect of IFs on cellular processes, changes in IF expression are often linked to changes in cellular function. The best example of this is the change from a keratin to a vimentin dominant IF network in cells that transition from a stationary to migratory state, a characteristic of epithelial to mesenchymal transition (EMT) (Chung, Rotty, and Coulombe 2013; Mendez, Kojima, and Goldman 2010; Aiello and Kang 2019).

Given the heterogeneity in IF expression in different cell types and the fact that different IF proteins have distinct mechanical properties, IFs are suggested to be the 'mechanical footprints' of the cell (Block et al. 2015). It can be hypothesized that IF expression and composition in the cell can be tailored to the mechanical properties of its environment, to accommodate a specific behaviour. In this review, we explore this hypothesis by giving an overview of how IFs are involved in mechanoreciprocity between cell and environment, how IFs facilitate migration through 3D environments, and how they protect the cell against the damaging consequences of confined migration.

1. Mechanoreciprocity in tissue mechanics and IF organisation

The physical properties of tissues within an organism are highly diverse. Besides differences in cell types and cellular organisation, every tissue has a unique composition and architecture of ECM, leading to differences in topology and rigidity (Barnes, Przybyla, and Weaver 2017). The rigidity or stiffness of tissue describes the amount of force necessary to induce deformation of the substrate and is often described with the elastic modulus (E). The physiological range of stiffness's within the body ranges from very soft tissues with elastic moduli below 1 kPa, like brain, lung, or adipose tissue, to stiffer tissues like muscle and bone in the range of 10 kPa and 1 GPa

respectively (Barnes et al., 2017). For many physiological processes, it is essential that cells can sense the mechanical properties of their environment and can respond to it to maintain homeostasis(Humphrey, Dufresne, and Schwartz 2014). In the continuum of cell-tissue interactions, cells are constantly monitoring the mechanical and structural information of their environment to translate this into biochemical signals in a process termed mechanotransduction (Hoffman, Grashoff, and Schwartz 2011). In the first step of this process, forces acting on the cell typically lead to conformational changes in mechanosensitive molecules. Examples of mechanosensitive responses upon force are the opening of mechanically gated ion channels or exposure of binding sites for protein interactions (Hayakawa, Tatsumi, and Sokabe 2012; Klotzsch et al. 2009; Botello-Smith et al. 2019). The mechanosensitive response can subsequently trigger a signalling transduction cascade, leading to a mechanoresponse. In many cases, these mechanoresponses provide a feedback loop to the upstream mechanosensitive structures, providing a mechanism for cellular adjustment to the characteristics of its environment (Hoffman, Grashoff, and Schwartz 2011).

1.1 Mechanoresponsiveness of the IF network

Multiple lines of evidence indicate that the composition and organisation of the IF network are sensitive to the mechanical properties of the environment. First of all, the expression levels of different IF proteins appears to be dependent on the characteristics of the environment. A proteomic screen of U251-MG glioblastoma cells injected in either the flank or the brain of nude mice identified cytosolic and nuclear IFs as some of the most differentially expressed proteins. Whereas the protein levels of lamin A, GFAP, and vimentin were upregulated in the rigid environment of the flank, the soft environment of the brain led to an increase in nestin and lamin B1 and B2 (Swift et al. 2013). Another study found differences in solubility of vimentin in human mesenchymal stem cells (MSCs), endothelial cells, and fibroblasts cultured on substrates with different rigidities. The solubility of vimentin exhibited a biphasic response with peak solubility levels around 5 kPa, and a smaller soluble pool on the softest and stiffest substrate (Murray, Mendez, and Janmey 2014). Also, the organisation of the IF network is influenced by substrate rigidity. In glioma cells, the IF network is concentrated around the cell centre on soft substrates, whereas the network is extending more towards the cell periphery when cultured on stiffer substrates (Pogoda et al. 2014; 2017). Fluid shear force is another mechanical stimulus that leads to the reorganisation of the IF network. In response to shear force, the solubility of keratin 8 and 18 is decreased and the mesh size distribution is shifted towards the periphery of alveolar epithelial cells, leading to a local increase in stiffness (Sivaramakrishnan et al. 2008; Flitney et al. 2009). In addition to tissue rigidity, cells can also respond to the geometry

of the tissue, although responsiveness to topology appears to be IF type-specific. The organisation of vimentin is not directly affected by subtle changes in shape in fibroblasts cultured on micropatterns. It does, however, indirectly affect the cellular response to topology by affecting the distribution of microtubules (Shabbir et al. 2014). The lack of responsiveness of vimentin to geometrical cues was also found in pancreatic carcinoma cells cultured on aligned or random electrospun nanofibers. In these cells, however, the keratin network did respond to the alignment of the fibres (Wang et al. 2019). Together, these studies highlight the mechanoresponsive properties of the IF network and the heterogeneity of distinct IF family members in this response.

1.2 Contribution of IFs to cell and tissue mechanics

In addition to the physical environment influencing the composition and organisation of IFs, IFs can also contribute to the mechanical properties of the tissue. First of all, IFs can change tissue mechanics by affecting cellular stiffness. The contribution of IFs to the mechanical properties of the cell has been studied for different IF proteins, in many different cell types, and using a variety of techniques (Charrier and Janmey 2016). Although most studies show that IFs contribute to cellular mechanics under low strain conditions, the effect is modest in comparison to other cytoskeletal components, like the actomyosin cortex. The effect of IFs on the mechanics, however, becomes more apparent when cells are exposed to larger or repeated deformations or stressors (Charrier and Janmey 2016), as we will discuss later in this review. Interesting to note is that the contribution of IFs to cell mechanics is dependent on the characteristics of the substrate. In mesenchymal stem cells, loss of vimentin reduces the deformability of the cell when cells are placed on 4% agarose hydrogels. However, this effect of depletion of vimentin is lost when cells are plated on a softer substrate (Sharma et al. 2017). Also in mouse embryonic fibroblasts, vimentin contributes little to cellular mechanics on soft substrates, but it increases the stiffness of cells when cells are plated on stiffer substrates, such as glass (Mendez, Restle, and Janmey 2014). In addition to cellular stiffness, cells can also contribute to tissue mechanics by exerting traction forces on the local environment. Early studies already linked the IF network to cellular contractility, by showing that fibroblasts lacking vimentin had a diminished ability to deform 3D collagen gels (Eckes et al. 1998). A later study confirmed this and further showed that the contribution of vimentin to cellular contraction in collagen gels only occurred in conditions where cell-matrix interactions were dominant over cell-cell interactions. When the same experiment was repeated using higher densities of cells, this effect was lost (Mendez, Restle, and Janmey 2014). Altogether, the effects of tissue mechanics on IF network organisation and vice versa stress the interdependency of the two and highlight the role of IFs in mechanoreciprocity (Fig. 1). Given the involvement of IF

proteins in many different cellular processes, the mechanoresponsive adaptation of the IF network has implications for cellular behaviour and could be a mechanism of the cell to adapt to the mechanical properties of its environment. In the next paragraph, we will explore this idea by describing how mechanoreciprocity plays a role in the process of 3D cell migration, and how changes in the IF network might affect this process.

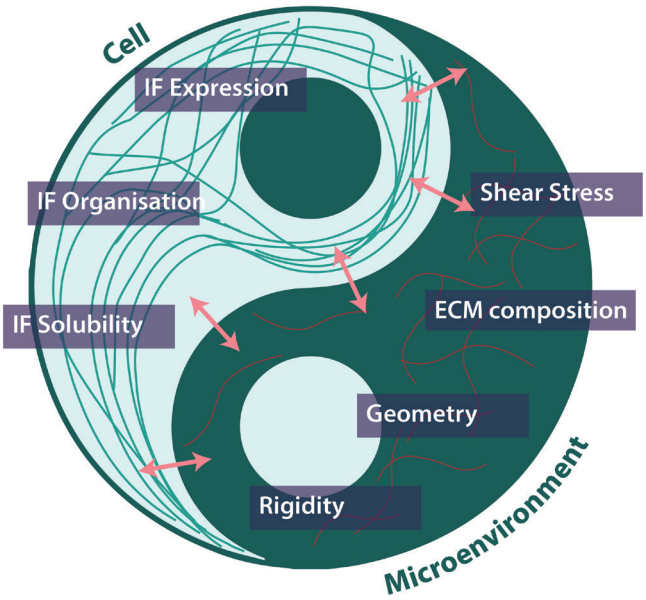

Figure 1. IFs as integrative components of cell-microenvironment reciprocity.

2. IFs contribute to different modes of 3D cell migration.

Cells can adopt different migration strategies when migrating through 3D environments. The used strategy is both dependent on the cell-intrinsic properties and the characteristics of the environment (van Helvert, Storm, and Friedl 2018). The composition and architecture of the ECM, i.e. the type and amount of ECM molecules, the degree of crosslinking, and geometry of the substrate, can be sensed by the cell and can drive certain migration modes, such as mesenchymal, amoeboid and lobopodial migration (Yamada and Sixt 2019). In the next section, we describe how IFs can contribute to different migration strategies, partly based on what we know from studies in 2D. Although IFs are also involved in collective cell migration (De Pascalis and Etienne-Manneville 2017), in this part we focus on single-cell migration modes.

2.1 IFs in mesenchymal migration

In environments with a high ligand density and substrate rigidity, cells adopt a spindle-

like shape and facilitate movement by attaching to and pulling on the substrate, a process called mesenchymal migration (Yamada and Sixt 2019). Compared to the other modes of 3D migration, mesenchymal cell migration shows the most resemblance with migration on flat surfaces and is dependent on dynamic integrin adhesions complexes, such as focal adhesions (FA), and actomyosin contractions (Doyle et al. 2015; Jacquemet, Hamidi, and Ivaska 2015; Doyle and Yamada 2016). The FA-complexes that are facilitating the adhesion to the ECM are part of a mechanosensing machinery that can be described as a 'molecular clutch' (Elosegui-Artola et al. 2016). The motor-clutch hypothesis proposes that for an optimum migration speed, the number of motors (F-actin and myosin motors) and clutches (integrins and linker-proteins) are in balance with the substrate rigidity (Elosegui-Artola et al. 2016). Although the motor-clutch hypothesis has been mainly studied in 2D migration models, there are strong implications that similar mechanisms take place during 3D migration. Within 3D collagen gels with different rigidities, increased adhesion protein dynamics and decreased adhesion stability was observed in softer collagen gels. This balance can be shifted by changing the availability of integrin ligands or contractility of the cell (Doyle et al. 2015).

Although the role of IF proteins in 3D mesenchymal migration has not been extensively investigated, many studies in 2D link the IF network to this form of migration and different components of the molecular clutch (Box 1). Mechanoreciprocity between tissue mechanics and IF network organisation might affect the molecular clutch dynamics during cell migration, especially given the opposing effects of different IF family members on FA dynamics. Vimentin has been extensively studied in FA dynamics and is often associated with reinforcement of the formation and maturation of FAs. Phosphorylated vimentin regulates the trafficking of β1 integrin and promotes β1 integrin activation on the cell surface (Ivaska et al. 2005; Rizki, Mott, and Bissell 2007; Fortin et al. 2010; Kim et al. 2010). Also, the recruitment of vimentin to FAs through plectin promotes the activation of focal adhesion kinase (FAK) and downstream targets (Burgstaller et al. 2010; Chang et al. 2012; Gregor et al. 2014; Hyder et al. 2014; Havel et al. 2015). The expression of the IF protein nestin, on the other hand, has an opposite effect on β1 integrin and FAK dynamics in pancreatic cancer cells. In these cells, not up but downregulation of nestin promotes cell membrane localisation, clustering and activation of α5β1 integrin complexes and causes relocation of pFAK to FAs (Hyder et al. 2014). Also, keratin is often described as a negative regulator of FA formation and maturation. A recent publication shows that in migrating keratinocytes, contractile forces generated through FA signalling result in a counterbalancing feedback loop through keratin 14-plectin-integrin α6β4 at the level of hemidesmosomes. Upon loss of hemodesmosomal constraint, FAs can grow further and generate more traction force, leading to increased FAK signalling and initiation of PI3K-YAP signalling (Wang et al. 2020). Although cell adhesion on 2D substrates shares similarities with 3D

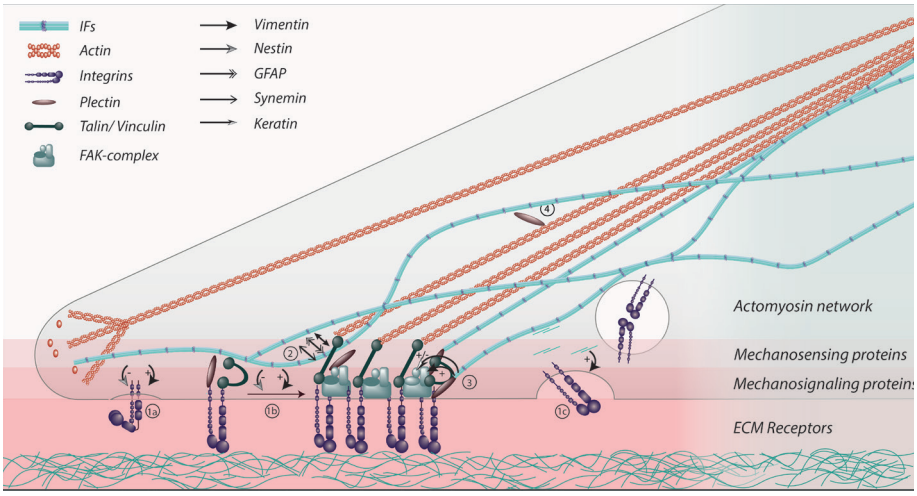

Box 1. Molecular clutch – IF interplay. For successful 3D migration, the forces that a cell exerts on the tissue must be proportional to the mechanical characteristics of the environment, also termed mechanoreciprocity (Paszek and Weaver 2004; van Helvert, Storm, and Friedl 2018). The molecular clutch model describes the dynamic interplay between different proteins that mediate force transmission between the cell and the ECM. In this model, balanced force transmission from the actomyosin motors to the substrate through ECM receptors involves mechanosensing molecules, including talin, vinculin, tensin and zyxin, and mechanosignaling proteins like FAK, Paxillin and Src among others (Elosegui-Artola et al. 2016; Case and Waterman 2015). IFs interact with different components of the molecular clutch. (1) At the level of ECM receptors, IFs are involved in the regulation of the bioavailability of integrins by regulating their activation (1a), clustering (1b), and recycling (1c). Vimentin can directly interact with the integrin β3 and induces clustering of integrin β3 proteins (Kim et al. 2016; Bhattacharya et al. 2009). Also, integrin β1 trafficking and activation are promoted by phosphorylated vimentin (Ivaska et al. 2005; Rizki, Mott, and Bissell 2007; Fortin et al. 2010; H. Kim et al. 2010; Chang et al. 2012), whereas nestin has the opposite effect on integrin β1 bioavailability (Hyder et al. 2014). (2) IFs can directly interact with the mechanosensitive adaptor proteins, as has been described for GFAP and vimentin with talin and vinculin (De Pascalis et al. 2018), and α and β synemin with talin, vinculin, zyxin (Leube, Moch, and Windoffer 2015). (3) Activity of mechanosignaling proteins like focal adhesion kinase (FAK) and downstream targets are influenced by the recruitment of vimentin through plectin (Burgstaller et al. 2010; Gregor et al. 2014; Hyder et al. 2014; Havel et al. 2015). Keratins both negatively (Keratin 6) and positively (keratin 8/18) influence FAK-Src signalling (Rotty and Coulombe 2012; Bordeleau et al. 2012). (4) Lastly, IFs also interact with the molecular clutch at the level of the actomyosin network. Vimentin negatively regulates RhoA activity and contractility by controlling phosphorylation levels of GEF-H1 (Jiu et al. 2017). On the other hand vimentin, GFAP and nestin have positive effects on actomyosin force distribution and orientation (Costigliola et al. 2017; De Pascalis et al. 2018).

substrates (Doyle and Yamada 2016), an extra layer of complexity is introduced with the additional dimension. Whereas the adhesion molecules are only on one side of the cell in 2D migration, the ECM adhesion sides are localised in all directions in 3D. Besides, migration within 3D matrices can induce local differences in ECM rigidity, as a consequence of fibril buckling (Doyle and Yamada 2016). Since IF-FA interactions have mainly been studied in 2D systems, it remains to be investigated how IFs regulate FA dynamics in 3D matrices.

Another characteristic of mesenchymal cell migration is the high proteolytic activity of the migrating cells, used to remodel the ECM to overcome physical barriers (Wolf et al. 2013). Proteolytic activity in mesenchymal migration is often associated with finger-like protrusions termed ´invadopodia´. Invadopodia are F-actin rich protrusions that are enriched in ECM- and membrane-remodelling proteins and are typically associated with highly invasive cell types (Sibony-Benyamini and Gil-Henn 2012). In invasive bladder cancer cells and fibrosarcoma cells, vimentin forms a scaffold that enables the formation of invadopodia through interaction with plectin and CARMIL2 (Sutoh Yoneyama et al. 2014; Lanier, Kim, and Cooper 2015). Although vimentin is not present in invadopodia right after formation, IFs start to infiltrate the structure as it matures. This shift in vimentin localisation is necessary for the elongation and maturation of invadopodia (Schoumacher et al. 2010).

2.2 IFs in lobopodial and amoeboid migration

In addition to using focalised traction forces to pull on the ECM, cells can also move by pushing the cell body towards the substrate through actin protrusions, a process termed amoeboid migration. This form of migration is stimulated by confinement and a low number of adhesion sites and does not require proteolytic activity (Liu et al. 2015). Although the contribution of IFs to amoeboid migration has not been widely studied, two recent publications found opposite effects of the presence of vimentin on the amoeboid migration speed (Lavenus et al. 2020; Stankevicins et al. 2019). The absence of vimentin promoted amoeboid migration speed in melanoma cells, whereas it limited the speed of bone-marrow-derived macrophages. Despite this discrepancy, both papers describe a role for vimentin in protecting the cell against mechanical migration-associated stress (Lavenus et al. 2020; Stankevicins et al. 2019).

A third mode of migration that cells can use in 3D environments, is lobopodial-dependent migration. Lobopodial migration is a hybrid form of migration, where cells generate both bleb-like protrusions typical for amoeboid migration and generate traction forces on the ECM like in mesenchymal migration (Yamada and Sixt 2019). During lobopodial migration, the nucleus acts as a piston to compartmentalise the cell into anterior high-pressure and posterior low-pressure zones. Vimentin is involved

in this process, as actomyosin contractility acts through nesprin-3a on the vimentin network to pull the nucleus forward and therewith increase cytosolic pressure in the anterior compartment (Petrie, Koo, and Yamada 2014). Whether this role is restricted to vimentin or whether other IFs are also involved in lobopodial migration, remains to be investigated.

3. The contribution of IFs to mechanical resilience

Migration through 3D environments can lead to exposure to mechanical stress. In particular, when cells are confined by the ECM and/or tightly adherent cells, they are exposed to compressive forces from the ECM and tensile forces from the actomyosin network (McGregor, Hsia, and Lammerding 2016; Yamada and Sixt 2019). As discussed earlier, although the contribution of IFs is moderate when cells are exposed to small strains, the contribution of IFs to the mechanics of the cell becomes more evident when cells are exposed to larger strains or repeated mechanical stress. The mechanical resilience of IFs became apparent from a recent study in which 3D hydrogels with mouse embryonic fibroblasts (mEFs) were stretched. In this study, wild-type mEFs were compared to vimentin-deficient cells and vimentin 'ghost cells'. In the latter, actin, microtubules, and cell membranes were dissolved, leaving only the intact IF network behind (Hu et al. 2019). Upon a single large deformation, the cytoplasmic toughness of wild-type mEFs was larger than that of both the vimentin-deficient and the vimentin "ghost cells". Repeated exposure to strain led to significant cytoplasm softening in wild-type cells and even more in vimentin depleted cells, indicating damage and disassembly of other cytoskeletal structures. In contrast, the cytoplasm of vimentin ghost cells showed little softening, even after 100 cycles of deformation. The authors further showed that vimentin was involved in distributing the strain over a larger area within the cytoplasm, decreasing the local burden at the place where the strain was applied (Hu et al. 2019). These findings corroborate earlier studies in 2D, in which it was shown that vimentin has little effect on a single deformation event, but stabilised the elastic moduli of mEFs cells upon exposure to repeated compressions or large deformations (Mendez, Restle, and Janmey 2014). Thus, by distributing strain and maintaining integrity in response to major mechanical stressors, IFs play an important role in cellular mechanical resilience.

To understand how IFs contribute to the mechanical resilience of the cell, IF proteins have been studied *in vitro* to characterise their mechanical properties. Three mechanical features of IFs set the protein networks apart from actin filaments and microtubules and this potentially explains their resilient behaviour in cells. First of all, IFs are more flexible and stretchable compared to actin filaments and microtubules (Block et al. 2015). IFs can be extended over two to three times their original length before filaments rupture (Qin, Kreplak, and Buehler 2009). A possible underlying

mechanism for this phenomenon is a transition from α-helices to β-sheets in the coiled-coil domain of each dimer upon stretching, which accounts for a doubling in dimer length (Qin, Kreplak, and Buehler 2009). Besides, it has been postulated that sections of tetramers can detach and reattach a few units further down to enable an extension of the filament, whilst thinning the filament (Qin, Kreplak, and Buehler 2009). Another characteristic of IFs is that the network can undergo strain stiffening: whereas at low strains the filaments are largely elastic, in response to large deformations the network gets stiffer (Block et al. 2015). This characteristic is likely linked to the protein sequence of the IF tail region and to the ability to form permanent cross-links in the IF network (Lin et al. 2010). *In vitro*, the mechanical properties of the different members of the IF family are heterogeneous due to the difference in amino-acid sequence and polyelectrolytic properties (Block et al. 2015). How this heterogeneity affects cellular mechanical resilience *in vivo* remains to be further elucidated.

3.1 IFs and nuclear envelope integrity during confined migration

Recently, different research groups have shown that the IF network plays an important role in protecting the nucleus from migration-induced mechanical stress (Patteson et al. 2019; Stankevicins et al. 2019; Lavenus et al., 2020). During confined migration, the deformability of the nucleus can be a rate-limiting factor (Friedl and Alexander 2011). Higher nuclear deformability can promote migration, but at the same time can increase the chance of rupture of the nuclear envelope, extrusion of chromatin, and consequently DNA damage and apoptosis (McGregor, Hsia, and Lammerding 2016). Nuclear IF proteins lamin A and C are involved in maintaining nuclear envelope integrity during confined migration and depletion of these proteins promotes nuclear deformation at the costs of increased nuclear damage (Denais et al. 2016). In addition to the nuclear lamins on the inside, the dense network of cytosolic IFs forms a cage-like structure around the nucleus called a perinuclear net (Dupin, Sakamoto, and Etienne-Manneville 2011; Patteson, et al. 2019). This IF perinuclear net is coupled to the nuclear envelope through nesprin-3 and plectin, proteins that are part of the *linker of nucleus skeleton and cytoskeleton* (LINC) *complex* (Ketema et al. 2013; McGregor, Hsia, and Lammerding 2016). Recently, it became evident that vimentin protects the nucleus from mechanical stress during confined migration. Whereas vimentin increases the speed of migration of mEFs on flat surfaces, vimentin slows down migration of mEFs in 3D collagen matrix or in 3D microchannels that mimic tissue confinement (Patteson, Pogoda, et al. 2019). The increase in speed in vimentin-deficient mEFs in 3D environments, however, comes at the cost of more frequent nuclear ruptures, perturbed nuclear shape, and increased migration-induced DNA damage. The increased vulnerability of these cells under compression is associated with a reduction in cytoplasmic stiffness above the nucleus,

indicating that larger cell deformability in vimentin-deficient cells leads to an increase in cell damage (Patteson et al. 2019). Also, during amoeboid migration, vimentin is involved in protecting the nucleus from compressive forces. Both in carcinoma cells and bone-marrow-derived macrophages, a decrease in vimentin is associated with altered nuclear shape, increased nuclear rupture, and apoptosis upon amoeboid migration (Stankevicins et al. 2019; Lavenus et al., 2020). In the former, also an increase in double-strand breaks was reported (Stankevicins et al. 2019). Although mechanical resilience of IFs during confined migration has only been studied in the context of the nucleus, it is possible that IFs are also involved in mechanical protection of other organelles during migration. Indeed, in mEFs the vimentin network was shown to constrain the diffuse-like movement of organelles, therewith promoting stability (Guo et al. 2013). Whether this has implications for cell migration has yet to be determined. Another question that remains to be answered is whether different IF proteins are equally well suited to protect the nucleus from damage during confined migration, or whether this is a vimentin specific property. GFAP, nestin, and keratins are also known to have a high protein density around the nucleus and are part of the perinuclear cage (Dupin, Sakamoto, and Etienne-Manneville 2011; Sivaramakrishnan et al. 2008). How these proteins affect nuclear envelope integrity during migration is currently unknown.

Conclusions

The diverse roles of IFs in 2D cell migration is well established (Leduc and Etienne-Manneville 2015; Chung, Rotty, and Coulombe 2013). IFs regulate cell polarisation (Dupin, Sakamoto, and Etienne-Manneville 2011), lamellopodia formation (Jiu et al. 2015), FA dynamics (Gregor et al. 2014; Burgstaller et al. 2010; Leube, Moch, and Windoffer 2015), and actomyosin dynamics (Jiu et al. 2017; Costigliola et al. 2017; De Pascalis et al. 2018; Pan et al. 2008), and are therefore an essential component of the cell migration machinery. Although migration through tissues depends on the similar molecular players as in 2D, it has become evident that 3D migration requires a more adaptive response of cells to the chemical and mechanical properties of the environment (van Helvert, Storm, and Friedl 2018; Yamada and Sixt 2019). Based on findings in the literature described in this review, we propose that IFs are particularly relevant for cell migration within a 3D-context. The diversity and mechanoresponsiveness of the protein family allow cells to precisely fine-tune the IF network to adapt to the mechanical characteristics of the tissue environment. IFs further play a dual role during 3D migration, as specific IF proteins both are involved in the regulation of different migration modes, and can protect the cell against migration induced stress due to the unique mechanical properties of the cell. We, therefore, conceptualise IFs as essential contributors to cell-environment mechanoreciprocity and propose that the IF

composition can be tailor-fit to the mechanical needs of a migrating cell. So far, only a number of studies have investigated IF function in 3D migration dynamics. How the different IF proteins respond to alterations in tissue mechanics and how this further affects locomotion in 3D remains to be further elucidated in future research.

Acknowledgements

This study was funded by the Dutch Cancer Society [KWF 101123], and the T and P Bohnenn Foundation (P.R).

References

Aiello, Nicole M., and Yibin Kang. 2019. "Context-Dependent EMT Programs in Cancer Metastasis." *Journal of Experimental Medicine* 216 (5): 1016–26. https://doi.org/10.1084/jem.20181827.

Barnes, J. Matthew, Laralynne Przybyla, and Valerie M. Weaver. 2017. "Tissue Mechanics Regulate Brain Development, Homeostasis and Disease." *Journal of Cell Science* 130 (1): 71–82. https://doi.org/10.1242/jcs.191742.

Bhattacharya, Ramona, Annette M. Gonzalez, Phillip J. DeBiase, Humberto E. Trejo, Robert D. Goldman, Frederick W. Flitney, and Jonathan C.R. Jones. 2009. "Recruitment of Vimentin to the Cell Surface by β3 Integrin and Plectin Mediates Adhesion Strength." *Journal of Cell Science* 122 (9): 1390–1400. https://doi.org/10.1242/jcs.043042.

Block, Johanna, Viktor Schroeder, Paul Pawelzyk, Norbert Willenbacher, and Sarah Köster. 2015. "Biochimica et Biophysica Acta Physical Properties of Cytoplasmic Intermediate Filaments." *BBA - Molecular Cell Research* 1853 (11): 3053–64. https://doi.org/10.1016/j.bbamcr.2015.05.009.

Bordeleau, François, Marie Eve Lapierre, Yunlong Sheng, and Normand Marceau. 2012. "Keratin 8/18 Regulation of Cell Stiffness-Extracellular Matrix Interplay through Modulation of Rho-Mediated Actin Cytoskeleton Dynamics." *PLoS ONE* 7 (6): 1–10. https://doi.org/10.1371/journal.pone.0038780.

Botello-Smith, Wesley M., Wenjuan Jiang, Han Zhang, Alper D. Ozkan, Yi Chun Lin, Christine N. Pham, Jérôme J. Lacroix, and Yun Luo. 2019. "A Mechanism for the Activation of the Mechanosensitive Piezo1 Channel by the Small Molecule Yoda1." *Nature Communications* 10 (1). https://doi.org/10.1038/s41467-019-12501-1.

Burgstaller, Gerald, Martin Gregor, Lilli Winter, and Gerhard Wiche. 2010. "Keeping the Vimentin Network under Control: Cell-Matrix Adhesion-Associated Plectin 1f Affects Cell Shape and Polarity of Fibroblasts." *Molecular Biology of the Cell* 21 (19): 3362–75. https://doi.org/10.1091/mbc.E10-02-0094.

Case, Lindsay B., and Clare M. Waterman. 2015. "Integration of Actin Dynamics and Cell Adhesion by a Three-Dimensional, Mechanosensitive Molecular Clutch." *Nature Cell Biology* 17 (8): 955–63. https://doi.org/10.1038/ncb3191.

Chang, In Ae, Myung-Jin Oh, Min Hee Kim, Seung-Kiel Park, Byung G. Kim, and Uk Namgung. 2012. " Vimentin Phosphorylation by Cdc2 in Schwann Cell Controls Axon Growth via B1-integrin Activation ." *The FASEB Journal* 26 (6): 2401–13. https://doi.org/10.1096/fj.11-199018.

Charrier, Elisabeth E., and Paul A. Janmey. 2016. *Mechanical Properties of Intermediate Filament Proteins. Methods in Enzymology*. 1st ed. Vol. 568. Elsevier Inc. https://doi.org/10.1016/bs.mie.2015.09.009.

Chung, Byung-min, Jeremy D Rotty, and Pierre A Coulombe. 2013. "Networking Galore : Intermediate

Filaments and Cell Migration." *Current Opinion in Cell Biology* 25 (5): 600–612. https://doi.org/10.1016/j.ceb.2013.06.008.

Costigliola, Nancy, Liya Ding, Christoph J. Burckhardt, Sangyoon J. Han, Edgar Gutierrez, Andressa Mota, Alex Groisman, Timothy J. Mitchison, and Gaudenz Danuser. 2017. "Vimentin Fibers Orient Traction Stress." *Proceedings of the National Academy of Sciences of the United States of America* 114 (20): 5195–5200. https://doi.org/10.1073/pnas.1614610114.

Denais, C.M, Gilbert, R. M., Isermann, P., McGregor, A. L., te Lindert, M., Weigelin, B., Davidson, P. M.,. Friedl, P, Wolf, K., Lammerding, J.. 2016. "2016 Nuclear Envelope Rupture and Repair during Cancer Cell Migration." *Science* 352 (6283): 353–58. https://doi.org/10.1126/science.aad7297.

Doyle, Andrew D., Nicole Carvajal, Albert Jin, Kazue Matsumoto, and Kenneth M. Yamada. 2015. "Local 3D Matrix Microenvironment Regulates Cell Migration through Spatiotemporal Dynamics of Contractility-Dependent Adhesions." *Nature Communications* 6. https://doi.org/10.1038/ncomms9720.

Doyle, Andrew D., and Kenneth M. Yamada. 2016. "Mechanosensing via Cell-Matrix Adhesions in 3D Microenvironments." *Experimental Cell Research* 343 (1): 60–66. https://doi.org/10.1016/j.yexcr.2015.10.033.

Dupin, Isabelle, Yasuhisa Sakamoto, and Sandrine Etienne-Manneville. 2011. "Cytoplasmic Intermediate Filaments Mediate Actin-Driven Positioning of the Nucleus." *Journal of Cell Science* 124 (Pt 6): 865–72. https://doi.org/10.1242/jcs.076356.

Eckes, Beate, Dagmar Dogic, Emma Colucci-Guyon, Ning Wang, Andrew Maniotis, Donald Ingber, Alexandra Merckling, et al. 1998. "Impaired Mechanical Stability, Migration and Contractile Capacity in Vimentin Deficient Fibroblasts." *Journal of Cell Science* 111 (13): 1897–1907.

Elosegui-Artola, Alberto, Roger Oria, Yunfeng Chen, Anita Kosmalska, Carlos Pérez-González, Natalia Castro, Cheng Zhu, Xavier Trepat, and Pere Roca-Cusachs. 2016. "Mechanical Regulation of a Molecular Clutch Defines Force Transmission and Transduction in Response to Matrix Rigidity." *Nature Cell Biology* 18 (5): 540–48. https://doi.org/10.1038/ncb3336.

Flitney, Eric W., Edward R. Kuczmarski, Stephen A. Adam, and Robert D. Goldman. 2009. "Insights into the Mechanical Properties of Epithelial Cells: The Effects of Shear Stress on the Assembly and Remodeling of Keratin Intermediate Filaments." *The FASEB Journal* 23 (7): 2110–19. https://doi.org/10.1096/fj.08-124453.

Fortin, Shannon, Marie Le Mercier, Isabelle Camby, Sabine Spiegl-Kreinecker, Walter Berger, Florence Lefranc, and Robert Kiss. 2010. "Galectin-1 Is Implicated in the Protein Kinase c ε/Vimentin-Controlled Trafficking of Integrin-β1 in Glioblastoma Cells." *Brain Pathology* 20 (1): 39–49. https://doi.org/10.1111/j.1750-3639.2008.00227.x.

Friedl, Peter, and Stephanie Alexander. 2011. "Cancer Invasion and the Microenvironment: Plasticity and Reciprocity." *Cell* 147 (5): 992–1009. https://doi.org/10.1016/j.cell.2011.11.016.

Gregor, Martin, Selma Osmanagic-Myers, Gerald Burgstaller, Michael Wolfram, Irmgard Fischer, Gernot Walko, Guenter P. Resch, Almut Jörgl, Harald Herrmann, and Gerhard Wiche. 2014. "Mechanosensing through Focal Adhesion-Anchored Intermediate Filaments." *FASEB Journal* 28 (2): 715–29. https://doi.org/10.1096/fj.13-231829.

Guo, Ming, Allen J. Ehrlicher, Saleemulla Mahammad, Hilary Fabich, Mikkel H. Jensen, Jeffrey R. Moore, Jeffrey J. Fredberg, Robert D. Goldman, and David A. Weitz. 2013. "The Role of Vimentin Intermediate Filaments in Cortical and Cytoplasmic Mechanics." *Biophysical Journal* 105 (7): 1562–68. https://doi.org/10.1016/j.bpj.2013.08.037.

Havel, L S, E R Kline, A M Salgueiro, and A I Marcus. 2015. "Vimentin Regulates Lung Cancer Cell Adhesion through a VAV2–Rac1 Pathway to Control Focal Adhesion Kinase Activity." *Oncogene* 34 (15): 1979–90. https://doi.org/10.1038/onc.2014.123.

Hayakawa, Kimihide, Hitoshi Tatsumi, and Masahiro Sokabe. 2012. "Mechano-Sensing by Actin Filaments and Focal Adhesion Proteins." *Communicative and Integrative Biology* 5 (6): 572–77. https://doi.org/10.4161/cib.21891.

Helvert, Sjoerd van, Cornelis Storm, and Peter Friedl. 2018. "Mechanoreciprocity in Cell Migration." *Nature Cell Biology* 20 (1): 8–20. https://doi.org/10.1038/s41556-017-0012-0.

Herrmann, Harald, and Ueli Aebi. 2016. "Intermediate Filaments: Structure and Assembly." *Cold Spring Harbor Perspectives in Biology* 8 (11). https://doi.org/10.1101/cshperspect.a018242.

Hoffman, Brenton D., Carsten Grashoff, and Martin A. Schwartz. 2011. "Dynamic Molecular Processes Mediate Cellular Mechanotransduction." *Nature* 475 (7356): 316–23. https://doi.org/10.1038/nature10316.

Hu, Jiliang, Yiwei Li, Yukun Hao, Tianqi Zheng, Satish K. Gupta, German Alberto Parada, Huayin Wu, et al. 2019. "High Stretchability, Strength, and Toughness of Living Cells Enabled by Hyperelastic Vimentin Intermediate Filaments." *Proceedings of the National Academy of Sciences of the United States of America* 116 (35): 17175–80. https://doi.org/10.1073/pnas.1903890116.

Humphrey, Jay D., Eric R. Dufresne, and Martin A. Schwartz. 2014. "Mechanotransduction and Extracellular Matrix Homeostasis." *Nature Reviews Molecular Cell Biology* 15 (12): 802–12. https://doi.org/10.1038/nrm3896.

Hunter Lanier, M., Taekyung Kim, and John A. Cooper. 2015. "CARMIL2 Is a Novel Molecular Connection between Vimentin and Actin Essential for Cell Migration and Invadopodia Formation." *Molecular Biology of the Cell* 26 (25): 4577–88. https://doi.org/10.1091/mbc.E15-08-0552.

Hyder, Claire L., Glorianne Lazaro, Joanna W. Pylvänäinen, Maxwell W.G. Roberts, Susanna M. Qvarnström, and John E. Eriksson. 2014. "Nestin Regulates Prostate Cancer Cell Invasion by Influencing the Localisation and Functions of FAK and Integrins." *Journal of Cell Science* 127 (10): 2161–73. https://doi.org/10.1242/jcs.125062.

Ivaska, Johanna, Karoliina Vuoriluoto, Tuomas Huovinen, Ichiro Izawa, Masaki Inagaki, and Peter J. Parker. 2005. "PKCε-Mediated Phosphorylation of Vimentin Controls Integrin Recycling and Motility." *EMBO Journal* 24 (22): 3834–45. https://doi.org/10.1038/sj.emboj.7600847.

Jacquemet, Guillaume, Hellyeh Hamidi, and Johanna Ivaska. 2015. "Filopodia in Cell Adhesion, 3D Migration and Cancer Cell Invasion." *Current Opinion in Cell Biology* 36: 23–31. https://doi.org/10.1016/j.ceb.2015.06.007.

Jiu, Yaming, Jaakko Lehtimäki, Sari Tojkander, Fang Cheng, Harri Jäälinoja, Xiaonan Liu, Markku Varjosalo, John E. Eriksson, and Pekka Lappalainen. 2015. "Bidirectional Interplay between Vimentin Intermediate Filaments and Contractile Actin Stress Fibers." *Cell Reports* 11 (10): 1511–18. https://doi.org/10.1016/j.celrep.2015.05.008.

Jiu, Yaming, Johan Peränen, Niccole Schaible, Fang Cheng, John E. Eriksson, Ramaswamy Krishnan, and Pekka Lappalainen. 2017. "Vimentin Intermediate Filaments Control Actin Stress Fiber Assembly through GEF-H1 and RhoA." *Journal of Cell Science* 130 (5): 892–902. https://doi.org/10.1242/jcs.196881.

Ketema, M., M. Kreft, P. Secades, H. Janssen, and A. Sonnenberg. 2013. "Nesprin-3 Connects Plectin and Vimentin to the Nuclear Envelope of Sertoli Cells but Is Not Required for Sertoli Cell Function in Spermatogenesis." *Molecular Biology of the Cell* 24 (15): 2454–66. https://doi.org/10.1091/mbc.E13-02-0100.

Kim, Hugh, Fumihiko Nakamura, Wilson Lee, Claire Hong, Dolores Pérez-Sala, and Christopher A. McCulloch. 2010. "Regulation of Cell Adhesion to Collagen via β1 Integrins Is Dependent on Interactions of Filamin A with Vimentin and Protein Kinase C Epsilon." *Experimental Cell Research* 316 (11): 1829–44. https://doi.org/10.1016/j.yexcr.2010.02.007.

Kim, Jiyoon, Chansik Yang, Eun Jin Kim, Jungim Jang, Se-Jong Kim, So Min Kang, Moon Gyo Kim,

Hosung Jung, Dongeun Park, and Chungho Kim. 2016. "Vimentin Filaments Regulate Integrin–Ligand Interactions by Binding to the Cytoplasmic Tail of Integrin β3." *Journal of Cell Science* 129 (10): 2030–42. https://doi.org/10.1242/jcs.180315.

Klotzsch, Enrico, Michael L. Smith, Kristopher E. Kubow, Simon Muntwyler, William C. Little, Felix Beyeler, Delphine Gourdon, Bradley J. Nelson, and Viola Vogel. 2009. "Fibronectin Forms the Most Extensible Biological Fibers Displaying Switchable Force-Exposed Cryptic Binding Sites." *Proceedings of the National Academy of Sciences of the United States of America* 106 (43): 18267–72. https://doi.org/10.1073/pnas.0907518106.

Lavenus, Sandrine B., Sara M. Tudor, Maria F. Ullo, Karl W. Vosatka, and Jeremy S. Logue. 2020. "A Flexible Network of Vimentin Intermediate Filaments Promotes Migration of Amoeboid Cancer Cells through Confined Environments." *Journal of Biological Chemistry* 295 (19): 6700–6709. https://doi.org/10.1074/jbc.RA119.011537.

Leduc, Cécile, and Sandrine Etienne-Manneville. 2015. "Intermediate Filaments in Cell Migration and Invasion: The Unusual Suspects." *Current Opinion in Cell Biology* 32: 102–12. https://doi.org/10.1016/j.ceb.2015.01.005.

Leube, Rudolf E., Marcin Moch, and Reinhard Windoffer. 2015. "Intermediate Filaments and the Regulation of Focal Adhesion." *Current Opinion in Cell Biology* 32: 13–20. https://doi.org/10.1016/j.ceb.2014.09.011.

Lin, Yi Chia, Norman Y. Yao, Chase P. Broedersz, Harald Herrmann, Fred C. MacKintosh, and David A. Weitz. 2010. "Origins of Elasticity in Intermediate Filament Networks." *Physical Review Letters* 104 (5): 1–4. https://doi.org/10.1103/PhysRevLett.104.058101.

Liu, Yan Jun, Maël Le Berre, Franziska Lautenschlaeger, Paolo Maiuri, Andrew Callan-Jones, Mélina Heuzé, Tohru Takaki, Raphaël Voituriez, and Matthieu Piel. 2015. "Confinement and Low Adhesion Induce Fast Amoeboid Migration of Slow Mesenchymal Cells." *Cell* 160 (4): 659–72. https://doi.org/10.1016/j.cell.2015.01.007.

McGregor, Alexandra Lynn, Chieh Ren Hsia, and Jan Lammerding. 2016. "Squish and Squeeze - the Nucleus as a Physical Barrier during Migration in Confined Environments." *Current Opinion in Cell Biology* 40: 32–40. https://doi.org/10.1016/j.ceb.2016.01.011.

Mendez, M. G., D. Restle, and P. A. Janmey. 2014. "Vimentin Enhances Cell Elastic Behavior and Protects against Compressive Stress." *Biophysical Journal* 107 (2): 314–23. https://doi.org/10.1016/j.bpj.2014.04.050.

Mendez, Melissa G, Shin-Ichiro Kojima, and Robert D Goldman. 2010. "Vimentin Induces Changes in Cell Shape, Motility, and Adhesion during the Epithelial to Mesenchymal Transition." *FASEB Journal : Official Publication of the Federation of American Societies for Experimental Biology* 24 (6): 1838–51. https://doi.org/10.1096/fj.09-151639.

Murray, Maria E., Melissa G. Mendez, and Paul A. Janmey. 2014. "Substrate Stiffness Regulates Solubility of Cellular Vimentin." *Molecular Biology of the Cell* 25 (1): 87–94. https://doi.org/10.1091/mbc.E13-06-0326.

Omary, M Bishr. 2009. "Review Series Introduction ' IF-Pathies ': A Broad Spectrum of Intermediate Filament – Associated Diseases." *Journal of Clinical Investigation* 119 (7): 1756–62. https://doi.org/10.1172/JCI39894.1756.

Pan, Y., R. Jing, A. Pitre, B. J. Williams, and O. Skalli. 2008. "Intermediate Filament Protein Synemin Contributes to the Migratory Properties of Astrocytoma Cells by Influencing the Dynamics of the Actin Cytoskeleton." *The FASEB Journal* 22 (9): 3196–3206. https://doi.org/10.1096/fj.08-106187.

Pascalis, Chiara De, and Sandrine Etienne-Manneville. 2017. "Single and Collective Cell Migration: The Mechanics of Adhesions." *Molecular Biology of the Cell* 28 (14): 1833–46. https://doi.org/10.1091/mbc.E17-03-0134.

Pascalis, Chiara De, Carlos Pérez-González, Shailaja Seetharaman, Batiste Boëda, Benoit Vianay, Mithila Burute, Cécile Leduc, Nicolas Borghi, Xavier Trepat, and Sandrine Etienne-Manneville. 2018. "Intermediate Filaments Control Collective Migration by Restricting Traction Forces and Sustaining Cell–Cell Contacts." *The Journal of Cell Biology* 2017 (9), jcb.201801162. https://doi.org/10.1083/jcb.201801162.

Paszek, Matthew J., and Valerie M. Weaver. 2004. "The Tension Mounts: Mechanics Meets Morphogenesis and Malignancy." *Journal of Mammary Gland Biology and Neoplasia* 9 (4): 325–42. https://doi.org/10.1007/s10911-004-1404-x.

Patteson, Alison E., Katarzyna Pogoda, Fitzroy J. Byfield, Kalpana Mandal, Zofia Ostrowska-Podhorodecka, Elisabeth E. Charrier, Peter A. Galie, et al. 2019. "Loss of Vimentin Enhances Cell Motility through Small Confining Spaces." *Small* 15 (50), 1903180: 1–10. https://doi.org/10.1002/smll.201903180.

Patteson, Alison E., Amir Vahabikashi, Katarzyna Pogoda, Stephen A. Adam, Kalpana Mandal, Mark Kittisopikul, Suganya Sivagurunathan, Anne Goldman, Robert D. Goldman, and Paul A. Janmey. 2019. "Vimentin Protects Cells against Nuclear Rupture and DNA Damage during Migration." *The Journal of Cell Biology* 218 (12), jcb.201902046. https://doi.org/10.1083/jcb.201902046.

Petrie, Ryan J., Hyun Koo, and Kenneth M. Yamada. 2014. "Generation of Compartmentalized Pressure by a Nuclear Piston Governs Cell Motility in a 3D Matrix." *Science* 345 (6200): 1062–65. https://doi.org/10.1126/science.1256965.

Pogoda, Katarzyna, Robert Bucki, Fitzroy J. Byfield, Katrina Cruz, Tongkeun Lee, Cezary Marcinkiewicz, and Paul A. Janmey. 2017. "Soft Substrates Containing Hyaluronan Mimic the Effects of Increased Stiffness on Morphology, Motility, and Proliferation of Glioma Cells." *Biomacromolecules* 18 (10): 3040–51. https://doi.org/10.1021/acs.biomac.7b00324.

Pogoda, Katarzyna, Likang Chin, Penelope C. Georges, Fitzroy J. Byfield, Robert Bucki, Richard Kim, Michael Weaver, Rebecca G. Wells, Cezary Marcinkiewicz, and Paul A. Janmey. 2014. "Compression Stiffening of Brain and Its Effect on Mechanosensing by Glioma Cells." *New Journal of Physics* 16. https://doi.org/10.1088/1367-2630/16/7/075002.

Qin, Zhao, Laurent Kreplak, and Markus J. Buehler. 2009. "Hierarchical Structure Controls Nanomechanical Properties of Vimentin Intermediate Filaments." *PLoS ONE* 4 (10). https://doi.org/10.1371/journal.pone.0007294.

Rizki, Aylin, Joni D. Mott, and Mina J. Bissell. 2007. "Polo-like Kinase 1 Is Involved in Invasion through Extracellular Matrix." *Cancer Research* 67 (23): 11106–10. https://doi.org/10.1158/0008-5472.CAN-07-2348.

Rotty, Jeremy D., and Pierre A. Coulombe. 2012. "A Wound-Induced Keratin Inhibits Src Activity during Keratinocyte Migration and Tissue Repair." *Journal of Cell Biology* 197 (3): 381–89. https://doi.org/10.1083/jcb.201107078.

Schoumacher, Marie, Robert D. Goldman, Daniel Louvard, and Danijela M. Vignjevic. 2010. "Actin, Microtubules, and Vimentin Intermediate Filaments Cooperate for Elongation of Invadopodia." *Journal of Cell Biology* 189 (3): 541–56. https://doi.org/10.1083/jcb.200909113.

Shabbir, Shagufta H., Megan M. Cleland, Robert D. Goldman, and Milan Mrksich. 2014. "Geometric Control of Vimentin Intermediate Filaments." *Biomaterials* 35 (5): 1359–66. https://doi.org/10.1016/j.biomaterials.2013.10.008.

Sharma, Poonam, Zachary T. Bolten, Diane R. Wagner, and Adam H. Hsieh. 2017. "Deformability of Human Mesenchymal Stem Cells Is Dependent on Vimentin Intermediate Filaments." *Annals of Biomedical Engineering* 45 (5): 1365–74. https://doi.org/10.1007/s10439-016-1787-z.

Sibony-Benyamini, Hadas, and Hava Gil-Henn. 2012. "Invadopodia: The Leading Force." *European Journal of Cell Biology* 91 (11–12): 896–901. https://doi.org/10.1016/j.ejcb.2012.04.001.

Sivaramakrishnan, Sivaraj, James V. DeGiulio, Laszlo Lorand, Robert D. Goldman, and Karen M. Ridge.

2008. “Micromechanical Properties of Keratin Intermediate Filament Networks.” *Proceedings of the National Academy of Sciences of the United States of America* 105 (3): 889–94. https://doi.org/10.1073/pnas.0710728105.

Stankevicins, Luiza Da Cunha, Marta Urbanska, Daniel AD. Flormann, Emmanuel Terriac, Zahra Mostajeran, Annica K.B. Gad, Fang Cheng, John E. Eriksson, and Franziska Lautenschläger. 2019. “Vimentin Provides the Mechanical Resilience Required for Amoeboid Migration and Protection of the Nucleus.” *BioRxiv*, 720946. https://doi.org/10.1101/720946.

Sutoh Yoneyama, Mihoko, Shingo Hatakeyama, Tomonori Habuchi, Takamitsu Inoue, Toshiya Nakamura, Tomihisa Funyu, Gerhard Wiche, Chikara Ohyama, and Shigeru Tsuboi. 2014. “Vimentin Intermediate Filament and Plectin Provide a Scaffold for Invadopodia, Facilitating Cancer Cell Invasion and Extravasation for Metastasis.” *European Journal of Cell Biology* 93 (4): 157–69. https://doi.org/10.1016/j.ejcb.2014.03.002.

Swift, Joe, Irena L. Ivanovska, Amnon Buxboim, Takamasa Harada, P. C.Dave P. Dingal, Joel Pinter, J. David Pajerowski, et al. 2013. “Nuclear Lamin-A Scales with Tissue Stiffness and Enhances Matrix-Directed Differentiation.” *Science* 341 (6149). https://doi.org/10.1126/science.1240104.

Szeverenyi, Ildiko, Andrew J. Cassidy, Wang Chung Cheuk, Bernett T.K. Lee, John E.A. Common, Stephen C. Ogg, Huijia Chen, et al. 2008. “The Human Intermediate Filament Database: Comprehensive Information on a Gene Family Involved in Many Human Diseases.” *Human Mutation* 29 (3): 351–60. https://doi.org/10.1002/humu.20652.

Trepat, Xavier, Zaozao Chen, and Ken Jacobson. 2012. “Cell Migration.” *Comprehensive Physiology* 2 (4): 2369–92. https://doi.org/10.1002/cphy.c110012.

Wang, Wei, Alba Zuidema, Lisa Te Molder, Leila Nahidiazar, Liesbeth Hoekman, Thomas Schmidt, Stefano Coppola, and Arnoud Sonnenberg. 2020. “Hemidesmosomes Modulate Force Generation via Focal Adhesions.” *The Journal of Cell Biology* 219 (2). https://doi.org/10.1083/jcb.201904137.

Wang, Yiqun, Yi Lu, Jinkang Gong, and Yuan Yao. 2019. “Electrospun Nanofiber Regulates Assembly of Keratin and Vimentin Intermediate Filaments of PANC-1 Pancreatic Carcinoma Cells.” *Materials Science and Engineering C* 96 (October 2018): 616–24. https://doi.org/10.1016/j.msec.2018.11.072.

Wolf, Katarina, Mariska te Lindert, Marina Krause, Stephanie Alexander, Joost te Riet, Amanda L. Willis, Robert M. Hoffman, Carl G. Figdor, Stephen J. Weiss, and Peter Friedl. 2013. “Physical Limits of Cell Migration: Control by ECM Space and Nuclear Deformation and Tuning by Proteolysis and Traction Force.” *Journal of Cell Biology* 201 (7): 1069–84. https://doi.org/10.1083/jcb.201210152.

Yamada, Kenneth M., and Michael Sixt. 2019. “Mechanisms of 3D Cell Migration.” *Nature Reviews Molecular Cell Biology*, no. Box 1. https://doi.org/10.1038/s41580-019-0172-9.

CHAPTER 3

Determining glioma cell invasion and proliferation in *ex vivo* organotypic brain slices using whole-mount immunostaining and tissue clearing

Jessy V. van Asperen[1], Emma J. van Bodegraven[1], Pierre A.J.T. Robe[2], Elly M. Hol[1]

[1] Department of Translational Neurosciences, UMC Utrecht Brain Center, University Medical Center Utrecht, Utrecht University, 3584 CG Utrecht, The Netherlands
[2] Department of Neurology and Neurosurgery, University Medical Center Utrecht Brain Center, Utrecht University, 3584 CG Utrecht, The Netherlands

Manuscript in preparation
(lay-out according to STAR protococl, Cell Press)

Abstract

The *ex vivo* organotypic brain slice invasion model is commonly used to study the growth dynamics of gliomas, primary brain tumours that are known for their invasive behaviour (Claes, Idema and Wesseling, 2007; Pencheva *et al.*, 2017). Here we describe a protocol where the *ex vivo* organotypic slice invasion model is combined with whole-mount immunostaining, tissue clearing and 3D reconstruction, to visualise and quantify the invasion of glioma cells. In addition, we describe a method to determine the proliferation rate of the cells within this model.

Graphical Abstract

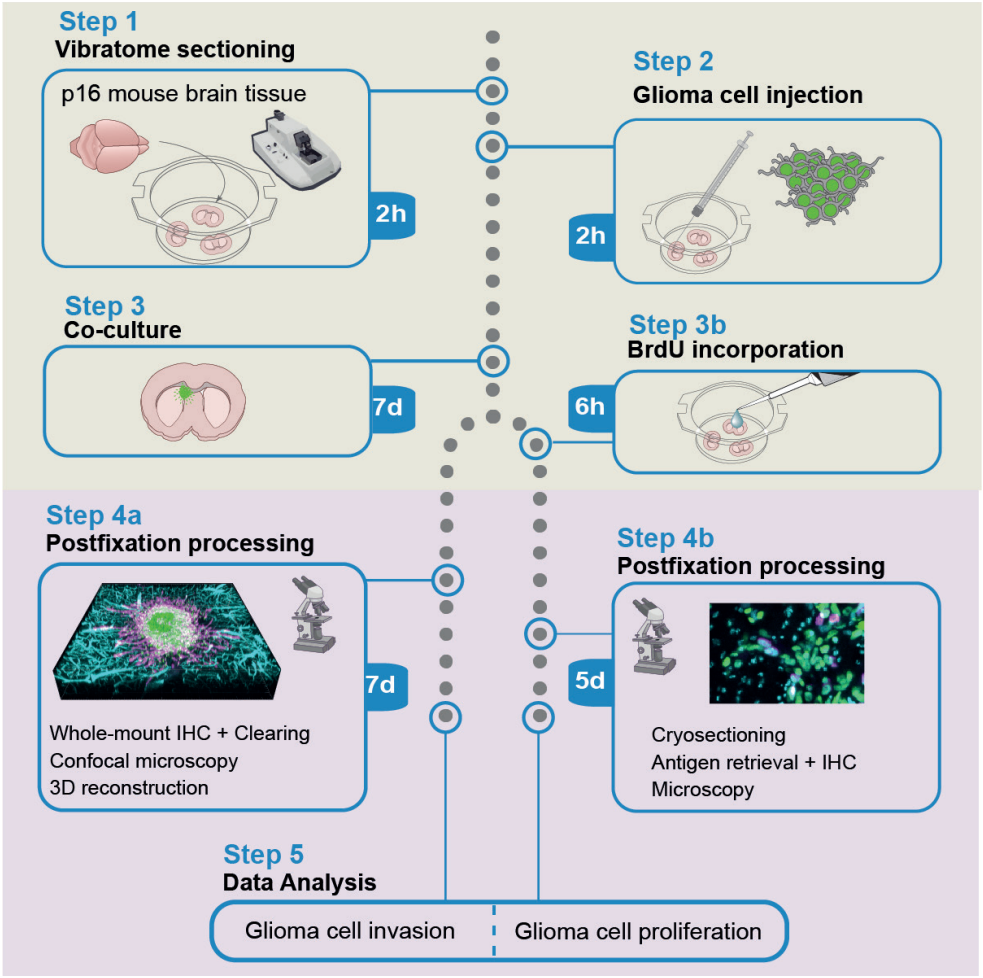

Before You Begin

This protocol requires the use of mouse brain tissue. All animal experiments should be performed following relevant governmental and institutional guidelines. All experiments described here were approved by the animal welfare body Utrecht and the Central Authority for Scientific Experiments on Animals of the Netherlands (CCD, license: AVD115002016532).

Generation and expansion of fluorescently labelled glioma cell lines

Timing: 10 days

The protocol and analysis steps described in this paper are based on U251-MG cells of which the nuclei are fluorescently labelled with H2B-mNeonGreen and/ or H2B-mCherry. We have also used this protocol successfully with other glioma cell lines such as GL261, U87, and primary glioblastoma cell lines. Cytosolic- or membrane-bound fluorophores can also be used to visualise the glioma cells, however, the quantification steps described in this protocol are optimised for nuclear labelling. We do not recommend the use of fluorescent dyes for this protocol, as the fluorescent dye is lost during the clearing steps (steps 41, 42).

1. Plate 1 x 10^6 cells in a 6-well plate (9.6 cm^2)
2. Twenty-four hours after plating, add lentivirus-H2B-mNeonGreen or lentivirus-H2B-mCherry to the cells with a multiplicity of infection (MOI) of 1 to 10

CRITICAL: Transduction of cells with lentiviruses should be performed in a biosafety level 2 certified laboratory.

3. When the cells reach 70% confluency, passage the cells to two new wells and select the labelled cells with antibiotics, dependent on the resistance gene present in the lentivirus construct. In our experiments, we used 1 µg/mL puromycin to select the H2B-mNeonGreen positive cells and 10 µg/mL blasticidin to select H2B-mCherry positive cells.

Note: The concentration of the antibiotic is dependent on the cell line and antibiotic batch. Determine the concentration needed for selection beforehand with an antibiotic kill curve.

4. Expand the selected population in a T25 or T75 flask before the start of the experiment.

Note: When transduced cells are cultured for longer periods of time, non-transduced

cells can slowly take over and decrease the percentage of fluorescently labelled cells. To avoid this, adding a low concentration of antibiotics to the standard culture medium is recommended. We added 1/5th of the concentration used for the selection of cells to the culture medium for maintenance.

Preparation of equipment and materials for mouse brain collection and vibratome slicing

Timing: 30 minutes

Right before the start of the experiment, perform the following preparations:

5. Prepare the culture plates for collection of the *ex vivo* organotypic brain slices
    a. Add 1.5 mL recovery medium with 25% fetal bovine serum (FBS) to a 6-well plate.
    b. Place cell culture inserts into the recovery medium with 25% FBS using a forceps.
    c. Place the plate at 37 °C to preheat in a humidified 5% CO_2 incubator until further use.

Note: optionally, the *ex vivo* organotypic brain slices can be collected first in cell culture inserts placed in recovery medium without FBS to avoid exposure of the recovery medium with 25% FBS to the open air. In this case, prepare an additional 6-well plate where the 25% FBS of the recovery medium is replaced by DMEM/F-12 medium.

6. Transfer 100 mL artificial cerebrospinal fluid (aCSF) to a sterile flask and keep it on ice.
7. Transfer 25 mL aCSF to a 50 mL tube for collection of the mouse brain tissue.
8. Clean the vibratome and additional equipment.
    a. Clean the vibratome and working space around it with 70% ethanol.
    b. Clean the vibratome collection container and place it in the vibratome.
    c. Fill the space around the vibratome container with ice.
    d. Sterilise the vibratome equipment (razor blades, platform, brushes, and spoons) by incubating it in the vibratome bucket with a layer of 70% ethanol until further use.

Optional: The vibratome can be placed in a laminar flow cabinet to reduce the risk of contamination with microbes. This is however not required when aseptic techniques are applied.

Key Resources Table

Reagent or resource	Source	Identifier
Antibodies		
Chicken anti-vimentin (dilution 1:1500)	Chemicon	AB5733, RRID: AB_11212377
Rabbit anti-laminin (dilution 1:1000)	Sigma Aldrich	L9393, RRID: AB_477163
Rat anti-BrdU (dilution 1:500)	Bio-Rad	OBT0030S, RRID: AB_609570
Donkey anti-chicken Alexa Fluor Cy5 (1:1000)	Jackson Immuno Research	703-175-155, RRID: AB_2340365
Donkey anti-rabbit Alexa Fluor Cy3 (1:1000)	Jackson ImmunoResearch Labs	711-166-152, RRID: AB_2313568
Donkey anti-rabbit Alexa Fluor 647 (1:1000)	Jackson ImmunoResearch Labs	711-606-152, RRID: AB_2340625
Chemicals, peptides, and recombinant proteins		
DMEM/F-12	Gibco	11320033
DMEM/F-12 GlutaMAX™ supplement	Gibco	10565018
L-Glutamine	Gibco	25030081
Phosphate buffered saline (PBS) 10x	Gibco	14200-067
Penicillin-Streptomycin (10,000 U/mL)	Gibco	15140122
Puromycin Dihydrochloride	Gibco	A1113803
Fetal bovine serum (FBS)	Biowest	S181H
Blasticidin	InvivoGen	ant-bl-1
Recombinant human EGF	Peprotech	AF-100-15-A
Recombinant human FGF-basic	Peprotech	AF-100-18B
5-Bromo-2'-deoxyridine	Sigma-Aldrich	B5002-1G
HEPES (238.30 g/mol)	Sigma-Aldrich	7365-45-9
Sodium azide (65.01 g/mol)	Sigma-Aldrich	S2002-100G
Saponin	Sigma-Aldrich	47036
D-Glucose (198.17 g/mol)	Sigma Aldrich	16301-1KG
Boric acid (61.83 g/mol)	Merck KGaA	1001650500
NaHCO3 (84.01 g/mol)	Merck KGaA	144-55-8
NaH_2PO_4 (137.99 g/mol)	Merck KGaA	10049-21-5
$MgCl_2$ (203.30)	Merck KGaA	7791-18-6
$CaCl_2$ (147.02)	Merck KGaA	10035-04-8
Glycerol	Merck KGaA	55-81-5
Paraformaldehyde	Merck KGaA	1.04005.1000
Hydrochloric acid fuming 37%	Merck KGaA	100317
2-Methylbutan	Carl Roth	3927.1
KCL (74.55 g/mol)	VWR chemicals	7447-40-7
Gelatin	VWR Chemicals	24360.233
Thimoresal	Gerbu Biotechnik GmbH	1031.0010
Normal Donkey Serum	Jackson ImmunoResearch	RRID: AB_2337258
Triton X-100	Roche Diagnostics GmbH	40139421
Tissue Tek	Sakura	4583
RapiClear 1.47	SunJin Lab. Co	#RC147001
Hoechst 33528	Thermo Fischer Scientific	H3569
FluorSave™ Reagent	Millipore	345789

Experimental models: Cell lines		
U251-MG	ECACC	09063001
Experimental models: Organisms/strains		
C57BL6J	Charles Rivers Laboratories	Strain code 027
Recombinant DNA		
pLenti6-H2B-mCherry	Addgene	#89766
pLV-H2B-mNeonGreen	Laboratory of Hugo Snippert (Drost *et al.*, 2015)	N/A
Software and algorithms		
ImageJ (version 1.53c)	N/A	RRID: SCR_003070
Imaris 8.4 – 9.4	Bitplane	RRID:SCR_007370, https://Imaris.oxinst.com/
Other		
Falcon® Permeable Support for 6-well Plate with 1.0 µm Transparent PET Membrane, Sterile	Corning	353102
Corning 500 mL Bottle Top Vacuum Filter, 0.22 µm	Merck	CLS431117
Corning 50 mL centrifuge tubes	Merck	CLS430829-500EA
Scott Duran Flask 1L	VWR	215-1595
Scott Duran Flask 100 mL	VWR	215-1592
Forceps	Fine Science Tools	11080-02
Fine Scissors	Fine Science Tools	14184-09
Surgical Scissors	Fine Science Tools	14101-14
Loctite 401 glue	Henkel Adhesives	N/A
Stainless Steel Blade	Campden Instruments Limited	752/1/SS
Surgical Blade	BBraun	BB510
Hamilton 0.5 uL syringe model 7000.5 KH	Hamilton	86250
Micromanipulator model MM-3	Narishige group	N/A
GJ-8 magnetic stand	Narishige group	N/A
Iron plate	Narishige group	N/A
Leica MS5 stereomicroscope	Leica Microsystems	N/A
Horizontal orbital shaker, benchmark incu-shaker mini	Benchmark Scientific Inc, USA	H1001-M
iSpacers	SunJin Lab co.	#IS002
Peel-A-way embedding moulds	Sigma-Aldrich	E6032
VT1000S Vibratome	Leica Biosystems	1404723512
Leica CM 1950 cryostat	Leica Biosystems	**1491950C**
LSM 880 confocal microscope	Zeiss	N/A
AxioVert A1 epifluorescent microscope	Zeiss	N/A
AxioScope A1 epifluorescent microscope	Zeiss	N/A

Materials and Equipment

Artificial cerebrospinal fluid (aCSF)

Reagent	Final Concentration	Amount
HEPES	10 mM	2.84 g
$NaHCO_3$	21 mM	1.76 g
NaH_2PO_4	1.2 mM	164 µg
KCl	2.5 mM	185 µg
$MgCl_2$	2 mM	410 µg
$CaCl_2$	2 mM	220 µg
D-glucose	5 mM	999 µg
Glycerol	250 mM	25 mL
ddH_2O	N/A	Up to 1 L
Total	**N/A**	**1 L**

After dissolving the chemicals in 800 µL ddH2O, measure and adjust the pH and fill up to 1 L. Afterwards, filter using a 0.22 µm bottle-top vacuum filter and store the aCSF at 4 °C. aCSF can be used until precipitates start to form.

Recovery medium

Reagent	Final Concentration	Amount
HEPES	5 mM	0.297 g
$NaHCO_3$	0.7% (w/v)	1.76 g
Penicillin/streptavidin	1% (v/v)	2.5 mL
Fetal bovine serum*	25% (v/v)	62.5 mL*
DMEM/F-12	N/A	185 mL
Total	**N/A**	**250 mL**

Dissolve the HEPES and NaHCO3 in 185 mL DMEM/F-12, filter through a 0.22 µm bottle-top vacuum filter. Add penicillin/streptavidin and store at 4 °C for weeks.
*Prepare a stock of recovery medium without FBS and add fresh FBS to the volume needed for the experiment.

Neural Stem Cell (NSC) medium

Reagent	Final Concentration	Amount
DMEM/F-12 with GlutaMAX™	N/A	14.82 mL
Penicillin/streptavidin	1% (v/v)	150 uL
EGF (10 µg/mL)	10 ng/mL	15 µL
FGF (10 µg/mL)	10 ng/mL	15 µL
Total	**N/A**	**15 mL**

After adding the EGF and FGF, the medium should be stored at 4 °C and be used within a week. Adjust the volume to the amount needed for a 1-week experiment.

PBS-Gelatin-Triton X-100 (PBS-GT) buffer

Reagent	Final Concentration	Amount
Gelatin	0.2% (w/v)	0.5 g
Triton-X-100	0.5% (v/v)	1.25 mL
Thimerosal	0.01% (w/v)	25 ug
PBS (10x, pH 7.4)	1x	25 mL
ddH_2O	N/A	up to 250 mL
Total	**N/A**	**250 mL**

Buffer can be stored for 2 weeks at 4 °C

CRITICAL: Thimerosal contains mercury and should be handled with extra caution. Solutions containing this compound should be handled in the fume hood. Thimerosal can be replaced by sodium azide (0.01%), this chemical is also toxic and should be handled in the fume hood.

4% PFA in PBS (pH 7.4)

Reagent	Final Concentration	Amount
Paraformaldehyde	4%	4 g
PBS (10x, pH 7.4)	1x	10 mL
ddH_2O	N/A	up to 100 mL
Total	**N/A**	**100 mL**

Dissolve the paraformaldehyde in 50 mL ddH2O with 1 M NaOH by heating the solution up to 60 °C. Add 10x PBS, let the solution cool down and adjust the pH to 7.4. Filter the solution, aliquot and freeze the aliquots at -20 °C for long-term storage. Avoid repeated thaw-freeze cycles.

Blocking buffer

Reagent	Final Concentration	Amount
10% Triton-X-100 in PBS	0.5% (v/v)	0.5 mL
Normal Donkey Serum	5.0% (v/v)	0.5 mL
PBS (10x, pH 7.4)	1x	1 mL
ddH_2O	N/A	8 mL
Total	**N/A**	**10 mL**

Store at 4 °C or -20 °C for 1 week or long-term storage, respectively.

2N HCL

Reagent	Final Concentration	Amount
Hydrochloric acid (37%)	2 mol/L	16.6 mL
ddH_2O	N/A	83.4 mL
Total	**N/A**	**250 mL**

Solution is stable at room temperature.

0.1M Borate Buffer (pH 8.5)

Reagent	Final Concentration	Amount
Boric acid	0.1M	6.18 g
ddH_2O	N/A	up to 100 mL
Total	**N/A**	**1 L**

Dissolve in 800 mL and adjust the pH to 8.5. The solution is stable at room temperature.

Step-by-Step Method Details

Dissection of postnatal day 16 mouse brains

Timing: 30 minutes

1. Decapitate a 16 days-old C57BL/6 mouse using scissors.
2. Peel away the skin and meninges of the head until the skull becomes visible.
3. Place ultra-fine scissors in the spinal cord and cut until the cerebellum is reached.
4. Carefully peel away the skull meninges using tweezers until the brain is uncovered.
5. With ultra-fine scissors make a cut rostral of the olfactory bulb to disconnect the olfactory nerves.
6. Place forceps caudally under the brain and transfer the brain from the skull into a 50 mL tube containing 25 mL aCSF and place it on ice.
7. Repeat the procedure for the other mice when multiple brains are needed.

Preparation of *ex vivo* organotypic brain slices using the vibratome

Timing: 45 minutes

The *ex vivo* organotypic brain slice protocol described below is adapted from Pencheva et al., 2017.

8. Take the vibratome equipment out of the bucket with 70% ethanol and let everything air-dry.
9. Pour the aCSF with the brain(s) into a sterile Petri dish and remove the olfactory bulb and cerebellum using a sterile razor blade.

10. Place the brain on the razor blade with the rostral part facing upward and remove residual aCSF from the caudal part by lightly touching the brain-blade interface with a paper tissue.
11. Place a drop of glue on the vibratome platform and transfer the brain to the glue with the rostral part facing up (Fig. 1a).

Note: two additional brains can be transferred to the same plate to slice three brains simultaneously. In this case, make sure that all brains are aligned and oriented in the same direction.

12. Place the vibratome platform with the mounted brain tissue into the vibratome container and fixate.
13. Fill the container with cold aCSF and place a filter tip connected to CO_2 into the bucket to carbonate the aCSF.
14. Turn on the vibratome, set the frequency to 7 Hz and the slicing thickness to 350 µm.

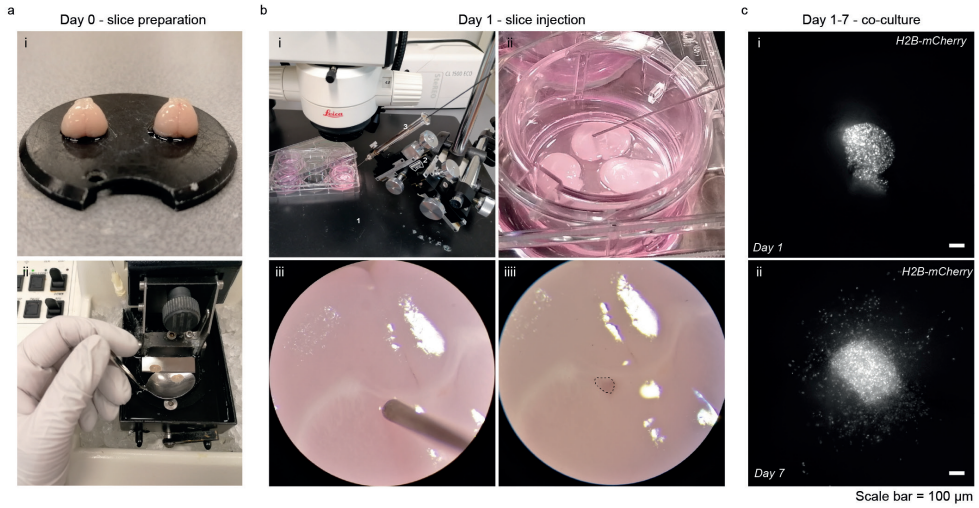

Figure 1. Preparation and injection of ex vivo organotypic slices. (a) Example images of slice preparation on day 0. i. Dissected mouse brains in the correct orientation on the vibratome platform. ii. The vibratome set-up during tissue collection. (b) Injection of slices using a micromanipulator. i. Image of the experimental set-up, with a magnetic stand (1), a micromanipulator (2), and a Hamilton syringe (3). ii, iii. Zoom-in on an organotypic brain slice in a cell-culture insert with the Hamilton syringe inserted into the lateral ventricle of the brain slice. iiii. Image of the organotypic brain slice after injection with the glioma cells. The dotted line indicates the location of the injected cells. (c) Epifluorescent images of H2B-mCherry expressing injected U251-MG cells on day 1 (i) and day 7 (ii) in culture. Images are taken with an inverted epifluorescent microscope. Cells in focus are migrating at the membrane/ brain slice interface. Scale bar = 100 µm

15. Start trimming off the rostral region of the brain and stop when the lateral ventricles become visible.
16. Take the culture plate with the cell inserts out of the incubator and start collecting tissue with visible lateral ventricles. To collect the tissue, place a sterile spoon underneath the blade and carefully transfer the tissue to the spoon using a sterile brush (Fig. 1a). Pour off most of the aCSF and transfer the brain slice to a cell culture insert.
17. After collecting four slices per insert, remove the residual aCSF using a P1000 pipette with filter tip and take the plate to a cell culture laminar flow cabinet.
18. Wash the slices once with sterile PBS.

Optional: When the slices are collected in recovery medium without FBS, transfer the cell culture inserts to a culture plate with recovery medium + 25% FBS after the PBS wash.

19. Place the plate with cell culture inserts containing the brain slices in recovery medium + 25% FBS into a 37 ˚C with 5% CO_2 incubator for recovery of the brain slices and culture overnight.

Injection of glioma cell lines into the organotypic brain slices

Timing: 2 - 4h

One day after the generation of the organotypic brain slices, glioma cell mixes can be prepared for injection into the *ex vivo* organotypic brain slices (Video 1). The timing needed for this step is dependent on the number of cell lines and the number of brain slices that will be used in the experiment.

20. Passage the cells used for the experiment with standard passaging methods.
21. Make cell suspensions of 25 000 cells/ µL. A minimal volume of 5 µL (125 000 cells) is needed.

Optional: The invasive and proliferative properties of the experimental group can be directly compared to an internal control group. When choosing for this experimental set-up, mix cells of the internal control cells with fluorophore A one to one with the experimental group expressing fluorophore B.

22. Prepare a 6-well plate with 1 mL neural stem cell (NSC)-medium per insert.
23. Take the cell culture inserts with *ex vivo* organotypic brain slices from the incubator. Dip the inserts two times in 1 mL PBS. Remove the remaining recovery medium from the inserts and transfer the inserts to the 6-well plate with NSC-medium.

24. Set up the micromanipulator at the dissection microscope and fixate the Hamilton syringe in the micromanipulator. Clean your working space with 70% ethanol. Clean the syringe by washing it first with acetone (1x) and, subsequently, multiple times with 70% ethanol. Finally, rinse the syringe with PBS.
25. Place the 6-well plate with the organotypic brain slices under the dissection microscope and place the micromanipulator in such a way that the syringe is in the centre of view at 4x magnification when touching the organotypic brain slices (Fig. 1b).
26. Mix the cell suspension with a normal pipette and directly take up 0.5 µL with the syringe.
27. Using the micromanipulator, move the syringe to the brain slice. Slowly insert the syringe +/- 50 µm into the lateral ventricle at an angle of approximately 45 ° and afterwards retract it 40 µm out of the tissue. Inject the cell suspension into the lateral ventricle at low speed (+/- 30 seconds per 0.5 µL), while preventing the cells to flush over the tissue (Fig. 1b, Video 1). Slowly take out the syringe after injection.
28. Rinse the syringe with PBS multiple times before injecting the next cell line.
29. After finishing the injections, rinse the syringe with PBS, 70% ethanol and acetone.
30. Inspect the organotypic brain slices with a fluorescent microscope to check the presence of fluorescently labelled cells (Fig. 1c). Afterwards, place the culture plate in the incubator to culture the *ex vivo* organotypic brain slices.

Culturing and fixation of the *ex vivo* organotypic brain slices

Timing: 7d

31. Replace the medium of the injected organotypic brain slices once every 2 or 3 days by transferring the inserts into a new well with 1 mL of fresh NSC-medium.
32. Wash the cell culture inserts containing the brain slices once with PBS and fixate in 2 mL 4% PFA in PBS overnight.
33. The next day, wash the inserts 3 times with PBS and store at 4 °C until further use

Note : The migratory patterns of the glioma cells can be followed during the culturing period using epifluorescence microscopy (Fig. 1c). Note however that the cells that can be observed with an inverted microscope are the cells that migrate on the membrane rather than into the tissue. To visualise and analyse the cells migrating into the tissue, follow the steps described below.

Pause point: The fixated organotypic brain slices can be stored in PBS for multiple weeks before further processing. Anti-fungal agents can be added when the slices are not used within a month.

Whole-mount immunostaining and tissue clearing

Timing: 6d

Whole-mount immunostaining methods can be used to analyse the 3D invasion pattern of the glioma cells and to visualise glioma cell features or mouse brain structures, like the glioma cell cytoskeleton or blood vessels. Below, we describe a co-immunostaining for the extracellular matrix (ECM) protein laminin and the intermediate filament protein vimentin. At the injection site, glioma cells deposit extracellular matrix proteins, which allows for distinction between the tumour core and invasive front based on laminin staining. Vimentin can be used to visualise the larger cellular processes of the glioma cells. The described protocol is an adaptation of the whole-mount immunostaining protocol developed by (Belle et al., 2014) and the RapiClear 1.47 clearing method developed by the SunJin lab (www.sunjinlab.com, n.d.; Bekkouche *et al.*, 2020).

34. Cut the membrane from the inserts around the individual brain slices using a scalpel and transfer it to a 24-well plate.
35. Permeabilise the brain slices in 2% PBST (2% Triton-X100 in PBS) at room temperature for 4 hours.
36. Add blocking buffer (PBS-GT, materials and methods) to the brain slices and incubate at room temperature overnight.

CRITICAL: The PBS-GT contains thimerosal (a mercury solution) and should be handled with caution.

37. Add primary antibodies to PBS-GT with 0.1% saponin, add the mix to the brain slices, and incubate at 37 ˚C on a horizontal shaker (70 rpm) for 72 hours. Here we used rabbit anti-laminin (1:1 000) and chicken anti-vimentin (1:1 500) antibodies.
38. Wash the brain slices 6 times with PBS-T (0.5% Triton-X100 in PBS) for 1 hour.
39. Add secondary antibodies to PBS-GT with 0.1% saponin, add to the brain slices, and incubate at 37 ˚C on a horizontal shaker (70 rpm) for 24 hours. Protect from light by covering the well plate with aluminium foil. Here we used donkey anti-rabbit-Cy3 and donkey anti-chicken-AF647 secondary antibodies
40. Wash the brain slices 6 times with PBS-T for 1 hour (total of 6 hours).
41. Pre-warm RapiClear 1.47 solution at 37 ˚C and add 300 µL to each brain slice. Place on a horizontal shaker at 37 ˚C and incubate for a minimum of 45 minutes until the brain slice is transparent. The used Rapiclear solution can be

reused maximally three times.

42. Place an iSpacer (Fig. 2a) on a glass microscopy slide and transfer the brain slices to the microscopy slide. Multiple brain slices can be mounted on one glass microscopy slide. Fill the iSpacer with fresh RapiClear solution and seal with a coverslip. Use clear nail polish to seal the edges of the coverslip. Store the microscopy slides at 4 ˚C until further use.

Confocal imaging and image processing

Timing: 1h/ brain slice

43. Place the microscopy slide with the cleared brain slices on the stage of a confocal microscope and navigate to the region of interest.
44. We used a 10x objective to capture all tumour cells and to create a 3D reconstruction at the macroscopic level. Higher magnification can be used when smaller parts of the tumours are imaged and higher resolution is needed. Adjust the laser power and gain to optimise the signal based on background and fluorescent signal.
45. Adjust the number and size of tiles and the top and bottom of the z-stack in such a way that all cells are captured. Make sure that the pixel size and step size remain constant when imaging different samples within your experiment. We used a pixel size of 1.77 μm/pixel and a step size of 6.07 μm as a minimal XY and Z resolution to allow quantification.
46. Stitch the tiled images using the confocal software or using the 'Stitching of 3D images' plugin in ImageJ. We used four tiled images of 576 x 576 pixels each to capture the tumour region.

Annotation and selection of the tumour core based on extracellular matrix deposits using ImageJ.

Timing: 15 min/ brain slice

During the culture period, the glioma cells locally deposit ECM proteins. This local deposit of ECM in combination with ECM of the basement membranes of the blood

>Figure 2. Whole-mount immunostaining and tissue clearing of ex vivo organotypic slices. (a) Image of four brain slices placed within an iSpacer on a microscope glass, covered and cleared with RapiClear, and mounted with a coverslip. (b) 3D projection image of a brain slice injected with H2B-mNeonGreen (green) expressing U251-MG cells. The mouse brain vasculature is stained with laminin (cyan) and the glioma-cell cytoskeleton with vimentin (magenta). (c) Higher magnification image of individual glioma cells migrating along the mouse brain vasculature. (d) Invasion of mCherry expressing U251-MG cells (magenta) surrounded by GFAP-expressing mouse brain astrocytes (green). Scale bar = 100 μm

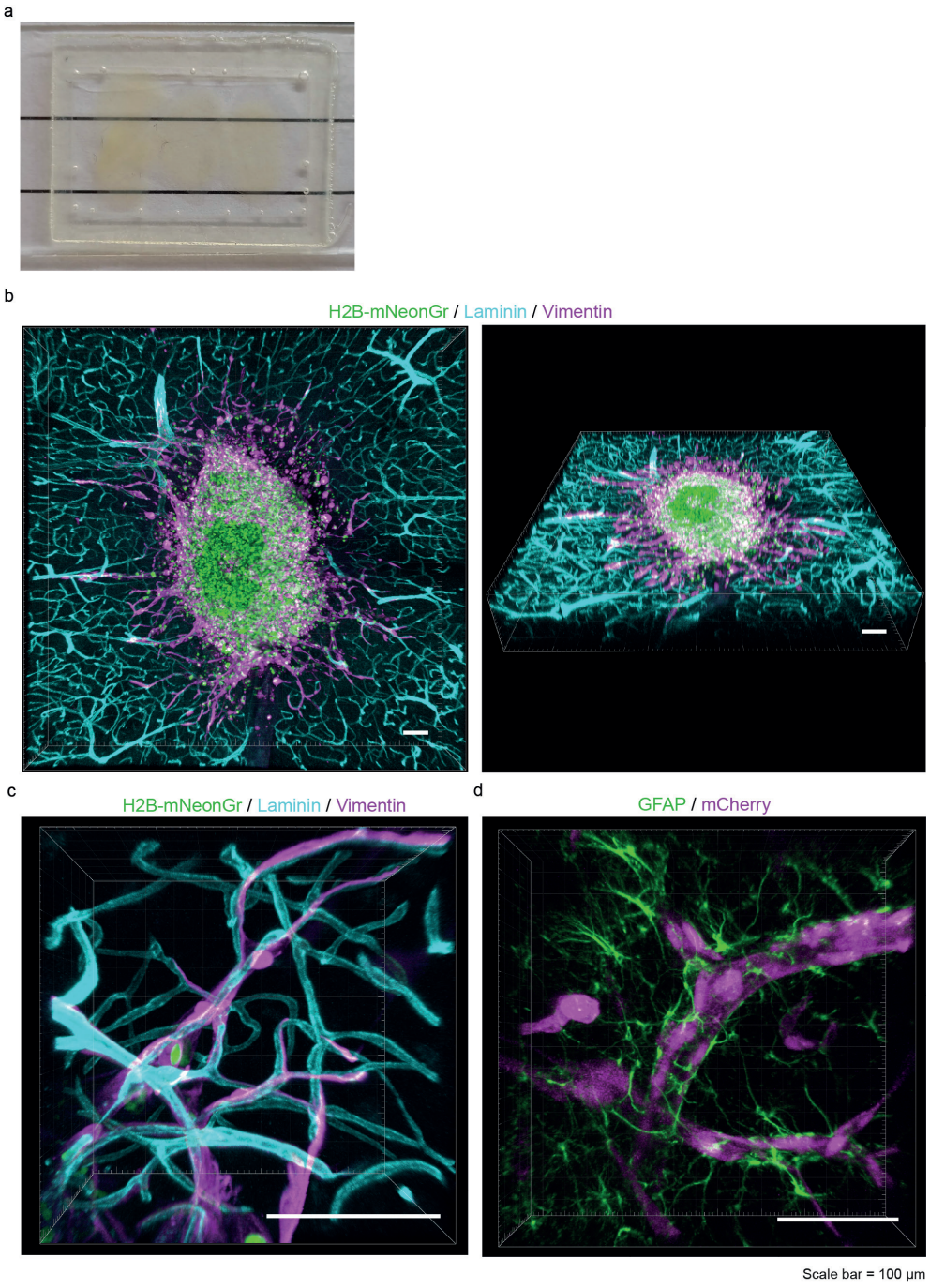
a
b
H2B-mNeonGr / Laminin / Vimentin
c
H2B-mNeonGr / Laminin / Vimentin
d
GFAP / mCherry
Scale bar = 100 µm

vessels allows for the distinction between cells that remained at the site of injection (the tumour core) and the cells that invaded the mouse brain tissue (Fig.3a). In this step, we describe how the staining patterns of the laminin staining can be used to determine the tumour core.

47. Open the confocal-generated and tiled image in ImageJ. This file should consist of minimally two channels: a channel with the nuclei and a channel with laminin staining. Duplicate the file and go to one of the z-planes in which the nuclei are clearly visible.

Optional: Before the start of the analysis, use a filename randomiser plugin to blind the images when comparing different experimental conditions.

48. Open the Brightness & Contrast function and linearly increase the laminin signal by adjusting the maximum (Fig. 3a, step 2). The laminin secreted by the injected glioma cells will become visible, whereas the laminin signal from the blood vessels will be overexposed at this point. Use the laminin ECM depos it signal in combination with the density of the nuclei to draw a region of interest (ROI) around the tumour core and add this to the ROI manager (Fig. 3a, step 2 and 3).
49. To delete the laminin signal of the blood vessels, delete the signal outside of the ROI created in the previous step (Fig. 3a, step 4). Go to the next z-plane and check whether the created ROI still fits the tumour core, adjust the ROI if necessary, and repeat the action. Repeat this until only the laminin signal of the ECM deposits in the tumour core are visible and all blood vessels are deleted.
50. Add the created laminin tumour core channel to the original file and save (Fig. 3a, step 5).

Analysis of the distribution of nuclei in tumour core and invasive front using Imaris software

Timing: 10 min/ brain slice

51. Import the adjusted files into the Imaris Software and open the first file in the 'Surpass' environment.

>Figure 3. Image processing and analysis steps to quantify invasion of glioma cells. (a) Creation of a tumour core in ImageJ. Open a z-project in ImageJ (1) and increase the brightness/contrast within the laminin channel to reveal the ECM deposits of the injected glioma cells (2). Draw an ROI around the ECM deposit (3) and remove the laminin signal outside of the ROI (4). Repeat these steps for different z-planes. Duplicate the created channel and merge it with the original file (5). (b) Analysis steps in Imaris to quantify invasion. Open the file created in ImageJ in the Imaris software. With the 'Create Surface' tool,

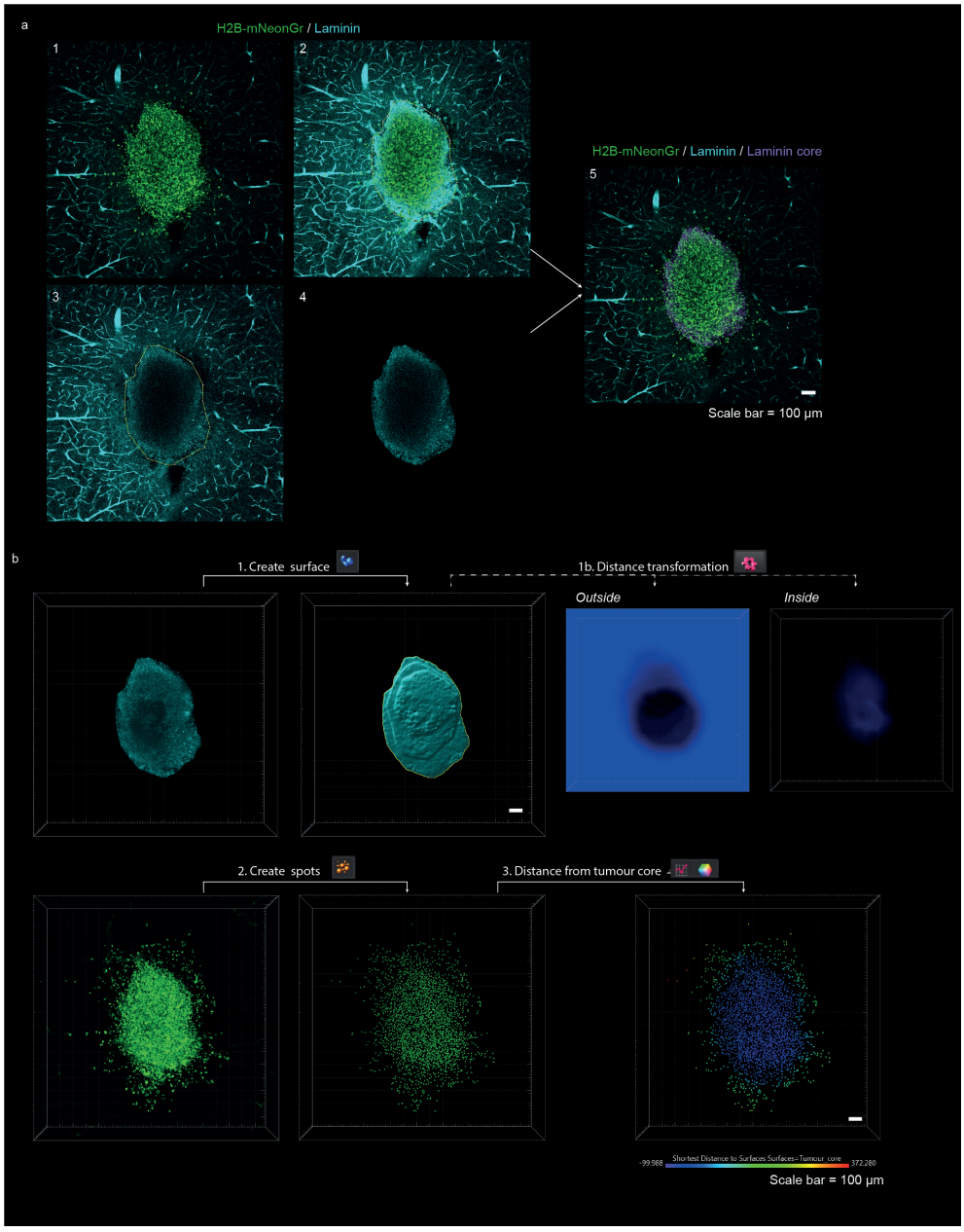

create a surface of the tumour core (1). In Imaris version 9.5 or older, use the Distance transformation option to create new channels where the signal intensity represents the distance to or in the tumour core (1b). In newer versions, this step can be replaced by selecting the option 'Shortest Distance Calculation' in the first step of creating a surface. Create spots of the H2B-mNeonGreen channel with the 'Create Spots' tool (2). In the newly created spots, the software can calculate, display (3), and export the distance to the surface created in (1). Scale bar = 100 µm

52. Create a surface (Fig. 3b, step 1a)
    a. In version 9.5 or higher, the first panel in the new surface option is 'algorithm settings'. In this panel select 'shortest distance calculation'.
    b. Select the source channel corresponding to the created deposited laminin signal. Select the smooth function. In our experiments, we chose a 'surface detail' of 5 μm.
    c. In the next panel, set the threshold based on absolute intensity. In our experiments, we set the threshold at 2.00.
    d. In the next panel, additional filters can be applied to the created surface. This step can be skipped.
53. Create spots of the individual nuclei in the image (Fig. 3b, step 2a)
    a. In version 9.5 or higher, the first panel in the new surface option is 'algorithm settings'. In this panel select 'shortest distance calculation'.
    b. Select the source panel corresponding to the nuclei of the injected glioma cells. For spot detection in our experiments, we chose an 'Estimated XY Diameter' of 11 μm. Select 'Model PSF-elongation along Z-axis', in our experiments we choose an 'Estimated Z Diameter' of 22 μm. Select 'Background subtraction'.
    c. In the next panel, filters can be applied to the created spots based on the quality of the signal. This step will affect the number of spots that are created and therefore the outcome of your measurements. It is important to optimise these settings. Finish the creation of the spots by clicking on the green arrows.
    d. Inspect the spots that are created. 'Background spots' can be manually deleted in the 'Edit' panel.

The next step in the analysis is dependent on the version of Imaris

Version 8.4 – 9.4

54. Perform distance transformation on the created surface (Fig. 3b, step 1b)
    a. Select the created surface and click on 'Tools'.
    b. Select the second option: 'Distance Transformation'. This will start a MatLab Script embedded within the Imaris Software. First, select 'Outside SurfaceObject'. After running this script, a new channel will be added, in which the intensity of the signal corresponds to the distance to the outside of the surface
    c. Repeat the 'Distance Transformation' script for the 'Inside SurfaceObject' option. An additional channel will be added in which the intensity of the

signal corresponds to the inside of the surface.

55. Calculate the distance from the individual spots (nuclei) to the created surface (tumour core, Fig. 3b, step 3)
    a. Select the created spots, click on 'Statistics' and go to 'Detailed'.
    b. In the second dropdown menu, select 'Intensity Center Ch= x Img 1', in which Ch = x corresponds to the channel that was created with the 'Outside SurfaceObject' distance transformation of the surface. The displayed values correspond to the closest distance of individual spots to the border of the surface. Values of 0 correspond to nuclei within the tu mour core, whereas values higher than 0 correspond to nuclei invaded into the tissue. Click on the 'Save' Icon to export the data as an excel file.
    c. Repeat the 'Intensity Center Ch= x Img 1' step for the channel corre sponding to the 'Inside SurfaceObject' of the distance transformation. The displayed values correspond to the closest distance of individual spots to the border of the surface. Values of 0 correspond to nuclei outside of the tumour core, whereas values higher than 0 correspond to nuclei within the tumour core. Click on the 'Save' Icon to export the data as an excel file.
    d. To visualise the distribution of nuclei, click on the 'Color' icon. For 'Color Type', select 'Statistics Coded' and in the dropdown menu select 'Intensity Center Ch= x Img 1'. This allows colour coding of either the 'Outside SurfaceObject' or 'Inside SurfaceObject'

Imaris version 9.5 or higher

56. In the newer versions of Imaris, selection of the 'Shortest Distance Calculation' during the first step of creating a new surface (step 52a) or spots (step 53a) allows you to skip the distance transformation steps described in steps 54 and 55.
57. Calculate the distance from the individual spots (nuclei) to the created surface (tumour core, Fig. 3b, step 3)
    a. Click on 'Statistics 'and go to 'Detailed'
    b. In the dropdown menu, select 'Shortest Distance to Surfaces Surfaces = x' in which x corresponds to the name of the surface created earlier. The displayed values correspond to the closest distance between the individual spots and the border of the surface, with positive values representing nu clei outside of the surface (invaded into the tissue) and negative values representing nuclei within the surface (within the tumour core). Click on the 'Save' Icon to export the list as an excel file.

58. After exporting the data on invasion distance from every brain slice, copy the columns with the invasion distances into a single file for further statistical anal ysis. The number of invading and non-invading cells can be determined and a histogram can be made to show the distribution of cells within the brain slice (Fig. 4b).

Determining proliferation rate of glioma cells in the organotypic brain slices: BrdU assay

Timing: 6 hours

Alternative to the whole-mount immunostaining method, after fixation the *ex vivo* organotypic brain slices can be further sectioned with a cryostat. This allows for immunostainings with antibodies that are not compatible with the whole-mount immunostaining method. In the next session, we describe how a BrdU assay can be performed on glioma cells injected into organotypic brain slices, to determine the level of proliferation of these cells.

59. Prepare the organotypic brain slices and inject the glioma cells as described before, up to point 31 of this protocol.
60. On the 7th day after injection, place a drop of 50 μL 40 mM BrdU in NSC-medium on top of the lateral ventricles containing the glioma cells and incubate at 37 ˚C in a humidified 5% CO_2 incubator for 6 hours (Fig. 5a).
61. After 6 hours of incubation with BrdU, fixate and wash the tissue as described in steps 32 and 33 of this protocol.

Cryosectioning of fixated organotypic brain slices

Timing: 3 days

62. Cut the membrane of the insert around the individual brain slices and transfer to an embedding mould.
63. Submerge the brain slices in a 30% sucrose in PBS solution (pH = 7.2) and incubate at 4 ˚C for 48 hours. Upon incubation in the sucrose solution, the brain slices should have sunk to the bottom of the embedding mould.
64. Remove the sucrose solution and wash the slices once with PBS.
65. Add Tissue Tek to the brain slices and snap freeze by placing the embedding moulds in 2-Methylbutan (-55 ˚C) on dry-ice for 2 minutes until the Tissue Tek is frozen.
66. Transfer the snap-frozen brain slices to a cryostat with a chamber temperature of -20 ˚C and an objective temperature of -18 ˚C.
67. Use the cryostat to section the brain slices into 20 μm sections and mount the

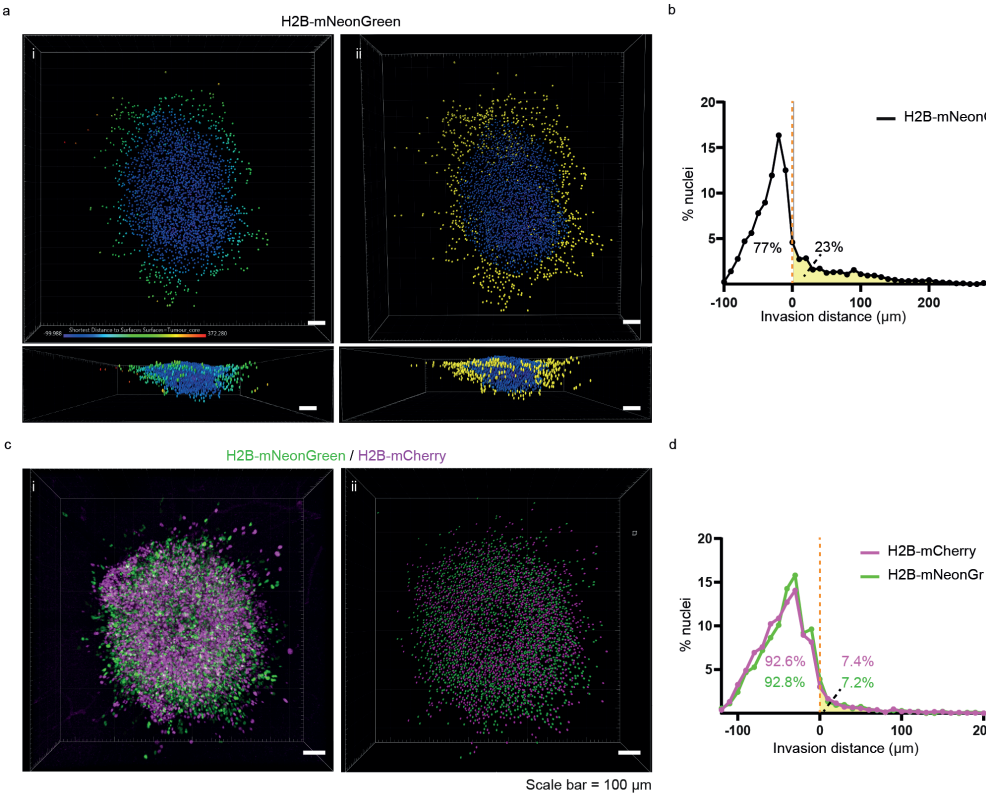

Figure 4. Quantification of cell invasion. (a) 3D projection of individual nuclei. (i) Every nucleus is colour coded based on the closest distance to the border of the tumour core. In panel (ii) the nuclei that have a value larger than 0 um are depicted in yellow representing the invading population of cells. (b) Histogram of invasion distance represents the distribution of cells in the tumour core (AUC = white) and tissue (AUC = yellow) of the 3D representation displayed in (a). The percentage of cells in the tissue or tumour core is printed. (c) Confocal image (i) and 3D projection (ii) of mixed H2B-mCherry (magenta) and H2B-mNeonGreen (green) expressing cells. (d) Histogram of invasion distances show overlapping invasion patterns for the H2B-mCherry and H2B-mNeonGreen expressing cells with a similar genetic background. Scale bar = 100 µm

sections on SuperFrost Plus Adhesion microscope slides (Fig. 5b). Collect the tissue on different microscopy slides in a series of four or five.

Note: take time to orient the brain slice at the right angle relative to the knife of the cryostat, so that it matches the cutting surface of the vibratome sections.

68. Upon collection of all tissue, let the sections dry at room temperature until the Tissue Tek has evaporated. Store the microscopy slides at -20 ˚C or directly proceed to the immunofluorescence staining.

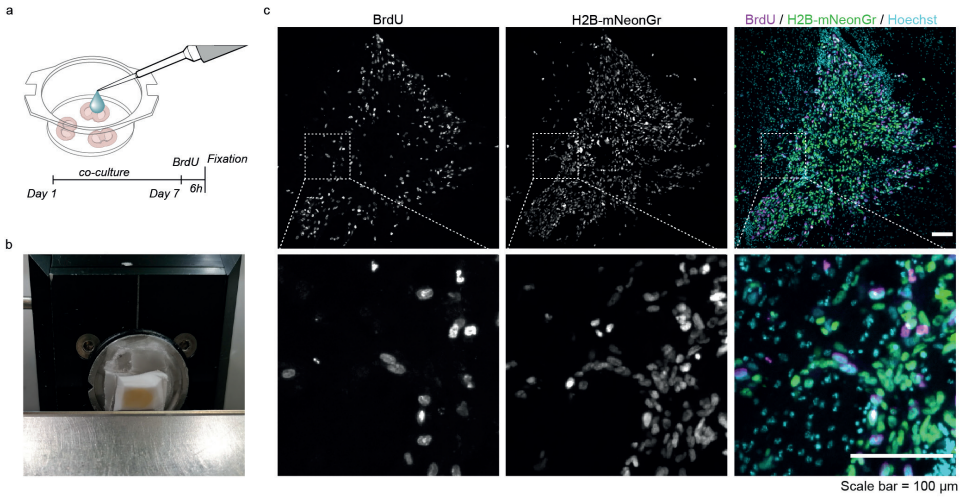

Figure 5. BrdU assay to determine proliferation. (a) Schematic representation of BrdU assay. (b) Example image of a fixated organotypic brain slice embedded in Tissue Tek within the cryostat chamber. (c) Sectioned organotypic brain slice injected with H2B-mNeonGreen (green) cells, stained with BrdU (magenta) and counterstained with Hoechst (cyan). Scale bar = 100 µm

BrdU Immunofluorence staining of tissue sections

Timing: 2 days

69. Take out the glass microscope slides from -20 ˚C and air dry.
70. Wash the tissue three times with PBS to get rid of the remaining traces of Tissue Tek.
71. Perform antigen retrieval on the tissue sections.
72. Cover the tissue sections with HCl 2N and incubate at 37 ˚C for 30 minutes.
73. Incubate the tissue sections in Borate Buffer at room temperature for 15 minutes.
74. Wash three times in PBS (pH = 7.2) with 0.25% Triton-X100.
75. Incubate the tissue sections in blocking buffer at room temperature for 90 minutes (see 'materials and equipment' for blocking solution used in this protocol).
76. Incubate the tissue with BrdU primary antibodies at 4 ˚C overnight. Dilute the antibodies in blocking buffer diluted 1:1 in PBS. In our experiments, we used rat anti-BrdU (1:500)
77. Make a humidified chamber by placing wet paper tissues in the incubation box.
78. Wash the tissue sections three times with PBS.
79. Incubate the tissue sections with secondary antibodies in a humidified chamber at room temperature for 1 hour, protected from light. Dilute the antibodies in PBS with 0.25% triton and counterstain with Hoechst (1:1 000) or an alternative nuclear stain. In our experiments, we used donkey anti-rat-AF647

(1:1000) secondary antibodies.

80. Wash the tissue sections three times with PBS, protected from light.
81. Mount the glass microscope slides with a coverslip
    a. Remove the PBS by holding the glass microscope slide vertically on a paper tissue
    b. Place three drops of FluorSave reagent or an alternative mounting solution on one side of the microscopy slide.
    c. Place a 25 x 60 mm coverslip with one edge on top of the mounting solution drops and slowly lower it to spread the mounting solution over the microscopy slide. Avoid making bubbles.
    d. Remove excess mounting solution by placing the microscope slide on a paper tissue.
    e. Let the microscope slide dry overnight before imaging with epifluorescence microscopy or alternative imaging methods.

Expected Outcomes

By combining *ex vivo* organotypic invasion model with whole-mount immunostaining and tissue clearing, you can reconstruct the invasion patterns of labelled glioma cells of interest. In our hands, this methodology was used to visualise perivascular invasion of H2B-mNeonGreen labelled U251-MG cells along laminin-stained blood vessels. By using vimentin-staining, the cytoskeleton of individually invading glioma cells was visualised (Fig. 2b,c). Additionally, mouse astrocytes can be stained using antibodies against glial fibrillary acidic protein (GFAP, Fig. 2d), to study interactions between astrocytes and glioma cells. The analysis steps described here are optimised for nuclear labelling, but successful visualisation of invasion patterns is also expected when cytosolic labels are used (Fig. 2d). Using these analysis steps, you can quantify the number of invaded cells and the distribution of cells in the tissue (Fig. 4a,b). To cope with variation between samples, an internal control can be included in the experimental design, in which control cells with a different fluorescent label are co-injected with the experimental cells (step 20, Fig. 4c,d). We used this strategy to compare the invasive capacities of U251-MG cells with different cytoskeletal GFAP networks (van Asperen *et al.*, 2021).

After BrdU-incorporation, cryosectioning of the *ex vivo* organotypic brain slices, and BrdU-staining, nuclear staining of BrdU-positive cells are anticipated (Fig. 5). By dividing the number of BrdU-positive nuclei by the total number of nuclei, the percentage of mitotic cells within a specific time-frame can be calculated.

Limitations

The co-culture method described in this protocol allows investigation of glioma cell invasion and proliferation in a brain-like environment where brain geometrical cues and ECM compositions are mimicked and maintained. We did not investigate the host-cell – glioma cell interaction in this model, as the effect of the culture conditions may be a limitation for these types of questions. For instance, cell death of mouse brain cells is expected, and this will alter the physiology of the surrounding brain cells.

A limitation of the whole-mount immunostaining protocol is that not all primary antibodies fully penetrate the tissue or have a good signal-to-noise ratio. In our hands, the BrdU antibody was not compatible with the whole mount immunostaining protocol, explaining why we describe staining with this antibody on cryo-sectioned material. For clearing of the whole-mount immunostained tissue, we selected the RapiClear clearing method. There are multiple tissue clearing methods developed and published, each with their advantages, disadvantage, and suitability for types of tissues (Silvestri et al., 2016). The absence of shrinkage and non-laborious protocol makes RapiClear a suitable clearing method for organotypic brain slices, however, a disadvantage is that we observed a difference in signal intensity over the Z-axis, indicating suboptimal clearing. Therefore, this method is less suitable for quantitative measurements of signal intensity between samples. Also during the analysis of distribution of nuclei using the Imaris software, there might be a selection bias during the quality threshold filtering (step 53c) of nuclei that are more superficial. Since we observe that most cells migrate in the XY direction, we do not expect that this bias will have major effects on the outcome of the analysis, nevertheless using an internal control (step 21) can be considered to cope with this bias. Lastly, the tissue-clearing steps described in this protocol are incompatible with cellular dyes, therefore visualisation of cells and tissues is dependent on fluorescent proteins and immunostainings.

Troubleshooting

Problem 1:

Steps 15, 16: The vibratome slicing leads to irregular brain slices, curled up tissue or loosening of the mounted brain.

Potential Solution:

Solution 1: Optimise the amount of glue used when mounting the mouse brain to the platform (step 11). Too little glue can cause partial detachment of the brain during the slicing, resulting in irregular and curled up slices. When too much glue is used, it can cover the part of the brain that will be collected during the slicing and disturb the vibratome slicing. Aim for a drop of glue the size of a pea.

Solution 2: Replace the razor blade. The razor blade can be re-used multiple times, but after a couple of re-uses, it will become blunt and disturb the slicing.

Solution 3: When the tissue has become a little loose, it can help to place a brush directly behind the tissue to avoid movement.

Problem 2:

Step 27: Injection of the cells leads to a flow of cells on top of the tissue, or underneath the tissue.

Potential Solution:

Injection of the cells works best when the cells can fill up pre-existing free space like the ventricles or the space created with the syringe itself. In the XY axis, place the syringe in the tissue in the same line as the longest axis of the ventricle to stimulate a smooth flow of cells. In the XZ axis, place the syringe right below the surface of the tissue so that there is sufficient space available for the cells and direct injection on the membrane of the cell culture insert is avoided. Another solution is to decrease the speed of injection. Lastly, in our experience, there is more overflow of cells when the slices are washed right before injection, as a layer of liquid remains on top of the slice that promotes the flow of cells. We, therefore, do not recommend washing the top of the brain slices right before injections.

Problem 3:

Step 30: The injected cells look deformed or unhealthy after injection.

Potential Solution:

When the syringe is improperly washed with PBS after cleaning with ethanol, the cells may look deformed after injection and will not invade the tissue. To avoid this, wash the syringe repeatedly with PBS before taking up cells and do not clean the syringe with ethanol in-between the injection steps.

Problem 4:

Step 44: Weak signal-to-noise ratio of the fluorescent protein expressed by the cells.

Potential Solution:

The brain slice tissue can give rise to a high background, which can lead to a weak signal-to-noise ratio when the intensity of the fluorescent protein is low. Consider using a different fluorescent protein with better intensity or include a fluorescent protein-

specific antibody during the whole-mount immunostaining protocol.

Problem 5:

Step 67: Only half of the tissue is collected during the cryosectioning

Potential Solution:

The angle of the tissue relative to the knife is essential to collect a section of the entire brain slice during cryosectioning. Take more time in fine-tuning the angle of the knife after making the first slices to be sure that the tissue is sectioned correctly.

Acknowledgments

We thank Youri Adolfs for the help with the whole-mount immunostaining protocol and Imaris Software analysis, and Loïs Aitatus for the help with making the video. This study was funded by the Dutch Cancer Society [KWF 101123], and the T and P Bohnenn Foundation (P.R).

Author Contributions

J.v.A. performed the data collection, formal analysis, methodology, and wrote the original draft. E.v.B. performed methodology, and reviewed and edited the manuscript. P.R. performed supervision, and reviewed and edited the manuscript. E.H. performed funding acquisition, project administration, methodology, supervision, and reviewed and edited the manuscript.

References

van Asperen, J. *et al.* (2021) 'GFAP splice variants fine-tune glioma cell invasion and and tumour dynamics by modulating migration persistence', *bioRxiv*, pp. 1–47. Available at: https://doi.org/10.1101/2021.08.19.456978.

Bekkouche, B. M. B. *et al.* (2020) 'Comparison of Transparency and Shrinkage During Clearing of Insect Brains Using Media With Tunable Refractive Index', *Frontiers in Neuroanatomy*, 14(November), pp. 1–19. doi: 10.3389/fnana.2020.599282.

Belle, M. *et al.* (2014) 'A Simple Method for 3D Analysis of Immunolabeled Axonal Tracts in a Transparent Nervous System', *Cell Reports*, 9(4), pp. 1191–1201. doi: 10.1016/j.celrep.2014.10.037.

Claes, A., Idema, A. J. and Wesseling, P. (2007) 'Diffuse glioma growth: A guerilla war', *Acta Neuropathologica*, 114(5), pp. 443–458. doi: 10.1007/s00401-007-0293-7.

Drost, J. *et al.* (2015) 'Sequential cancer mutations in cultured human intestinal stem cells', *Nature*, 521(7550), pp. 43–47. doi: 10.1038/nature14415.

Pencheva, N. *et al.* (2017) 'Identification of a Druggable Pathway Controlling Glioblastoma Invasiveness', *Cell Reports*, 20(1), pp. 48–60. doi: 10.1016/j.celrep.2017.06.036.

www.sunjinlab.com (no date) 'Mouse Brain Quick Guide ':

Supplementary material

Video 1. Injection of glioma cell mixes into the ex vivo organotypic brain slices


4

CHAPTER 4

GFAP splice variants fine-tune glioma cell invasion and tumour dynamics by modulating migration persistence

Jessy V. van Asperen[1#], Rebeca Uceda-Castro[2#], Claire Vennin[2], Jacqueline A. Sluijs[1], Emma J. van Bodegraven[1], Andreia S. Margarido[2], Pierre A.J.T. Robe[3], Jacco van Rheenen[2†], Elly M. Hol[1†]

[1] Department of Translational Neurosciences, UMC Utrecht Brain Center, University Medical Center Utrecht, Utrecht University, 3584 CG Utrecht, The Netherlands
[2] Division of Molecular Pathology, Oncode Institute, The Netherlands Cancer Institute, Amsterdam, The Netherlands
[3] Department of Neurology and Neurosurgery, University Medical Center Utrecht Brain Center, Utrecht University, 3584 CG Utrecht, The Netherlands

[#] These authors contributed equally

[†] These authors jointly supervised this work

Scientific Reports. 2022. 12 (424)
doi: 10.1038/s41598-021-04127-5

Abstract

Glioma is the most common form of malignant primary brain tumours in adults. Their highly invasive nature makes the disease incurable to date, emphasizing the importance of better understanding the mechanisms driving glioma invasion. Glial fibrillary acidic protein (GFAP) is an intermediate filament protein that is characteristic for astrocyte- and neural stem cell-derived gliomas. Glioma malignancy is associated with changes in GFAP alternative splicing, as the canonical isoform GFAPα is downregulated in higher-grade tumours, leading to increased dominance of the GFAPδ isoform in the network. In this study, we used intravital imaging and an *ex vivo* brain slice invasion model. We show that the GFAPδ and GFAPα isoforms differentially regulate the tumour dynamics of glioma cells. Depletion of either isoform increases the migratory capacity of glioma cells. Remarkably, GFAPδ-depleted cells migrate randomly through the brain tissue, whereas GFAPα-depleted cells show a directionally persistent invasion into the brain parenchyma. This study shows that distinct compositions of the GFAP network lead to specific migratory dynamics and behaviours of gliomas.

Introduction

Glioblastoma multiforme (GBM, grade IV glioma) is the most common and most aggressive tumour of the central nervous system, with an incidence of 3 per 100,000 people and a crude median survival of 9 months after diagnosis (Ho et al. 2014). GBM is currently incurable and this is for a large part due to the highly invasive nature of glioma cells (Bellail et al. 2004; Hatoum, Mohammed, and Zakieh 2019; Birbrair 2017). Standard-of-care treatment for GBM consists of surgical tumour resection, followed by chemo- and radiotherapy, but fails to fully eradicate highly invasive glioma cells. As a consequence, patients often relapse after treatment and the tumour rapidly re-grows.

The intermediate filament (IF) protein glial fibrillary acid protein (GFAP) is a signature type III IF protein of glioma cells that has been implicated in tumour migration (Moeton et al. 2014; Stassen et al. 2017; van Bodegraven et al. 2019a). The role of IFs in glioma invasion and migration has only gained attention recently (Leduc and Etienne-Manneville 2015). With over 70 genes encoding different IF proteins, the IF family is one of the largest human gene families and IF expression patterns are highly cell- and tissue type-specific (Peter and Stick 2015). Changes in the composition of the IF network are associated with alterations in malignancy. For example, during the epithelial-to-mesenchymal (EMT) transition, a process linked to increased cellular invasiveness and cancer progression (Zhang and Weinberg 2018), the IF network of cancer cells with an epithelial origin changes from a keratin-dominant to a vimentin-dominant network (Thiery et al. 2009; Mendez, Kojima, and Goldman 2010; Sharma et al. 2019). In addition, breast cancer invasion is linked to changes in the IF network, with

a switch from keratin 8 to keratin 14 expression in invasive cells (Cheung et al. 2013). GFAP is an IF protein that is classically used to identify malignancies of glial origin, such as astrocytomas and glioblastomas (Duffy and Rapport 1982). In addition to GFAP, gliomas can heterogeneously express a combination of IFs including vimentin, synemin, and nestin (Skalli et al. 2013), which are located within the same filament in the cell (Leduc and Manneville 2017). GFAP is differentially spliced, and GFAPα and GFAPδ are the two isoforms that are most highly expressed and best studied. The GFAPδ isoform results from alternative splicing with a 3' polyadenylation event, where the last two exons 8 and 9 of GFAPα are replaced by exon 7a, leading to an alternative 42 amino acid C-terminal tail (Blechingberg et al. 2007; Nielsen et al. 2002). The two isoforms have different assembly properties (Moeton et al. 2016), protein interactions (Nielsen et al. 2002; Nielsen and Jørgensen 2004), and differ in their expression patterns, with GFAPα predominantly expressed in mature astrocytes and GFAPδ in the neurogenic niches of the human brain (van den Berge et al. 2010; Roelofs et al. 2005).

In previous studies, we and others have shown that glioma malignancy is associated with alterations in GFAP splice isoform levels (Blechingberg et al. 1994; Andreiuolo et al. 2009; Heo et al. 2012; Brehar et al. 2015; Stassen et al. 2017; Choi et al. 2009; van Bodegraven et al. 2019b). As such, RNA sequencing analysis of the cancer genome atlas (TCGA) database showed that increasing glioma malignancy grades are associated with a lower overall expression of GFAP and a shift towards higher levels of the alternative splice variant GFAPδ relative to GFAPα (Stassen et al. 2017). Increasing the GFAPδ/α ratio *in vitro* leads to an upregulation of genes encoding proteins that are involved in the interactions between cells and the extracellular matrix (ECM) such as laminins, integrins, and matrix metalloproteinase 2 (MMP-2, Moeton et al. 2014; 2016; Stassen et al. 2017; van Bodegraven et al. 2019a). Besides, immunohistochemical analysis of glioma tissue samples linked GFAPδ expression to an altered cellular morphology (Choi et al. 2009; Heo et al. 2012) and to more invasive tumours based on neuroimaging (Brehar et al. 2015). Although these observations are suggestive for changed glioma cell behaviour upon alterations in GFAP isoform expression, a full characterisation of changed behaviour has not yet been performed.

In this study, we investigated how manipulation of GFAP isoform expression affects human glioma cell invasion and growth dynamics *ex vivo* and *in vivo*. We longitudinally monitored the growth patterns of a total of twelve clones of U251-MG glioma cells depleted from either the GFAPα or the GFAPδ isoform in *ex vivo* organotypic mouse brain slices and in mouse brains *in vivo* with intravital imaging. We show that manipulation of the GFAP network strongly affects the motility of glioma cells and tumour growth patterns. GFAPδ-KO cells form denser tumours, have increased motility compared to control tumours and migrate randomly, whereas GFAPα-KO cells show a more diffuse growth pattern and migrate more persistently towards the brain parenchyma.

Results

GFAP isoform expression differs between low- and high-grade gliomas.

Using differential gene expression analysis of RNA sequencing data from the The Cancer Genome Atlas (TCGA, https://www.cancer.gov/tcga), we previously showed that the ratio of splice variants GFAPα and GFAPδ differs between low grade- and high-grade gliomas (Stassen et al. 2017). Since this publication, 37 additional patient samples were included in the TCGA database. We therefore re-analysed the RNA sequencing data of the updated TCGA cohort and confirmed our previously reported findings. Whereas canonical splice variant GFAPα was significantly decreased in grade IV glioma compared to lower grades glioma (grade II and III, Supp. Fig. 1a), the expression of alternative splice variant GFAPδ was not different between the different grades (Supp. Fig. 1b). Thus, there is an increased dominance of GFAPδ in high- versus lower-grade glioma, as illustrated by the significant increase in the GFAPδ/α ratio (Fig. 1a).

Modification of GFAP isoform expression using CRISPR-Cas9.

To understand how the different ratios of GFAPδ/α affect the behaviour of the tumour cells, we modified GFAP isoform expression in the U251-MG human glioma cell line using CRISPR-Cas9 technology, as previously performed in van Bodegraven et al. 2019a. A set of two single guide RNAs (sgRNAs) were used to delete the DNA region encoding the 41 or 42 amino acid tail of GFAPα and GFAPδ, respectively. To create a GFAPα knockout (KO), the intronic regions before and after exon 8 and 9 were targeted, whereas the GFAPδ-KO cells were created by flanking the intronic regions before and after exon 7a (Fig.1b, Supp. Fig. 2b,d). In addition to the six cell clones previously generated in van Bodegraven et al. 2019 (CRISPR set A: CTL1, CTL2, GFAPδ-KO1, GFAPδ-KO2, GFAPα-KO1, GFAPα-KO2), we engineered six extra cell clones a using different set of sgRNAs (CRISPR set B: CTL3, CTL4, GFAPδ-KO3, GFAPδ-KO4, GFAPα-KO3, GFAPα-KO4) to create a total of twelve clones. Exonic depletion was confirmed with polymerase chain reaction (PCR) (Supp. Fig. 2a,c) and sequencing (Supp. Fig. 2b,d). Targeting the exonic region led to a significant decrease in mRNA levels of the corresponding isoform (Supp. Fig. 2e,f,g) and an increase (GFAPα-KO) or decrease (GFAPδ-KO) of the GFAPδ/α mRNA ratio (Fig. 1c) and the GFAPδ/GFAPpan protein ratio (Fig. 1d,e, Supp. Fig. 2h,i). The cell clones showed normal IF network formation, except for GFAPα-KO clone 3, where occasional network collapses were observed (Supp. Fig. 2j). This GFAPα-KO clone 3 had the highest GFAPδ/GFAPpan protein ratio (Fig. 1d), confirming that there is a limit to the level of GFAPδ that can be incorporated into the network (Moeton et al. 2016; Perng et al. 2008).

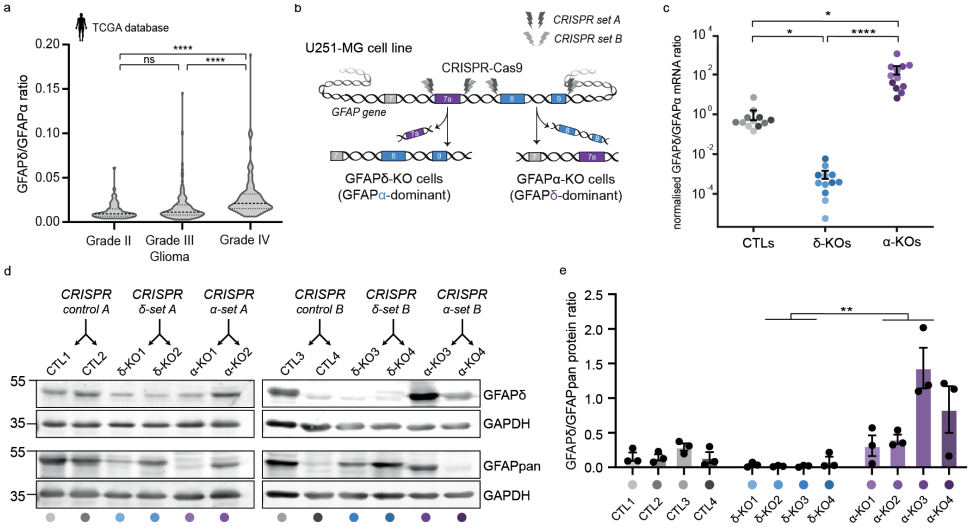

Figure 1. GFAPδ/GFAPα ratio in the TCGA database and generation of GFAP isoform KO clones to regulate the GFAPδ/GFAPα ratio in U251-MG glioma cells. (a) Violin plots of the GFAPδ/GFAPα ratio in tumour samples of grade II (n= 64), grade III (n= 130), and grade IV (n= 153) astrocytoma, obtained from normalised isoform expression data of the TCGA database. Significance was determined using a Kruskal-Wallis test followed by a Dunn's multiple comparisons test. (b) Schematic illustration of the GFAP gene with the CRISPR-Cas9-targeted locations to generate GFAPδ- and GFAPα-KO cell clones. GFAPδ-KO and GFAPα-KO cell clones were generated using two sets of sgRNAs (CRISPR set A and B) and four clones per isoform-KO were selected and characterised, leading to a total of 12 cell clones. (c) GFAPδ/GFAPα mRNA ratio of the GFAP isoform KO cells and controls, represented on a log10 scale. Depletion of exon 7a (GFAPδ-KO) leads to a decrease in the GFAPδ/ GFAPα ratio compared to the control cells, whereas depletion of exons 8 and 9 (GFAPα-KO) leads to an increase in the ratio. n=12 biological repeats per group, derived from 4 clones per condition represented with different colour hues. Significance was determined using a Kruskal-Wallis test followed by a Dunn's multiple comparisons test. (d) Protein levels of GFAPδ and all GFAP isoforms (GFAPpan) in the 12 different cell clones generated with the different CRISPR sets (CRISPR control A, CRISPR δ-set A, CRISPR α-set A, CRISPR control B, CRISPR δ-set B, CRISPR α-set B) determined with Western blot. Full-lenth blots are presented in Supplementary Fig.6. (e) Quantification of GFAPδ/GFAPpan levels in the 12 different cell clones. Significance was determined using a Kruskal-Wallis test followed by a Dunn's multiple comparisons test. The data is shown as mean ± S.E.M, *p < 0.05, **p < 0.01, ***p < 0.001, ****p < 0.0001, ns = not significant.

Depletion of GFAP isoforms increases cell invasion in *ex vivo* organotypic brain slices.

To study how modulation of the GFAP network affects cell invasion in a physiologically relevant environment, we adapted the *ex vivo* organotypic brain slice model described by ref. (Pencheva et al. 2017). *Ex vivo*, 350 µm thick brain slices of p15-17 mouse pups were prepared and cultured in an air-liquid interface. The twelve cell clones were transduced with H2B-mNeonGreen to visualise the nuclei and were injected into the

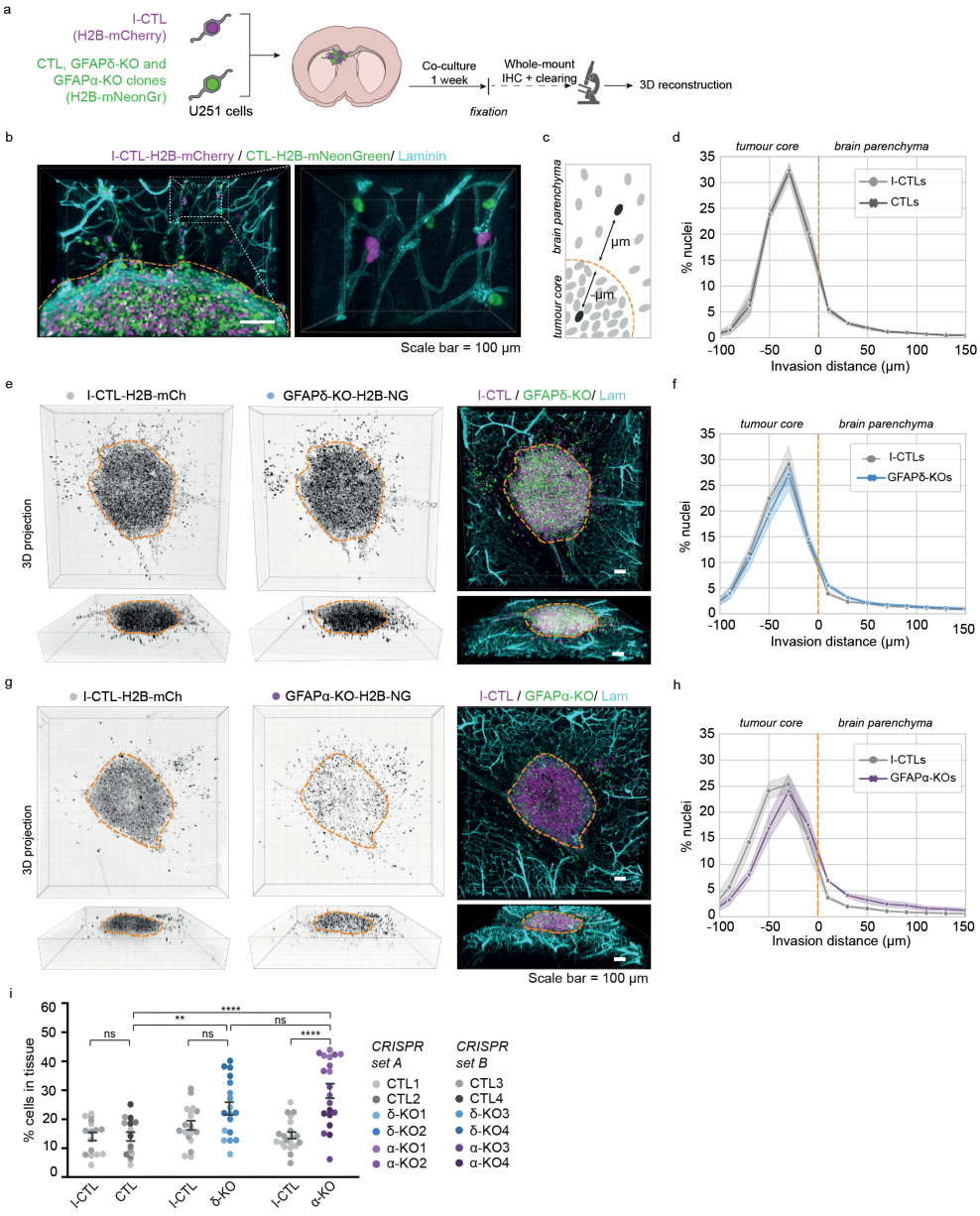

Figure 2. Modification of GFAP isoform expression affects macroscopic growth patterns in organotypic brain slice cultures. (a) Schematic of experimental set-up: H2B-mNeonGreen expressing control (CTL), GFAPδ-KO and GFAPα-KO cell clones are injected in organotypic brain slices together with an H2B-mCherry expressing internal control (I-CTL) and co-cultured for one week. After fixation, whole-mount immunofluorescent staining, and clearing, confocal images are used to create a 3D reconstruction of the invasion patterns. (b) Representative image of I-CTL1 (magenta) and CTL1 (green) cells within the organotypic brain slice model. Invading cells are mainly found around the mouse brain vasculature (laminin, cyan). Laminin deposits in the tumour core can be used to distinguish stationary cells

lateral ventricles of the organotypic brain slice using a micromanipulator. The twelve H2B-mNeonGreen expressing cells (4 CTLs, 4 GFAPδ-KOs, 4 GFAPα-KOs) were co-injected with an internal control clone (I-CTL, CRISPR set A: CTL1, CRISPR set B: CTL3) that expressed H2B-mCherry. The brain slices injected with U251-MG cells were kept in culture for one week (Fig. 2a). Upon fixation of the *ex vivo* slices, we applied whole-mount immunofluorescent staining for laminin and used RapiClear tissue clearing (Bekkouche et al. 2020). Subsequently, we used confocal imaging to create a three-dimensional (3D)-reconstruction of the invasion patterns of the cells in the brain slice (Fig. 2b, Supp. Fig. 3). Laminin expression was not only observed along the blood vessels but deposits produced by the glioma cells were also observed at the injection site where the cell density was the highest (Fig. 2b, Supp. Fig. 3). We used this laminin expression pattern to distinguish cells within the tumour core from cells that had invaded into the mouse brain tissue (Supp. Fig. 3).

First, we compared the distribution of nuclei of the CTLs, GFAPδ-KOs, and GFAPα-KOs to that of the I-CTLs. We calculated the distance of every individual nucleus from the boundary of the tumour core and plotted the distribution of the cells within different distance bins (Fig. 2c). As expected, the distribution plot of H2B-mNeonGreen expressing CTLs overlapped with that of the H2B-mCherry expressing I-CTLs (Fig. 2d, Supp. Fig. 4a). The distribution of nuclei of the GFAPδ-KO cells slightly deviated from the I-CTL line (Fig. 2e,f, Supp. Fig. 4b), but the clearest alteration in distribution was observed in the GFAPα-KO cells. Whereas I-CTL cells have the highest density of cells in the tumour core, the GFAPα-KO cells showed a more diffuse growth pattern (Fig. 2g, Supp. Fig. 4c). When plotting the distribution of cells, a shift in cell density towards the tumour border and tissue was observed (Fig. 2h), indicating more invasion. We next quantified the percentage of cells in the tissue as a measure for invasion and indeed observed a higher percentage of invading GFAPα-KO cells in comparison to its I-CTL and in comparison to the CTLs (Fig. 2i). Whereas GFAPδ-KO

from cells invading the tissue, indicated with the orange dotted line. (c) Schematic depicting the method used to quantify the distribution of nuclei in the organotypic brain slices. (d) Distribution of nuclei of all I-CTL and CTL cells in the organotypic brain slices (n=16 independent experiments, 4 different clones). (e) Representative images of invasion pattern of GFAPδ-KO clone 1 and I-CTL 1. (f) Distribution of nuclei of all GFAPδ-KO and I-CTL cells in the organotypic brain slices (n=18 independent experiments, 4 different clones). (g) Representative image of the invasion pattern of GFAPα-KO clone 2 and I-CTL 1. (h) Distribution of nuclei of all GFAPα-KO cells and I-CTL cells in the organotypic brain slices (n= 20 independent experiments, 4 different clones). (i) Quantification of the percentage of invaded cells per condition, n= 16 (CTLs), n=18 (GFAPδ-KO), and n= 20 (GFAPα-KO) injected organotypic brain slices derived from 4 different clones (CRISPR set A and B) per condition. Significance was determined using a two-way ANOVA followed by Tukey's multiple comparisons test. Scale bar = 100 μm. The data is shown as mean ± S.E.M, *$p < 0.05$, **$p < 0.01$, ***$p < 0.001$, ****$p < 0.0001$, ns = not significant. NG= mNeonGreen, mCh = mCherry, Lam = laminin.

had similar percentages of invading cells compared to its I-CTL, a higher percentage of invading cells was measured in comparison to the CTLs (Fig. 2i).

To confirm the effect of downregulating GFAPα on tumour distribution patterns, we repeated the *ex vivo* organotypic brain slice invasion experiment with U251-MG cells transduced with an shRNA against the 3'UTR of GFAPα (Supp. Fig. 5a), as earlier published in Moeton et al. 2014. Targeting GFAPα at the mRNA level led to a diffuse growth pattern and more invading cells, similar to the observations seen in CRISPR-Cas9 modified cells (Supp. Fig. 5).

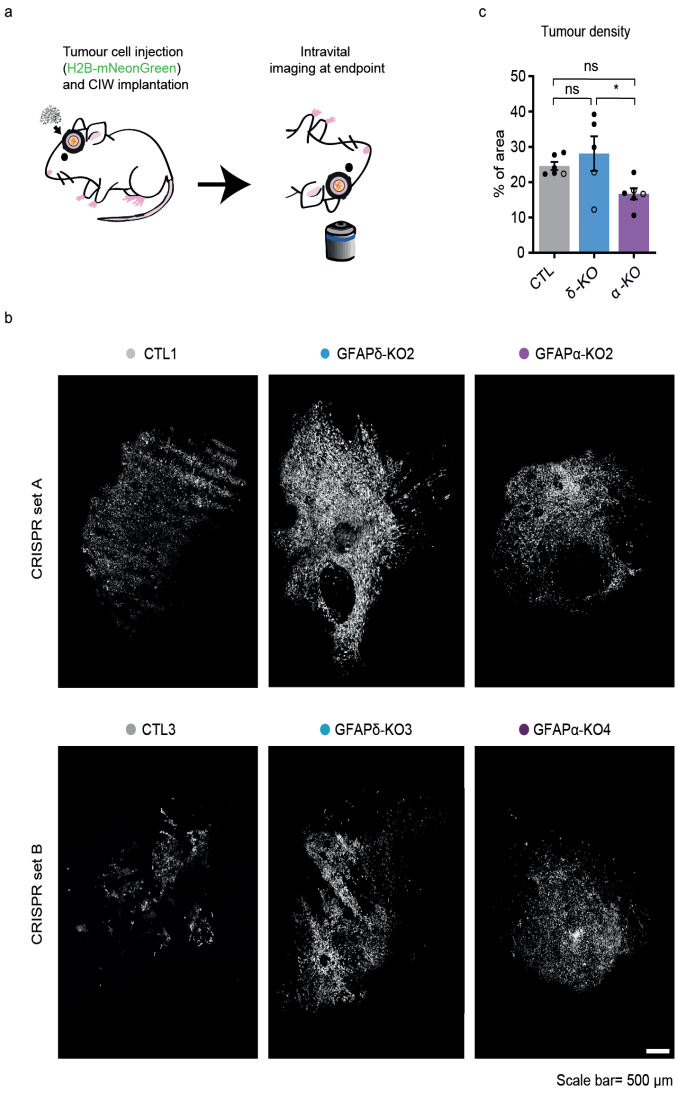

Depletion of GFAPα isoform leads to more diffuse tumours *in vivo*

Next, we aimed to study the GFAP-modulated cells in an *in vivo* setting where a functional vasculature is present, and where it is possible to follow tumour progression over time. We used intravital microscopy (IVM), which allows to longitudinally visualise tumour cell behaviour at the single-cell level in a living organism (Margarido et al. 2020). Per condition, we separately injected two H2B-mNeonGreen expressing clones with the most extreme GFAPδ/α ratio (CTL 1, GFAPδ-KO 2, and GFAPα-KO 2 from CRISPR set A, CTL 3, GFAPδ-KO 3, and GFAPα-KO 4 from CRISPR set B) into NOD-Scid IL2Rgnull (NSG) mice. Tumour development was followed using a cranial imaging window (CIW). An overview image of the tumour at the endpoint was taken, when a well-established tumour with similar size had formed (Fig. 3a, b). To quantify the tumour density, we calculated the number of individual cells in the total tumour area. We observed that tumours generated by the GFAPδ-KO were significantly denser than tumours generated by the GFAPα-KO cells (Fig. 3b,c). This suggested that GFAPα-KO cells have a more diffuse growth pattern compared to GFAPδ-KO cells.

Depletion of GFAP isoforms increases motility and alters invasion patterns *in vivo*

To further gain insight into the migratory behaviour of GFAP-modulated glioma cells *in vivo*, we again made use of the CIW to longitudinally study invasive behaviours at the single-cell level. At endpoint, a series of time-lapse z-stack images of the tumour was acquired for 6 hours with a time interval of 45 minutes (Fig. 4a). The movement of individual glioma cells was determined by tracking their migration path over time in 3D-reconstructed time-lapse movies (Fig. 4b). Data concerning migration velocity, speed, persistence, and directionality were extracted from the tracks. This showed that depletion of either GFAPδ or GFAPα isoform leads to an increase in the percentage of

<Figure 3. In vivo tumour growth dynamics in GFAP-modulated tumours. (a) Schematic overview of the experimental setup. U251-MG GFAP-modulated cell clones expressing H2B-NeonGreen were implanted in the brain of NSG mice under a CIW. Time-lapse intravital imaging was performed through a CIW to study the tumour growth dynamics of each tumour type. (b) Representative 3D reconstructed tile-scans showing distinct tumours generated by different GFAP-modulated clones. Two clones engineered with different CRISPR-Cas9 sgRNAs are presented (CTL1, GFAPδ-KO2 and GFAPα-KO2 from CRISPR set A and CTL3, GFAPδ-KO3 and GFAPα-KO4 from CRISPR set B). Scale bar = 500μm. (c) Quantification of tumour density for each indicated tumour type. n=6 (CTLs), n=5 (GFAPδ-KO), and n= 6 (GFAPα-KO) mice. All tumours were imaged when they had filled half the imaging window (endpoint), which was between 13 and 35 days after the cranial window implantation, except for one CTL1 tumour which reached endpoint after 72 days . Black dots represent clones from CRISPR set A (CTL1, GFAPδ-KO2, GFAPα-KO2) and white dots represent clones from CRISPR set B (CTL3, GFAPδ-KO3, GFAPα-KO4) .The data is shown as mean ± S.E.M, *$p < 0.05$, **$p < 0.01$, ***$p < 0.001$, ****$p < 0.0001$, ns = not significant, one-way ANOVA followed by Tukey's multiple comparisons test.

motile cells compared to the CTL (Fig. 4c). While the GFAPδ-KO cells migrate faster than the CTL cells (Fig. 4d, e), they move with less persistence compared to the GFAPα-KO and CTL cells (Fig. 4f). Considering that directionality is an important factor for invasion, we analysed the directionality patterns in each tumour type and determined whether the cells were migrating towards the tumour core or the brain parenchyma (Alieva et al. 2019). This demonstrated that GFAPα-KO cells migrate more towards the brain parenchyma while the CTL cells and GFAPδ-KOs migrate more randomly (Fig. 4 b,g). Indeed, this data is in line with our observation that GFAPα-KO tumours are more diffuse than GFAPδ-KO tumours (Fig. 3b, c).

It has been recently shown that nucleus stiffness and cell deformability plays an important role in cell motility. For instance, to move in a three-dimensional ECM, the nucleus of a cell must squeeze through the narrow spacing within the brain parenchyma (McGregor, Hsia, and Lammerding 2016; Wolf et al. 2013; Ivkovic et al. 2012). In our model, we observed a significant increase in the nuclear axis length of GFAPα-KOs compared to CTLs (Fig. 4h), which may contribute to the increased ability of GFAPα-KO to infiltrate the brain parenchyma.

Discussion

The invasive nature of glioma makes the disease highly aggressive and hard to treat. Therefore, precisely understanding the mechanisms driving invasion of glioma cells is crucial for the development of new anti-invasive treatment strategies. In this study, we investigated the role of GFAP isoforms in glioma cell invasion, using an organotypic brain slice invasion model and intravital imaging through a CIW. We show that the GFAPδ/α ratio affects the macroscopic growth patterns of glioma cells both *ex vivo* and

>Figure 4. In vivo migratory behaviour of tumour cells with different GFAPδ/α ratios. (a) Schematic representation of implantation of CIW and intravital time-lapse imaging over 6 hours with an interval of 45 minutes. (b) Representative still images from a time-lapse movie showing migratory tumour cells in different GFAP-modulated tumours (CTL1, GFAPδ-KO2, GFAPα-KO2) . Red lines highlight individual tumour cell tracks. Scale bar=20 μm. Corresponding plots represent tracks from a common origin showing the direction of the tumour cells either towards the tumour core or the brain parenchyma. (c) Percentage of motile (cell displacement > 2 μm/hour) and static cells for each tumour type. (d) Quantification of cell displacement of motile cells for the indicated tumour type. (e) Cell speed of motile cells for the different cell clones (μm/h). (f) Cell persistence of motile cells in the different cell clones. Black dots represent clones from CRISPR set A (CTL1, GFAPδ-KO2, GFAPα-KO2) and white dots clones from CRISPR set B (CTL3, GFAPδ-KO3, GFAPα-KO4) . (g) Tukey-style whiskers plot of the centre of mass displacement of individual positions of each condition. (h) Quantification of nuclear cell length in the different cell clones. % of cells with a length higher than 30 μm is represented. n=4 (CTLs), n=5 (GFAPδ-KO), and n=5 (GFAPα-KO) CIW mice implanted with 2 different cell clones, one of each CRISPR set. The data is shown as mean ± S.E.M, *$p < 0.05$, **$p < 0.01$, ***$p < 0.001$, ****$p < 0.0001$, ns = not significant, one-way ANOVA or two-way ANOVA followed by Tukey's multiple comparisons test.

in vivo by regulating cell migration speed, directionality, and persistence. Importantly, we demonstrate that GFAPδ-KO cells show increased motility compared to CTL and GFAPα-KO cells *in vivo*, but move randomly. GFAPα-KO cells, on the other hand, move more persistently and have a strong tendency to migrate towards the brain parenchyma. These dynamics of the GFAPα-KO cells lead to a more diffuse infiltration pattern into the brain parenchyma.

Earlier studies that investigated the role of GFAP in cell motility and migration have been somewhat inconsistent. As such, GFAP expression has been linked to both higher (De Pascalis et al. 2018; Lepekhin et al. 2001) and lower (Rutka et al. 1994; Elobeid et al. 2000; Moeton et al. 2014) velocities of cell migration. Also, shRNA mediated knockdown of GFAPα decreased cell velocity in an earlier *in vitro* study (Moeton et al.

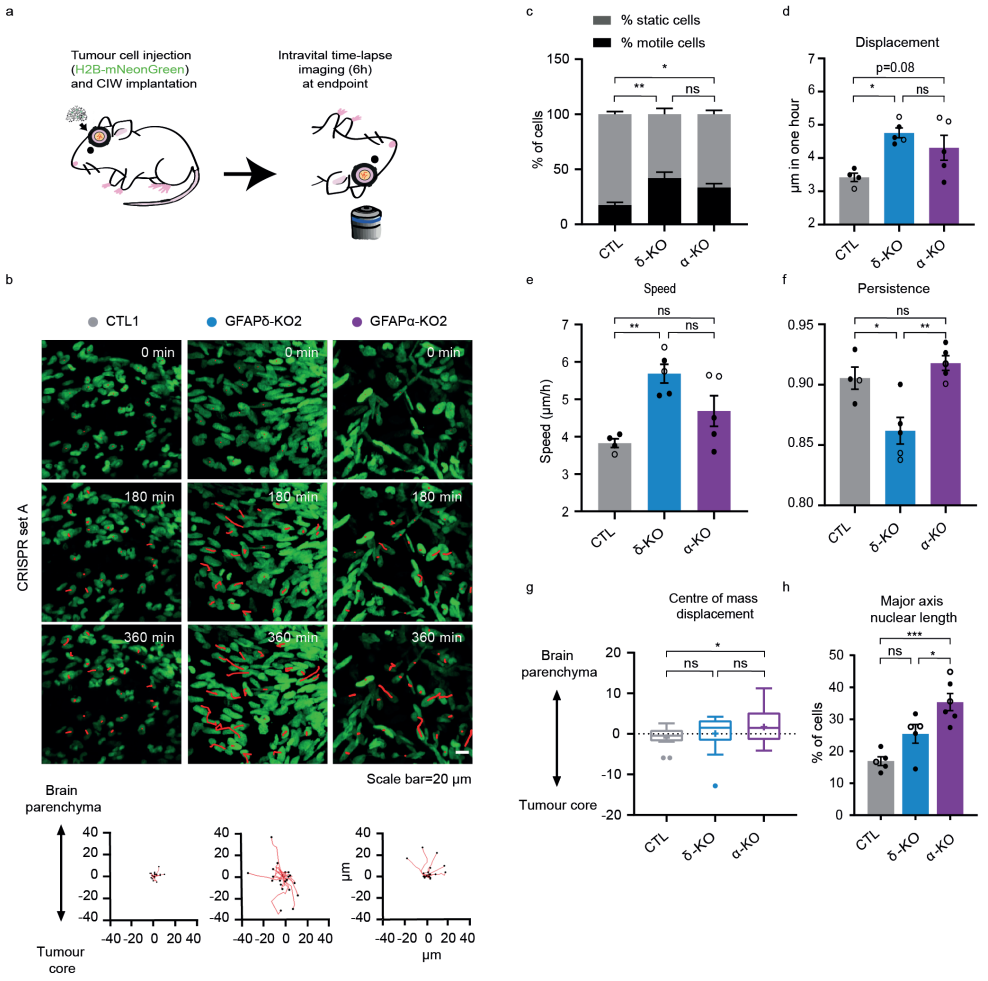

2014), which is inconsistent with the phenotype we describe here. The effect of GFAP depletion on cell behaviour might not only be isoform dependent, but also influenced by the cell-environmental context (Alieva et al. 2019), which may explain discrepancies between earlier studies performed in 2D. Our study is the first, to our knowledge, to investigate the role of GFAP and its isoforms within the physiological context of the brain. We find that depletion of both isoforms leads to an increase in the number of motile cells, as well as an increase in cell displacement and speed (Fig. 4c,d,e). Therefore, cell-intrinsic motility and velocity may not be dependent on the GFAPδ/α ratio, but on modification of the GFAP network in general. In contrast to motility and velocity, we demonstrate that directionality and persistence of cell migration is GFAP isoform dependent. Previous studies have shown that the IF network can promote migration persistence by modulating microtubule organisation and cell polarity (Gan et al. 2016; Shabbir et al. 2014; Schaedel et al. 2021; De Pascalis et al. 2018). Whether the absence of GFAPα or dominance of GFAPδ regulates directional migration similarly remains to be elucidated. The directionality of migration and invasion can also be steered by extrinsic factors such as ECM composition and topology (Petrie, Doyle, and Yamada 2009). For instance, adhesive interaction of the cell with the extracellular microenvironment as well as remodelling of the ECM are required to migrate efficiently through the extracellular space (Trepat, Chen, and Jacobson 2012). MMPs are responsible for the degradation of a large range of ECM proteins and GBM cells have been shown to overexpress MMP2 and 9 (Forsyth et al. 1999). In line with this, we showed in our previous work that modulation of the GFAPα isoform affects genes involved in the compositions of the ECM and extracellular space (Stassen et al. 2017). In addition, we previously demonstrated that GFAPα-KO cells produce more laminin and overexpress MMP2 by activating signaling pathways up- and downstream of dual-specificity phosphatase 4 (Moeton et al. 2014; van Bodegraven et al. 2019a).This might contribute to the higher ability of these cells to invade the brain parenchyma persistently. Additionally, it has been shown that immune cells, including macrophages and microglia, also promote glioma invasion (Broekman et al. 2018; Markovic et al. 2005; Chen et al. 2021). Considering that our experiments were performed in immunodeficient NOD-SCID mice, it remains to be elucidated whether interactions with immune cells potentially affect the invasive behaviour of glioma cells with different GFAPδ/α ratios.

The findings of this study contribute to our understanding on how a switch in the GFAPδ/α ratio in grade IV glioma patients may affect the aggressiveness of these tumours. Increased dominance of GFAPδ in grade IV glioma tumours has been reported by multiple studies (Andreiuolo et al. 2009; Choi et al. 2009; Heo et al. 2012; Stassen et al. 2017, reviewed in van Bodegraven et al. 2019b), and was confirmed by analysis of the updated TCGA database (Fig. 1a). Similarly, Brehar and colleagues reported that patients with highly invasive tumours, based on pre-operative MRI, had

increased percentages of GFAPδ positive cells (Brehar et al. 2015). Glioma tumours are known to be highly heterogeneous. This heterogeneity appears to be not only between patients but also between single cells within a tumour (Patel et al. 2014; Szerlip et al. 2012; Meyer et al. 2015), therefore it is likely that the same tumour is composed of a mix of cells with a high and low GFAPδ/α ratio and these distinct cell populations may contribute to different behaviour. Together, it can be hypothesised that a larger population of high GFAPδ/α ratio cells in grade IV tumours contributes to infiltration of the brain parenchyma and subsequent relapse after therapy. Further work is needed to understand the contribution of the GFAPδ/α ratio to the infiltrative growth of low and high-grade glioma tumours in clinical samples, for instance using intravital imaging in patient-derived xenografts (Zeng et al. 2020).

How the shift in GFAP isoform expression is established in grade IV tumours is currently unknown. Alternative splice events are known to occur more frequently in tumour tissue in comparison to non-malignant cells (Kahles et al. 2018), and dysregulation of the splicing machinery drives glioma aggressiveness (Fuentes-Fayos et al. 2020). Recently, it was discovered that hypoxia can induce adult-to-foetal splicing transitions in glioma, regulated by muscle blind-like proteins (MBNL, Voss et al. 2020). Hypoxia is considered an important driver of glioma invasion and is typically associated with grade IV gliomas (Gérard et al. 2019; Jensen et al. 2014). GFAP has multiple predicted binding motifs for the hypoxic-associated splicing factor MBNL (Paz et al. 2010). The link between hypoxia, GFAP alternative splicing, and cell invasion remains to be investigated.

In summary, our work demonstrates the importance of GFAP isoforms in fine-tuning glioma invasion and tumour dynamics. Together, the increased understanding of the mechanisms driving the invasive behaviours of different GFAP positive populations that form glioma tumours will help develop better anti-invasive therapeutic strategies in the future.

Materials and Methods

Cell lines and culture

The cell identity of malignant glioma cell line U251-MG (obtained from Lars Ruether, Institut für Neuropathologie, Universitätsklinikum Münster, Münster, Germany) was confirmed by short terminal repeat analysis (Eurofins Scientifc, Luxembourg city, Luxembourg). All cells were cultured in DMEM high glucose (Gibco 41966052) mixed 1:1 with Ham's F10 nutrient mix (Gibco 22390025) supplemented with 10% fetal bovine serum (Gibco 10270106/ Biowest S181H) and 1% penicillin/streptomycin (Gibco 15140122) at 37 °C in a humidified incubator with 5% CO_2. Cells were routinely tested negative for mycoplasma contamination.

Mice

For the generation of organotypic slice cultures, 15-17 day- old C57BL6J male and female mice were used. C57BL6J mice were obtained from Charles Rivers Laboratories and bred in-house. The animals were kept under a normal 12:12h light-dark cycle with lights off at 19:00, at room temperature (21 +/- 2 ºC) and at 40-70% humidity conditions, and were fed with chow and water ad libitum.

For intravital imaging experiments, NOD-Scid IL2Rgnull male and female mice (NSG), aged 8 to 20 weeks at the time of cranial window implantation were used. Mice were housed in individually ventilated cage and received food and water *ad libitum*. All experimental protocols used in this manuscript were in accordance with ARRIVE guidelines, national regulations, and ethical guidelines and were approved by the Centrale Commissie Dierproeven (CCD) and the Instantie voor Dierenwelzijn (IvD).

TCGA RNA sequencing data collection and analysis

Expression data of GFAP splice variants from the Cancer Genome Atlas (TCGA) was extracted using the TSVdb webtool (http://tsvdb.com)(Sun et al. 2018). Normalised RSEM (RNA-Seq by Expectation Maximization) count estimates from TCGA Lower Grade Glioma (TCGA-LGG) and glioblastoma multiforme (TCGA-GBMs) projects were extracted and matched with the sample ID to clinical data on histological subtype and malignancy grade downloaded from the TCGA database: https://www.cancer.gov/tcga. The GFAPα and GFAPδ normalised expression levels and GFAPδ/α ratios were compared in data from 64 grade II astrocytomas, 130 grade III astrocytomas and 153 GBMs.

Generation of CRISPR-Cas9 plasmids

Single guide RNAs (sgRNAs) targeting the intronic regions before and after exon7a (GFAPδ-KO) or exon 8 and 9 (GFAPα-KO) were designed using web resources of the Broad Institute (http://tools.genome-engineering.org/, Ran et al. 2013) or CRISPOR.org (http://crispor.tefor.net/, Concordet and Haeussler 2018) and were selected based on proximity to exons and MIT and CFD specificity score (Doench et al. 2016). The sgRNA complementary oligonucleotide templates (Supp. Table 1) were cloned into pSpCas9(BB)-2A-Puro (Addgene, #48139) or pSpCas9(BB)-2A-GFP (Addgene, #48138) plasmids after BbsI (Thermo Fisher Scientific) digestion. Plasmids were isolated using a Maxiprep kit (LabNed) and the sequence was verified by Sanger sequencing (Macrogen, Amsterdam, The Netherlands). Per GFAP isoform, two sets of CRISPR-Cas9 plasmids were generated (CRISPR δ-set A, CRISPR δ-set B, CRISPR α-set A, CRISPR α-set B, Supp. Table 1). Empty plasmids were used as a control (CRISPR

control A and CRISPR control B). The sgRNAs cloned into the pSpCas9(BB)-2A-Puro plasmid (CRISPR control A, δ-set A, α-set A) and the cell clones generated with these plasmids (CTL1, CTL2, δ-KO1, δ-KO2, α-KO1, α-KO2) have been described in van Bodegraven et al. 2019a. The sgRNA pairs cloned into the pSpCas9(BB)-2A-GFP plasmid (CRISPR control B, δ-set B, α-set B) and the cell clones generated with these plasmids (CTL3, CTL4, δ-KO3, δ-KO4, α-KO3, α-KO4) are first described in this paper.

For cell transfection of the CRISPR-Cas9 construct and clonal expansion, U251-MG cells were seeded at a density of 0.8 to 1.2 x 10^5 cells in an uncoated 6-well plate. Twenty-four hours after seeding, the sets of CRISPR-Cas9 plasmids (1 μg DNA total) with the sgRNAs upstream and downstream of the targeted exons of the GFAP isoforms were co-transfected using polyethylenimine (PEI, 166 ng/mL final concentration). Cells transfected with the pSpCas9(BB)-2A-Puro plasmids (CRISPR set A) were treated with 1 μg/mL puromycin (Sigma-Aldrich, 58-58-2) 24 hours after transfection and were selected for 96 hours. The drug-resistant pool was expanded and cell clones were generated by single-cell sorting cells into 96-well plates using fluorescence-activated cell sorting (FACS; FACSAria II Cell Sorter). Cells transfected with the pSpCas9(BB)-2A-GFP plasmids (CRISPR set B) were selected for GFP using FACS (FACSAria II Cell Sorter) 48 hours after transfection. The GFP-positive pool was expanded and cell clones were generated by plating cells at low densities in 96-well plates (0.5 cell/well). The 96-well plates were inspected for colony formation and cell clones were expanded.

Selection of CRISPR-Cas9 targeted cell clones

PCR screening was used to identify cell clones in which the targeted DNA region in the GFAP gene was depleted. Genomic DNA was isolated from cell pellets of the cell clones. Cells were lysed in 5 mM Twris HCl (pH 8.8) at 95°C for 10 minutes and treated with proteinase K at 56°C for 30 minutes. The CRISPR-Cas9 targeted DNA region was amplified using primers described in Supp. Table 1, using the FirePol PCR Master Mix (Solis BioDyne, 04-12-00S15). PCR products were separated on a 1.5% agarose gel containing SYBR Safe (Thermo Fisher Scientific, S33102) and GFAP isoform KO clones were identified based on the presence of predicted smaller PCR products. Depletion of the targeted DNA region was confirmed by isolating the amplified DNA of the PCR product using the PureLink Quick Gel Extraction Kit (Thermo Fisher Scientific, K210012) and Sanger sequencing (Macrogen, Amsterdam, The Netherlands).

shRNA construct design

Lentiviral shRNA expression plasmids targeting GFAPα or non-targeting controls were generated as described in Moeton et al. 2014. In short, lentiviral shRNA expression plasmids from the RNAi Consortium (TRC) Mission library were obtained from Sigma-Aldrich (TRCN0000083733)(Root et al. 2006). A human shRNA construct against nucleotides 2674-2694 in the 3' untranslated region of the GFAPα transcript or a SHC002 non-targeting construct (NTC) with no homology to human sequences were cloned into the pLKO.1 backbone. It was attempted to create shRNAs targeting the transcript of GFAPδ, however we were unsuccessful in significantly downregulating this isoform (data not shown).

Lentiviral production and transduction of cells

Lentiviruses encoding NTC or GFAPα shRNA were produced as described in Moeton et al. 2014. U251-MG cells were transduced with lentiviral particles encoding NTC or GFAPα shRNA with a multiplicity of infection (MOI) of 0.5. Three days after transduction, cells were selected by treatment with 1 μg/mL puromycin (Gibco, A1113803) to create stable cell lines.

All U251-MG GFAP-modulated cells (with CRISPR-Cas9 or shRNAs) and controls were transduced with lentiviruses to induce expression of H2B-mNeonGreen or H2B-mCherry. The pLV-H2B-mNeonGreen-IRES-puro plasmid was a gift from Dr. Hugo Snippert (Drost et al. 2015), the pLenti6-H2B-mCherry plasmid was a gift from Torsten Wittmann (Addgene plasmid # 89766). Lentiviral particles were produced with standard third-generation lentiviral protocol. In short, 2 x 10^7 293T cells (ATCC, ATCC-CRL-11268) were plated in a 15 cm^2 dish and transfected the next day with a total of 51.6 μg DNA of an envelope plasmid (pMD2.G), packaging plasmids (pMDLg/pRRE and pRSV-Rev) and pLV-H2B-mNeonGreen-IRES-puro or pLenti6-H2B-mCherry plasmid using PEI (166 ng/mL final concentration). The medium was replaced 24 hours after transfection. After 48 hours, the medium containing virus particles were collected and filtered through a 0.22 μm filter. The supernatants were ultracentrifuged at 22,000 rpm (rotor 70Ti, Beckman ultracentrifuge) at 16 °C for 2 hours and 40 minutes. The pellet was resuspended in PBS + 0.5% BSA (Sigma), aliquoted and stored at -80°C until further use. The viral titre was determined by transducing 293T cells with a dilution series of the virus. The viral titre was estimated in transducing units (TU) / mL by counting the number of transduced fluorescent cells 48 hours after transduction. The GFAP-modulated cells were transduced with H2B-mNeonGreen and H2B-mCherry lentiviral particles with an MOI of 1. Cells were passaged once and positive cells were selected by keeping the cells in medium containing 1.5 μg/mL puromycin (H2B-mNeonGreen clones) or 10 μg/mL blasticidin (H2B-mCherry clones) for three days.

Western blot analysis

Total protein was extracted from cultured cells scraped in suspension buffer [0.1M NaCl, 0.01 M Tris HCl (pH 7.6), 0.001 M EDTA, and Complete EDTA-free protease inhibitor cocktail (Roche)] and sonicated (2 x 10 seconds) in an ultrasonic bath. An equal amount of 2 x SDS loading buffer [100 μM Tris (pH 6.8), 4% SDS, 20% glycerol, 5% 2-ME, and bromophenol blue] was added to the cell suspension, samples were heated at 95 °C for 5 minutes and DNA was broken down by pushing the sample through a 25-gauge needle. Equal amounts of sample were loaded on a 10% SDS-page gel and proteins were separated by electrophoresis. Proteins were then blotted on a 0.45-μm pore size nitrocellulose membrane (GE Healthcare) using a wet/tank transfer blotting system (Biorad, 170390). Membranes were blocked in blocking buffer (50 mM Tris pH 7.4, 150 mM NaCl, 0.25% (w/v) gelatin, 0.5% Triton-X100) for 10 minutes and incubated with primary antibodies (Supp. Table 2) in blocking buffer overnight at 4 °C. Membranes were washed with TBS with 1% Tween (TBS-T) three times for 10 minutes and then incubated with secondary antibodies (Supp. Table 2) in blocking buffer at room temperature for 1 hour. After three washing steps with TBS-T and one washing step with MilliQ, the membrane blots were scanned with the Odyssey Clx Western Blot Detection System (Li-Cor Biosciences). The background-corrected signal intensity of bands corresponding to the GFAPpan and GFAPδ proteins were measured and normalised against the intensity levels of glyceraldehyde 3- phosphatedehydrogenase (GAPDH) bands on the same blots.

RNA isolation, cDNA isolation and real-time quantitative PCR

For RNA extraction of cultured cells, cells were seeded on poly-D lysine (PDL)-coated wells of a 24-well plate at a density of 4×10^4 cells. After three days in culture, cells were lysed in TRIzol (Thermo Fisher Scientific, 15596026) and RNA was extracted using standard TRIzol-chloroform extraction methods. RNA concentration and purity were measured using Varioscan Flash (Thermo Fisher Scientific). 200 to 500 ng of RNA were used to prepare cDNA using the QuantiTect Reverse Transcription Kit (Qiagen, 205311) according to the manufacturer's protocol. The generated cDNA was used for real-time quantitative PCR using the SYBR Green Master mix in a QuantStudio 6 Flex Real-Time PCR system (Thermo Fisher Scientific, 4309155) using the primers listed in Supp. Table 1. Expression values were calculated by transforming Ct values (2^{-Ct}) and were normalised to the mean value of the transformed Ct values of the reference genes GAPDH and Alu element Jurka (Alu- J).

Immunocytochemistry

For immunocytochemistry on cultured cells, cells were seeded on PDL-coated coverslips in a 24-well plate at a density of 2×10^4 cells. After three days in culture, the cells were fixed in 4% paraformaldehyde (PFA) dissolved in phosphate buffer saline (PBS), pH 7.4 for 30 minutes. Cells were washed in PBS, incubated in a blocking buffer (50 mM Tris pH 7.4, 150 mM NaCl, 0.25% (w/v) gelatine, and 0.5% triton X-100) at room temperature for 15 min, and afterwards with primary antibodies (Supp. Table 2) in blocking buffer overnight at 4°C. Coverslips were washed with PBS and incubated with secondary antibodies (Supp. Table 2) and Hoechst 33528 (1:1000, Thermo Fisher Scientific, H3569) in blocking buffer at room temperature for 1 hour. After washing steps with PBS, the coverslips were mounted on microscopy slides with Mowiol (0.1 M tris-HCl pH 8.5, 25% glycerol, 10% Mowiol (Merck Millipore, 81381). The samples were imaged using a Zeiss Axioscope A1 microscope with a 40x objective.

Generation of Organotypic Brain Slices

For the generation of organotypic brain slices, the protocol of Pencheva et al., 2017 was adapted (Pencheva et al. 2017). Postnatal day 15 – 17 C57BL6/J pups were decapitated, the brains were dissected and captured in ice-cold artificial cerebrospinal fluid (aCSF, pH7.2: 10 mM Hepes, 21 mM $NaHCO_3$, 1.2 mM NaH_2PO_4, 2.5 mM KCl, 2 mM $MgCl_2$, 2 mM $CaCl_2$, 5 mM D-glucose, 250 mM glycerol in milliQ). The brains were transferred to a petri dish and cerebellum and olfactory bulbs were removed. The cerebrum was glued to the vibratome cutting stage using a drop of Loctite 401 glue (Henkel Adhesives) with the rostral part facing upwards. The vibratome cutting stage was mounted on a VT1000S vibratome (Leica Biosystems,1404723512) and tissue was fully submerged in carbonated ice-cold aCSF. Coronal brain slices of 350 µm were cut with a speed of 0.1 mm/s and a frequency of 7 Hz. Slices with visible lateral ventricles were transferred to 1.0-µm porous membrane inserts (Corning®, 353102) in a 6-well plate with slicing medium [DMEM:F12 (Gibco, 11320), 1% L-Glutamine (Gibco, 25030123), 5 mM HEPES, 21 mM $NaHCO_3$ and 1% pen/strep (Gibco, 15140122], with a maximum of 4 slices per transwell insert. Residual aCSF was removed from the inserts, the brain slices were washed with PBS and the transwells were transferred to 1.5 mL recovery medium (DMEM:F12, 25% FBS, 1% L-Glutamine, 5 mM HEPES, 21 mM $NaHCO_3$ and 1% P/S) below the transwells, allowing the slices to be cultured at the air-liquid interface. The slices were cultured at 37 °C in a humidified incubator with 5% CO_2 overnight. The next day, the transwells were dipped twice in PBS and transferred to a 6-well plate containing NSC medium (DMEM:F12 – GlutaMAX, 1% pen/strep, 10 ng/mL EGF (Peprotech, AF-100-15-A), 10 ng/mL FGF (Peptrotech, AF-100-18B) before injection of cells.

Organotypic brain slice invasion assay

Cells were counted using the Countess 3 FL Automated Cell Counter (Thermo Fischer Scientific, AMQAF2000) and suspensions of 2.5×10^5 cells/ µl were prepared. For the mixed cell injections, H2B-mNeonGreen expressing cells were mixed at a 1:1 ratio with H2B-mCherry expressing internal control cells. For the CRISPR-Cas9 modulated cells, CTL-1-H2B-mCherry was used as an internal control (I-CTL1) for the CRISPR-set-A clones(CTL 1 and 2, GFAPδ-KO 1 and 2, GFAPα-KO 1 and 2), and CTL-3-H2B-mCherry was used as an internal control (I-CTL2) for the CRISPR- set-B clones (CTL 3 and 4, GFAPδ-KO 3 and 4, GFAPα-KO 3 and 4). For the shRNA modulated cells, NTC-H2B-mCherry was used as an internal control. A Hamilton 0.5 µL syringe model 7000.5 KH (Hamilton, 86250) was assembled on a Narishige micromanipulator model MM-3 (Narishige group) and was placed on the magnetic board of a Leica MS5 dissection microscope (Leica Biosystems), using a Narishige GJ-8 magnetic stand (Narishige group). The syringe was rinsed with acetone, 70% ethanol, and PBS before use. Before injection, the cell suspension was mixed and 0.5 µL was taken up by the syringe. The needle was placed into the lateral ventricle of the brain slice by moving 50 µm into the tissue and 40 µm out. The cell suspension was slowly injected into the lateral ventricle of the mouse brain tissue, filling up the lateral ventricle without overflowing on the tissue. The medium of the organotypic brain slices was replaced every 2-3 days. One week after injection of the cells, the brain slices were washed with PBS and fixed in 4% PFA in PBS at 4 °C overnight.

Whole-mount immunostaining and RapiClear clearing

For whole-mount immunostaining of the organotypic brain slices, we used the method described in Belle et al. 2014. The porous membrane surrounding the brain tissue was cut out and transferred to a 24-well dish. The tissue was permeabilised in 2% Triton-X-100 (Roche, 40319421) in PBS and subsequently incubated in PBSGT blocking solution (0.2% gelatin, 0.5% Triton-X-100, 0.01 % thimerosal or 0.2 % sodium azide in 1x PBS), for a minimum of 4 hours at room temperature. Primary antibodies were diluted in PBSGT + 0.1% saponin, 300 µL was added to the tissue and incubated on a horizontal shaker (70 rpm) at 37 °C for 3 days. Tissue injected with mixed H2B-mNeonGreen/ H2B-mCherry cells were incubated with rabbit anti-laminin antibodies (1:1000, Supp. Table 2). The empty wells were filled with PBS to avoid evaporation of the primary antibody mix. The tissue was washed 6 times in PBS with 0.25% Triton-X-100 for one hour. Secondary antibodies were diluted in PBSGT + 0.1% saponin and the mix was spun down to precipitate aggregates. 300 µL was added to the tissue and incubated on a horizontal shaker (70 rpm) at 37 °C for 24h. The tissue was washed 6 times in PBS with 0.25% Triton-X-100 for one hour. For tissue clearing of the organotypic brain slices,

we selected the RapiClear protocol developed by SunJin Lab, as this protocol does not lead to tissue shrinkage and the protocol is non-laborious (Bekkouche et al. 2020; www.sunjinlab.com, n.d.). For tissue clearing, the brain slices were transferred to iSpacers (SunJin Lab Co., #IS002) mounted on microscope slides and 300 µL of RapiClear 1.47 (SunJin Lab Co, #RC147001) was added on the brain slices. The slices were cleared at 37 ºC on a horizontal shaker (30 rpm) for 45 minutes, mounted with a coverslip in RapiClear 1.47, and sealed with transparent nail polish. The cleared brain slices were imaged using an LSM 880 (Zeiss) confocal microscope equipped with a 3-channel QUASAR Detection Unit (000000-2078-293). The entire population of injected cells was imaged with a 10x objective (N-Achroplan 10x, 420940-990-000) at 1.77 µm pixel resolution Z-plane increments of 6.63 µm and using image tiling. Smaller regions were imaged using a 20x objective (LD Plan-NEOFLUAR 20x, 421350-9970-000) at 0.42 µm pixel resolution and 3.39 µm Z-plane increments.

Quantification of cell invasion in ex vivo slices

Cell invasion in the organotypic brain slices was quantified in the confocal generated images using ImageJ (1.53c) and Imaris software (version 8.4). Upon blinding, images were excluded from analysis when errors had occurred during the injections of cells (overflowing of tissue, large populations of unhealthy looking cells). Using ImageJ software, image tiling was used to reconstruct the entire population of injected cells. The tiled z-stack consisted of an H2B-mNeonGreen and H2B-mCherry channel with the nuclei of the injected glioma cells and a laminin channel staining the mouse vasculature. In addition to staining the vasculature, laminin also gave rise to a diffuse staining at the location where tumour density was highest, as shown by H2B-mCherry/H2B-mNeonGreen signal. This staining of the ECM deposits generated by the tumour cells was used to draw a boundary between the tumour core and the mouse tissue (Supp. Fig.3) in the different z-planes. An additional channel was generated in which only the tumour core laminin staining was selected. The stitched images with additional laminin-channel were imported into the Imaris Software (version 8.4). The 'create surface' function was used to generate a 3D surface of the laminin tumour core signal (background subtraction, estimated diameter 17.8, threshold =2, voxels =1). The 'create spots' function was used to generate individual spots (11 µm + PSF-elongation along the Z-axis) of the H2B-mCherry nuclei using a standardised Quality threshold filter, adjusted so that cells in all z-planes were detected. Using the same function, the same number of H2B-mNeonGreen spots was generated. The 'distance transformation' function was used for the tumour core surface, generating a new channel where the intensity of the signal represented the distance from the 'outside surface object' or 'inside surface object'. The Imaris software was used to calculate for every H2B-mCherry and

H2B-mNeonGreen nucleus the distance to the tumour core, using the 'intensity center' calculation within the "statistics" function. The excel file was exported and histograms of the distances (bin size 20 µm) were created using the NumPy package of the Python software (Harris et al. 2020).

Tumour cell injection and cranial window implantation (CWI) surgery

Two clones per condition generated by two different sgRNA were used for the *in vivo* experiments: CTL 1 (CRISPR-set-A) and 3 (CRISPR-set-B), GFAPδ-KO 2 (CRISPR-set-A) and 3 (CRISPR-set-B), and GFAPα-KO 2 (CRISPR-set-A) and 4 (CRISPR-set-B). Clones with the most extreme GFAPδ/α ratio were selected, except for the GFAPα-KO clone 3 as network collapses were observed in this line. Per injection, 100,000 U251-MG cells were resuspended in 3µl of PBS and injected the same day as the cranial window was implanted. CWI was performed as previously described (Alieva et al. 2017). In short, mice were sedated with 4% isoflurane inhalation for inducing anaesthesia and 1.5-2% during surgery. The hair from the back of the neck up to the eyes was shaved. Next, the mouse head was firmly fixed with ear bars in a stereotaxic device. Eye ointment was applied to prevent the animal's eyes from drying out. Next, the skin was cut circularly. After scraping the periosteum underneath to the edges of the skull, a circular groove of 5 mm diameter was drilled over the right parietal bone. After craniotomy, the dura mater was removed with a fine forceps. Next, tumour cells were injected stereotactically using a 10 µl Hamilton syringe with a 2 pt style needle in the middle of the craniotomy at a depth of 0.5 mm. The exposed brain was sealed with silicone oil and a 6 mm coverslip glued on top. Dental acrylic cement (Vertex) was applied on the skull surface to cover the edge of the coverslip and a 3D printed plastic ring was glued around the coverslip to provide fixation to the microscope. A single dose of 100 µg/kg of buprenorphine (Temgesic, Indivior Europe Limited) was administered before the surgery and the day after surgery. In addition Rimadyl in water was administered 24 hours before CIW implantation and for a total of 72 hours (Zoetis). After surgery, the mice were provided food and water *ad libitum*. Mice were closely monitored twice per week.

Intravital imaging

Mice were anaesthetised in an induction chamber with 4.0% isoflurane. Next, they were placed face-up in a custom-designed imaging box. A 3D printed imaging plate facilitated CWI fixation. Isoflurane was introduced through the facemask and ventilated by an outlet on the other side of the box. To study cell migration, time-lapse images of several positions of the tumour volume were acquired every 45 minutes for a maximum of 6 hours, during which the climate chamber surrounding the microscope was kept

at 37 °C and the mouse body temperature was monitored with a rectal thermometer. For each position, images of the complete z stack of the tumour were acquired, with a step size of 3 µm. Imaging was performed on an inverted Leica SP8 multiphoton microscope with a chameleon Vision-S (Coherent Inc., Santa Clare, CA, www.coherent.com). This microscope is equipped with a 25x (HCX IRAPO NA0.95 WD 2.5mm) water objective with four non-descanned detectors (NDDs). The NDDs detected the following wavelengths: NDD1 <455 nm, NDD2 455–505 nm, NDD3 500–550 nm, NDD4 555–680 nm. H2B-mNeonGreen was excited with 944 nm and detected with NDD3. Scanning was performed in a bidirectional mode at 400 Hz and 12 bit, with a zoom of 1, and 512 × 512 pixels.

Quantification of tumour density

Density was calculated at endpoint. A tumour was considered endpoint when approximately 50% or more of the cover slip of the imaging window was covered with tumour cells. All tumours included in the analysis were imaged between 13 and 35 days after the cranial window was implanted, except for one CTL1 which reached endpoint 72 days after window implantation due to a miss injection. To quantify the tumour density, we calculated the number of individual cells in the total tumour area. The quantification was done using ImageJ (U. S. NIH, Bethesda, Maryland, USA).

Tracking migration of tumour cells

All mice that were succesfully imaged for 6 hours were included in the analysis. The analysis were done in a blinded manner. The tracking of migratory cells was done as previously described (Alieva et al. 2017). After imaging, acquired z-stacks were corrected for z and xy shifts with Huygens Professional software program (version20.10). Up to 300 cells per mouse were tracked manually with an ImageJ plugin ("MTrackJ" Rasband, W.S., ImageJ, U. S. NIH, Bethesda, Maryland, USA). At the start of each movie, a random cell was selected. The XY position was determined over time and the displacement, speed and persistence for each cell were calculated by Excel (Microsoft). The spatial average of all cell positions was used to measure the centre of mass displacement. For each border position, the centre of mass along the Y-axis was measured by the 'Chemotaxis and Migration Tool'. Calculation of the centre of mass (M_{end}). i= index of single cells, n= number of cells, $X_{i,end}$ $Y_{i,end}$ = coordinates of the respective endpoint.

$$M_{end} = \frac{1}{n}\sum_{i=1}^{n}(x_{i,end},\ Y_{i,end})$$

Statistical analysis

The normality of data was tested using the Shapiro-Wilk test. For all normally distributed measurements, one-way ANOVA (when >2 means were compared) or two-way ANOVA followed by Tukey's multiple comparisons test were used to determine significance, set to $p < 0.05$. For non-normally-distributed measurements, a Kruskal-Wallis test (when >2 means were compared) followed by Dunn's multiple comparisons test were used to determine significance. All p values were two-tailed. Levels of significance were set as follows: ns > 0.05, *0.05 ≤ p > 0.01, **0.01 ≤ p > 0.001, ***0.001 ≤ p > 0.0001, ****p ≤ 0.0001. Error bars are presented as mean ± S.E.M. All statistical analyses were performed using GraphPad Prism software (version 9.1.2, GraphPad Software, USA).

Acknowledgements

The results shown here are partly based on data generated by The Cancer Genome Atlas Research Network (https://www.cancer.gov/tcga). The authors thank all members of the Hol and van Rheenen labs for thoughtful discussion. This study was funded by the Dutch Cancer Society [KWF 101123, R.U.C, J.v.A, J.v.R, E.H.], a HFSP fellowship (C.V.), the Portuguese Foundation for Science and Technology (FCT, GABBA program-PD/BD/105748/2014, A.S.M.), the T and P Bohnenn Foundation (P.R) and the Josef Steiner Foundation (J.v.R).

Author Contributions

R.U.C and J.v.A. performed conceptualisation, data collection, formal analysis, methodology, and wrote the original draft. C.V. performed conceptualisation, methodology, supervision, and reviewed and edited the manuscript. J.S. performed data collection, methodology, and reviewed and edited the manuscript. E.v.B. performed conceptualisation, methodology, and reviewed and edited the manuscript. A.S.M. performed methodology, and reviewed and edited the manuscript. P.R. performed conceptualisation, methodology, supervision, and reviewed and edited the manuscript. J.v.R. performed conceptualisation, funding acquisition, project administration, methodology, supervision, and reviewed and edited the manuscript. E.H. performed conceptualisation, funding acquisition, project administration, methodology, supervision, and reviewed and edited the manuscript.

References

Alieva, Maria, Verena Leidgens, Markus J. Riemenschneider, Christoph A. Klein, Peter Hau, and Jacco van Rheenen. 2019. "Intravital Imaging of Glioma Border Morphology Reveals Distinctive Cellular Dynamics and Contribution to Tumor Cell Invasion." Scientific Reports 9 (1): 1–11. https://doi.org/10.1038/s41598-019-38625-4.

Alieva, Maria, Andreia S. Margarido, Tamara Wieles, Erik R. Abels, Burcin Colak, Carla Boquetale, Herke Jan Noordmans, Tom J. Snijders, Marike L. Broekman, and Jacco van Rheenen. 2017. "Preventing Inflammation Inhibits Biopsy-Mediated Changes in Tumor Cell Behavior." Scientific Reports 7 (1): 7529. https://doi.org/10.1038/s41598-017-07660-4.

Andreiuolo, Felipe, Marie Pierre Junier, Elly M. Hol, Catherine Miquel, Leila Chimelli, Nadine Leonard, Hervé Chneiweiss, Catherine Daumas-Duport, and Pascale Varlet. 2009. "GFAPδ Immunostaining Improves Visualization of Normal and Pathologic Astrocytic Heterogeneity." Neuropathology 29 (1): 31–39. https://doi.org/10.1111/j.1440-1789.2008.00936.x.

Bekkouche, Bo M.B., Helena K.M. Fritz, Elisa Rigosi, and David C. O'Carroll. 2020. "Comparison of Transparency and Shrinkage During Clearing of Insect Brains Using Media With Tunable Refractive Index." Frontiers in Neuroanatomy 14 (November): 1–19. https://doi.org/10.3389/fnana.2020.599282.

Bellail, Anita C., Stephen B. Hunter, Daniel J. Brat, Chalet Tan, and Erwin G. Van Meir. 2004. "Microregional Extracellular Matrix Heterogeneity in Brain Modulates Glioma Cell Invasion." International Journal of Biochemistry and Cell Biology 36 (6): 1046–69. https://doi.org/10.1016/j.biocel.2004.01.013.

Belle, Morgane, David Godefroy, Chloé Dominici, Céline Heitz-Marchaland, Pavol Zelina, Farida Hellal, Frank Bradke, and Alain Chédotal. 2014. "A Simple Method for 3D Analysis of Immunolabeled Axonal Tracts in a Transparent Nervous System." Cell Reports 9 (4): 1191–1201. https://doi.org/10.1016/j.celrep.2014.10.037.

Berge, Simone A. van den, Jinte Middeldorp, C. Eleana Zhang, Maurice A. Curtis, Brian W. Leonard, Diego Mastroeni, Pieter Voorn, Wilma D.J. van de Berg, Inge Huitinga, and Elly M. Hol. 2010. "Longterm Quiescent Cells in the Aged Human Subventricular Neurogenic System Specifically Express GFAP-δ." Aging Cell 9 (3): 313–26. https://doi.org/10.1111/j.1474-9726.2010.00556.x.

Birbrair, Alexander. 2017. "Stem Cell Microenvironments And Beyond." Advances in Experimental Medicine and Biology, vol 1041. Springer, Cham. https://doi.org/10.1007/978-3-319-69194-7_1

Blechingberg, Jenny, Holm, Ida E., Nielsen, Karsten B., Jensen, Torben H., Jørgensen, Arne L., Nielsen, Anders L. 2007. "Identification and Characterization of GFAPj, a Novel Glial Fibrillary Acidic Protein Isoform." Glia 55: 487-507. https://doi.org/10.1002/glia.

Blechingberg, Jenny, Søren Lykke-andersen, Torben Heick Jensen, Arne Lund Jørgensen, and Anders Lade Nielsen. 2007. "Regulatory Mechanisms for 3'-End Alternative Splicing and Polyadenylation of the Glial Fibrillary Acidic Protein, GFAP, Transcript." Nucleic Acids Research 35 (22): 7636–50. https://doi.org/10.1093/nar/gkm931.

Bodegraven, Emma J. van, Jessy V. van Asperen, Pierre A.J. Robe, and Elly M. Hol. 2019. "Importance of GFAP Isoform-Specific Analyses in Astrocytoma." Glia 67 (8): 1417–33. https://doi.org/10.1002/glia.23594.

Bodegraven, Emma J. van, Jessy V. van Asperen, Jacqueline A. Sluijs, Coen B.J. van Deursen, Miriam E. van Strien, Oscar M.J.A. Stassen, Pierre A.J. Robe, and Elly M. Hol. 2019. "GFAP Alternative Splicing Regulates Glioma Cell-ECM Interaction in a DUSP4-Dependent Manner." FASEB Journal : Official Publication of the Federation of American Societies for Experimental Biology 33 (11): 12941–59. https://doi.org/10.1096/fj.201900916R.

Brehar, Felix Mircea, Dorel Arsene, Lacramioara Aurelia Brinduse, and Mircea Radu Gorgan. 2015. "Immunohistochemical Analysis of GFAP-δ And Nestin in Cerebral Astrocytomas." Brain Tumor Pathology 32 (2): 90–98. https://doi.org/10.1007/s10014-014-0199-8.

Broekman, Marike L., Sybren L. N. Maas, Erik R. Abels, Thorsten R. Mempel, Anna M. Krichevsky, and Xandra O. Breakefield. 2018. "Multidimensional Communication in the Microenvirons of Glioblastoma." Nature Reviews Neurology 14 (8): 482-495. https://doi.org/10.1038/s41582-018-0025-8.

Chen, Houminji, Ming Li, Yanwu Guo, Yongsheng Zhong, Zhuoyi He, Yuting Xu, and Junjie Zou. 2021.

"Immune Response in Glioma ' s Microenvironment." Innovative surgical sciences 5(3-4): 115-125. https://doi.org/10.1515/iss-2019-0001

Cheung, Kevin J., Edward Gabrielson, Zena Werb, and Andrew J. Ewald. 2013. "Collective Invasion in Breast Cancer Requires a Conserved Basal Epithelial Program." Cell 155 (7): 1639–51. https://doi.org/10.1016/j.cell.2013.11.029.

Choi, Kyung-Chan, Sung-Eun Kwak, Ji-Eun Kim, Seung Hun Sheen, and Tae-Cheon Kang. 2009. "Enhanced Glial Fibrillary Acidic Protein-δ Expression in Human Astrocytic Tumor." Neuroscience Letters 463 (3): 182–87. https://doi.org/10.1016/j.neulet.2009.07.076.

Concordet, Jean Paul, and Maximilian Haeussler. 2018. "CRISPOR: Intuitive Guide Selection for CRISPR/Cas9 Genome Editing Experiments and Screens." Nucleic Acids Research 46 (W1): W242–45. https://doi.org/10.1093/nar/gky354.

Doench, John G., Nicolo Fusi, Meagan Sullender, Mudra Hegde, Emma W. Vaimberg, Katherine F. Donovan, Ian Smith, et al. 2016. "Optimized SgRNA Design to Maximize Activity and Minimize Off-Target Effects of CRISPR-Cas9." Nature Biotechnology 34 (2): 184–91. https://doi.org/10.1038/nbt.3437.

Drost, Jarno, Richard H. Van Jaarsveld, Bas Ponsioen, Cheryl Zimberlin, Ruben Van Boxtel, Arjan Buijs, Norman Sachs, et al. 2015. "Sequential Cancer Mutations in Cultured Human Intestinal Stem Cells." Nature 521 (7550): 43–47. https://doi.org/10.1038/nature14415.

Duffy, Philip E, and Maurice M Rapport. 1982. "The relationship of glial fibrillary acidic protein to the shape, motility, and differentiation of human astrocytoma cells". Experimental cell research 139(1), 145-157. https://doi.org/10.1016/0014-4827(82)90328-7

Elobeid, A., E. Bongcam-Rudloff, B. Westermark, and M. Nistér. 2000. "Effects of Inducible Glial Fibrillary Acidic Protein on Glioma Cell Motility and Proliferation." Journal of Neuroscience Research 60 (2): 245–56. https://doi.org/10.1002/(SICI)1097-4547(20000415)60:2<245::AID-JNR14>3.0.CO;2-1.

Forsyth, P. A., H. Wong, T. D. Laing, N. B. Rewcastle, D. G. Morris, H. Muzik, K. J. Leco, et al. 1999. "Gelatinase-A (MMP-2), Gelatinase-B (MMP-9) and Membrane Type Matrix Metalloproteinase-1 (MT1-MMP) Are Involved in Different Aspects of the Pathophysiology of Malignant Gliomas." British Journal of Cancer 79 (11–12): 1828–35. https://doi.org/10.1038/sj.bjc.6990291.

Fuentes-Fayos, Antonio C., Mari C. Vázquez-Borrego, Juan M. Jiménez-Vacas, Leire Bejarano, Sergio Pedraza-Arévalo, Fernando L-López, Cristóbal Blanco-Acevedo, et al. 2020. "Splicing Machinery Dysregulation Drives Glioblastoma Development/Aggressiveness: Oncogenic Role of SRSF3." Brain : A Journal of Neurology 143 (11): 3273–93. https://doi.org/10.1093/brain/awaa273.

Gan, Zhuo, Liya Ding, Christoph J. Burckhardt, Jason Lowery, Assaf Zaritsky, Karlyndsay Sitterley, Andressa Mota, et al. 2016. "Vimentin Intermediate Filaments Template Microtubule Networks to Enhance Persistence in Cell Polarity and Directed Migration." Cell Systems 3 (3): 252-263.e8. https://doi.org/10.1016/j.cels.2016.08.007.

Gérard, Michael, Aurélien Corroyer-Dulmont, Paul Lesueur, Solène Collet, Michel Chérel, Mickael Bourgeois, Dinu Stefan, et al. 2019. "Hypoxia Imaging and Adaptive Radiotherapy: A State-of-the-Art Approach in the Management of Glioma." Frontiers in Medicine 6 (June). https://doi.org/10.3389/fmed.2019.00117.

Harris, Charles R., K. Jarrod Millman, Stéfan J. van der Walt, Ralf Gommers, Pauli Virtanen, David Cournapeau, Eric Wieser, et al. 2020. "Array Programming with NumPy." Nature 585 (7825): 357–62. https://doi.org/10.1038/s41586-020-2649-2.

Hatoum, Adam, Raihan Mohammed, and Omar Zakieh. 2019. "The Unique Invasiveness of Glioblastoma and Possible Drug Targets on Extracellular Matrix." Cancer Management and Research 11: 1843–55. https://doi.org/10.2147/CMAR.S186142.

Heo, Dong Hwa, Se Hoon Kim, Kyung-Moo Yang, Yong Jun Cho, Keung Nyun Kim, Do Heum Yoon, and

Tae-Cheon Kang. 2012. "A Histopathological Diagnostic Marker for Human Spinal Astrocytoma: Expression of Glial Fibrillary Acidic Protein-δ." Journal of Neuro-Oncology 108 (1): 45–52. https://doi.org/10.1007/s11060-012-0801-z.

Ho, Vincent K.Y., Jaap C. Reijneveld, Roelien H. Enting, Henri P. Bienfait, Pierre Robe, Brigitta G. Baumert, and Otto Visser. 2014. "Changing Incidence and Improved Survival of Gliomas." European Journal of Cancer 50 (13): 2309–18. https://doi.org/10.1016/j.ejca.2014.05.019.

Ivkovic, Sanja, Christopher Beadle, Sonal Noticewala, Susan C. Massey, Kristin R. Swanson, Laura N. Toro, Anne R. Bresnick, Peter Canoll, and Steven S. Rosenfeld. 2012. "Direct Inhibition of Myosin II Effectively Blocks Glioma Invasion in the Presence of Multiple Motogens." Molecular Biology of the Cell 23 (4): 533–42. https://doi.org/10.1091/mbc.E11-01-0039.

Jensen, Randy L., Michael L. Mumert, David L. Gillespie, Anita Y. Kinney, Matthias C. Schabel, and Karen L. Salzman. 2014. "Preoperative Dynamic Contrast-Enhanced MRI Correlates with Molecular Markers of Hypoxia and Vascularity in Specific Areas of Intratumoral Microenvironment and Is Predictive of Patient Outcome." Neuro-Oncology 16 (2): 280–91. https://doi.org/10.1093/neuonc/not148.

Kahles, André, Kjong Van Lehmann, Nora C. Toussaint, Matthias Hüser, Stefan G. Stark, Timo Sachsenberg, Oliver Stegle, et al. 2018. "Comprehensive Analysis of Alternative Splicing Across Tumors from 8,705 Patients." Cancer Cell 34 (2): 211-224.e6. https://doi.org/10.1016/j.ccell.2018.07.001.

Leduc, Cécile, and Sandrine Etienne-Manneville. 2015. "Intermediate Filaments in Cell Migration and Invasion: The Unusual Suspects." Current Opinion in Cell Biology 32: 102–12. https://doi.org/10.1016/j.ceb.2015.01.005.

Leduc, Cécile, and Sandrine Etienne Manneville. 2017. "Regulation of Microtubule-Associated Motors Drives Intermediate Filament Network Polarization" 216 (6): 1689–1704. https://doi.org/10.1083/jcb.201607045.

Lepekhin, Eugene A., Camilla Eliasson, Claes Henric Berthold, Vladimir Berezin, Elisabeth Bock, and Milos Pekny. 2001. "Intermediate Filaments Regulate Astrocyte Motility." Journal of Neurochemistry 79 (3): 617–25. https://doi.org/10.1046/j.1471-4159.2001.00595.x.

Margarido, Andreia S., Laura Bornes, Claire Vennin, and Jacco van Rheenen. 2020. "Cellular Plasticity during Metastasis: New Insights Provided by Intravital Microscopy." Cold Spring Harbor Perspectives in Medicine 10 (11): 1–21. https://doi.org/10.1101/cshperspect.a037267.

Markovic, Darko S., Rainer Glass, Michael Synowitz, Nico Van Rooijen, and Helmut Kettenmann. 2005. "Microglia Stimulate the Invasiveness of Glioma Cells by Increasing the Activity of Metalloprotease-2." Journal of Neuropathology and Experimental Neurology 64 (9): 754–62. https://doi.org/10.1097/01.jnen.0000178445.33972.a9.

McGregor, Alexandra Lynn, Chieh Ren Hsia, and Jan Lammerding. 2016. "Squish and Squeeze - the Nucleus as a Physical Barrier during Migration in Confined Environments." Current Opinion in Cell Biology 40: 32–40. https://doi.org/10.1016/j.ceb.2016.01.011.

Mendez, Melissa G, Shin-Ichiro Kojima, and Robert D Goldman. 2010. "Vimentin Induces Changes in Cell Shape, Motility, and Adhesion during the Epithelial to Mesenchymal Transition." FASEB Journal : Official Publication of the Federation of American Societies for Experimental Biology 24 (6): 1838–51. https://doi.org/10.1096/fj.09-151639.

Meyer, Mona, Jüri Reimand, Xiaoyang Lan, Renee Head, Xueming Zhu, Michelle Kushida, Jane Bayani, et al. 2015. "Single Cell-Derived Clonal Analysis of Human Glioblastoma Links Functional and Genomic Heterogeneity." Proceedings of the National Academy of Sciences of the United States of America 112 (3): 851–56. https://doi.org/10.1073/pnas.1320611111.

Moeton, Martina, Regina Kanski, Oscar M J A Stassen, Jacqueline A. Sluijs, Dirk Geerts, Paula Van Tijn, Gerhard Wiche, Miriam E. Van Strien, and Elly M. Hol. 2014. "Silencing GFAP Isoforms in Astrocytoma Cells Disturbs Laminin-Dependent Motility and Cell Adhesion." FASEB Journal 28 (7): 2942–54. https://doi.org/10.1096/fj.13-245837.

Moeton, Martina, Oscar M J A Stassen, Jacqueline A. Sluijs, Vincent W N van der Meer, Liselot J. Kluivers, Hedde van Hoorn, Thomas Schmidt, Eric A J Reits, Miriam E. van Strien, and Elly M. Hol. 2016. "GFAP Isoforms Control Intermediate Filament Network Dynamics, Cell Morphology, and Focal Adhesions." Cellular and Molecular Life Sciences 73 (21): 4101–20. https://doi.org/10.1007/s00018-016-2239-5.

Nielsen, Anders Lade, Ida E. Holm, Marianne Johansen, Bjarne Bonven, Poul Jørgensen, and Arne Lund Jørgensen. 2002. "A New Splice Variant of Glial Fibrillary Acidic Protein, GFAP Epsilon, Interacts with the Presenilin Proteins." Journal of Biological Chemistry 277 (33): 29983–91. https://doi.org/10.1074/jbc.M112121200.

Nielsen, Anders Lade, and Arne Lund Jørgensen. 2004. "Self-Assembly of the Cytoskeletal Glial Fibrillary Acidic Protein Is Inhibited by an Isoform-Specific C Terminus." Journal of Biological Chemistry 279 (40): 41537–45. https://doi.org/10.1074/jbc.M406601200.

Pascalis, Chiara De, Carlos Pérez-González, Shailaja Seetharaman, Batiste Boëda, Benoit Vianay, Mithila Burute, Cécile Leduc, Nicolas Borghi, Xavier Trepat, and Sandrine Etienne-Manneville. 2018. "Intermediate Filaments Control Collective Migration by Restricting Traction Forces and Sustaining Cell–Cell Contacts." The Journal of Cell Biology 217(9): 3031-3044 https://doi.org/10.1083/jcb.201801162.

Patel, A P, I Tirosh, J J Trombetta, A K Shalek, S M Gillespie, H Wakimoto, D P Cahill, et al. 2014. "Single-Cell RNA-Seq Highlights Intratumoral Heterogeneity in Primary Glioblastoma." Science 344 (6190): 1396–1401. https://doi.org/10.1126/science.1254257.

Paz, Inbal, Martin Akerman, Iris Dror, Idit Kosti, and Yael Mandel-Gutfreund. 2010. "SFmap: A Web Server for Motif Analysis and Prediction of Splicing Factor Binding Sites." Nucleic Acids Research 38 (SUPPL. 2): 1–5. https://doi.org/10.1093/nar/gkq444.

Pencheva, Nora, Mark C. de Gooijer, Daniel J. Vis, Lodewyk F.A. Wessels, Tom Würdinger, Olaf van Tellingen, and René Bernards. 2017. "Identification of a Druggable Pathway Controlling Glioblastoma Invasiveness." Cell Reports 20 (1): 48–60. https://doi.org/10.1016/j.celrep.2017.06.036.

Perng, M, Shu-Fang Wen, Terry Gibbon, Jinte Middeldorp, Jacqueline Sluijs, and and Roy A. Quinlan, Elly M. Hol. 2008. "Glial Fibrillary Acidic Protein Filaments Can Tolerate the Incorporation of Assembly-Compromised GFAP-δ, but with Consequences for Filament Organization and αB-Crystallin Association." Molecular Biology of the Cell 82 (4): 327–31. https://doi.org/10.1091/mbc.E08.

Peter, Annette, and Reimer Stick. 2015. "Evolutionary Aspects in Intermediate Filament Proteins." Current Opinion in Cell Biology 32: 48–55. https://doi.org/10.1016/j.ceb.2014.12.009.

Petrie, Ryan J., Andrew D. Doyle, and Kenneth M. Yamada. 2009. "Random versus Directionally Persistent Cell Migration." Nature Reviews Molecular Cell Biology 10 (8): 538–49. https://doi.org/10.1038/nrm2729.

Ran, F Ann, Patrick D Hsu, Jason Wright, Vineeta Agarwala, David A Scott, and Feng Zhang. 2013. "Genome Engineering Using the CRISPR-Cas9 System." Nat Protoc 8 (11): 2281–2308. https://doi.org/10.1038/nprot.2013.143.

Roelofs, Reinko F., David F. Fischer, Simone H. Houtman, Jacqueline A. Sluijs, Wendy Van Haren, Fred W. Van Leeuwen, and Elly M. Hol. 2005. "Adult Human Subventricular, Subgranular, and Subpial Zones Contain Astrocytes with a Specialized Intermediate Filament Cytoskeleton." Glia 52 (4): 289–300. https://doi.org/10.1002/glia.20243.

Root, David E., Nir Hacohen, William C. Hahn, Eric S. Lander, and David M. Sabatini. 2006. "Genome-Scale Loss-of-Function Screening with a Lentiviral RNAi Library." Nature Methods 3 (9): 715–19. https://doi.org/10.1038/nmeth924.

Rutka, J T, S L Hubbard, K Fukuyama, K Matsuzawa, P B Dirks, and L E Becker. 1994. "Effects of Antisense Glial Fibrillary Acidic Protein Complementary DNA on the Growth, Invasion, and

Adhesion of Human Astrocytoma Cells." Cancer Res. 54(12): 3267-3272

Schaedel, Laura, Charlotta Lorenz, Anna V Schepers, Stefan Klumpp, and Sarah Köster. 2021. "Vimentin intermediate filaments stabilize dynamic microtubules by direct interactions." Nature Communications 12(1): 1-12. https://doi.org/10.1038/s41467-021-23523-z.

Shabbir, Shagufta H., Megan M. Cleland, Robert D. Goldman, and Milan Mrksich. 2014. "Geometric Control of Vimentin Intermediate Filaments." Biomaterials 35 (5): 1359–66. https://doi.org/10.1016/j.biomaterials.2013.10.008.

Sharma, Pooja, Sarah Alsharif, Arwa Fallatah, and Byung Min Chung. 2019. "Intermediate Filaments as Effectors of Cancer Development and Metastasis: A Focus on Keratins, Vimentin, and Nestin." Cells 8 (5): 497. https://doi.org/10.3390/cells8050497.

Skalli, Omar, Ulrika Wilhelmsson, Charlotte Örndahl, Boglarka Fekete, Kristina Malmgren, Bertil Rydenhag, and Milos Pekny. 2013. "Astrocytoma Grade IV (Glioblastoma Multiforme) Displays 3 Subtypes with Unique Expression Profiles of Intermediate Filament Proteins." Human Pathology 44 (10): 2081–88. https://doi.org/10.1016/j.humpath.2013.03.013.

Stassen, Oscar M.J.A., Emma J. van Bodegraven, Fabrizio Giuliani, Martina Moeton, Regina Kanski, Jacqueline A. Sluijs, Miriam E. van Strien, Willem Kamphuis, Pierre A.J. Robe, and Elly M. Hol. 2017. "GFAPδ/GFAPα Ratio Directs Astrocytoma Gene Expression towards a More Malignant Profile." Oncotarget 8 (50): 88104–21. https://doi.org/10.18632/oncotarget.21540.

Sun, Wenjie, Ting Duan, Panmeng Ye, Kelie Chen, Guanling Zhang, Maode Lai, and Honghe Zhang. 2018. "TSVdb: A Web-Tool for TCGA Splicing Variants Analysis." BMC Genomics 19 (1): 1–7. https://doi.org/10.1186/s12864-018-4775-x.

Szerlip, Nicholas J., Alicia Pedraza, Debyani Chakravarty, Mohammad Azim, Jeremy McGuire, Yuqiang Fang, Tatsuya Ozawa, et al. 2012. "Intratumoral Heterogeneity of Receptor Tyrosine Kinases EGFR and PDGFRA Amplification in Glioblastoma Defines Subpopulations with Distinct Growth Factor Response." Proceedings of the National Academy of Sciences of the United States of America 109 (8): 3041–46. https://doi.org/10.1073/pnas.1114033109.

Thiery, Jean Paul, Hervé Acloque, Ruby Y.J. Huang, and M. Angela Nieto. 2009. "Epithelial-Mesenchymal Transitions in Development and Disease." Cell 139 (5): 871–90. https://doi.org/10.1016/j.cell.2009.11.007.

Trepat, Xavier, Zaozao Chen, and Ken Jacobson. 2012. "Cell Migration." Comprehensive Physiology 2 (4): 2369–92. https://doi.org/10.1002/cphy.c110012.

Voss, Dillon M., Anthony Sloan, Raffaella Spina, Heather M. Ames, and Eli E. Bar. 2020. "The Alternative Splicing Factor, MBNL1, Inhibits Glioblastoma Tumor Initiation and Progression by Reducing Hypoxia-Induced Stemness." Cancer Research 80 (21): 4681–92. https://doi.org/10.1158/0008-5472.can-20-1233.

Wolf, Katarina, Mariska te Lindert, Marina Krause, Stephanie Alexander, Joost te Riet, Amanda L. Willis, Robert M. Hoffman, Carl G. Figdor, Stephen J. Weiss, and Peter Friedl. 2013. "Physical Limits of Cell Migration: Control by ECM Space and Nuclear Deformation and Tuning by Proteolysis and Traction Force." Journal of Cell Biology 201 (7): 1069–84. https://doi.org/10.1083/jcb.201210152.

www.sunjinlab.com. n.d. "Mouse Brain Quick Guide :" Accessed 4 Oct 2017.

Zeng, Wenxin, Zhaohua Tang, Yongguo Li, Guangnian Yin, Zili Liu, Jie Gao, Yan Chen, and Feilan Chen. 2020. "Patient-Derived Xenografts of Different Grade Gliomas Retain the Heterogeneous Histological and Genetic Features of Human Gliomas." Cancer Cell International 20 (1): 1–12. https://doi.org/10.1186/s12935-019-1086-5.

Zhang, Yun, and Robert A Weinberg. 2018. "Epithelial-to-Mesenchymal Transition in Cancer: Complexity and Opportunities EMT: A Naturally Occurring Transdifferentia-Tion Program." Frontiers of Medicine 12 (4): 1–13. https://doi.org/10.1007/s11684-018-0656-6.

Supplementary Data

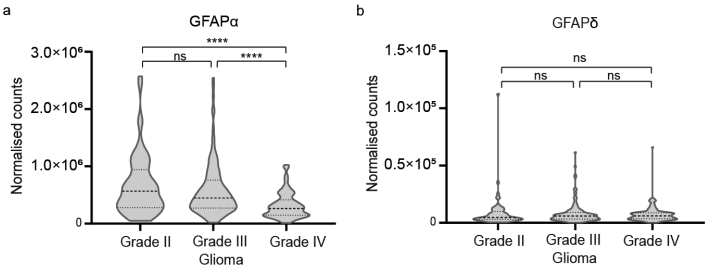

Supp. Fig. 1. GFAP isoform expression in different grades of astrocytoma. Violin plots of GFAPα and GFAPδ levels in tumour samples of grade II (n= 64), grade III (n= 130), and grade IV (n= 153) astrocytoma, obtained from normalised isoform expression data of the TCGA database. GFAPα levels (a) are decreased in grade IV astrocytoma, whereas GFAPδ levels (b) remain constant. Significance was determined using a Kruskal-Wallis test followed by Dunn's multiple comparisons test. The data is shown as mean ± S.E.M, *p < 0.05, **p < 0.01, ***p < 0.001, ****p < 0.0001, ns = not significant.

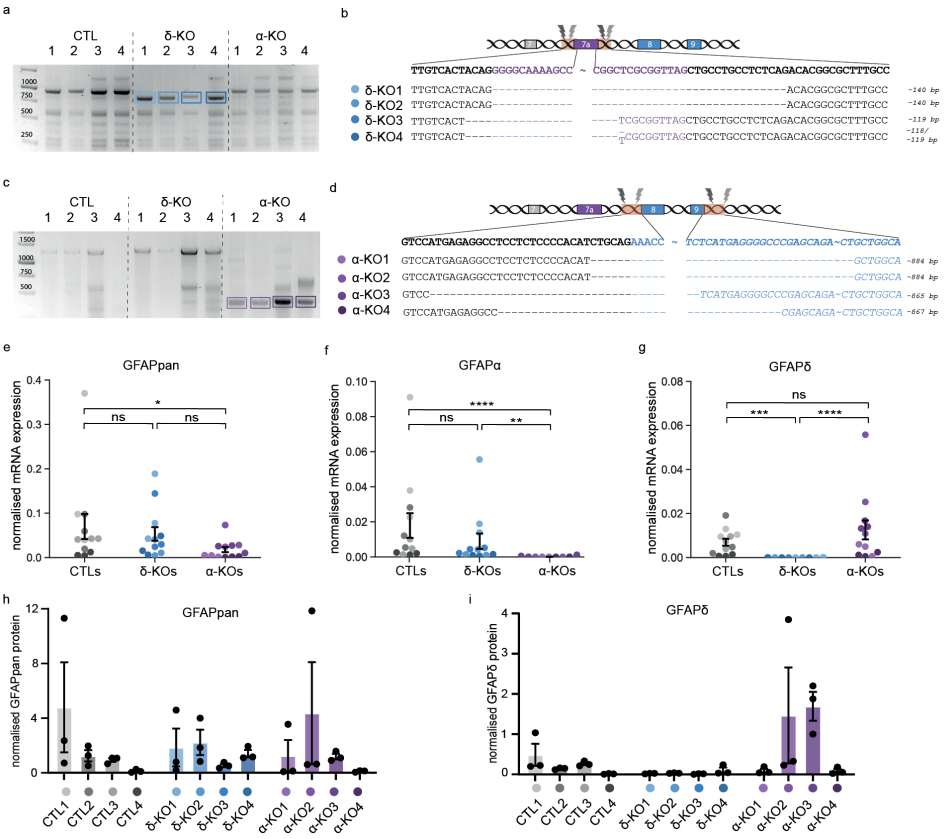

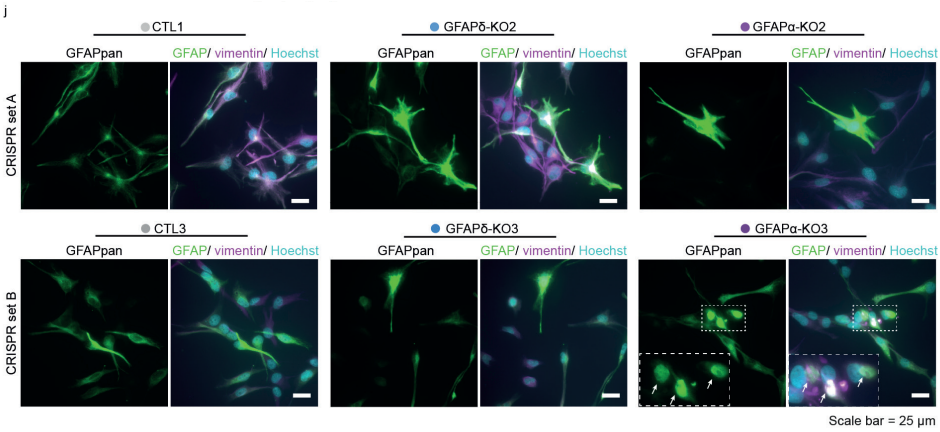

Supp. Fig. 2. Characterisation of the GFAP-modulated cells. (a,b) PCR amplification and sequencing of the GFAP gene around exon 7a. GFAPδ-KO cells have a deletion of 140 bp (GFAPδ-KO 1 and 2, CRISPR δ-set A) or 118/119 bp (GFAPδ-KO 3 and 4, CRISPR δ-set B) of exon 7a. (c,d) PCR amplification and sequencing of the GFAP gene around exons 8 and 9. GFAPα -KO cells have 884 bp deletion (GFAPα-KO 1 and 2, CRISPR α-set A) or 865/867 bp deletion (GFAPα-KO 3 and 4, CRISPR α-set B) of exons 8 and 9. (e-g) mRNA levels of GFAPpan (e), GFAPα (f), and GFAPδ (h) normalised against GAPDH and AluJ. Deletion of exon 7a (GFAPδ-KO cells) leads to a significant reduction in GFAPδ mRNA levels, but not to a reduction in GFAPα or GFAPpan. Deletion of exons 8 and 9 (GFAPα-KO cells) leads to a significant reduction in both GFAPα and GFAPpan levels, but not in GFAPδ mRNA levels. n= 12 individual experiments per group, derived from 4 clones per condition represented with different colour hues. Significance was determined using a Kruskal-Wallis test followed by Dunn's multiple comparisons test. (h,i) Protein levels of GFAPpan (g) and GFAPδ (h) normalised against GAPDH. (j) The GFAP network in six different cell clones (CRISPR set A: CTL1, GFAPδ-KO3, GFAPα-KO3, CRISPR set B: CTL3, GFAPδ-KO2, GFAPα-KO2) shown with immunofluorescence. GFAP is integrated in the IF network (shown with vimentin) in all cell clones. IF network collapses were occasionally observed in GFAPα-KO3, indicated with white arrows. Scale bar = 25 µm. The data is shown as mean ± S.E.M, *$p < 0.05$, **$p < 0.01$, ***$p < 0.001$, ****$p < 0.0001$, ns = not significant.

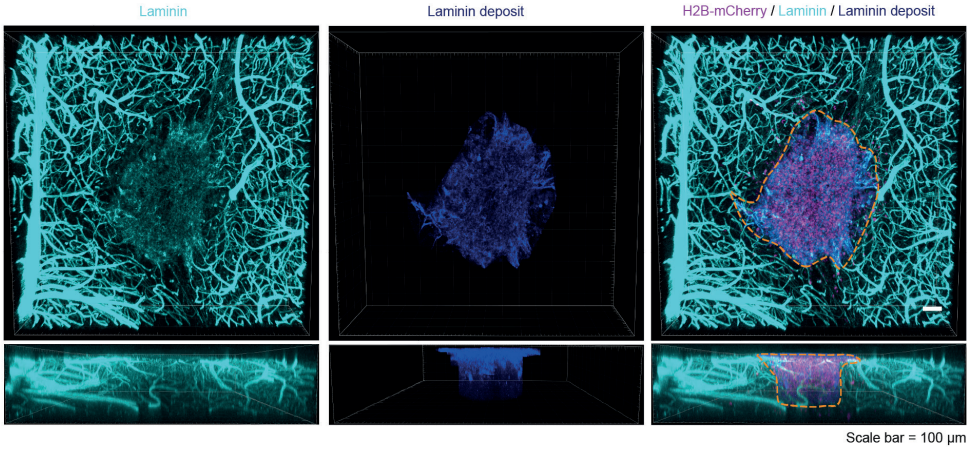

Supp. Fig. 3. Laminin staining can be used to distinguish tumour core from invading cells. Overexposure of laminin reveals background staining that colocalizes with the highest density of H2B-mCherry nuclei at the site of injection. This laminin deposit is used to distinguish cells in the tumour core versus cells that invaded the tissue, indicated with the orange dotted line. Scale bar = 100 µm.

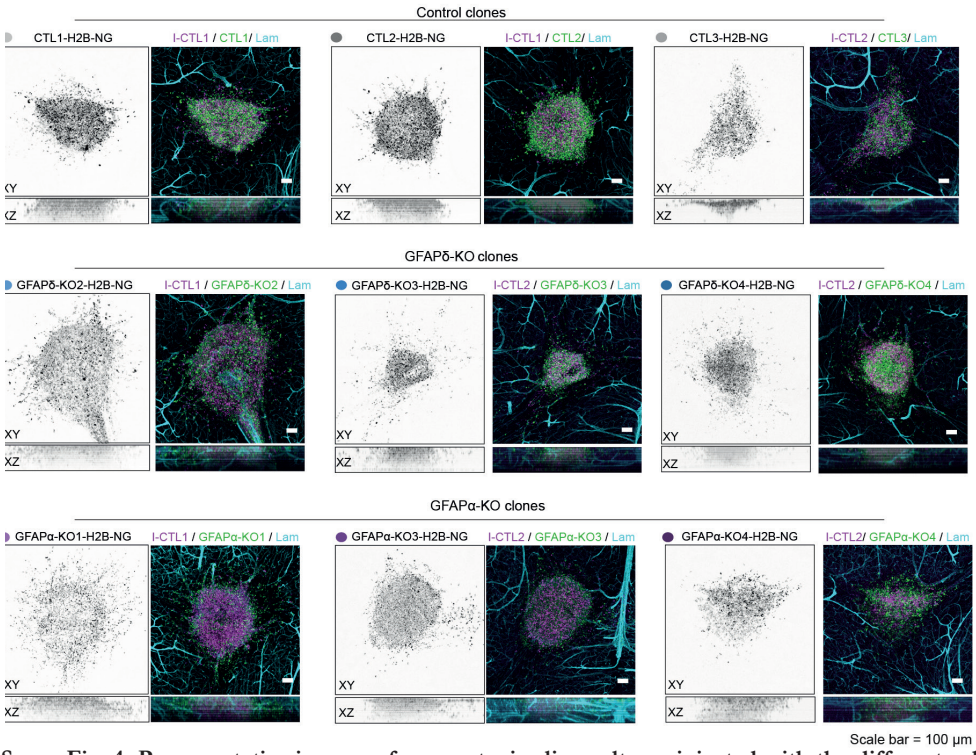

Supp. Fig. 4. Representative images of organotypic slice cultures injected with the different cell clones. Representative images of injected I-CTL-H2B-mCherry cells together with H2B-mNeonGreen expressing CTL clones (a), GFAPδ-KO clones (b) or GFAPα-KO clones (c). Scale bar = 100 µm. NG= mNeonGreen, Lam = laminin.

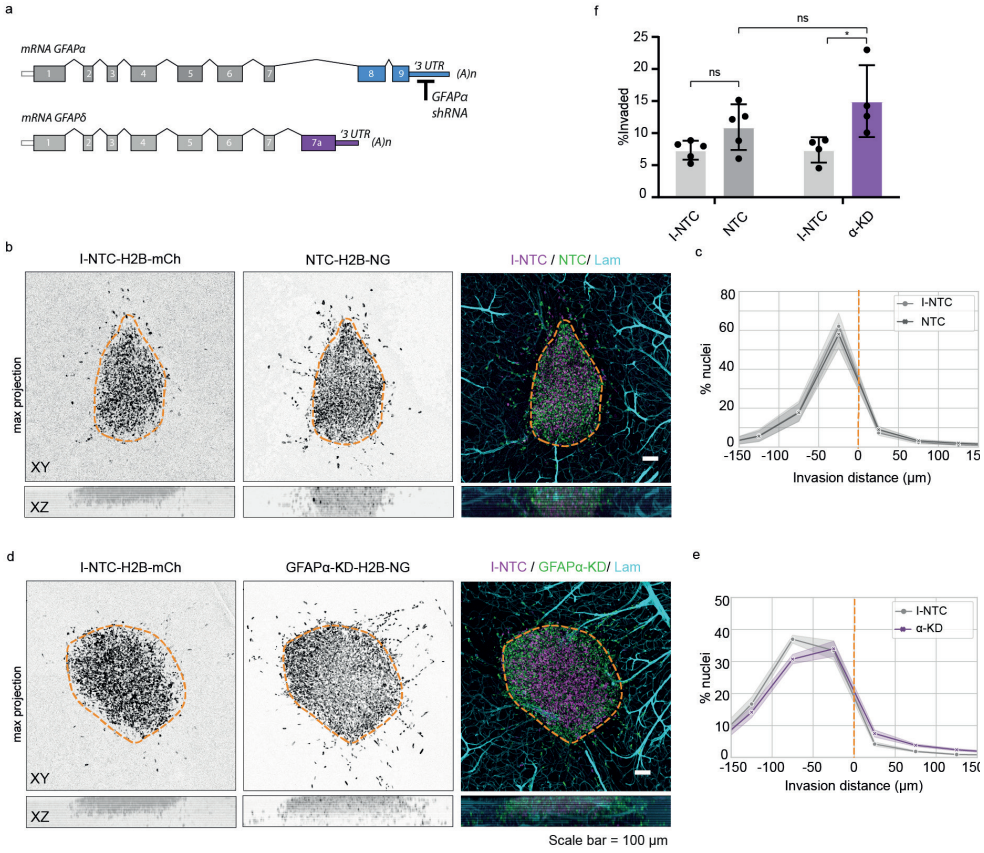

Supp. Fig. 5. Invasion patterns of GFAPα-KD cells. (a) Schematic illustration of GFAPα shRNA target site. (b,c) I-NTC and NTC show similar distribution patterns of nuclei in organotypic brain slices. Histograms show the percentage of nuclei per 50 µm bins, with negative values representing cells within the tumour core and positive values representing cells in the mouse brain tissue (n= 5 independent experiments). (d,e) GFAPα-KD cells show a more diffuse growth pattern in comparison to I-NTC cells and a shift in cell distribution towards the mouse tissue (n=4 independent experiments). (f) Quantification of the percentage of invaded cells. GFAPα-KD cells show higher percentages of cell invasion in comparison to the I-NTCs, but not in comparison to the NTCs. Significance was determined using a two-way ANOVA followed by Tukey's multiple comparisons test. Scale bar = 100 µm. The data is shown as mean ± S.E.M, $^{**}p < 0.05$, $^{**}p < 0.01$, $^{***}p < 0.001$, $^{****}p < 0.0001$, ns = not significant. I-NTC = internal non-targeting control, NTC = non-targeting control, NG = mNeonGreen, mCh = mCherry, Lam = laminin, UTR = untranslated region.

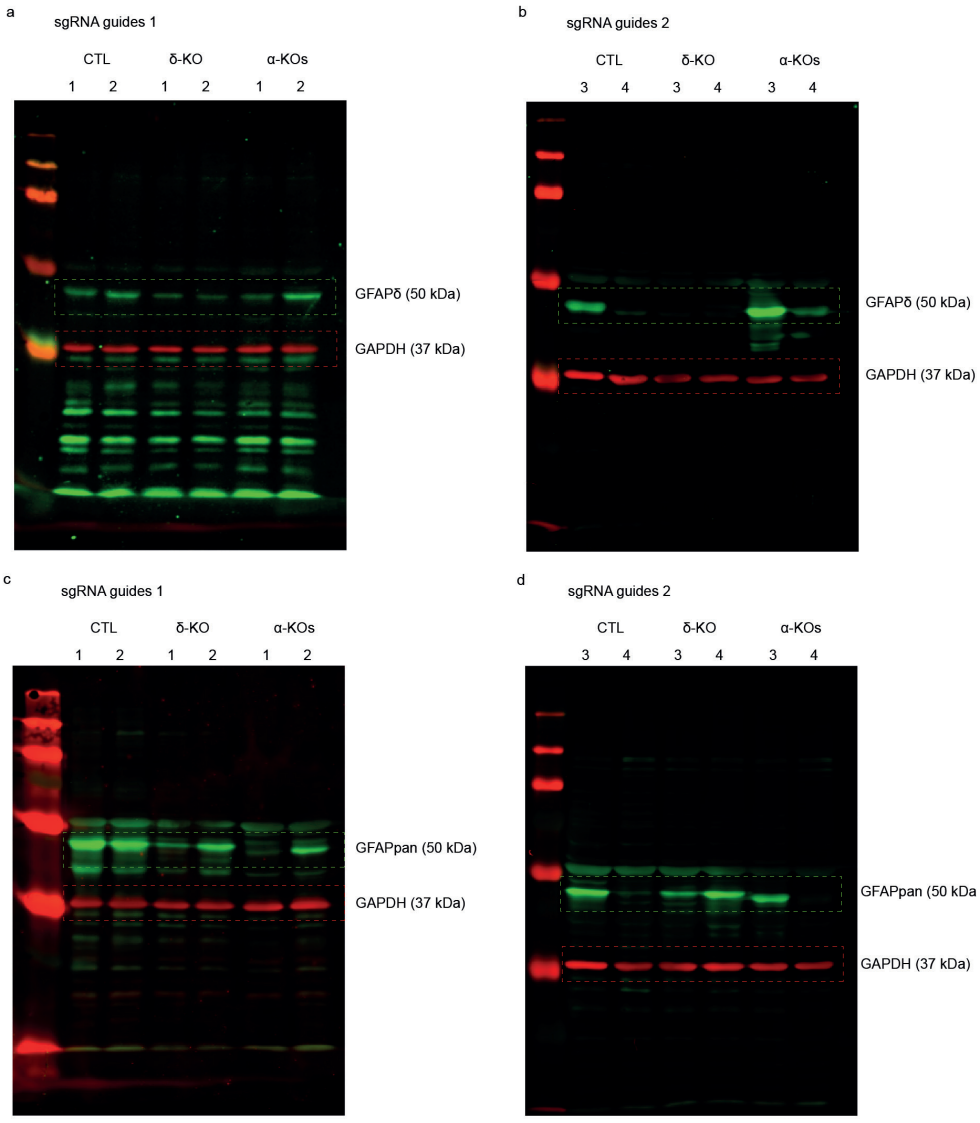

Supp. Fig. 6. Protein levels of GFAPδ and all GFAP isoforms (GFAPpan) in the 12 different cell clones determined with Western blot. (a,b) Full-length blots of GFAP and GAPDH. Single blots were stained with primary antibodies rabbit anti-GFAPδ and mouse anti-GAPDH and with secondary antibodies donkey anti-rabbit IRDye800 and donkey anti-mouse AF647 (Table S2). (c,d) Full-length blots of GFAP and GAPDH. Single blots were stained with primary antibodies rabbit anti-GFAPpan and mouse anti-GAPDH and with secondary antibodies donkey anti-rabbit IRDye800 and donkey anti-mouse AF647 (Supp. Table 2). All antibodies were characterised in Moeton et al., 2016.

Supp. Table 1. Overview of oligonucleotides

Name	Target	Oligonucleotide 1 (5' > 3')	Oligonucleotide 2 (5' > 3')
CRISPR-guides			
GFAPα-KO sgRNAs set A	*GFAP* gene intron 7	CACCGGGCTGGTTTCTGCAGATGTG	AAACCACATCTGCAGAAACCAGCCC
	GFAP gene '3 UTR exon 9	CACCGGATAGTTGCTCCGCCTCTGC	AAACGCAGAGGCGGAGCAACTATCC
GFAPα-KO sgRNAs set B	*GFAP* gene intron 7	CACCGCAGGCTGGTTTCTGCAGATG	AAACCATCTGCAGAAACCAGCCTGC
	GFAP gene '3 UTR exon 9	CACCGCTCGGGCCCCTCATGAGACG	AAACCGTCTCATGAGGGGCCCGAGC
GFAPδ-KO sgRNAs set A	*GFAP* gene intron 6	CACCGTAACTGCTTGTCACTACAGG	AAACCCTGTAGTGACAAGCAGTTAC
	GFAP gene intron 7	CACCGGGCAAAGCGCCGTGTCTGAG	AAACCTCAGACACGGCGCTTTGCCC
GFAPδ-KO sgRNAs set B	*GFAP* gene intron 6	CACCGTTTAACTGCTTGTCACTACA	AAACTGTAGTGACAAGCAGTTAAAC
	GFAP gene intron 7	CACCGAATGGAACGCCGCCGGCTCG	AAACCGAGCCGGCGGCGTTCCATTC
shRNA-guides			
shRNA GFAPα	GFAPα transcript nt 2674–2694	CCCTTCTTACTCACACACAAA	na
NTC	na	CAACAAGATGAAGAGCACCAA	na
PCR primers			
GFAPα	*GFAP* gene 44,907,012- 44,908,284	TAGGCTCTCTCTGCTCGGTT	GAGGGCGATGTAGTAGGTGC
GFAPδ	*GFAP* gene 44,910,531- 44,909,596	GTTGCTCCAGACTGGGACTG	CATTTCAGGGCCAATGCAAG
qPCR primers			
AluJ	Repeat sequence AluJ	CAACATAGTGAAACCCCGTCTCT	GCCTCAGCCTCCCGAGTAG
GAPDH	GAPDH transcript	TGCACCACCAACTGCTTAGC	GGCATGGACTGTGGTCATGA
GFAPα	GFAP transcript 1 (α) 2776 - 2890	CCCACTCTGCTTTGACTGAGC	CCTTCTTCGGCCTTAGAGGG
GFAPδ	GFAP transcript 2 (δ) 1167 - 1263	TCCAACCTGCAGATTCGAGG	TTGGTATAACTCGTATTGTGAGGCTT
GFAPpan	GFAP transcript 1,2 453 - 551	GACCTGGCCACTGTGAGG	GGCTTCATCTGCTTCCTGTC

Abbreviations: AluJ = Alu element Jurka, GAPDH = Glyceraldehyde 3-phosphate dehydrogenase, GFAP = glial fibrillary acidic protein, qPCR = quantitative polymerase chain reaction, sgRNA= single guide RNA, shRNA= short hairpin RNA, PCR = polymerase chain reaction, UTR= untranslated region

Supp. Table 1. List of antibodies

Antibody	Product number, Company	(WM)-IF	WB
Chicken anti-vimentin	AB5733, Chemicon, Temecula, CA, USA	1:1500	-
Mouse anti-GAPDH	MAB374, Chemicon, Temecula, CA, USA	-	1:2000
Rabbit anti-GFAP	#Z0334, Dako (Agilent), Santa Clara, CA, USA	1:1000	1:50000
Rabbit anti-GFAPδ	Manufactured in house. Bleeding date: 27-11-2003 (purified in 2004)	-	1:2000
Rabbit anti-laminin	L9393, Sigma Aldrich, St Louis, MO, USA	1:1000	-
Donkey anti-chicken Cy3	703-175-155, Jackson Immuno Research, West Grove, PA, USA	1:1000	-
Donkey anti-mouse AF647	703-606-150, Jackson Immuno Research, West Grove, PA, USA	-	1:2000
Donkey anti-rabbit Cy3	711-166-152, Jackson Immuno Research, West Grove, PA, USA	1:1000	-
Donkey anti-rabbit AF647	711-606-152, Jackson Immuno Research, West Grove, PA, USA	1:1000	-
Goat anti-rabbit IRDye800	926-32211, LI-COR, 4647 Superior Street Lincoln, NE, USA	-	1:5000

Abbreviations: AF= Alexa Fluor, GAPDH= Glyceraldehyde 3-phosphate dehydrogenase, GFAP = glial fibrillary acidic protein


5

CHAPTER 5

GFAP protects glioma cells against migration induced damage, nuclear fragmentation, and accidental cell death during confined cell invasion

Jessy V. van Asperen[1], Loïs J. Aitatus[1], Jacqueline A. Sluijs[1], A. Katherine Tan[1,2], Marieke Krepel[1], Pierre A.J.T. Robe[2], Jan Lammerding[3], Elly M. Hol[1]

[1] Department of Translational Neurosciences, UMC Utrecht Brain Center, University Medical Center Utrecht, Utrecht University, 3584 CG Utrecht, The Netherlands
[2] Department of Neurology and Neurosurgery, University Medical Center Utrecht Brain Center, Utrecht University, 3584 CG Utrecht, The Netherlands
[3] Weill Institute for Cell and Molecular Biology, Cornell University, Ithaca, NY 14853, USA

Manuscript in preparation

Abstract

The invasive nature of diffuse gliomas is a major challenge in the treatment of this tumour. During glioma invasion, the confined environment of the brain parenchyma forces invading cells to actively deform their cell shape and nucleus, which can lead to exposure to migration induced mechanical stress. Intermediate filament (IF) proteins have unique mechanical properties that can protect cells against large mechanical strains. In this study, we investigated the roles of IF proteins glial fibrillary acidic protein (GFAP) and vimentin in glioma migration through confinement. Using a combination of *ex vivo* organotypic brain slices and microfluidic devices, we discovered that exposure of glioma cells to physical constraint can lead to a caspase-3/7 independent form of nuclear fragmentation and accidental cell death. Migration induced nuclear fragmentation is exacerbated by loss of GFAP, but not vimentin, and is associated with more frequent rupture of the nuclear envelope. This study shows that GFAP protects the nucleus against migration induced damage in confined environments.

Introduction

Diffuse gliomas are a form of primary brain tumours that are characterised by their highly invasive nature (Sahm et al. 2012; Claes, Idema, and Wesseling 2007). Even though gliomas rarely metastasises to tissues outside the central nervous system, local cell invasion into the brain parenchyma causes therapy evasion and the formation of satellite tumours, hampering the treatment of the disease (Ho et al. 2014; Cuddapah et al. 2014). In addition, glioma cell invasion may also contribute to tumour-related epilepsy (Venkataramani et al. 2019), further impacting the quality of life of glioma patients.

During cell invasion, glioma cells use a migration strategy that resembles the migration pattern of neural progenitors. Cells move in a saltatory fashion characterised by bursts of movement followed by immobile periods (Farin et al. 1994; Watkins and Sontheimer 2011). One of the hypothesised factors contributing to this saltatory movement pattern is the confined environment of the brain (Beadle 2010; Ivkovic et al. 2012; Picariello et al. 2019; Agarwal et al. 2018). The brain parenchyma is densely packed with cell bodies, cellular processes, and extracellular matrix (ECM) proteins that together create a physical barrier impeding glioma cell invasion (Thorne and Nicholson 2006). Proteolytic activity and ECM remodelling capacities of glioma cells can partially obliterate these barriers (Forsyth et al. 1999; Yamada and Sixt 2019), yet glioma cells are required to actively deform their cell shape to infiltrate the tissue (Beadle 2010). Particularly myosin-II dependent deformation and translocation of the nucleus, the largest and stiffest organelle of the cell, can be a rate-limiting factor in migration through confinement (Friedl, Wolf, and Lammerding 2011; Beadle 2010; Picariello et al. 2019;

Davidson et al. 2014). In other types of cancer, it is known that large deformations of the nucleus leads to exposure to mechanical stress and can result in nuclear envelope (NE) rupture (Denais et al. 2016; Raab et al. 2016) and DNA damage (Pfeifer et al. 2018; Shah et al. 2021; Xia et al. 2019). This effect on nuclear- and chromatin integrity can have negative consequences for tumour cell survival (Patteson, Vahabikashi, et al. 2019; Harada et al. 2014), but can also promote tumour progression by increasing genomic instability and stimulating invasive behaviour (Nader et al. 2021; Irianto et al. 2017; Bakhoum et al. 2018).

The intermediate filament (IF) protein family is an important player in the protection of cells against cellular stress (Toivola et al. 2010). Within the context of NE integrity, the protective role of nuclear IF proteins lamin A/C and to a lesser extend lamin B are well established (Denais et al. 2016; Harada et al. 2014), but more recent evidence points towards involvement of cytoplasmic IFs as well (Patteson, Vahabikashi, et al. 2019; Stankevicins et al. 2020; Tudor et al. 2019). IF proteins have unique mechanical properties that allow the filaments to resist large mechanical strains (Qin, Kreplak, and Buehler 2009; Hu et al. 2019; Block et al. 2015). The IF network forms a cage-like structure around the nucleus that is coupled to the NE through the *linker of nucleus skeleton and cytoskeleton* (LINC) complex (Dupin, Sakamoto, and Etienne-Manneville 2011; Patteson, Vahabikashi, et al. 2019; Ketema et al. 2013; McGregor, Hsia, and Lammerding 2016). In migrating fibroblasts (Patteson, Vahabikashi, et al. 2019), carcinoma cells (Tudor et al. 2019), and macrophages (Stankevicins et al. 2019), the perinuclear vimentin cage protects the nucleus from migration-induced DNA damage, rupture, and apoptosis. In glioma cells, the IF network consist out of glial fibrillary acidic protein (GFAP), vimentin, nestin, and synemin (Skalli et al. 2013). Splice isoforms GFAPδ and GFAPα differentially regulate the invasion dynamics of glioma cells and affect the shape of nuclei during *in vivo* invasion (van Asperen et al. 2021), yet whether GFAP and other IF proteins also play a role in maintaining nuclear integrity during tissue infiltration is currently unknown. The involvement of the glial IF network in controlling nuclear positioning (Dupin, Sakamoto, and Etienne-Manneville 2011), indicates a close cytosolic-NE interaction that may benefit NE integrity during migration.

In this study, we investigated the role of IF proteins GFAP and vimentin in glioma invasion in *ex vivo* organotypic mouse brain slices and microfluidic confined migration devices. We show that GFAP and vimentin have different effects on nuclear mechanics and stability in U251-MG cells during confined migration. We describe a novel role for GFAP in protecting NE integrity during migration induced stress. Loss of GFAP in U251-MG glioma cells is associated with more frequent nuclear fragmentation events upon exposure to physical constraint and leads to accidental cell death. Susceptibility to fragmentation of the nucleus is associated with more frequent cytosol-nucleoplasm exchange, but not with altered nuclear mechanics.

Results

Manipulation of the glioma IF network leads to nuclear fragmentation in the organotypic brain slice invasion model.

GFAP and vimentin are both important components of the glioma IF network. To investigate whether the two components of the IF network have different roles, we depleted GFAP or vimentin in U251-MG cells by targeting specific exons of the respective genes with CRISPR-Cas9 technology (Supp. Fig. 1a). Clonal lines were selected and depletion of either IF protein was confirmed using quantitative PCR, immunostaining, and Western blot (Supp. Fig. 1b,c). Whereas depletion of GFAP had no effect on vimentin RNA expression levels, remarkably depletion of vimentin led to a decrease in GFAP expression as well (Supp. Fig. 1b,c). Whereas IF networks were still visible in the CTL and GFAP-KO cells, GFAP had a diffuse protein expression pattern in the Vim-KO cells (Supp. Fig. 1d).

Earlier studies performed in our lab showed that manipulation of the GFAPδ/α ratio in glioma cells affects their invasive capacities (van Asperen et al. 2021). To test whether full depletion of GFAP or Vimentin had a similar effects, H2B-mNeonGreen expressing GFAP- and Vimentin-KO cells were injected into *ex vivo* organotypic mouse brain slices together with an internal control line expressing H2B-mCherry to directly compare their migratory behaviours, as described in van Asperen et al. 2021 (Fig. 1a). We first quantified the distribution of cells within the tumour core and at the invasive front. Although the density of tumour cells was deviant in the GFAP-KO cells (Fig. 1b), when comparing the percentages of nuclei in the tissue as a measure for invasion, no significant differences were observed between the conditions (Fig. 1c). Nevertheless, in higher magnification images we observed an aberrant nuclear morphology in GFAP-KO cells. Both within the tumour core and at the invasive front, fragments of H2B-mNeonGreen positive GFAP-KO nuclei were observed (Fig. 1d), whereas these fragments were less noticeable in CTL and Vim-KO slices (Supp. Fig. 2). We quantified the area of the H2B-mNeonGreen nuclei in the *ex vivo* organotypic brain slices and calculated the percentage of H2B-mNeonGreen nuclei that had an area smaller than 15 μm^2 as a measure for nuclear fragments. Indeed, we found that the proportion of nuclear fragments was higher in the Vim-KO cells in comparison the CTL cells, but the most striking increase in percentage of nuclear fragments was observed in *ex vivo* organotypic brain slices injected with the GFAP-KO cells (Fig. 1e). This increase in nuclear fragments was observed in both the tumour core and in the invading cells, whereas Vim-KO cells only had an increase in fragments in the tumour core (Fig. 1e).

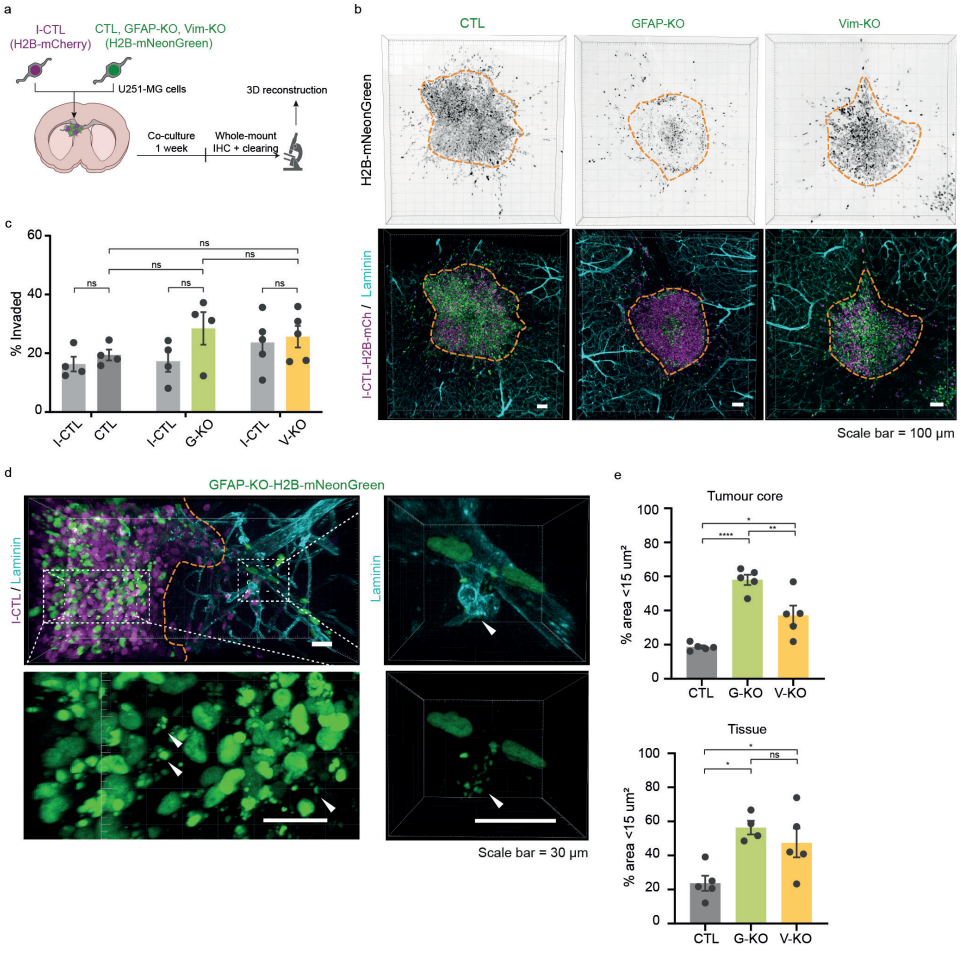

Figure 1. Modification of the IF network in U251-MG affects nuclear integrity in ex vivo organotypic brain slice cultures. (a) Schematic of the experimental set-up of the ex vivo organotypic brain slice invasion assay. (b) Representative images of invasion patterns of H2B-mNeonGreen expressing CTL, GFAP-KO, and Vim-KO cells (black in upper panel, green in lower panel) co-injected with H2B-mCherry expressing I-CTL cells (magenta). The mouse brain vasculature is immunolabeled with laminin antibodies (cyan). Orange dotted line represents the border between tumour core and invaded cells. Scale bar = 100 µm. (c) Quantification of the percentage of invaded cells per condition, n= 4 (CTLs), n=4 (GFAP-KO), and n= 5 (Vim-KO) injected organotypic brain slices from independent experiments. Significance was determined using a two-way ANOVA followed by Tukey's multiple comparisons test. (d) Higher magnification representative image of GFAP-KO-H2B-mNeonGreen cells and I-CTL-H2B-mCherry cells within an organotypic brain slice. Orange dotted line represents the border between tumour core and invaded cells. H2B-mNeonGreen nuclear fragments of can be observed in both the tumour core (lower left panel) and in the proximity of invaded cells (right panels). Examples of nuclear fragments are indicated with arrow heads. Scale bar = 30 µm. (e) Quantification of percentage of H2B-mNeonGreen areas with a surface smaller than 15 μm^2 within the tumour core (upper graph) and in the tissue (lower graph), n= 5 injected organotypic brain slices from independent experiments. Significance was determined using a one-way ANOVA followed by a Tukey's multiple comparisons test. The data is shown as mean ± S.E.M, *p < 0.05, **p < 0.01, ***p < 0.001, ****p < 0.0001, ns = not significant.

Loss of GFAP induces nuclear fragmentation during confined migration

Cell invasion requires cells to deform the cell nucleus, which can impact NE integrity (Denais et al. 2016; Raab et al. 2016). Also within the tumour core, cells are highly motile (Alieva et al. 2019), which can expose the cells to physical strains. To investigate whether nuclear fragmentation was a consequence of migration through confinement, we made use of microfluidic devices in which tissue confinement is mimicked with PDMS pillars (Fig. 2a, Davidson et al. 2015). The H2B-mNeonGreen expressing CTL, GFAP-KO, and Vim-KO cells were seeded in the microfluidic chambers and confined migration was followed with time-lapse imaging for 14 hours, starting 24 hours after seeding (Fig. 2b). We first compared the capacity of cells to migrate through confined spaces by investigating the migration speed and success rate. We found no major differences in the percentage of successful transits of cells migrating through 1 and 2 × 5 μm² confinements (Fig. 2c). We did however observe that both GFAP-KO and Vim-KO cells were slower when migrating through 2 × 5 μm² constrictions, but had a similar transit time compared to CTL cells when migrating through 1 and 15 × 5 μm² confinements (Fig. 2d, Supp. Fig. 3a). More strikingly, however, was the effect of

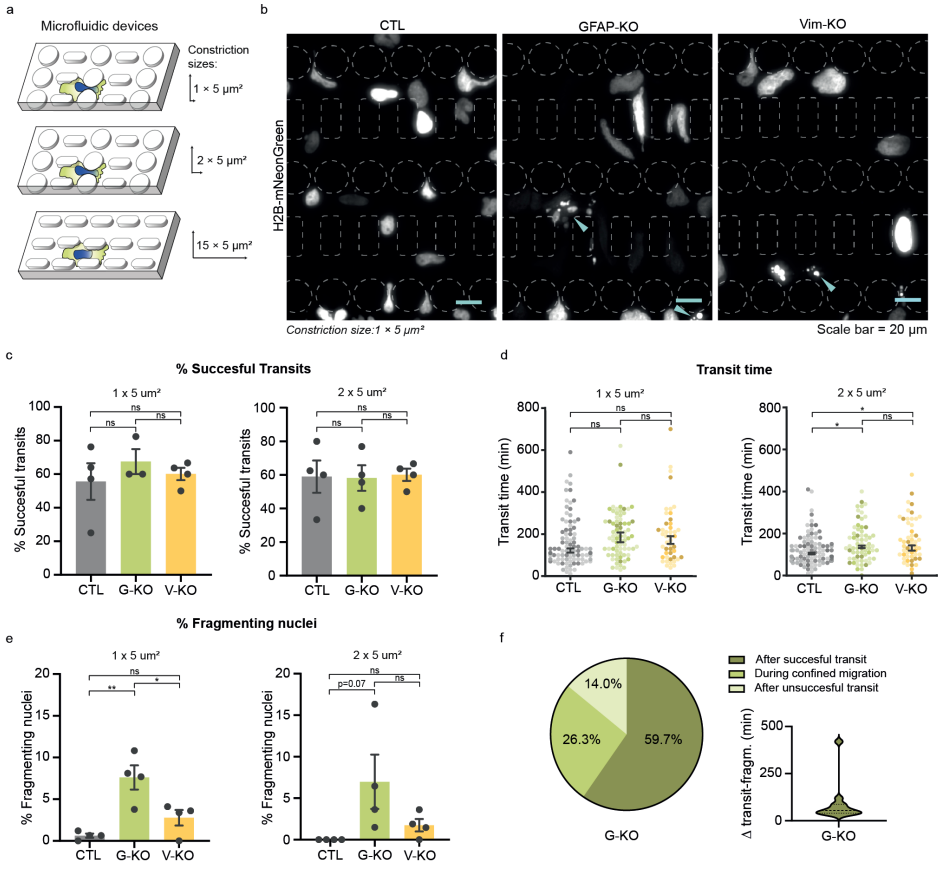

confined migration on the nuclear integrity of GFAP-KO cells. In the GFAP-KO cells, we frequently observed nuclear fragmentation events within the microfluidic devices (Fig. 2b). We quantified the percentage of cells that showed nuclear fragmentation and indeed found a significant increase in the GFAP-KO cells in comparison to the CTL- and Vim-KO cells (Fig. 2e). Of the fragmenting nuclei in the GFAP-KO cells, the fragmentation event mostly took place after successful transition through at least one confined area (59.7%, Fig. 2f) and occurred with a median of 55 minutes (Fig. 2f, 95% CI = 40 - 90 minutes) after successfully migrating through a constriction. Nuclear fragmentation events, however, also took place while cells were still in the confined area (26.3%, Fig. 2f), or when cells had attempted to go through confinement but were unsuccessful (14.0%, Fig. 2f).

We next repeated the experiment in a different clone of the GFAP-KO cells (GFAP-KO2). Also in these cells, more nuclear fragmentations were observed compared to CTL2 cells (Supp. Fig. 3b). GFAP is regulated by alternative splicing, and the ratio between the isoforms GFAPα and GFAPδ in the network affects the migration patterns of glioma cells (van Asperen et al. 2021). To test whether loss of either GFAPα or GFAPδ also leads to a nuclear fragmentation phenotype, we repeated the experiments with two GFAPα-KO and two GFAPδ-KO cell clones. Although nuclear fragmentation events were observed, there were no significant differences in the percentage of events between the CTL, GFAPα-KO, and GFAPδ-KO cell clones (Supp. Fig. 3c). We did observe a small effect on the percentage of successful transits and the transit time for two of the cell clones (Supp. Fig. 3d,e). GFAPα-KO1 had a higher percentage of successful transits and a faster transit time in comparison to CTL2, whereas GFAPδ-KO2 cells were slower when migrating through 2 × 5 μm^2 constrictions. However, these differences were not observed in the other clones (Supp. Fig. 3d,e).

< Figure 2. Confined migration leads to nuclear fragmentation in GFAP-KO cells. (a) Schematic of the experimental set-up of the microfluidic confined migration devices, with constriction sizes of 1 × 5 μm^2, 2 × 5 μm^2, and of 15 × 5 μm^2 as a non-confined control. (b) Representative images of CTL, GFAP-KO and Vim-KO-H2B-mNeonGreen cells in the microfluidic confined migration devices with a constriction size of 1 × 5 μm^2. Arrow heads indicate nuclear fragments. Scale bar = 20 μm. (c) Quantification of percentage of successful transits in 1 × 5 μm^2 (left panel) and 2 × 5 μm^2 (right panel) constrictions. N= 4 independent experiments. (d) Quantification of transit time in 1 × 5 μm^2 (left panel) and 2 × 5 μm^2 (right panel) constrictions. The median transit time per independent experiment was determined, n= 4 independent experiments. The scatter plots show the transit time of individual nuclei, colour saturation represents different independent experiments. (e) Quantification of percentage of fragmenting nuclei in 1 × 5 μm^2 (left panel) and 2 × 5 μm^2 (right panel) constrictions. N= 4 independent experiments. (f) Percentage of GFAP-KO cells that fragmented after a successful transit, during a successful transit or after an unsuccessful transit. Violin-plot shows the distribution of time between successful transit and nuclear fragmentation of the GFAP-KO cells. Error bars in graphs represent mean ± S.E.M, *$p < 0.05$, **$p < 0.01$, ns = not significant. In all panels, significance was determined using a one-way ANOVA followed by a Tukey's multiple comparisons test.

Susceptibility of GFAP-KO cells to nuclear fragmentation is associated with altered nuclear morphology, but not with differences in nuclear mechanics.

To unravel whether the nuclear fragmentation events are linked to general alterations in nuclear morphology and mechanics, we first tested whether intact GFAP- and Vim-KO cells had alterations in nuclear size by comparing the area of nuclei of cells migrating through the unconfined 15 × 5 μm^2 control channels. Both GFAP-KO and Vim-KO nuclei had an increased area in comparison to the control nuclei, most prominently the GFAP-KO cells (Fig. 3a,b). The increase in nuclear size was also found in U251-cells transduced with shRNA against the GFAP transcript (Supp. Fig. 4b), although in this line, no nuclear fragmentations were observed (data not shown). No difference in nuclear size was however observed GFAP-KO2 (Supp. Fig. 4a), neither in the cell clones depleted for GFAPα or GFAPδ (Supp. Fig. 4c).

To test whether nuclear mechanics were altered in the IF-modulated cells, we used a micropipette aspiration microfluidic device to quantify the deformation dynamics of the GFAP-KO and Vim-KO cells (Davidson et al. 2019). Vim-KO cells showed a more rapid deformation in comparison to both CTL and GFAP-KO cells (Fig. 3c,d), but no differences were observed between the GFAP-KO cells and CTL cells (Fig. 3c,d), neither between the CTLs and GFAPα-KO and GFAPδ-KO cells (data not shown). These findings show that manipulation of GFAP can lead to alterations in nuclear size, but the increased susceptibility to nuclear fragmentation in the GFAP-KO cells cannot be explained by a difference in nuclear mechanics.

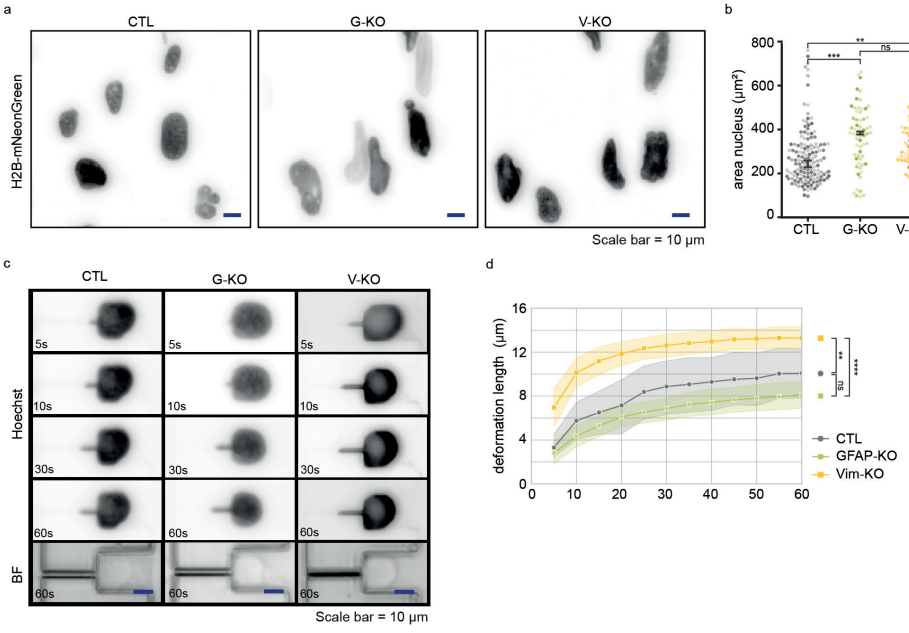

Nuclear fragmentation is proceeded by loss of nuclear envelope integrity

We decided to focus on the CTL and GFAP-KO cells only and next tested whether nuclear fragmentations were linked to a loss of NE integrity. We transduced H2B-mCherry expressing GFAP-KO and CTL cells with a nuclear localisation signal (NLS)-GFP construct to follow NE ruptures during confined migration (Fig. 4a). We first quantified the percentage of cells that had cytosolic NLS during at least one time-point whilst moving through confinement, indicating NE rupture. In the CTL cells, we observed a higher percentage of cells with at least one NE rupture when comparing cells moving through the first versus second/third row of confinement (Fig. 4b). The percentage of cells with NE ruptures was significantly higher in GFAP-KO cells compared to the CTLs, both in the first row of confinement as well as in the second/third row, where the percentage of cells with at least one NE rupture reached a mean of 92.57% (+/ 13.55%, Fig. 4b). We next investigated the NE repair time after successful transit through a confinement and found no differences in repair time between the CTL and GFAP-KO cells, neither after constriction 1 nor after constriction 2 (Fig. 4c).

We next traced fragmenting GFAP-KO cells from the start of confined migration to fragmentation and plotted the intensity of H2B-mCherry and NLS-GFP signal in the nuclei (Fig. 4d,e). We observed that NLS-signal intensity in the nucleus decreased upon the start of the confined migration and did not return to baseline upon successful migration. After the start of fragmentation, the NLS-GFP signal further decreased in the fragmented nuclei, whereas H2B-mCherry signal went up due to condensation of the chromatin (Fig. 4e). Together, these findings indicate that there is a frequent exchange in cytoplasm and nucleoplasm during confined migration and that the NE rupture is not fully repaired before fragmentation takes place.

<Figure 3. Morphological and mechanical characteristics of the nuclei in IF-modulated cells. (a) Representative image of nuclei of CTL, GFAP-KO and Vim-KO cells migrating through 15 × 5 μm^2 control channels. (b) Quantification of the area of the nucleus in 15 × 5 μm^2 control channels, the nuclei of both GFAP-KO and Vim-KO cells have an increased size. The median value of the nuclear area per independent experiment was determined, n=4 independent experiments. The scatter plots show the area of individual nuclei, the colour saturation represent the independent experiments. Significance was determined using a one-way ANOVA followed by a Tukey's multiple comparisons test. (c) Representative images of deformation dynamics nuclei as measured with microfluidic micropipette aspiration devices. Nuclei were stained with Hoechst 33342 and images were acquired every 5 seconds. (d) Quantification of nuclear deformation the during the first 60 seconds. The median nuclear deformation per timepoint per independent experiment was determined, n= 5 independent experiments. Significance was determined using a Kruskal-Wallis test followed by Dunn's multiple comparisons over all timepoints combined. Error bars in graphs represent mean ± S.E.M, $^{**}p < 0.01$, $^{***}p < 0.001$, $^{****}p < 0.0001$, ns = not significant.

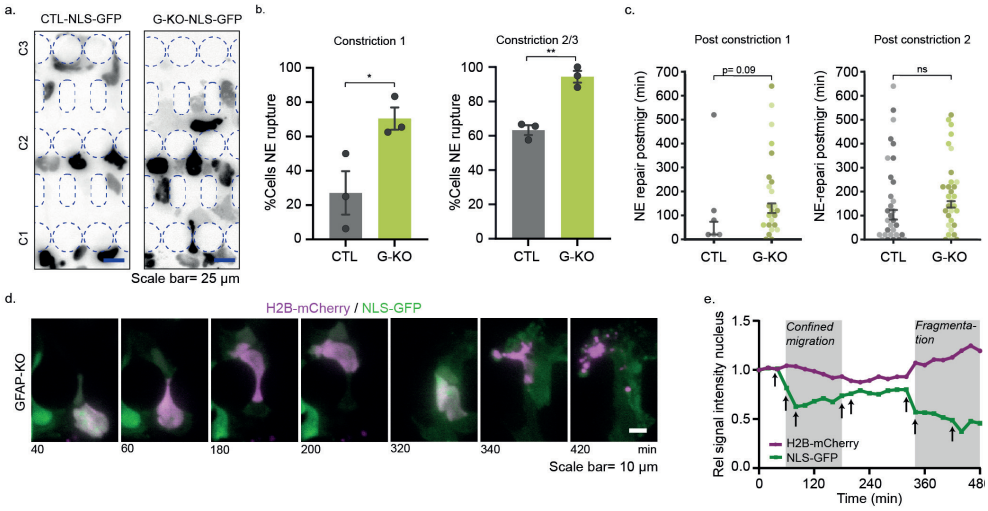

Figure 4. Loss of GFAP is associated with more NE ruptures. (a) Representative image of CTL and GFAP-KO cells transduced with NLS-GFP in microfluidic devices with 1 × 5 µm^2 constrictions. C1, C2, C3 = constriction row 1, 2 and 3. Scale bar = 25 µm. (b) Quantification of the percentage of cells with at least one NE rupture during migration through the first constriction (left panel) or through the second/third constriction (right panel). N=3 independent experiments. Significance was determined with an unpaired t-test. (c) Quantification of the time between NE rupture and repair after successful transit through the first constriction (left panel) or second constriction (right panel). The median value of the NE repair time per independent experiment was determined, n= 3 independent experiments. Significance was determined with an unpaired t-test. The scatter plots show the transit time of individual nuclei, colour saturation represents different independent experiments. (d) Time-lapse sequence of a H2B-mCherry/ NLS-GFP double positive GFAP-KO nucleus that fragments after a successful transit. Scale bar = 10 µm. (e) Relative signal intensity of H2B-mCherry and NLS-GFP within the nucleus displayed in (d) over the course of confined migration and fragmentation. NLS-GFP signal drops after start of migration and is not restored to baseline levels before the fragmentation event. Black arrows indicate the time sequences displayed in panel (d). Error bars in graphs represent mean ± S.E.M, *p < 0.05, **p < 0.01, ns = not significant

Nuclear fragmentation is followed, but not proceeded, by caspase-3/7 activity and/or cell death

Condensation and fragmentation of chromatin is a characteristic feature of apoptosis, and this is a downstream effect of caspase-3 activity (D'Arcy 2019). We therefore next tested whether nuclear fragmentation in GFAP-KO cells was a form of apoptosis and was proceeded by caspase-3 activity. When repeating the microfluidic confined migration assay with a caspase-3/7 reporter in the medium, we observed that nuclear fragmentation was not proceeded by caspase-3/7 activity. After fragmentation, however, caspase-3/7 activity was occasionally observed (Fig. 5a). We did observe that living GFAP-KO cells in the microfluidic devices had unexpected 'background' activity of caspase-3/7 in the cytoplasm, which was not observed in the CTLs (Fig. 5b). To test whether non-apoptotic forms of cell death were underlying the nuclear fragmentation, we repeated

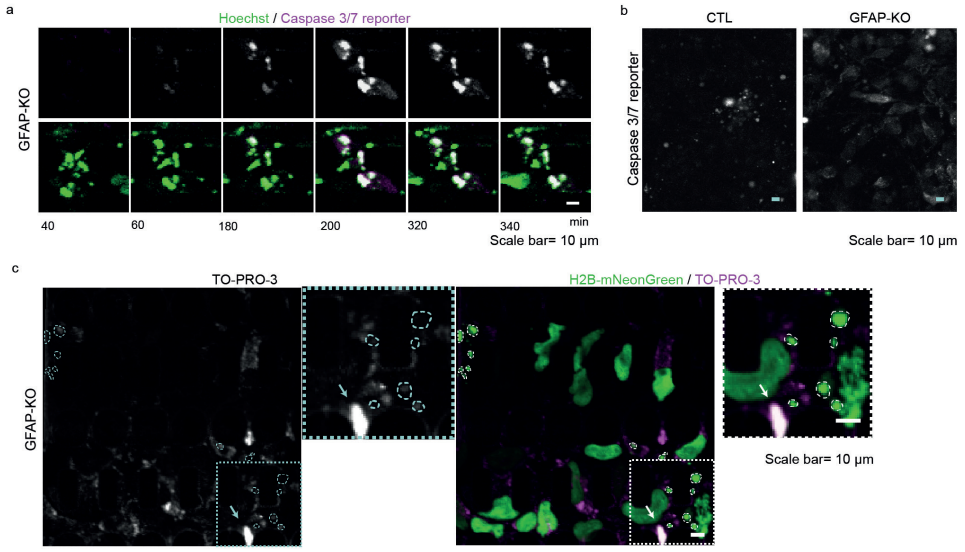

Figure 5. Nuclear fragmentation can result in cell death, but is not proceeded by Caspase 3/7 activity or TO-PRO-3 positivity. (a) Time-lapse sequence of a fragmenting GFAP-KO nucleus where Caspase-3/7 becomes active post-fragmentation. No Caspase-3/7 activity is observed before the fragmentation event. (b) Representative image of background activity of Caspase-3/7 in the cytosol of living CTL and GFAP-KO cells. (c) Representative image of microfluidic device with TO-PRO-3 negative fragmented nuclei. The outlines of nuclear fragments are represented with dashed circles. The arrow indicates a TO-PRO-3 positive dead nucleus. Scale bar = 10 µm.

the experiment with TO-PRO-3 in the medium. This nuclear dye is impermeable for living cells but visualises the nuclei upon cell death. Similarly to caspase-3/7 activity, TO-PRO-3 positivity was frequently observed after nuclear fragmentation, but fragmenting cells were TO-PRO-3 negative before the fragmentation event. These findings indicate that nuclear fragmentation occurs while the cell is still alive, but that the event itself is harmful for the cell and causes cell death.

Nuclear fragmentation in primary glioma cells.

To investigate whether the nuclear fragmentation and cell death phenotype is relevant not only for U251-MG but also other glioma cell lines, we repeated the CRISPR-Cas9 induced GFAP-KO in a primary glioma cell line (KT1937) that we obtained from surgical material. A GFAP-KO clonal line was created using the same sgRNA as described before and this clone was compared to clonal control (C-CTL) cells, as well as to the parental non-clonal KT1937 (PL) line (Fig. 6a). GFAP was successfully knocked out in the KT1937 GFAP-KO lines as indicated with Western blot and immunofluorescent staining (Fig. 6b,c). The three cell lines were seeded in the confined

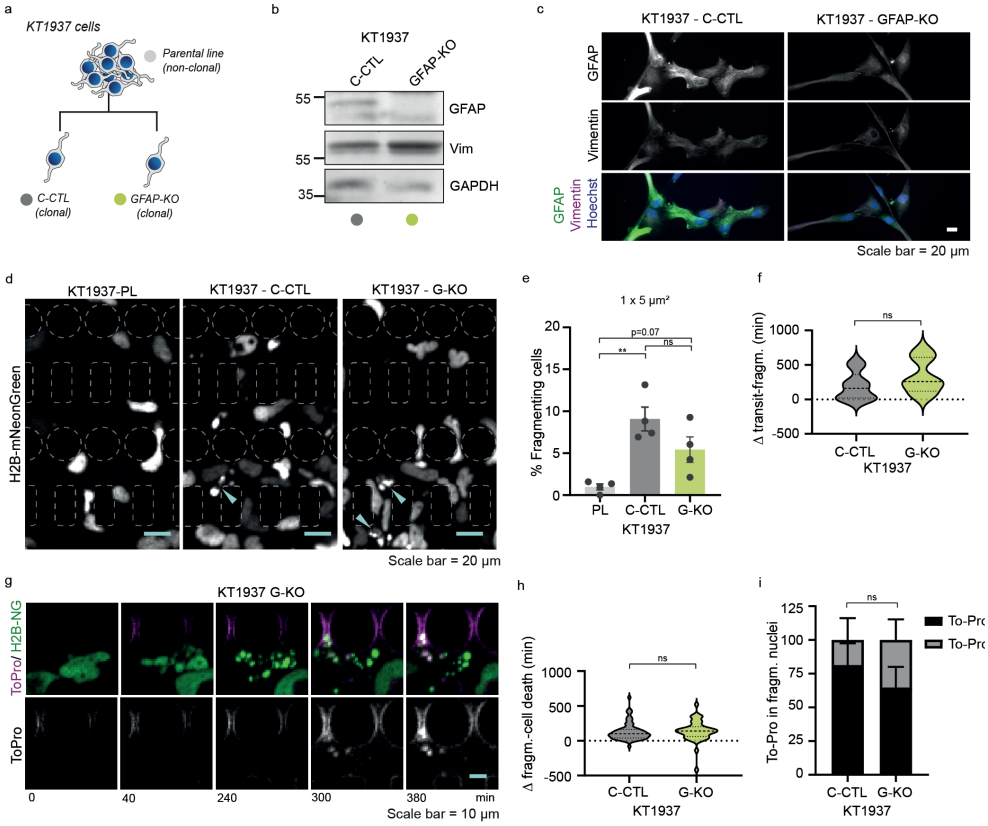

Figure 6. Nuclear fragmentation events are observed in primary glioma cell line KT1937, but protection by GFAP is less evident. (a) Schematic of the non-clonal parental line KT1937 and clonal control (C-CTL) and GFAP-KO cells used. GFAP-KO was induced using CRISPR-Cas9 strategy. (b) Protein levels of GFAP and Vim in the KT1937 C-CTL and GFAP-KO cells. (c) The IF network in the C-CTL and GFAP-KO cells as shown with immunofluorescence with GFAP and vimentin antibodies. Scale bar = 20 µm. (d) Representative images of KT1937-PL, C-CTL and GFAP-KO H2B-mNeonGreen expressing cells in the microfluidic confined migration devices with a constriction size of 1 × 5 µm^2. Arrow heads indicate vnuclear fragments. Scale bar = 20 µm. (e) Quantification of percentage of fragmenting nuclei in 1 × 5 µm^2 constrictions. N= 4 independent experiments, significance was determined using a one-way ANOVA followed by a Tukey's multiple comparisons test. (f) Quantification of time between successful transit and fragmentation of the nucleus in C-CTL and GFAP-KO cells. The median value per independent experiment was determined, n= 3 independent experiments. Significance was determined with an unpaired t-test. (g) Time-lapse sequence of a GFAP-KO cell that fragments and becomes TO-PRO-3 positive. (h) Quantification of time between fragmentation of the nucleus and cell death in C-CTL and GFAP-KO cells. The average value per independent experiment was determined, n= 4 independent experiments. Significance was determined with an unpaired t-test. (i) Percentage of nuclear fragments that are TO-PRO-3+ or TO-PRO-3- in C-CTL and GFAP-KO cells. N=4 independent experiments, significance was determined with an unpaired t-test. Error bars in graphs represent mean ± S.E.M, **p < 0.01, ns = not significant.

migration devices (Fig. 6d), TO-PRO-3 was added to the culture media, and nuclear fragmentations and cell death events were counted. Although a trend towards more nuclear fragmentations was observed in the KT1937 GFAP-KO cells compared to the non-clonal KT1937 PL cells, to our surprise the most frequent fragmentations were observed in the KT1937 C-CTL cells (Fig. 6f.). There was no difference in the time span from successful transit through confinement to nuclear fragmentation between the KT1937 C-CTL and GFAP-KO cells (Fig. 6f). We next investigated whether the nuclear fragmentation was also associated with cell death, and indeed observed TO-PRO-3 positivity of nuclear fragments after fragmentation (Fig. 6g). In some cases, TO-PRO-3 positivity was observed before nuclear fragmentation (Fig. 6h). The median time between fragmentation and cell death was 100 vs 140 minutes in the KT1937 C-CTL and GFAP-KO cells, respectively; and 95% of the cells died within 416 vs 360 minutes, which was not significantly different (Fig. 6h). We next counted the number of cells that were imaged for at least 416 minutes and were still TO-PRO-3 negative after this time period. Of the fragmenting nuclei, 18.4% and 35.3% (C-CTL and GFAP-KO) were still To-Pro negative 416 minutes after fragmenting (Fig. 6i). Together, these findings show that the nuclear fragmentation phenotype is not specific for U251-MG cells, but also occur in primary glioma cells, although dependence on GFAP here is less evident. It further shows that most primary glioma cells die after nuclear fragmentation, although cell death is not observed in all fragmenting cells.

Discussion

Diffuse gliomas are known for their invasive character (Sahm et al. 2012; Claes, Idema, and Wesseling 2007), and this makes it a major challenge to successfully treat this disease. In this study, we show that the IF protein GFAP contributes to maintaining NE integrity during glioma invasion and migration. We show that nuclei of glioma cells without GFAP more frequently fragment into small pieces after cells are exposed to physical constraint in *ex vivo* organotypic brain slice cultures and microfluidic confined migration devices. Condensation and fragmentation of chromatin is typically a characteristic feature of apoptosis (D'Arcy 2019; Galluzzi et al. 2018), but in the GFAP-KO cells, nuclear fragmentation was not proceeded by increased caspase-3/7 activity, indicating that apoptotic pathways are not involved. As the event itself does kill the cell, we deliberate that loss of GFAP makes the invading glioma cell more susceptible to accidental cell death, a non-regulated form of cell death that is caused by extreme mechanical or chemical insults (Galluzzi et al. 2015; Galluzzi et al. 2018).

In earlier work, we discovered that GFAP has splice isoform dependent roles in regulating migration persistence during glioma invasion (van Asperen et al. 2021; van Bodegraven et al. 2019). The role of GFAP in protecting the cell against migration

induced damage, however, appears to be isoform independent. Neither depletion of GFAPα nor GFAPδ alone was sufficient to induce the nuclear fragmentation phenotype or cause alterations in nuclear shape, in contrast to what we expected based on earlier findings (van Asperen et al. 2021). The GFAPα and GFAPδ isoforms differ in the last 41/42 amino acids of the tail-region, therefore it is most likely that the protective function of GFAP can be attributed to the head or rod domain of the protein. Also, loss of vimentin does not impact nuclear integrity to the same extent as full loss of GFAP, although higher percentages of nuclear fragments were observed in *ex vivo* organotypic brain slices (Fig. 1e). Loss of vimentin does however impact nuclear mechanics, which is in line with what was earlier described in mouse embryonic fibroblasts (Patteson, Pogoda, et al. 2019; Patteson, Vahabikashi, et al. 2019). These different effects on nuclear mechanics can likely be explained by the observation that general GFAP levels are also decreased in Vim-KO cells and perinuclear organisation of IFs is diminished, whereas perinuclear vimentin structures are still observed in the GFAP-KO cells (Supp. Fig. 1d). This further suggests that at least part of the mechanism behind the nuclear fragmentation phenotype is not dependent on the IF cage structure itself, but more on general levels of (soluble) GFAP. It cannot, however, be ruled out that some of the phenotypes we observed are dependent on the perinuclear cage, for instance, the effect on nuclear size or frequency in NE ruptures. Although we have not tested NE ruptures in Vim-KO cells, an increased frequency in NE ruptures upon confinement was also observed in vimentin-null mouse embryonic fibroblasts (Patteson, Vahabikashi, et al. 2019). Therefore, both perinuclear cage dependent and independent functions of GFAP most likely contribute to the protection of the nucleus against migration induced fragmentation.

NE rupture upon nuclear deformation has been widely described and is known to negatively impact genomic stability (Denais et al. 2016; Raab et al. 2016; Nader et al. 2021; Shah et al. 2021). This can partly be explained by spillage of nuclear repair factors into the cytosol or exposure of the chromatin to cytoplasmic nucleases (Irianto et al. 2017b; Nader et al. 2021). A disturbance in cytoplasmic/ nucleoplasmic localisation of proteins likely contributes to the nuclear fragmentation phenotype in the GFAP-KO cells, as we observed that the NLS-GFP signal in the nucleus did not restore to baseline after the start of confined migration (Fig. 5e). In breast cancer cells, DNA damage is induced by leakage of the exonuclease TREX1 into the nucleoplasm after NE rupture (Nader et al. 2021). Whether TREX1, which is normally involved in the resolution of post-mitotic chromatin bridges (Maciejowski et al. 2020), is dysregulated in GFAP-KO glioma cells remains to be investigated. However, so far there is only evidence that TREX1 leads to DNA damage foci and not to complete fragmentation of the nucleus (Nader et al. 2021).

During apoptosis, DNA fragmentation is catalysed by the caspase-activated

DNAse/DNA fragmentation factor40 (DFF40), which is released upon cleavage of its binding partner caspase-activated DNAse/DNA fragmentation factor45 (DFF45) by caspase-3 (Liu et al. 1998; Enari et al. 1998). A yeast two-hybrid system identified GFAP as a binding partner of the DFF45 subunit, and *in vitro* incubation of the two proteins with caspase-3 showed that GFAP protects DFF45 from cleavage by caspase-3 (Hanus, Kalinowska-Herok, and Widlak 2010). DFF45 (and its interaction with GFAP) is therefore an interesting candidate to follow up on in the search for mechanisms underlying the nuclear fragmentation phenotype. For the activation of the DFF40/DFF45 complex, caspase-3 activity is required (Liu et al. 1998). Although a full activation of caspase 3/7 was not observed before nuclear fragmentation, we did observe an unexpected 'background' activity of caspase-3/7 in the cytosol of GFAP-KO cells. As GFAP itself is also a target of caspase-3 (Zhang et al. 2014) and thus can act as a sink for caspases, we hypothesise that the nuclear fragmentation is a result of a double-hit model where lack of GFAP in combination with dysregulated caspase-3 activity and

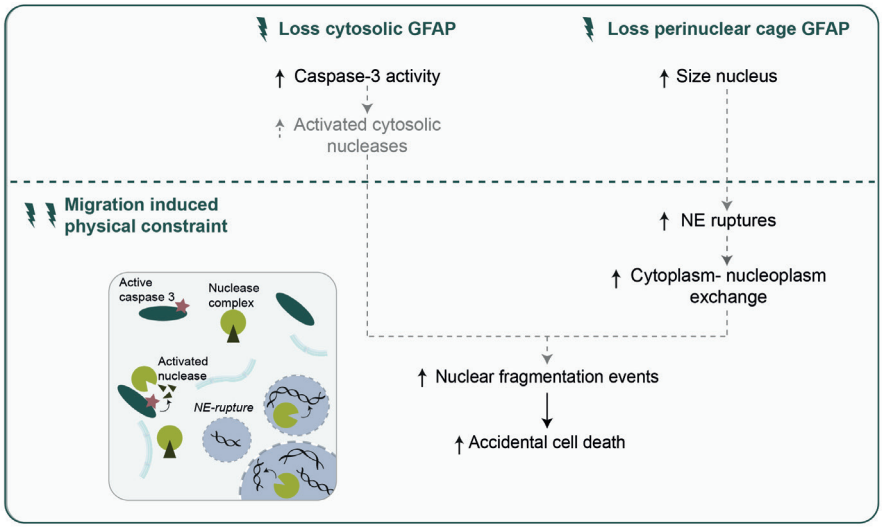

Figure 7. Hypothesised model for the increased susceptibility to nuclear fragmentation and accidental cell death in GFAP-depleted U251-MG cells. With normal GFAP expression, cytosolic GFAP is proposed to bind cytosolic nuclease-complexes to prevent activation by active caspase-3." Loss of cytosolic GFAP": background caspase-3/7 activity is increased for reasons unknown, which is proposed to lead to an increase in activated cytosolic nucleases. "Loss perinuclear cage GFAP": absence of GFAP in the perinuclear cage is proposed to lead to an increased size of the nucleus. This phenotype is also observed when perinuclear GFAP is lost in Vim-KO cells. The disturbance of nuclear shape if thought to underlie the frequency in NE ruptures and the associated cytoplasm-nucleoplasm exchange after exposure to "Migration induced physical constraint". The combination of the two events increases the change that activated cytosolic nucleases enter the nucleus and fragment the DNA and chromatin. This leads to irreversible damage to the nucleus and accidental cell death. Black words and lines represent observations from current study. Grey words and (dashed) lines represent hypothesised mechanisms and actions.

NE rupture upon physical constraint leads to chromatin exposure to exonucleases (Fig. 7).

At last, although we observed nuclear fragmentation in a primary glioblastoma cell line, indicating that this phenotype is relevant for glioma biology, the importance of GFAP in this cell line was less evident. GFAP depleted cells showed a trend towards more nuclear fragmentations in comparison to the parental cell line, but to our surprise, clonal control cells with GFAP were even more vulnerable for nuclear fragmentations when compared to the GFAP-KO clone. Glioblastomas are highly heterogeneous (Sottoriva et al. 2013; Patel et al. 2014; Meyer et al. 2015), therefore there may be clonal differences in the susceptibility for migration induced nuclear fragmentation. Further characterisation of different primary glioma cell lines and clones can help to determine which other factors contribute to the susceptibility for this phenotype. Factors that are known to contribute to NE stability, like chromatin state, nuclear lamina characteristics, and NE repair proteins are primary suspects to this end (Denais et al. 2016; Raab et al. 2016; Nava et al. 2020; Stephens, Banigan, and Marko 2018).

A better understanding of the nuclear fragmentation phenotype may help to identify novel mechanisms to kill (invading) glioma cells in the future. Yet, it is important to consider the possible effect on genomic instability. Although most cells that underwent nuclear fragmentation died within 7 hours (Fig. 6h), a significant proportion was still TO-PRO negative after this time (Fig. 6i). We cannot rule out that these cells die after the time-window of our experimental set-up, but the survival of these cells can have a detrimental effect on genomic stability (Irianto et al. 2017a; Bakhoum et al. 2018). This needs to be shown by studying DNA damage and genomic instability of the fragmenting and non-fragmenting glioma cells in future research.

In conclusion, our work demonstrates that exposure of glioma cells to physical constraint can lead to fragmentation of the nucleus that is followed by accidental cell death. In U251-MG cells, nuclear fragmentation is exacerbated by a loss of GFAP and is associated with more frequent ruptures of the nuclear envelope. Together, this research sheds new light on the consequence of confined migration on the nuclear integrity of glioma cells and describes a novel role for the GFAP protein in protecting glioma cells from migration induced stress.

Materials and Methods

Cell lines and culture

The human glioma cell line U251-MG (from Lars Ruether, Institut für Neuropathologie, Universitätsklinikum Münster, Münster, Germany) was cultured in DMEM high glucose (Gibco 41966052), Ham's F10 nutrient mix (Gibco 11550043) with 10% fetal bovine serum (Gibco 10270-106), and 1% penicillin-streptomycin (Gibco 15140122). The cell

identity of this line was confirmed by short terminal repeat analysis (Eurofins Scientifc, Luxembourg city, Luxembourg). The KT1937-line was obtained from a resected glioblastoma tumour as described previously in Robe et al. 2004, after obtaining the informed consent of the patient (informed consent TITMAG 16-342/16-340 reviewed by the Medical Ethical Committee of the University Medical Center Utrecht, the Netherlands). Histopathological grading was done by a dedicated neuro-pathologist. Biopsies were cut under sterile conditions into 0.5-1 mm pieces and put in a T75 culture flask with DMEM/F-12 medium supplemented with 10% FCS and 1% penicillin-streptomycin (Gibco 15140122). The same medium supplemented with GlutaMAX™ (Gibco 10565018) was used for the subsequent culture period. All cells were cultured at 37 ˚C in a humidified atmosphere and 5% CO_2, and were routinely tested negative for mycoplasma contamination.

Generation of GFAP and vimentin KO-lines using CRISPR-Cas9

GFAP- and vimentin-KO lines were generated using CRISPR-Cas9, as earlier described (van Bodegraven et al. 2019; van Asperen et al. 2021). For the generation of GFAP-KO lines, a single guideRNA (sgRNA) targeting exon 1 of the GFAP gene (5'-CACCGAAATCCACCCGGGTCGGGAG-3' and 5'-AAACCTCCCGACCCGGGTGGATTTC-3') was designed using the CRISPOR.org (http://crispor.tefor.net/) tool (Concordet and Haeussler 2018). For the generation of Vim-KO lines, a sgRNA targeting exon 2 of the vimentin gene (5- CACCGTGGACGTAGTCACGTAGCTC and 5'-AAACGAGCTACGTGACTACGTCCAC-3') was designed according to earlier published work from Jiu et al. 2015. The sgRNA complementary oligonucleotide templates were cloned into the pSpCas9(BB)-2A-GFP plasmid (Addgene, #48138). U251-MG cells were seeded at a density of 4.0×10^4 cells in multiple uncoated 24-well wells and were transfected with 400 ng plasmid per well using polyethylenimine (166 ng/mL final concentration). The GFP-positive cells were single-cell sorted into 96-well plates using FACS (FACSAria II Cell Sorter) 24 hours after transfection. The CTL, GFAPδ-KO and GFAPα-KO cells used in this study were generated as earlier described (van Bodegraven et al. 2019). The KT1937-GFAP-KO line was generated by transfecting 4.0×10^5 KT1937-cells in an uncoated 6-well plate with 1 μg plasmid using lipofectamine 2000 (Thermo Fisher Scientific, 11668030). The GFP-positive cells were selected using FACS 48 hours after transfection. The GFP-positive pool was expanded and cell clones were generated by plating cells at low densities in 96-well plates (0.5 cell/well). Clonal control KT-1937 cells were generated by the transfecting the parental lines with the empty plasmids. Clonal KO lines were selectewd based on real-time quantitative PCR and Western Blot expression of GFAP and vimentin.

RNA isolation, cDNA isolation and real-time quantitative PCR

RNA isolation, cDNA isolation, and real-time quantitative PCR were performed as previously described (van Asperen et al., 2021). In short, cells were seeded at a density of 4×10^4 cells on poly-D lysine (PDL)-coated wells of a 24-well plate, cultured for three days and RNA was extracted using standard TRIzol (Thermo Fisher Scientific, 15596026) -chloroform extraction methods. 500 ng of RNA was used to prepare cDNA using the QuantiTect Reverse Transcription Kit (Qiagen, 205311) according to the manufacturer's protocol. The generated cDNA was used for real-time quantitative PCR using the SYBR Green Master mix in a QuantStudio 6 Flex Real-Time PCR system (Thermo Fisher Scientific, 4309155) using the primers listed in Supp. Table 1. Expression values were calculated by transforming Ct values (2^{-Ct}) and were normalised to the mean value of the transformed Ct values of the reference genes GAPDH and Alu element Jurka (Alu- J).

Immunocytochemistry

Immunocytochemistry on cultured cells was performed as previously described (van Asperen et al., 2021). Cells were seeded on PDL-coated coverslips and fixed after three days in culture in 4% paraformaldehyde (PFA) dissolved in phosphate buffer saline (PBS), pH 7.4 for 30 minutes. Coverslips were blocked in blocking buffer (50 mM Tris pH 7.4, 150 mM NaCl, 0.25% (w/v) gelatin, 0.5% Triton-X100), followed by primary and secondary antibody staining in blocking buffer with the antibodies listed in Supp. Table 2. The coverslips were mounted on microscopy slides with Mowiol (0.1 M tris-HCl pH 8.5, 25% glycerol, 10% Mowiol (Merck Millipore, 81381) and imaged using a Zeiss Axioscope A1 microscope with a 40x objective.

Western blot analysis

Western blot analysis on cultured cells was performed as previously described (van Asperen et al., 2021). Cell pellets in suspension buffer (0.1M NaCl, 0.01 M Tris HCl (pH 7.6), 0.001 M EDTA, and Complete EDTA-free protease inhibitor cocktail (Roche)) mixed one to one with 2x SDS loading buffer (100 μM Tris (pH 6.8), 4% SDS, 20% glycerol, 5% 2-ME, and bromophenol blue) were loaded on a 10% SDS-page gel and proteins were separated by electrophoresis. Proteins were blotted on a 0.45-μm pore size nitrocellulose membrane (GE Healthcare) using a wet/tank transfer blotting system (Biorad, 170390). The membranes were blocked in blocking buffer (50 mM Tris pH 7.4, 150 mM NaCl, 0.25% (w/v) gelatin, 0.5% Triton-X100), followed by primary and secondary antibody staining in blocking buffer with the antibodies listed in Supp. Table 2.The membrane blots were scanned with the Odyssey Clx Western Blot Detection System (Li-Cor Biosciences).

Generation of fluorescently labeled cell lines

Lentiviral particles were generated using a third generation protocol. The pLV-H2B-mNeonGreen-IRES-puro plasmid was a gift from Dr. Hugo Snippert (Drost et al. 2015), the pLenti6-H2B-mCherry plasmid was a gift from Torsten Wittmann (Addgene plasmid # 89766). The pLV-NLS-copGFP-puro plasmid is described in Denais et al. 2016. Cells were transduced with H2B-mNeonGreen or H2B-mCherry lentiviral particles with an MOI of 1. Cells were passaged once and positive cells were selected by keeping the cells in medium containing 1.5 μg/mL puromycin (H2B-mNeonGreen clones) or 10 μg/mL blasticidin (H2B-mCherry clones) for three days. H2B-mCherry cells were subsequently transduced with pLV-NLS-copGFP with an MOI of 2 to generate H2B-mCherry-NLS-copGFP-double positive cells.

Mice

For the generation of organotypic slice cultures, 15-17 day- old C57BL6/J female and male mice were used. C57BL6/J mice were obtained from Charles Rivers Laboratories and bred in-house. All experiments were in in accordance with national regulations and ethical guidelines and were approved by the Centrale Commissie Dierproeven (CCD) and the Instantie voor Dierenwelzijn (IvD).

Ex vivo organotypic brain slice generation and image analysis

The organotypic brain slice invasion assay was performed as previously described (van Asperen et al., 2021). Briefly, 350 μm coronal sections of brains of postnatal day 15 – 17 C57BL6J pups were prepared using a VT1000S vibratome (Leica Biosystems,1404723512) and transferred to 1.0-μm porous membrane inserts (Corning®, 353102) in 1.5 mL recovery medium [DMEM:F12, 25% FBS, 1% L-Glutamine, 5 mM HEPES, 21 mM $NaHCO_3$ and 1% P/S], and cultured at 37 °C in a humidified incubator with 5% CO_2 overnight. The next day, the inserts were transferred to NSC medium [DMEM/F12 – GlutaMAX, 1% pen/strep, 10 ng/mL EGF (Peprotech, AF-100-15-A), 10 ng/mL FGF (Peptrotech, AF-100-18B)]. H2B-mNeonGreen expressing GFAP-KO and Vim-KO cells were mixed one to one with internal control cells expressing H2B-mCherry and 1,25 $\times 10^4$ cells were injected into the lateral ventricles of the organotypic brain slice using a 0.5 μL Hamilton syringe (model 7000.5 KH, 86250). The medium of the organotypic brain slices was replaced every 2-3 days. One week after injection of the cells, the brain slices were washed with PBS and fixed in 4% PFA in PBS at 4 °C overnight. The slices were washed with PBS and the porous membrane surrounding the brain tissue was cut out and transferred to a 24-well dish to perform whole-mount immunostaining of laminin (Supp. Table 2) and RapiClear tissue clearing (van Asperen et al., 2021). The cleared brain slices were imaged using an LSM 880 (Zeiss) confocal

microscope equipped with a 3-channel QUASAR Detection Unit (000000-2078-293). The entire population of injected cells was imaged with a 10x objective (N-Achroplan 10x, 420940-990-000) at 1.77 μm/pixel resolution, Z-plane increments of 6.63 μm and using image tiling. Smaller regions were imaged using a 20x objective (LD Plan-NEOFLUAR 20x, 421350-9970-000) at 0.42 μm/pixel resolution and 3.39 μm Z-plane increments.

Quantification of cell invasion was performed using ImageJ and Imaris software as described in van Asperen et al, 2021. For the quantification of nuclear fragmentation, the 20x confocal images of the injected organotypic brain slices were opened in ImageJ and two max projections of 50 μm stacks were created per organotypic brain slice. A ROI was drawn around the cells in the tumour core based on laminin expression patterns, and the max projection was binarized. The 'Analyze Particles' function of ImageJ was used to calculate the size of particles in the tumour core and in the invaded cells.

Preparation of microfluidic devices

The microfluidic devices for the confined migration assay and micropipette aspiration assay were generated as earlier described (Davidson et al., 2014, Denais et al., 2016, Elacqua et al., 2018; Davidson et al., 2019). Briefly, silicon wafer moulds were fabricated by 2-layer SU-8 photolithography (Davidson et al., 2014). Polydimethylsiloxane (PDMS) replicates were made by mixing the two-component of the Sylgard 184 PDMS kit (Dow Corning) in a 10:1 ratio according to the manufacturer's instructions. After the mixing, the solution was degassed using a vacuum chamber and the PDMS was baked for 2 hours at 65 °C. The PDMS was removed from the mould, cut to size, and biopsy punches were used to cut out the medium reservoirs and cell-seeding ports. Glass coverslips or microscopy slides were pre-soaked in 0.2 M HCl. The devices and glass coverslips/ microscopy slides were rinsed repeatedly with isopropanol and water, dried, and placed in a plasma cleaner (Harrick Plasma) for 5 minutes. The devices were placed on the glass coverslips or microscopy slides and heated on a hot plate 95 °C for 1 minute.

Preparation and live-cell imaging of microfluidic confined migration devices

The microfluidic confined migration devices were sterilised with 70% ethanol. Functionalisation of the devices was done by rinsing the devices with MilliQ and incubating the devices with 10 μg/mL laminin. After rinsing the devices with PBS and cell culture media, cell suspensions of 8.3×10^3 cells/ μl were prepared and cells were loaded (5.0 to 10.0 $\times$ 10^4 cells per chamber) into the cell seeding ports of the devices. Cells were cultured inside the devices for either 24 or 48 hours before the start of the live-cell migration experiment. One hour before the start of live-cell imaging,

the medium of the microfluidic confined migration devices was changed to phenol-red free medium (U251-MG cells: DMEM or FluorBrite DMEM supplemented with 10% FBS, KT-1937 cells: DMEM/F12). For the TO-PRO-2 and Caspase-3/7-reporter experiments, phenol-red free medium containing TO-PRO-3 (1:1000, Thermo Fischer #T3605) or Caspase-3/7 Green detection reagent (1:400, CellEvent™ #10423) was added to the devices four hours before the start of the live-cell imaging experiment. The devices were covered with a glass coverslip to avoid evaporation of medium, and were mounted on an inverted Zeiss Observer Z1 (CCD camera, 20x air objective, NA=0.8) or Olympus Cell M (CCD camera, 20x air objective, NA= 0.5) epifluorescence microscope with incubation chamber set at 37 °C for live-imaging. The TO-PRO-3 and Caspase-3/7-reporter experiments were performed with a Olympus FluoView FV1000 confocal microscope. Cells were imaged every 10 or 20 minutes for a duration of 14 hours.

Quantification of confined migration assay

Cell transit time and the number of successful transits were calculated using a custom-developed MATLAB program developed as described in Elacqua, McGregor, and Lammerding 2018. The number of nuclear fragmentations, cell death events, and NE ruptures were manually counted using ImageJ software using the 'Cell Counter' function. A region of interest was drawn around the confined migration device and around the region of confinement. Individual nuclei were tracked and time frames in which a cell was within the area of confinement, showed nuclear fragmentation, NE rupture or cell death was listed. The total number of cells within the device at the last time frame was used to calculate the percentage of events. All manual analysis were performed on blinded image files.

Micropipette aspiration assay

The experimental procedure for the aspiration assay is described in Davidson et al., 2019. In short, the microfluidic devices were pre-treated with 2% bovine serum albumin (BSA) and 0.2% fetal bovine serum in PBS for 10 minutes. Cell suspensions of 1.0 to 5.0 × 10^6 cells/mL were prepared and cells were incubated with 10 μg/ml Hoechst 33342 for 10 minutes. Three Tygon S3 E-3603 tubes were plugged into the microfluidic device, and connected to a vial with the cell suspension, with perfusion buffer (PBS) and to a collection tube. Different pressures were applied to the different microfluidic inlets with a MCFS-EZ pressure controller (Fluigent), leading to a pressure of 7.0 kPa, 1.4 kPa, and atmospheric pressure in the cell suspension, perfusion buffer, and collection tube, respectively. The pressure difference stimulated the flow of cells through the microfluidic device and suction of cells into micropipette channels with a diameter of 3 × 5 μm. Time-lapse brightfield and fluorescent images were acquired

with a frequency of 5 seconds for a total of 5 min with an inverted Zeiss Observer Z1 (CCD camera, 20x air objective, NA=0.8). Devices were re-used after flushing out the cells by inserting a pipette tip into the outlet of the collection tube. Analysis of the deformation dynamics were calculated using a custom-developed MATLAB program (Davidson et al. 2019).

Statistical analysis

Experiments repeated on different dates were considered independent experiments. For outcome measures at individual cell level, the median or average per independent experiment was used for statistics depending on the distribution of the data. All statistical analyses were performed using the GraphPad Prism software (version 9.1.2, Graphpad Software, USA). Normality of the data was tested using the Shapiro-Wilk test. For all normally distributed measurements, an unpaired t-test, one-way ANOVA, or two-way ANOVA followed by Tukey's multiple comparisons test were used to determine significance, set to $p < 0.05$. For non-normally-distributed measurements, the Mann-Whitney test or Kruskal-Wallis test followed by Dunn's multiple comparisons test were used to determine significance. All p values were two-tailed. Levels of significance were set as follows: ns > 0.05, *$0.05 \leq p > 0.01$, **$0.01 \leq p > 0.001$, ***$0.001 \leq p > 0.0001$, ****$p \leq 0.0001$. Error bars are presented as mean ± S.E.M.

Acknowledgements

This study was funded by the Dutch Cancer Society [KWF 101123, J.v.A, E.H.] and the T and P Bohnenn Foundation (P.R).

Author Contributions

J.v.A. performed conceptualisation, data collection, formal analysis, methodology, and wrote the original draft. L.A. performed data collection, formal analysis and reviewed and edited the manuscript. J.S. and K.T. performed data collection, methodology, and reviewed and edited the manuscript. M.K performed formal analysis and reviewed and edited the manuscript. P.R. and J.L. performed conceptualisation, methodology, supervision, and reviewed and edited the manuscript. E.H. performed conceptualisation, funding acquisition, project administration, methodology, supervision, and reviewed and edited the manuscript.

References

Agarwal, Srishti, Priyadharshni Muniyandi, Toru Maekawa, and D. Sakthi Kumar. 2018. "Vesicular Systems Employing Natural Substances as Promising Drug Candidates for MMP Inhibition in Glioblastoma: A Nanotechnological Approach." *International Journal of Pharmaceutics* 551 (1–2): 339–61. https://doi.org/10.1016/j.ijpharm.2018.09.033.

Alieva, Maria, Verena Leidgens, Markus J. Riemenschneider, Christoph A. Klein, Peter Hau, and Jacco van Rheenen. 2019. "Intravital Imaging of Glioma Border Morphology Reveals Distinctive Cellular Dynamics and Contribution to Tumor Cell Invasion." *Scientific Reports* 9 (1): 1–11. https://doi.org/10.1038/s41598-019-38625-4.

Asperen, Jessy van, Rebeca Uceda-Castro, Claire Vennin, Jacqueline Sluijs, Emma J van Bodegraven, Andreia S Margarido, Pierre AJ Robe, Jacco van Rheenen, and Elly M Hol. 2021. "GFAP Splice Variants Fine-Tune Glioma Cell Invasion and and Tumour Dynamics by Modulating Migration Persistence." *BioRxiv*, 1–47. https://doi.org/10.1101/2021.08.19.456978.

Bakhoum, Samuel F., Bryan Ngo, Ashley M. Laughney, Julie Ann Cavallo, Charles J. Murphy, Peter Ly, Pragya Shah, et al. 2018. "Chromosomal Instability Drives Metastasis through a Cytosolic DNA Response." *Nature* 553 (7689): 467–72. https://doi.org/10.1038/nature25432.

Beadle. 2010. "The Role of Myosin II in Glioma Invasion of the Brain Christopher." *Seikagaku* 82 (4): 327–31. https://doi.org/10.1091/mbc.E08.

Block, Johanna, Viktor Schroeder, Paul Pawelzyk, Norbert Willenbacher, and Sarah Köster. 2015. "Biochimica et Biophysica Acta Physical Properties of Cytoplasmic Intermediate Filaments" *BBA - Molecular Cell Research* 1853 (11): 3053–64. https://doi.org/10.1016/j.bbamcr.2015.05.009.

Bodegraven, Emma J. van, Jessy V. van Asperen, Jacqueline A. Sluijs, Coen B.J. van Deursen, Miriam E. van Strien, Oscar M.J.A. Stassen, Pierre A.J. Robe, and Elly M. Hol. 2019. "GFAP Alternative Splicing Regulates Glioma Cell-ECM Interaction in a DUSP4-Dependent Manner." *FASEB Journal : Official Publication of the Federation of American Societies for Experimental Biology* 33 (11): 12941–59. https://doi.org/10.1096/fj.201900916R.

Claes, An, Albert J. Idema, and Pieter Wesseling. 2007. "Diffuse Glioma Growth: A Guerilla War." *Acta Neuropathologica* 114 (5): 443–58. https://doi.org/10.1007/s00401-007-0293-7.

Concordet, Jean Paul, and Maximilian Haeussler. 2018. "CRISPOR: Intuitive Guide Selection for CRISPR/Cas9 Genome Editing Experiments and Screens." *Nucleic Acids Research* 46 (W1): W242–45. https://doi.org/10.1093/nar/gky354.

Cuddapah, Vishnu Anand, Stefanie Robel, Stacey Watkins, and Harald Sontheimer. 2014. "A Neurocentric Perspective on Glioma Invasion." *Nature Reviews. Neuroscience* 15 (7): 455–65. https://doi.org/10.1038/nrn3765.

D'Arcy, Mark S. 2019. "Cell Death: A Review of the Major Forms of Apoptosis, Necrosis and Autophagy." *Cell Biology International* 43 (6): 582–92. https://doi.org/10.1002/cbin.11137.

Davidson, Patricia M., Celine Denais, Maya C. Bakshi, and Jan Lammerding. 2014. "Nuclear Deformability Constitutes a Rate-Limiting Step during Cell Migration in 3-D Environments." *Cellular and Molecular Bioengineering* 7 (3): 293–306. https://doi.org/10.1007/s12195-014-0342-y.

Davidson, Patricia M., Gregory R. Fedorchak, Solenne Mondésert-Deveraux, Emily S. Bell, Philipp Isermann, Denis Aubry, Rachele Allena, and Jan Lammerding. 2019. "High-Throughput Microfluidic Micropipette Aspiration Device to Probe Time-Scale Dependent Nuclear Mechanics in Intact Cells." *Lab on a Chip* 19 (21): 3652–63. https://doi.org/10.1039/c9lc00444k.

Davidson, Patricia M., Josiah Sliz, Philipp Isermann, Celine Denais, and Jan Lammerding. 2015. "Design of a Microfluidic Device to Quantify Dynamic Intra-Nuclear Deformation during Cell Migration through Confining Environments." *Integrative Biology (United Kingdom)* 7 (12): 1534–46. https://doi.org/10.1039/c5ib00200a.

Denais, Celine M., Rachel M. Gilbert, Philipp Isermann, Alexandra L. McGregor, Mariska Te Lindert, Bettina Weigelin, Patricia M. Davidson, Peter Friedl, Katarina Wolf, and Jan Lammerding. 2016. "Nuclear Envelope Rupture and Repair during Cancer Cell Migration." *Science* 352 (6283): 353–58. https://doi.org/10.1126/science.aad7297.

Drost, Jarno, Richard H. Van Jaarsveld, Bas Ponsioen, Cheryl Zimberlin, Ruben Van Boxtel, Arjan Buijs, Norman Sachs, et al. 2015. "Sequential Cancer Mutations in Cultured Human Intestinal Stem Cells." *Nature* 521 (7550): 43–47. https://doi.org/10.1038/nature14415.

Dupin, Isabelle, Yasuhisa Sakamoto, and Sandrine Etienne-Manneville. 2011. "Cytoplasmic Intermediate Filaments Mediate Actin-Driven Positioning of the Nucleus." *Journal of Cell Science* 124 (Pt 6): 865–72. https://doi.org/10.1242/jcs.076356.

Elacqua, Joshua J., Alexandra L. McGregor, and Jan Lammerding. 2018. "Automated Analysis of Cell Migration and Nuclear Envelope Rupture in Confined Environments." *PLoS ONE* 13 (4): 1–19. https://doi.org/10.1371/journal.pone.0195664.

Enari, Masato, Hideki Sakahira, Hideki Yokoyama, Katsuya Okawa, Akihiro Iwamatsu, and Shigekazu Nagata. 1998. "A Caspase-Activated DNase That Degrades DNA during Apoptosis, and Its Inhibitor ICAD." *Nature* 391 (6662): 43–50. https://doi.org/10.1038/34112.

Farin A, Suzuki SO, Weiker M, Goldman JE, Bruce JN, Canoll P. 1994. "Transplanted Glioma Cells Migrate and Proliferate on Host Brain Vasculature: A Dynamic Analysis." *American Journal of Tropical Medicine and Hygiene* 51 (5): 523–32. https://doi.org/10.1002/glia.

Forsyth, P. A., H. Wong, T. D. Laing, N. B. Rewcastle, D. G. Morris, H. Muzik, K. J. Leco, et al. 1999. "Gelatinase-A (MMP-2), Gelatinase-B (MMP-9) and Membrane Type Matrix Metalloproteinase-1 (MT1-MMP) Are Involved in Different Aspects of the Pathophysiology of Malignant Gliomas." *British Journal of Cancer* 79 (11–12): 1828–35. https://doi.org/10.1038/sj.bjc.6990291.

Friedl, Peter, Katarina Wolf, and Jan Lammerding. 2011. "Nuclear Mechanics during Cell Migration." *Current Opinion in Cell Biology* 23 (1): 55–64. https://doi.org/10.1016/j.ceb.2010.10.015.

Galluzzi, L., J. M. Bravo-San Pedro, I. Vitale, S. A. Aaronson, J. M. Abrams, D. Adam, E. S. Alnemri, et al. 2015. "Essential versus Accessory Aspects of Cell Death: Recommendations of the NCCD 2015." *Cell Death and Differentiation* 22 (1): 58–73. https://doi.org/10.1038/cdd.2014.137.

Galluzzi, Lorenzo, Ilio Vitale, Stuart A. Aaronson, John M. Abrams, Dieter Adam, Patrizia Agostinis, Emad S. Alnemri, et al. 2018. "Molecular Mechanisms of Cell Death: Recommendations of the Nomenclature Committee on Cell Death 2018." *Cell Death and Differentiation* 25 (3): 486–541. https://doi.org/10.1038/s41418-017-0012-4.

Hanus, Jakub, Magdalena Kalinowska-Herok, and Piotr Widlak. 2010. "Identification of Novel Putative Regulators of the Major Apoptotic Nuclease DNA Fragmentation Factor." *Acta Biochimica Polonica* 57 (4): 521–27. https://doi.org/10.18388/abp.2010_2438.

Harada, Takamasa, Joe Swift, Jerome Irianto, Jae-won Shin, Kyle R Spinler, Avathamsa Athirasala, Rocky Diegmiller, P C Dave P Dingal, Irena L Ivanovska, and Dennis E Discher. 2014. "But Softness Can Limit Survival" 204 (5): 669–82. https://doi.org/10.1083/jcb.201308029.

Ho, Vincent K.Y., Jaap C. Reijneveld, Roelien H. Enting, Henri P. Bienfait, Pierre Robe, Brigitta G. Baumert, and Otto Visser. 2014. "Changing Incidence and Improved Survival of Gliomas." *European Journal of Cancer* 50 (13): 2309–18. https://doi.org/10.1016/j.ejca.2014.05.019.

Hu, Jiliang, Yiwei Li, Yukun Hao, Tianqi Zheng, Satish K. Gupta, German Alberto Parada, Huayin Wu, et al. 2019. "High Stretchability, Strength, and Toughness of Living Cells Enabled by Hyperelastic Vimentin Intermediate Filaments." *Proceedings of the National Academy of Sciences of the United States of America* 116 (35): 17175–80. https://doi.org/10.1073/pnas.1903890116.

Irianto, Jerome, Yuntao Xia, Charlotte R. Pfeifer, Avathamsa Athirasala, Jiazheng Ji, Cory Alvey, Manu Tewari, et al. 2017. "DNA Damage Follows Repair Factor Depletion and Portends Genome Variation

in Cancer Cells after Pore Migration." *Current Biology* 27 (2): 210–23. https://doi.org/10.1016/j.cub.2016.11.049.

Ivkovic, Sanja, Christopher Beadle, Sonal Noticewala, Susan C. Massey, Kristin R. Swanson, Laura N. Toro, Anne R. Bresnick, Peter Canoll, and Steven S. Rosenfeld. 2012. "Direct Inhibition of Myosin II Effectively Blocks Glioma Invasion in the Presence of Multiple Motogens." *Molecular Biology of the Cell* 23 (4): 533–42. https://doi.org/10.1091/mbc.E11-01-0039.

Jiu, Yaming, Jaakko Lehtimäki, Sari Tojkander, Fang Cheng, Harri Jäälinoja, Xiaonan Liu, Markku Varjosalo, John E. Eriksson, and Pekka Lappalainen. 2015. "Bidirectional Interplay between Vimentin Intermediate Filaments and Contractile Actin Stress Fibers." *Cell Reports* 11 (10): 1511–18. https://doi.org/10.1016/j.celrep.2015.05.008.

Ketema, M., M. Kreft, P. Secades, H. Janssen, and A. Sonnenberg. 2013. "Nesprin-3 Connects Plectin and Vimentin to the Nuclear Envelope of Sertoli Cells but Is Not Required for Sertoli Cell Function in Spermatogenesis." *Molecular Biology of the Cell* 24 (15): 2454–66. https://doi.org/10.1091/mbc.E13-02-0100.

Liu, Xuesong, Peng Li, Piotr Widlak, Hua Zou, Xu Luo, William T. Garrard, and Xiaodong Wang. 1998. "The 40-KDa Subunit of DNA Fragmentation Factor Induces DNA Fragmentation and Chromatin Condensation during Apoptosis." *Proceedings of the National Academy of Sciences of the United States of America* 95 (15): 8461–66. https://doi.org/10.1073/pnas.95.15.8461.

Maciejowski, John, Aikaterini Chatzipli, Alexandra Dananberg, Kevan Chu, Eleonore Toufektchan, Leszek J. Klimczak, Dmitry A. Gordenin, Peter J. Campbell, and Titia de Lange. 2020. "APOBEC3-Dependent Kataegis and TREX1-Driven Chromothripsis during Telomere Crisis." *Nature Genetics* 52 (9): 884–90. https://doi.org/10.1038/s41588-020-0667-5.

McGregor, Alexandra Lynn, Chieh Ren Hsia, and Jan Lammerding. 2016. "Squish and Squeeze - the Nucleus as a Physical Barrier during Migration in Confined Environments." *Current Opinion in Cell Biology* 40: 32–40. https://doi.org/10.1016/j.ceb.2016.01.011.

Meyer, Mona, Jüri Reimand, Xiaoyang Lan, Renee Head, Xueming Zhu, Michelle Kushida, Jane Bayani, et al. 2015. "Single Cell-Derived Clonal Analysis of Human Glioblastoma Links Functional and Genomic Heterogeneity." *Proceedings of the National Academy of Sciences of the United States of America* 112 (3): 851–56. https://doi.org/10.1073/pnas.1320611111.

Nader, Guilherme Pedreira de Freitas, Sonia Agüera-Gonzalez, Fiona Routet, Matthieu Gratia, Mathieu Maurin, Valeria Cancila, Clotilde Cadart, et al. 2021. "Compromised Nuclear Envelope Integrity Drives TREX1-Dependent DNA Damage and Tumor Cell Invasion." *Cell* 184 (20): 5230-5246.e22. https://doi.org/10.1016/j.cell.2021.08.035.

Nava, Michele M., Yekaterina A. Miroshnikova, Leah C. Biggs, Daniel B. Whitefield, Franziska Metge, Jorge Boucas, Helena Vihinen, et al. 2020. "Heterochromatin-Driven Nuclear Softening Protects the Genome against Mechanical Stress-Induced Damage." *Cell* 181 (4): 800-817.e22. https://doi.org/10.1016/j.cell.2020.03.052.

Patel, A P, I Tirosh, J J Trombetta, A K Shalek, S M Gillespie, H Wakimoto, D P Cahill, et al. 2014. "Single-Cell RNA-Seq Highlights Intratumoral Heterogeneity in Primary Glioblastoma." *Science* 344 (6190): 1396–1401. https://doi.org/10.1126/science.1254257.

Patteson, Alison E., Katarzyna Pogoda, Fitzroy J. Byfield, Kalpana Mandal, Zofia Ostrowska-Podhorodecka, Elisabeth E. Charrier, Peter A. Galie, et al. 2019. "Loss of Vimentin Enhances Cell Motility through Small Confining Spaces." *Small* 15 (50), 1903180: 1–10. https://doi.org/10.1002/smll.201903180.

Patteson, Alison E., Amir Vahabikashi, Katarzyna Pogoda, Stephen A. Adam, Kalpana Mandal, Mark Kittisopikul, Suganya Sivagurunathan, Anne Goldman, Robert D. Goldman, and Paul A. Janmey. 2019. "Vimentin Protects Cells against Nuclear Rupture and DNA Damage during Migration." *The Journal of Cell* Biology 218 (12), jcb.201902046. https://doi.org/10.1083/jcb.201902046.

Pfeifer, Charlotte R., Yuntao Xia, Kuangzheng Zhu, Dazhen Liu, Jerome Irianto, Victor M. Morales

García, Leeza M. Santiago Millán, et al. 2018. "Constricted Migration Increases DNA Damage and Independently Represses Cell Cycle." *Molecular Biology of the Cell* 29 (16): 1948–62. https://doi.org/10.1091/mbc.E18-02-0079.

Picariello, Hannah S., Rajappa S. Kenchappa, Vandana Rai, James F. Crish, Athanassios Dovas, Katarzyna Pogoda, Mariah McMahon, et al. 2019. "Myosin IIA Suppresses Glioblastoma Development in a Mechanically Sensitive Manner." *Proceedings of the National Academy of Sciences of the United States of America* 116 (31): 15550–59. https://doi.org/10.1073/pnas.1902847116.

Qin, Zhao, Laurent Kreplak, and Markus J. Buehler. 2009. "Hierarchical Structure Controls Nanomechanical Properties of Vimentin Intermediate Filaments." *PLoS ONE* 4 (10). https://doi.org/10.1371/journal.pone.0007294.

Raab, M., M. Gentili, H. De Belly, H. R. Thiam, P. Vargas, A. J. Jimenez, F. Lautenschlaeger, et al. 2016. "ESCRT III Repairs Nuclear Envelope Ruptures during Cell Migration to Limit DNA Damage and Cell Death." *Science* 352 (6283): 359–62. https://doi.org/10.1126/science.aad7611.

Robe, Pierre A., Mohamed Bentires-Alj, Marianne Bonif, Bernard Rogister, Manuel Deprez, Heddi Haddada, Minh Tuan Nguyen Khac, et al. 2004. "In Vitro and in Vivo Activity of the Nuclear Factor-KB Inhibitor Sulfasalazine in Human Glioblastomas." *Clinical Cancer Research* 10 (16): 5595–5603. https://doi.org/10.1158/1078-0432.CCR-03-0392.

Sahm, Felix, David Capper, Astrid Jeibmann, Antje Habel, Werner Paulus, Dirk Troost, and Andreas Von Deimling. 2012. "Addressing Diffuse Glioma as a Systemic Brain Disease with Single-Cell Analysis." *Archives of Neurology* 69 (4): 523–26. https://doi.org/10.1001/archneurol.2011.2910.

Scherer, H.J. 1940. "Cerebral Astrocytomas And Their Derivatives" *The American Journal of Cancer* 42 (1): 1–15.

Shah, Pragya, Chad M. Hobson, Svea Cheng, Marshall J. Colville, Matthew J. Paszek, Richard Superfine, and Jan Lammerding. 2021. "Nuclear Deformation Causes DNA Damage by Increasing Replication Stress." *Current Biology* 31 (4): 753-765.e6. https://doi.org/10.1016/j.cub.2020.11.037.

Skalli, Omar, Ulrika Wilhelmsson, Charlotte Örndahl, Boglarka Fekete, Kristina Malmgren, Bertil Rydenhag, and Milos Pekny. 2013. "Astrocytoma Grade IV (Glioblastoma Multiforme) Displays 3 Subtypes with Unique Expression Profiles of Intermediate Filament Proteins." *Human Pathology* 44 (10): 2081–88. https://doi.org/10.1016/j.humpath.2013.03.013.

Sottoriva, Andrea, Inmaculada Spiteri, Sara G M Piccirillo, Anestis Touloumis, V Peter Collins, John C Marioni, Christina Curtis, Colin Watts, and Simon Tavaré. 2013. "Intratumor Heterogeneity in Human Glioblastoma Reflects Cancer Evolutionary Dynamics." *Proceedings of the National Academy of Sciences* 110 (10): 4009–14. https://doi.org/10.1073/pnas.1219747110.

Stankevicins, Luiza, Nicolas Ecker, Emmanuel Terriac, Paolo Maiuri, Rouven Schoppmeyer, Pablo Vargas, Ana Maria Lennon-Duménil, et al. 2020. "Deterministic Actin Waves as Generators of Cell Polarization Cues." *Proceedings of the National Academy of Sciences of the United States of America* 117 (2): 826–35. https://doi.org/10.1073/pnas.1907845117.

Stankevicins, Luiza da, Marta Urbanska, Daniel A.D. Flormann, Emmanuel Terriac, Zahra Mostajeran, Annica K.B. Gad, Fang Cheng, John E. Eriksson, and Franziska Lautenschläger. 2019. "Vimentin Provides the Mechanical Resilience Required for Amoeboid Migration and Protection of the Nucleus." *BioRxiv*, 1–23. https://doi.org/10.1101/720946.

Stephens, Andrew D., Edward J. Banigan, and John F. Marko. 2018. "Separate Roles for Chromatin and Lamins in Nuclear Mechanics." *Nucleus* 9 (1): 119–24. https://doi.org/10.1080/19491034.2017.1414118.

Thorne, R. G., and C. Nicholson. 2006. "In Vivo Diffusion Analysis with Quantum Dots and Dextrans Predicts the Width of Brain Extracellular Space." *Proceedings of the National Academy of Sciences* 103 (14): 5567–72. https://doi.org/10.1073/pnas.0509425103.

Toivola, D. M., P. Strnad, A. Habtezion, and M. B. Omary. 2010. "Intermediate Filaments Take the Heat as Stress Proteins." *Trends in Cell Biology* 20 (2): 79–91. https://doi.org/10.1016/j.tcb.2009.11.004.

Tudor, Sara M., Lavenus, Sandrine B., and Logue, Jeremy S. 2019. "A Flexible Network of Vimentin Intermediate Filaments Promotes the Migration of Amoeboid Cancer Cells through Confined Environments." *Ayaŋ* 8 (5): 55. https://doi.org/https://doi.org/10.1101/788810.

Venkataramani, Varun, Dimitar Ivanov Tanev, Christopher Strahle, Alexander Studier-Fischer, Laura Fankhauser, Tobias Kessler, Christoph Körber, et al. 2019. "Glutamatergic Synaptic Input to Glioma Cells Drives Brain Tumour Progression." *Nature* 573 (7775): 532–38. https://doi.org/10.1038/s41586-019-1564-x.

Watkins, S., and H. Sontheimer. 2011. "Hydrodynamic Cellular Volume Changes Enable Glioma Cell Invasion." *Journal of Neuroscience* 31 (47): 17250–59. https://doi.org/10.1523/JNEUROSCI.3938-11.2011.

Xia, Yuntao, Charlotte R. Pfeifer, Kuangzheng Zhu, Jerome Irianto, Dazhen Liu, Kalia Pannell, Emily J. Chen, et al. 2019. "Rescue of DNA Damage after Constricted Migration Reveals a Mechano-Regulated Threshold for Cell Cycle." *Journal of Cell Biology* 218 (8): 2542–63. https://doi.org/10.1083/JCB.201811100.

Yamada, Kenneth M., and Michael Sixt. 2019. "Mechanisms of 3D Cell Migration." *Nature Reviews Molecular Cell Biology*, no. Box 1. https://doi.org/10.1038/s41580-019-0172-9.

Zhang, Zhiqun, J. Susie Zoltewicz, Stefania Mondello, Kimberly J. Newsom, Zhihui Yang, Boxuan Yang, Firas Kobeissy, et al. 2014. "Human Traumatic Brain Injury Induces Autoantibody Response against Glial Fibrillary Acidic Protein and Its Breakdown Products." *PLoS ONE* 9 (3): 1–16. https://doi.org/10.1371/journal.pone.0092698.

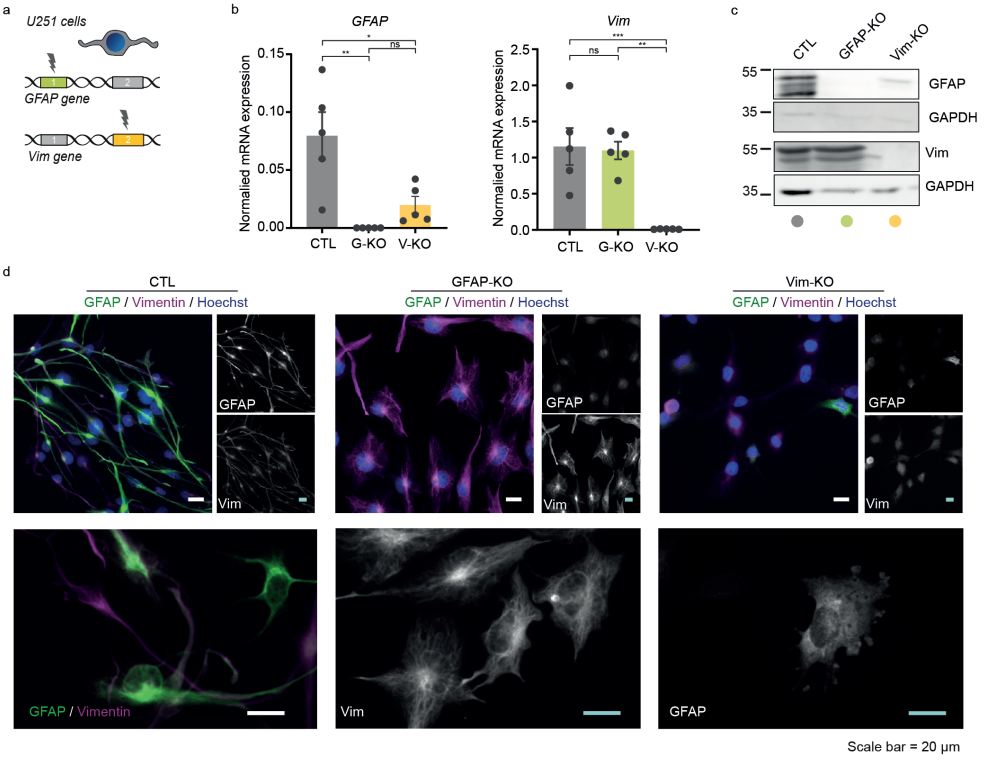

Supp. Fig 1. Generation and characterisation of GFAP and Vimentin-KO U251-MG cell clones. (a) Schematic of the CRISPR-Cas9 approach to generate GFAP-KO and Vim-KO cells. Exon 1 of the GFAP gene and exon 2 of vimentin gene were targeted to create KOs. (b) Normalised mRNA expression levels of GFAP (left panel) and vimentin (right panel) show a significant reduction in GFAP mRNA in the GFAP-KO cells but also Vimentin-KO cells, and reduction of vimentin mRNA in the Vim-KO cells. (c) Protein levels of GFAP and Vim in the different cell clones show an absence of the respective proteins in GFAP-KO and Vim-KO cells. N= 4 independent experiments, significance was determined using a one-way ANOVA followed by a Tukey's multiple comparisons test. (d) The IF network in the CTL, GFAP-KO and Vim-KO cells as shown with immunofluorescence with GFAP and vimentin antibodies. In the lower panel, higher magnification images of the remaining IF network are shown. Scale bar = 20 μm. Error bars in graphs represent mean ± S.E.M, *$p < 0.05$, **$p < 0.01$, ***$p < 0.001$, ns = not significant.

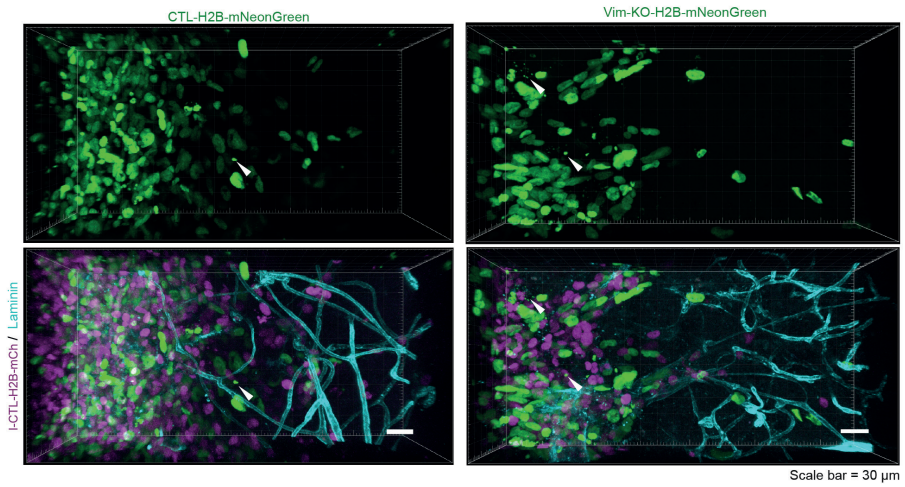

Supp. Fig 2. Representative image of CTL-H2B-mNeonGreen and Vim-H2B-mNeonGreen co-injected with I-CTL-H2B-mCherry cells within organotypic brain slice. Example image of only H2B-mNeonGreen only (green, upper panels) or merged images with I-CTL-H2B-mCherry (magenta) and the mouse-brain vasculature immunostained with laminin (cyan, lower panels). Examples of nuclear fragments are indicated with arrow heads. Scale bar = 20 μm

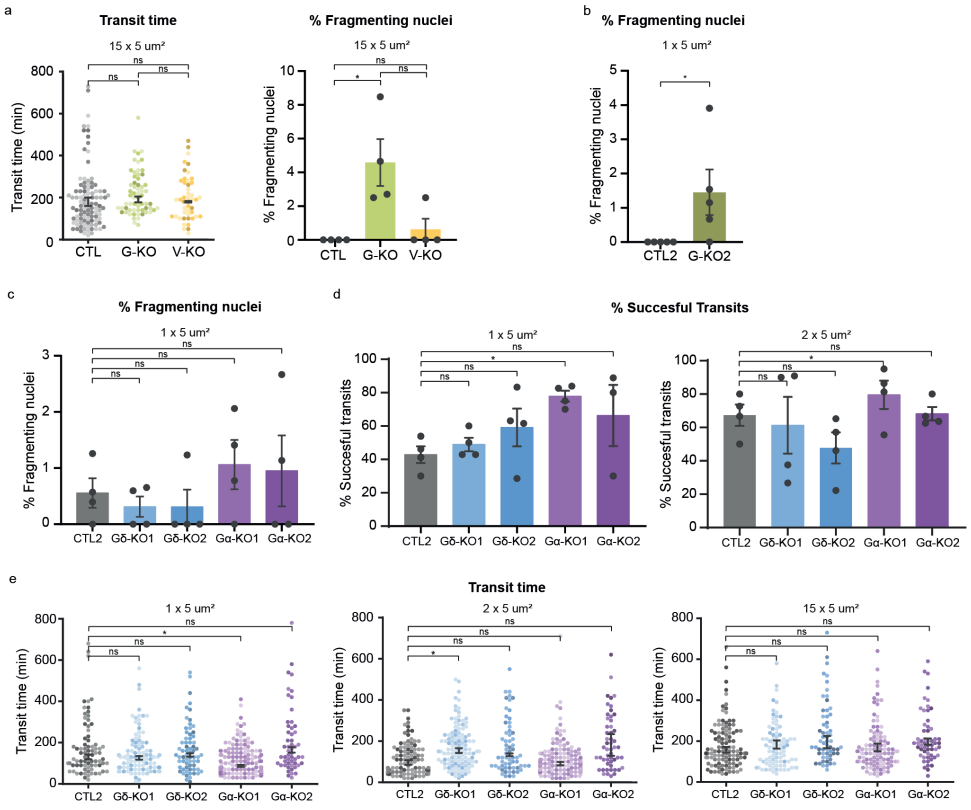

Supp. Fig 3. Quantification of successful transits, transit time and fragmentation events in non-confined conditions and additional GFAP-modulated cells. (a) Quantification of transit time (left panel) and percentage of fragmenting nuclei (right panel) in 15 × 5 μm^2 control channels (left panel). N= 4 independent experiments, significance was determined using a one-way ANOVA followed by a Tukey's multiple comparisons test. (b) Quantification of percentage of fragmenting nuclei in CTL and GFAP-KO clone 2 in 1 × 5 μm^2 constrictions. N= 4 independent experiments, significance was determined using an unpaired t-test. (c) Quantification of percentage of fragmenting nuclei GFAP isoform KO cells in 1 × 5 μm^2 constrictions. N= 4 independent experiments, significance was determined using a one-way ANOVA followed by a Tukey's multiple comparisons test. (d) Quantification of percentage of successful transits of GFAP isoform KO cells in 1 × 5 μm^2 (left panel) and 2 × 5 μm^2 (right panel) constrictions. N= 4 independent experiments, significance was determined using a one-way ANOVA followed by a Tukey's multiple comparisons test. (e) Quantification of transit time of GFAP isoform KO cells in 1 × 5 μm^2 (left panel), 2 × 5 μm^2 (middle panel) constrictions, and 15 × 5 μm^2 control channels (right panel). The median transit time per independent experiment was determined, n= 4 independent experiments. The scatter plots show the transit time of individual nuclei, colour saturation represents different independent experiments. Significance was determined using a one-way ANOVA followed by a Tukey's multiple comparisons test. Error bars in graphs represent mean ± S.E.M, *$p < 0.05$, ns = not significant.

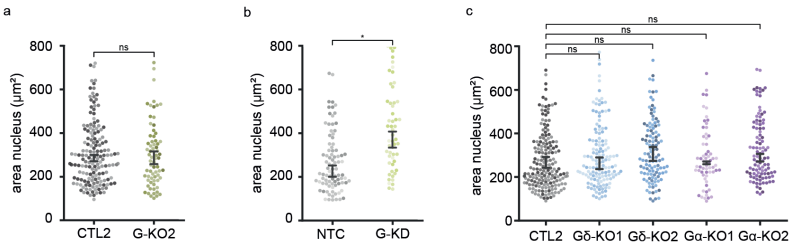

Supp. Fig 4. Morphological and mechanical characteristics of the nuclei of additional GFAP-modulated cells. (a) Quantification of the area of the nucleus of CTL and GFAP-KO clone 2 nuclei in 15 × 5 μm^2 control channels. The median area per independent experiment was determined, n= 4 independent experiments. Significance was determined using an unpaired t-test. (b) Quantification of the area of the nucleus of cells transduced with a shRNA against GFAP (G-KD) or a non-targeting control (NTC) in 15 × 5 µm control channels. The median area per independent experiment was determined, n= 4 independent experiments. Significance was determined using an unpaired t-test. (c) Quantification of the area of GFAP isoform modulated cells in 15 × 5 μm^2 control channels. The median area per independent experiment was determined, n= 4 independent experiments. Significance was determined using a one-way ANOVA followed by a Tukey's multiple comparisons test. In all panels, the scatter plots show the area of individual nuclei, colour saturation represents different independent experiments. Error bars in graphs represent mean ± S.E.M, *$p < 0.05$, ns = not significant.

Supp. Table 1. Primers used for quantitative PCR

Antibody	Product number, Company	(WM)-IF	WB
Chicken anti-vimentin	AB5733, Chemicon, Temecula, CA, USA	1:1500	-
Mouse anti-GAPDH	MAB374, Chemicon, Temecula, CA, USA	-	1:2000
Rabbit anti-GFAP	#Z0334, Dako (Agilent), Santa Clara, CA, USA	1:1000	1:50000
Rabbit anti-GFAPδ	Manufactured in house. Bleeding date: 27-11-2003 (purified in 2004)	-	1:2000
Rabbit anti-laminin	L9393, Sigma Aldrich, St Louis, MO, USA	1:1000	-
Donkey anti-chicken Cy3	703-175-155, Jackson Immuno Research, West Grove, PA, USA	1:1000	-
Donkey anti-mouse AF647	703-606-150, Jackson Immuno Research, West Grove, PA, USA	-	1:2000
Donkey anti-rabbit Cy3	711-166-152, Jackson Immuno Research, West Grove, PA, USA	1:1000	-
Donkey anti-rabbit AF647	711-606-152, Jackson Immuno Research, West Grove, PA, USA	1:1000	-
Goat anti-rabbit IRDye800	926-32211, LI-COR, 4647 Superior Street Lincoln, NE, USA	-	1:5000

Abbreviations: AluJ = Alu element Jurka, GAPDH = Glyceraldehyde 3-phosphate dehydrogenase, GFAP = glial fibrillary acidic protein, PCR = polymerase chain reaction.

Supp. Table 2. List of antibodies

Name	Forward primer (5' > 3')	Reverse primer (5' > 3')
AluJ	CAACATAGTGAAACCCCGTCTCT	GCCTCAGCCTCCCGAGTAG
GAPDH	TGCACCACCAACTGCTTAGC	GGCATGGACTGTGGTCATGA
GFAPpan	GACCTGGCCACTGTGAGG	GGCTTCATCTGCTTCCTGTC
Vim	CGTACGTCAGCAATATGAAAGTGTG	TCAGAGAGGTCAGCAAACTTGGA

Abbreviations: AF= Alexa Fluor, GAPDH= Glyceraldehyde 3-phosphate dehydrogenase, GFAP = glial fibrillary acidic protein, ICC= immunocytochemistry, WB = Western blot


6

CHAPTER 6

Investigation of glial fibrillary acidic protein (GFAP) in body fluids as a potential biomarker for glioma: a systematic review and meta-analysis

Jessy V. van Asperen[1#], Daria M. Fedorushkova1[1#], Pierre A.J.T. Robe[2†], Elly M. Hol[1†]

[1] Department of Translational Neurosciences, UMC Utrecht Brain Center, University Medical Center Utrecht, Utrecht University, 3584 CG Utrecht, The Netherlands
[2] Department of Neurology and Neurosurgery, University Medical Center Utrecht Brain Center, Utrecht University, 3584 CG Utrecht, The Netherlands

[#] These authors contributed equally

[†] These authors jointly supervised this work

Biomarkers. 2022. Feb 27(1):1-12
doi: 10.1080/1354750X.2021.2006313

Abstract

Introduction. Liquid biopsies are promising diagnostic tools for glioma. In this quantitative systematic review, we investigate whether the detection of intermediate filaments (IF) in body fluids can be used as a tool for glioma diagnosis and prognosis.

Materials and methods. We included all studies in which IF-levels were determined in patients with glioma and healthy controls. Of the 28 identified eligible studies, 12 focused on levels of GFAP in serum (sGFAP) and were included for metadata analysis.

Results. In all studies combined, 62.7% of all grade IV patients had detectable levels of sGFAP compared to 12.7% of healthy controls. sGFAP did not surpass the limit of detection in lower grade patients or healthy controls, but sGFAP was significantly elevated in grade IV glioma (0.12 ng/mL (0.06 – 0.18), $P < 0.001$) and showed an average median difference of 0.15 ng/mL (0.04 – 0.25, $P < 0.01$) compared to healthy controls. sGFAP levels were linked to tumour volume, but not to patient outcome.

Conclusion. The presence of sGFAP is indicative of grade IV glioma, but additional studies are necessary to fully determine the usefulness of GFAP in body fluids as a tool for grade IV glioma diagnosis and follow-up.
Keywords: glioblastoma multiforme; intermediate filament; cytoskeleton; biomarker; blood serum; GFAP

Clinical significance: This systematic review and meta-analysis shows that GFAP in serum is linked to grade IV glioma. The high heterogeneity between studies and relatively low sensitivity makes applicability of sGFAP as a biomarker however currently uncertain. Additional studies are necessary to investigate whether sGFAP can be used for the diagnosis or follow-up of specific subgroups of grade IV patients.

Introduction

Gliomas are tumours that arise from the glial cells in the brain (Louis et al. 2016). Glioma can occur in different malignancy grades with increasing malignancy: i.e. grade I = pilocytic astrocytoma, grade II = astrocytoma and oligodendroglioma, grade III = anaplastic astrocytoma and oligodendrocytoma, and grade IV = glioblastoma multiforme (GBM). This grading is based on various histopathological features (Louis et al. 2016). GBM is the most common primary malignant brain tumour, and the most severe of all gliomas. Due to its rapid progressive, heterogeneous nature, and diffuse spread in the brain, current treatment, consisting of chemotherapy, radiotherapy and/

or surgery, is unsuccessful in eradicating GBM (Aldape et al. 2019). This results in a five-year survival rate of 6.8% (Ostrom et al. 2019).

Tissue biopsies are widely used in the diagnosis of brain tumours. However, the procedure is highly invasive and potentially hazardous. In addition to the risk of neurological dysfunction, post-operative oedema and haemorrhage result in a mortality rate for biopsies of 0.5% to 3.5% (Yong and Lonser 2013). Furthermore, there is a notable inter- and intra-observer variability for histopathology of glioma biopsies (Mark, Beverly, and Edward 1996). Patients cannot undergo the invasive procedure repeatedly for longitudinal sampling due to the high risk. This complicates treatment monitoring in glioma patients, since neuro-imaging does not always provide proper correlation with treatment response (Neagu et al. 2015). Liquid biopsies can be a more objective, less invasive, and quicker diagnostic tool for glioma diagnosis or follow-up. It could aid in early detection of the tumour and possibly enable regular follow-up over time, allowing the monitoring of tumour progression and therapy response.

Emerging biomarkers in various types of cancer are intermediate filaments (IFs), which are cytoskeletal proteins (Sharma et al. 2019). The composition of the IF network varies greatly across various cell types. IFs play a role in many different cellular processes, from regulating the deformability and mechanical strength of the cell to various essential cellular mechanisms such as transmembrane transport and intracellular signalling (Etienne-Manneville 2018). In addition, IFs are involved in facilitating cell motility and migration, depending on the context, cell type, and type of IF (De Pascalis et al. 2018; Chung, Rotty, and Coulombe 2013). These functional characteristics of IFs are of interest considering the malignancy of glioma (Skalli et al. 2013; van Bodegraven et al. 2019a; Hohmann and Dehghani 2019). Glial fibrillary acid protein (GFAP) is an IF which is co-expressed with nestin and vimentin and is mainly present in the astrocytes and neural stem cells in the brain (Hol and Pekny 2015).

Because of the diverse roles of GFAP, its level in serum has been assessed for a variety of brain diseases (Messing and Brenner 2020). More specifically, GFAP is a novel biomarker for traumatic brain injury (TBI) (Shemilt et al. 2019) and a commercial test has recently been approved for use in the clinic by the U.S. Food and Drug Administration (The U.S. Food and Drug Administration 2018). While there is no consistent correlation between GFAP expression in tissue and glioma malignancy (reviewed in van Bodegraven et al. 2019a), we observed that the ratio between two splice variants of GFAP, GFAPα and δ, is correlated to glioma grade (Stassen et al. 2017; Middeldorp and Hol 2011; Hol and Pekny 2015). The release of GFAP by tumour cells and its diffusion to blood serum or other body fluids may however differ between tumour grades as a result of higher cell death/ proliferation and blood-brain permeability in tumours of higher grades. Serum or other body fluid GFAP levels might thus be of use in the clinical practice of neuro-oncology, for example as a diagnostic help in the case of doubtful MRI images

or to monitor treatment effect in glioma patients. A prerequisite to this end is to assess the level of intermediate filaments in the body fluids of glioma patients compared to healthy controls.

Results

Systematic Search

The search strategy resulted in 849 publications that were scanned on title and abstract by two researchers, independently. The 39 remaining studies that matched our inclusion criteria were evaluated in detail and 28 studies reporting on IF levels in body fluids of glioma patients were identified. Since only two out of 28 studies focussed on IF proteins other than GFAP (Husain et al. 2012; Ludwig et al. 2009), we decided to focus the systematic review on outcome measures regarding GFAP in body fluids of glioma patients (Fig. 1).

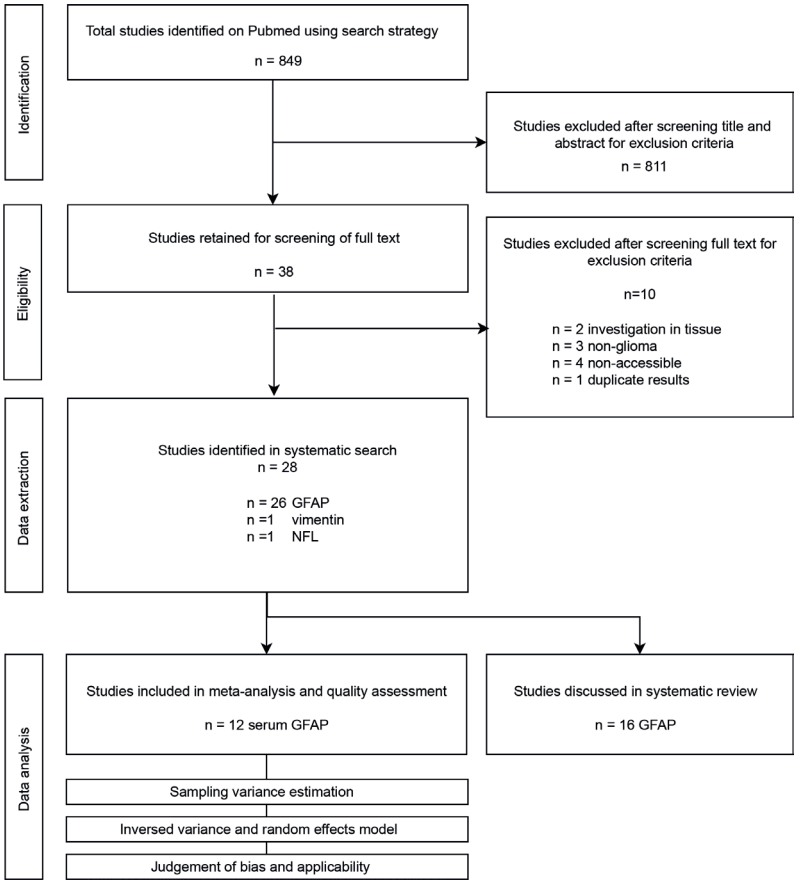

Figure 1. Preferred Reporting Items for Systematic Reviews and Meta-Analyses (PRISMA) diagram of included studies.

The majority of the identified studies reported on soluble GFAP protein levels in serum of glioma patients of different grades. The studies reporting on this outcome-measure were used for a meta-analysis. Other reported measures identified during the systematic search were on soluble GFAP levels in CSF, on numbers of GFAP positive tumour cells, immune cells, and extracellular vesicles, and on auto-antibodies against GFAP. The results of the studies not included in the meta-analysis are discussed per category.

Meta-analysis on GFAP levels in serum of glioma patients

Sixteen studies investigated the baseline levels of soluble serum GFAP (sGFAP) protein in the serum of glioma patients before treatment intervention, using antibody-based immunoassays. The reported outcome measures of twelve of these studies were used for a meta-analysis on sGFAP levels in different glioma grades and control group (Table 1). The remaining four studies categorised the patients differently by combining grade I/II and grade III/IV patients (Brommeland et al. 2007; Hepner et al. 2019; Shih et al. 2017; Urbanavičiūtė, Skauminas, and Skiriutė 2020) and were therefore not included in the meta-analysis, but will be discussed separately. The details on the control populations used in every study included in the meta-analysis are listed in Supp. Table 2.

First, we meta-analysed data on the percentage of subjects with detectable levels of GFAP in their serum in glioma patient and control groups, as reported by the twelve studies. Within the individual studies, a subject was considered positive for sGFAP (sGFAP$^+$) when the levels of sGFAP exceeded the lower limit of detection (LLOD) of the assay used, as determined by the authors and specified in Supp. Table 3. When combining all studies, the percentage of patients with detectable levels of sGFAP is 62.7% in grade IV glioma, in comparison to 12.7%, 17.2%, 10.7% and 15.1% in controls, grade I, grade II and grade III patients respectively (Fig. 2 and Supp. Table 4). The percentage sGFAP$^+$ grade IV patients showed large variation across studies, ranging from 29.1% (Gállego Pérez-Larraya et al. 2014) to 100% ((Husain et al. 2012), Fig 2B), although the latter study only included nine patients. sGFAP levels were detected using either the ElectroChemiLuminescence (ECL) technology from Roche (Husain et al. 2012; Baumgarten et al. 2018) or MesoScale Discovery (Lange et al. 2014), or the sandwich enzyme-linked sorbent assay (sELISA) from Biovendor (Kiviniemi et al. 2015; Ilhan-Mutlu et al. 2013; Jung et al. 2007; Lyubimova et al. 2020a; 2011a; van den Bossche et al. 2021; Vietheer et al. 2017) / Proteogenix (Gállego Pérez-Larraya et al. 2014). The single study that used the latter technique was also the study that reported the lowest percentage of sGFAP$^+$ grade IV patients. No large differences were however observed in percentage of sGFAP$^+$ subjects between studies that used the ECL methods versus the sELISA method from Biovendor. Most studies, regardless of the assay, used a LLOD within the range between 0.01 to 0.05 ng/mL to define a

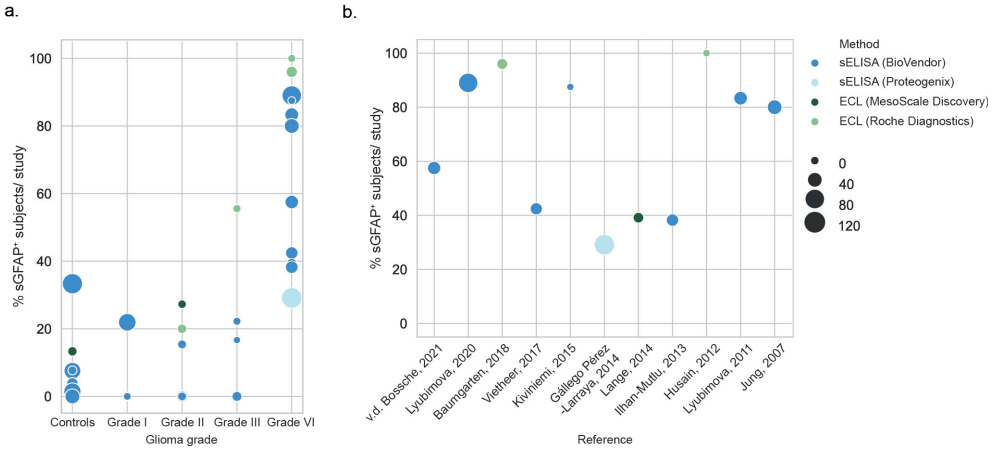

Figure 2. (a) A graphic overview of percentage of subjects with detectable levels of serum measured by different studies, grouped by glioma grade. (b) A graphic overview of percentage of grade IV patients positive for serum GFAP as measured by the individual studies. Size of the dot represents the number of grade IV patients included. Colours correspond to the method utilised in the study, of which the bright colours correspond to the studies included in the metadata analysis. Abbreviations: ECL = electrochemiluminescence; sELISA = sandwich Enzyme-Linked Immuno Sorbent Assay.

serum sample positive or negative for GFAP, with the exception of four studies (Supp. Table 3 van den Bossche et al. 2020; Lyubimova et al. 2011b; 2020b; Lange et al. 2014).

Next, we investigated the concentrations of soluble GFAP in the serum of glioma patients and controls by meta-analysing the mean/median sGFAP values reported by the different studies (Table 1, Supp. Table 5). When the mean/ median sGFAP levels were not reported, we extracted individual datapoints from the graphs to calculate the median sGFAP concentration for that study (Lange et al. 2014; van den Bossche et al. 2020). Assuming that GFAP is normally not present in serum, we first tested within the separate groups whether the basal sGFAP levels were significantly different from zero. The average estimated median of sGFAP levels were not significantly different from zero in healthy controls and grade I-III patients (0.00 ng/mL (0.00 – 0.00), Supp. Fig. 1 – 3), however a significant elevation was found in patients with glioma grade IV (0.12 ng/mL (0.06 – 0.18), $P < 0.001$, Fig 3a). Next, we determined the estimated median differences of sGFAP levels between the different groups by only including studies where sGFAP levels were directly compared. When directly comparing the sGFAP levels of grade IV patients to the levels of sGFAP in controls, an average median difference of 0.15 ng/mL (0.04 – 0.25, $P < 0.01$) was found (Fig. 3b). This significant difference was also apparent when comparing sGFAP of grade IV patients to grade III (0.10 ng/mL (0.02 – 0.19), $P < 0.05$), grade II (0.09 ng/mL (0.01 – 0.17), $P < 0.05$), and grade I (0.19 ng/mL (0.03 – 0.35), $P < 0.05$) (Supp. Fig. 4 - 6). However, no significant difference in sGFAP levels were found when comparing grade III to grade II, to grade I, or to con-

Table 1. An overview of studies quantifying GFAP protein levels in serum of grade IV patients and controls.*

Reference	Method	LLOD [ng/mL]	Reported values	GFAP [ng/mL] – Grade IV	n	sGFAP [ng/mL] – Controls	n
Van den Bossche et al (2020)	sandwich ELISA (BioVendor)	NA	Individual values	0.021 (0 – 0.84)	40	NA	NA
Lyubimova et al. (2020)	sandwich ELISA (BioVendor)	0.08	Median (IQR)	0.38 (0.14 - 1.28)	91	0.0 (0.0-0.0)	66
Baumgarten et al. (2018)	ECL (Elecsys® GFAP prototype test, Roche diagnostics)	0.05	All	0.16 (0 - 0.593) 0.18 (0.13)	25	NA	NA
Vietheer et al. (2017)	sandwich ELISA (BioVendor)	0.04	Median (IQR)	0.00 (0.00 - 0.22)	33	NA	NA
Tichy et al. (2016)	ECL (Elecsys® GFAP prototype test, Roche diagnostics)	0.05	Mean (SD)	0.23 (0.34)	33	NA	NA
Kiviniemi et al. (2015)	sandwich ELISA (BioVendor)	0.014	All	0.076 (0 – 0.387) 0.11 (0.12)	8	NA	NA
Gállego Pérez-Larraya et al. (2014)	sandwich ELISA (Proteogenix)	0.02	Mean (SD)	0.17 (0.53)	111	0.01 (0.02)	99
Lange et al. (2014)	ECL (MesoScale Discovery)	0.0156	Individual values	0.086 (0.0047-0.317)	21	0.086 (0.0047-0.317)	15
Ilhan-Mutlu et al. (2013)	sandwich ELISA (BioVendor)	0.03	Median (range)	0 (0 - 6.3)	34	0 (0 - 0.13)	26
Husain et al. (2012)	ECL (MesoScale Discovery)	0.04	All	0.09 (0.07 - 0.15) 0.10 (0.03)	9	NA	NA
Lyubimova et al. (2011)	sandwich ELISA (BioVendor)	0.1	Median (range)	0.212 (0.12 - 8.89)	42	0 (0 - 0.112)	69
Jung et al. (2007)	sandwich ELISA (BioVendor)	0.012	Median (range)	0.18 (0 –5.6)	50	0 (0 – 0)	50

*If all values were reported, both the median (range) and the mean (SD) are described. When individual data-points were reported, the data was extracted and the median (range) was calculated. Abbreviations: LLOD = lower limit of detection; n = number of subjects; NA = not available.

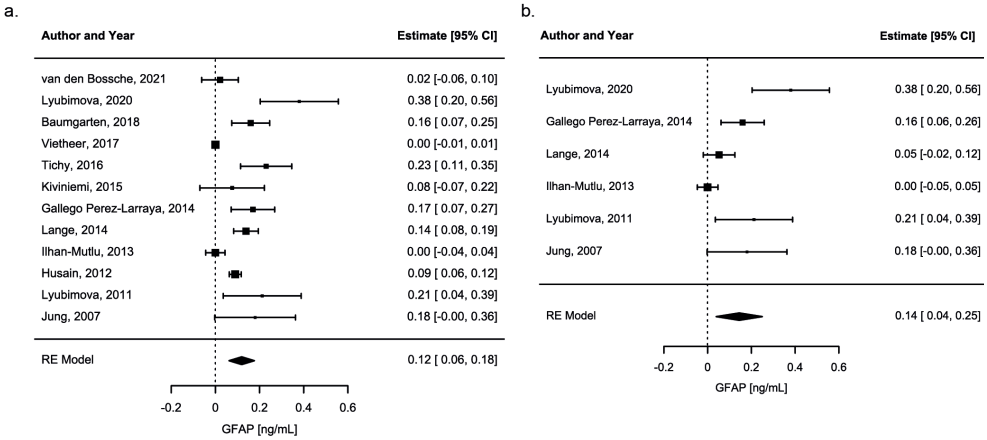

Figure 3. (a) A forest plot of average estimated median ($p < 0.0001$) GFAP levels in serum of grade IV patients, measured with sELISA or ECL, as meta-analysed with inverse variance and a random-effects model. Heterogeneity measures: tau2 = 0.0077; I2 = 93.33%. Squares indicate the observed outcome from individual studies and horizontal lines indicate its 95% confidence interval. The size of the square corresponds to the relative weight assigned in the pooled analysis using the random-effects model. The diamond at the bottom of the figure indicates the pooled median with 95% CI. (b) A forest plot of average estimated median difference ($p < 0.0001$) of sGFAP levels between grade IV patients and the control group as meta-analysed with inverse variance and a random-effects model. Heterogeneity measures: tau2 = 0.0132; I2 = 84.73%. Squares indicate the median difference between grade IV patients and controls from individual studies and horizontal lines indicate its 95% confidence interval. The size of the square corresponds to the relative weight assigned in the pooled analysis using the random-effects model. The diamond at the bottom of the figure indicates the pooled median difference with 95% CI.

trols (Supp. Fig. 7 - 10). Some studies compared the sGFAP levels of glioma patients to patients with brain metastases. Since our search did not focus on this patient group, we summarised these findings in Supp. Table 4, but did not include the brain metastasis group in the quantitative analysis.

Judgement of Bias and Applicability

Quality assessment of meta-analysed papers by the QUADAS-2 tool revealed that all studies were at risk of bias to some degree, mostly due to a lack of information about whether the results were interpreted without knowledge about the reference standard and vice versa (Supp. Table 6). Furthermore, not all controls were age- and sex-matched (Supp. Table 2). The funnel plot of the analysis showed qualitatively moderate asymmetry and thus moderate publication bias, which was further strengthened by the significant regression test for funnel plot asymmetry (Supp. Fig. 11).

Sensitivity and specificity analysis

Following the results of our meta-analysis, we conducted sensitivity and specificity analyses to determine the validity of sGFAP as a biomarker for grade IV glioma (Fig. 4a and 4b). The estimated sensitivity was between 29% and 89% for sGFAP levels for grade IV glioma compared to controls, while the specificity was relatively high (varying between 67% and 99%). SROC analysis showed an AUC of 0.885, but showed a wide range of variety (Fig. 4c) (Mandrekar 2010). This analysis was limited due to a small study sample.

Additional analyses of sGFAP

In addition to the studies included in the meta-analysis, four additional studies reported on sGFAP measurements in glioma using different conditions or groups. Brommeland and colleagues investigated the baseline levels of sGFAP in grade III and grade IV glioma combined and detected sGFAP in 16 out of 31 patients, with a mean of 239 ng/L (range 30 – 1210 ng/L). The authors described a tendency towards lower GFAP concentrations in grade III (87.5 ng/L) in comparison to grade IV (262 ng/L) patients, but information about the range of these measurements is lacking (Brommeland et al. 2007). Both Shih et al. and Urbanaviciute et al. compared sGFAP levels in grade I/II patients and grade III/IV patients combined. Both studies did not find a significant difference in sGFAP levels between the high- and low grade groups (Shih et al. 2017; Urbanavičiūtė, Skauminas, and Skiriutė 2020) or between glioma patients and controls (Urbanavičiūtė, Skauminas, and Skiriutė 2020). In the study by Shih and colleagues the

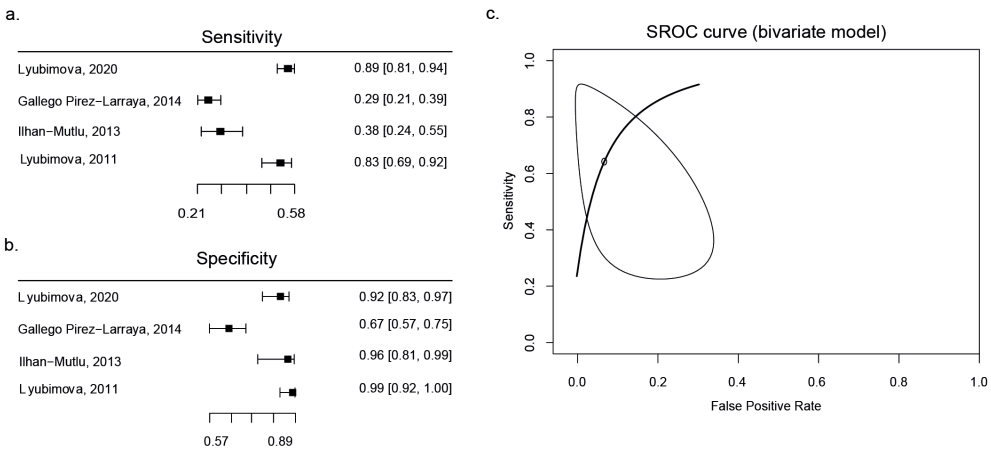

Figure 4. Forest plots of calculated sensitivity (a) and specificity (b) based on reported numbers of grade IV glioma and controls. Only studies with similar thresholds are shown. SROC curve (c) has been fitted using the bivariate model of Reitsma et al. as a linear mixed model with known variances of the random effects (Reitsma et al. 2005). An AUC of 0.885 was calculated.

mean level of sGFAP was even higher in the low grade glioma group (n=54, 0.281 +/- 0.522 ng/L) compared to the high grade group (n=20, 0.145 +/- 0.354 ng/L, Shih et al. 2017). Hepner and colleagues divided central nervous system (CNS) tumour patients into progressive- and stable disease groups, with high- and low grade gliomas but also other CNS tumours included in both categories. Higher levels of sGFAP were measured in both progressive- and stable disease groups in comparison to control samples (Hepner et al. 2019).

sGFAP association with patient outcome, treatment response and tumour characteristics

In addition to baseline sGFAP measurements, many studies investigated whether sGFAP levels correlate with patient outcome, treatment response and/or tumour characteristics, as summarised in Table 2. A clear correlation between sGFAP levels and overall survival (OS) and progression free survival (PFS) is lacking. Some studies report no association between sGFAP levels and OS or PFS (Shih et al. 2017; Gállego Pérez-Larraya et al. 2014; Vietheer et al. 2017). However, detection or an increase of sGFAP has also been linked to a less favourable outcome (Kiviniemi et al. 2015; Lyubimova et al. 2020a), as well as a (trend towards) more (Urbanavičiūtė, Skauminas, and Skiriutė 2020; Ilhan-Mutlu et al. 2013) favourable outcome of grade IV glioma patients. Of the studies that investigated treatment response, Baumgarten et al., Kiviniemi et al. and Husain et al. showed a significant increase of sGFAP in grade IV patients in the week after surgery (Husain et al. 2012; Baumgarten et al. 2018; Kiviniemi et al. 2015). However, Vietheer et al. showed decreased sGFAP levels in grade IV glioma patients 6-12 weeks after the surgery (Vietheer et al. 2017). There is thus a contrast between short-term effects and long-term effects of treatment of grade IV glioma on sGFAP levels.

sGFAP levels appear to be affected by the growth dynamics of the tumour, as studies showed that sGFAP correlates to tumour volume (Gállego Pérez-Larraya et al. 2014; Kiviniemi et al. 2015; Jung et al. 2007; Lyubimova et al. 2020a; Tichy et al. 2015), necrotic tumour volume (Kiviniemi et al. 2015), number of necrotic cells (Jung et al. 2007), and to the Ki67 proliferative index (Kiviniemi et al. 2015). A correlation between tumour volume and sGFAP levels was however not confirmed by others (Ilhan-Mutlu et al. 2013; Vietheer et al. 2017). The relation between tumour tissue GFAP expression and sGFAP levels is not clear, with one study describing higher levels of intratumoral GFAP in the patients with the highest sGFAP levels (Tichy et al. 2015), and two studies finding no correlation between the two measures (Kiviniemi et al. 2015; Jung et al. 2007).

The WHO glioma classification of 2016 includes IDH-1 genotyping, in which an IDH-1 mutation in the tumour tissue is associated with a better prognosis (Louis

Table 2. Overview of survival analyses and other correlations.*

Reference	Method	Association with survival?	Other correlations
Urbanaviciute et al. (2020)	sandwich ELISA (R&D systems)	Detection of sGFAP is not associated with OS in all glioma (p=0.3808, log-rank test, follow-up unknown), but is associated to favourable OS (p=0.0153) in grade IV patients	NA
Lyubimova et al. (2020)	sandwich ELISA (BioVendor)	sGFAP >0.2 ng/mL is associated to poor OS (p=0.028; log-rank test, follow-up at least five years).	A 'direct significant relationship of medium strength' between sGFAP and tumour volume (Spearman's test, data not shown). No correlations to tumour location in the brain (data not shown);
Vietheer et al. (2017)	sandwich ELISA (BioVendor)	sGFAP is not associated with OS or PFS (multivariate regression analysis, 78 weeks follow-up)	No correlation between tumour volume and sGFAP observed (Spearman rho = 0.048, p = 0.790).
Shih et al. (2017)	sandwich ELISA (BioVendor)	sGFAP is not associated with PFS (p = 0.653) or OS (p = 0.985; univariate analysis, follow-up at least 750 days).	NA
Tichy et al. (2016)	ECL (Elecsys® GFAP prototype test, Roche diagnostics)	NA	Significant correlation between grade IV tumour volume and sGFAP levels (Spearman rank R = 0.586, p=001).
Kiviniemi et al. (2015)	sandwich ELISA (BioVendor)	sGFAP > 0.014 ng/mL is associated to poor PFS in patients with primary high-grade glioma compared to patients with sGFAP ≤ 0.014 ng/ml (p = 0.008; log-rank test, 30 months follow-up).	Pre-operative sGFAP values significantly correlated to enhancing tumour volume and necrotic tumour volume in MRI-T1-Gad (r = 0.64; P = 0.005 and r = 0.73; P = 0.001, respectively). No correlation between tumour GFAP detected by IHC and sGFAP levels (p=0.761)
Gállego Pérez-Larraya et al. (2014)	sandwich ELISA (Proteogenix)	sGFAP > 0.5 ng/mL is not associated with OS or PFS (one-dimensional Cox model, 50 months follow up)	NA
Ilhan-Mutlu et al. (2013)	sandwich ELISA (BioVendor)	sGFAP is not associated with OS, but there is a trend towards more favourable OS of grade IV patients with detectable sGFAP as compared to patients without detectable sGFAP (log-rank test = 0.18, follow-up at least 40 months)	No correlation between neuroradiological characteristics and sGFAP observed
Jung et al. (2007)	sandwich ELISA (BioVendor)	NA	Significant correlation between tumour volume and sGFAP (Spearman Rho, CC=0.47; p<0.001) and necrotic volume and sGFAP levels (CC=0.49, p=0.004). No correlation between sGFAP and tissue GFAP expression
Brommeland et al. (2007)	sandwich ELISA	NA	GFAP > 150 ng/L and tumour size > 20 cm3 significantly associated (Multivariate linear regression, P < 0.0001, Spearman = 0.67).

* Whenever stated in the original research article, the applied statistical test and follow-up period was defined in brackets. Abbreviations: ELISA = Enzyme-Linked Immuno Sorbent Assay; PFS = progression free survival; OS = overall survival; NA = not available.

et al. 2016; Verhaak et al. 2010). In this meta-analysis, three reports incorporated this classification. Both Kiviniemi et al. and Vietheer et al. measured higher sGFAP levels in glioma grade IV patients with IDH-1 wildtype (IDHwt) status, compared to glioma grade IV with a IDH-1 mutation (IDHmut) (Kiviniemi et al. 2015; Vietheer et al. 2017). Urbanaviciute et al. however did not detect differences between the IDHwt and IDHmut groups (Urbanavičiūtė, Skauminas, and Skiriutė 2020). At last, Tichy and colleagues found higher rates of MGMT promotor methylation in patients with high sGFAP levels, but this correlation was not found by Kiviniemi et al (Kiviniemi et al. 2015; Tichy et al. 2015). Further molecular characterisation of the sGFAP positive and negative populations remains an important topic for further research.

GFAP protein levels in CSF of glioma patients

Three studies measured the levels of soluble GFAP in CSF (cGFAP) of glioma patients. Using radioimmunoassays, Syzmas et al. showed that the levels of cGFAP were elevated (range 4 - 50 µg/mL) in 5 patients with gliomas (of which 2 were grade IV glioma). In this study, no cGFAP levels above 3 µg/mL were detected in the non-glial tumour control group (Szymaś, Morkowski, and Tokarz 1986). Hayakawa et al. analysed the CSF of twelve grade IV glioma patients using a similar technique, and detected cGFAP levels above 25 ng/mL in eight patients, with cGFAP levels even reaching values above 500 ng/mL in three samples. Elevated cGFAP levels were detected in two out of ten astrocytoma patients and in none of the two oligodendroglioma patients or eight controls (Hayakawa et al. 1980). Both studies noted a large increase in cGFAP levels within the first days after surgery, followed by a gradual decrease (Szymaś, Morkowski, and Tokarz 1986; Hayakawa et al. 1980). Recently, GFAP was also detected in a proteomic screen on CSF samples of glioma patient. Although the overall abundance of the GFAP protein was low, in a small subset of patients the levels surpassed the threshold based on maximum levels measured in control samples. Interestingly, the cGFAP high patients had large, enhancing tumours with direct contact to the ventricles, indicating that tumour location plays a role in cGFAP levels. However, this MRI pattern was also observed in patients with low cGFAP levels. Since the calculated sensitivity levels of cGFAP as a marker for grade IV were low (25.45%), Schmid et al concluded that cGFAP does not appear to be a stable marker for all grade IV patients, nevertheless it may be clinically relevant for follow-up studies in patients with high levels (Schmid et al. 2021).

GFAP protein in extracellular vesicles and circulating cells

Previous studies have not only focused on soluble GFAP levels in serum and CSF of glioma patients, but also on the presence of GFAP in extracellular vesicles (EVs) and

circulating cells, as summarised in Table 3. EVs are membrane vesicles that are secreted by cells, including tumour cells, and contain proteins, RNAs and lipids. Larger EVs in the range of 100 to 1000 nm are termed microparticles, whereas vesicles smaller than 100 nm can be referred to as exosomes (Kao and Papoutsakis 2019). Blood samples of grade IV patients contained higher numbers of both GFAP positive microparticles and exosomes in comparison to control samples (Galbo et al. 2017; Lewis et al. 2019; Sartori et al. 2013), or higher levels of GFAP within EVs (Lewis et al. 2019). In addition to baseline differences, the number $GFAP^+$ microparticles increase upon surgical resection and show the highest numbers seven months after surgery (Sartori et al. 2013). Two of the three studies did not use permeabilisation steps in their sample preparation, indicating that the identified GFAP is expressed on the surface of the EVs and can potentially also be picked up by the sELISA and ECL studies described in the earlier meta-analysis. With exception of a single grade III patient that was included in the exosome study (Galbo et al. 2017), $GFAP^+$ EV levels have not been measured in grade II/III, therefore no conclusions can be drawn about the specificity of increased $GFAP^+$ EV levels for grade IV glioma.

In addition to EVs, also cells in the circulation of glioma patients are more frequently GFAP positive. Müller and colleagues detected $GFAP^+$ non-haematopoietic ($CD45^-$) cells in 20.6% of blood samples of grade IV glioma patients, whereas only a single blood sample contained GFAP positive cells in their control population. The authors found no significant difference between patients with primary and recurrent GBM tumours, nor was the presence of GFAP positive cells linked to overall survival. GFAP positive cells were however more frequently present in blood samples of patients with EGFR gene amplifications (Müller et al. 2014). A recent study performed by van den Bossche and colleagues found that the percentage of GFAP positive $CD16^+$ monocytes are indicative of brain tumours. Increased populations of these cells were found in blood samples of diffuse astrocytomas, oligodendrogliomas, grade IV gliomas and metastasis patients. The levels of $GFAP^+$ monocytes were directly compared to soluble sGFAP levels, but no correlation was found. Within grade IV patients, abundance of GFAP carrying monocytes correlated to tumour volume and was associated with shorter OS. The authors conclude that levels of $GFAP^+$ $CD16^+$ monocytes cannot be used to distinguish between different glioma grades, but have high sensitivity to detect brain lesions in general (van den Bossche et al. 2021).

GFAP auto-antibodies and miscellaneous measurements

In addition to GFAP protein measurements in body fluids, also GFAP auto-antibodies have been a focus of research. Ludwig et al. performed a serum auto-antibody screen against a peptide library and GFAP was identified as an informative antigen to

Table 3. Overview of GFAP measurements in extracellular vesicles and cells

Reference	Target	Method	GFAP antibody	Result
Sartori et al. (2013)	Microparticles	Flow cytometry: gating on particle size and annexin V positivity Detection of surface GFAP	Rabbit pc (DakoCytomation, Glostrup, Denmark)	Higher # of $GFAP^+$ and $GFAP^-$ MPs in grade IV glioma patients (n=61) compared to controls (n=20) Significant increase in $GFAP^-$ and $GFAP^+$ MPs 7 days to 7 months after surgery, greatest increase in GFAP+ MPs after 7 months.
Galbo et al. (2017)	Exosomes	Exosome isolation by ultracentrifugation Flow cytometry: gating on CD9-positivity Detection of surface GFAP	Mouse mc conjugated to AF488 (Biolegend, San Diego, CA)	Higher % of $GFAP^+$ exosomes in recurrent grade IV glioma patients (22.8%, n=8) compared to controls (2.9%, n=3)
Lewis et al. (2019)	Extracellular vesicles	EV isolation by single-step dielectrophoretic (DEP) separation Intravesicular GFAP labelling and quantification of IFI	Mouse mc conjugated to AF488 (BD Pharmingen)	IFI higher in 65% of grade IV glioma patients (n=17) compared to max intensity observed in controls (n=23) Sensitivity: 93%, Specificity: 38%, AUC: 0.65 (based on 15 grade IV patients and 8 controls)
Müller et al. (2014)	Circulating tumour cells (CTCs)	Centrifugation of cells on glass slides CD45 and GFAP labelling to identify $CD45^-$ CTCs	Rabbit pc (Dako, Glostrup, Denmark)	Higher % of $GFAP^+$ CTCs in blood of primary and recurrent GBM patients (20.6%, n=141) compared to controls (noncancer controls and brain metastasis patients, 3.7%, n=27). No correlation with overall survival. Higher % of $GFAP^+$ CTCs in tumours with EGFR amplification (28.6%, n=70) versus no amplification (14.1%, n=71)
Van den Bossche et al. (2020)	Monocytes	Flow cytometry: gating on FSC-area, SSC, HLA-DR, CD300e, CD14 and CD16 Detection of intracellular GFAP	Rabbit pc (Dako, Glostrup, Denmark)	Higher % of $GFAP^+$ $CD16^+$ monocytes in dif.astr. (n=28), oligod.g (n=32), grade IV glioma (n=145), and metastasis (n=21) patients compared to controls (n=38). Cut-off value of 0.6% $GFAP^+CD16^+$ monocytes gives sensitivity of 81%, specificity of 85%, AUC of 87% for detection any brain tumour. Grade IV patients with >20% $GFAP^+CD16^+CD14^-$ monocytes associated with decreased OS

Abbreviations: AUC= area under the curve, CTC = circulating tumour cells, dif. astr.= diffuse astrocytoma, FSC = forward scatter, HLA-DR = human leukocyte antigen complex, IFI= immunofluorescent intensity, mc= monoclonal, MP = microparticles, oligod.g = oligodendroglioma, OS= overall survival, pc

discriminate between serum of grade IV gliomas and that of controls (Ludwig et al. 2009). Auto-antibodies against GFAP were also identified in a two-dimensional western blot screen performed by Wei and colleagues, where antibodies against GFAP were detected in 5 out 20 patients. Upon further validation within a larger patient population using ELISA, the authors found a significant correlation between tumour grade and GFAP autoantibody levels. GFAP auto-antibodies were significantly elevated in grade III and grade IV sera respective of control samples, and correlated with tumour volume (Wei et al. 2013). Two additional studies on GFAP auto-antibodies showed mixed results. Koszewicz et al. failed to detect GFAP auto-antibodies in a group of 15 grade IV patients, but did detect GFAP reactivity in one of the eight grade II/III glioma patients (Koszewicz et al. 2016). Ruutiainen et al. on the other hand did detect elevated GFAP auto-antibodies in both CSF and serum of patients with brain tumours in comparison to the control group (Ruutiainen et al. 1981).

Discussion

In this systematic review, we investigated whether GFAP in body fluids can be used as a marker for (high grade) glioma. The majority of the identified studies reported on GFAP protein levels in serum (Fig. 2). In all antibody-based immunoassay studies combined, 62.7% of all grade IV glioma patients had detectable levels of GFAP in serum , with a median basal level of 0.12 ng/mL (0.06 – 0.18), compared to 12.7% of healthy controls with a median basal level of 0.00 ng/mL (0.00 – 0.00) (Fig. 2). Overall, higher sGFAP is associated with grade IV glioma and not with lower grades (Fig. 3, Supp. Fig. 1-3), and a similar trend is observed for soluble GFAP in CSF. The sGFAP level is not clearly related to patient prognosis of grade IV patients, but there is evidence for a correlation to tumour volume (Table 2). In addition to soluble GFAP levels in body fluids, multiple studies link grade IV glioma to increased levels of GFAP positive cells, EVs, and auto-antibodies against GFAP (van den Bossche et al. 2021; Galbo et al. 2017; Müller et al. 2014; Lewis et al. 2019; Sartori et al. 2013).

Quality assessment of meta-analysed papers showed that almost all studies were risk for bias, mostly because authors did not state whether the sGFAP results were interpreted without knowledge of the results of the reference standard, and vice versa (Supp. Table 6). It is however unlikely that the histopathological diagnosis of glioma samples were determined with prior knowledge about the level of sGFAP. However, whenever this was not explicitly stated, we had to give an 'unclear' assessment. It was difficult to obtain evidence for sGFAP levels in lower grade glioma. This is probably due to the fact that lower grade glioma has a lower prevalence in the population.

The funnel plot of sGFAP in grade IV glioma showed several studies outside of the 95% C.I., which revealed the high heterogeneity we have encountered between

studies (Supp. Fig. 11). One source of heterogeneity could be the different commercial kits that were used to determine the sGFAP levels. Also the fact that studies use different LLODs to determine sGFAP positive and negative samples is a likely source of heterogeneity and a limitation of the meta-analysis. Although most studies used LLODs within a similar range, not every study explicitly stated how the LLOD was determined, and whether values below the LLOD were defined as 0 or were taken along as originally measured (Supp. Table 3). Other factors likely to contribute to the variability between studies are the heterogeneity of the patient population, the relatively small number of patients included in each study, and the small number of studies in general. The limited number of studies is also reflected in the sensitivity and specificity outcomes. Although the high specificity indicates that an elevation of sGFAP discriminates grade IV patients from other glioma patients and controls, the sensitivity is limited. In addition, the wide range of the SROC curve (Fig. 4C) highlights that more studies are needed to conclusively determine sensitivity and specificity. For example, both Ilhan-Mutlu et al. and Vietheer et al. showed a zero median sGFAP level in grade IV glioma patients, illustrating the large variability in sGFAP levels within the group of GBM patients (Table 1). Further investigation into sGFAP positive- and negative subgroups of GBM patients is needed to determine the diagnostic value of sGFAP. So far, only three studies determined sGFAP in subgroups of patients classified according to WHO 2016 (Urbanavičiūtė, Skauminas, and Skiriutė 2020; Vietheer et al. 2017; Kiviniemi et al. 2015), and two of these studies showed that higher sGFAP levels are mainly associated with IDHwt tumours (Kiviniemi et al. 2015; Vietheer et al. 2017). Integration of additional genetic markers into sGFAP analysis may link the presence of sGFAP to specific molecular subgroups of GBM patients.

Although our meta-analysis shows that the presence of sGFAP is linked to grade IV glioma, the fact that not all grade IV patients have sGFAP and that sGFAP is occasionally detected in controls without malignancies makes the usefulness of sGFAP as a biomarker currently uncertain. Large prospective studies will have to determine the sensitivity and specificity of this tool. One clinical challenge in which the utility of sGFAP has not been tested yet, is in the differentiation between high-grade and low-grade non-enhancing tumours. The lack of contrast enhancement, associated with preservation of blood-brain barrier (BBB) integrity, is typically associated with low grade tumours. Nevertheless, in 30-40% of the cases non-enhancing gliomas are in fact grade IV tumours, which can lead to an underestimation of the aggressiveness of the tumour and delay in proper diagnosis and treatment (Hu et al. 2020). When sGFAP levels are elevated in grade IV irrespective of BBB permeability, sGFAP has the potential to help in the diagnosis of these hidden grade IV cases. An additional focus should be to monitor sGFAP levels within the sGFAP positive group over the progression of the disease and in response to different treatment regimes. This may help in determining

whether sGFAP levels can be used to monitor therapeutic response or can contribute to the distinction between progression and pseudo-progression.

GFAP is regulated by alternative splicing and the ratio between tissue expression levels of two splice variants, GFAPα and δ, correlates to glioma grade (Middeldorp and Hol 2011; Hol and Pekny 2015; Stassen et al. 2017; van Bodegraven et al. 2019b). An interesting future strategy is to measure the different GFAP isoforms in serum of grade IV glioma patients. The binding site of the anti-GFAP antibodies used to detect sGFAP could not be retrieved for all studies, but in the most widely used sELISA kit from BioVendor, the antibody is raised against an epitope in the coil 2B of the rod region of GFAP (AA 312-340) and therefore will pick up several different GFAP isoforms, including GFAPα and GFAPδ. Although measurements of the isoforms separately will not aid in improving the sensitivity issue of sGFAP as a biomarker, measurements of the GFAP isoforms in serum may help in predicting progression-free and overall survival.

Additional studies identified during this systematic review show that not only soluble GFAP levels are altered in grade IV patients, but also the levels of GFAP positive EVs and cells (Table 3). Since GFAP is a cytosolic protein, the fact that two studies detected GFAP on the surface of exosomes and microparticles is surprising. Surface expression of an IF protein is however not unique for GFAP, as surface vimentin has gained recent attention in respect to circulating gastric cancer cells (Liu et al. 2020), and viral infections (Ramos et al. 2020). EVs play an important role in tumour cell communication and progression (Becker et al. 2016), therefore further investigation into the source and function of GFAP positive EVs is an interesting focus of research. Since the studies focussing on GFAP in EVs did not include lower grade glioma patients, it is unknown whether GFAP positive EVs are specific for grade IV patients or all glioma patients. In the case of GFAP positive monocytes however, increased levels were not associated with any specific glioma grade, but were rather a sign of brain damage in general (van den Bossche et al. 2021).

This systematic review was initially set-up to investigate the presence of all IF proteins in body fluids of glioma patients, but apart from studies on GFAP, studies on other IFs in body fluids of glioma patients are scarce. Heppner et al. measured the levels of serum neurofilament light (NFl) in patients with progressive and stable brain tumours and found increased levels of NFl levels in patients with progressive CNS tumours (Hepner et al. 2019). In addition, Ludwig et al. identified auto-antibodies against vimentin in the serum of glioma patients of different grades (Ludwig et al. 2009). At last, vimentin was one of the upregulated proteins identified during a proteomic screen on CSF samples of grade IV glioma patients (Schmid et al. 2021). Particularly IF proteins vimentin and nestin are interesting targets to further test as glioma biomarkers, as expression levels of these proteins negatively correlate with progression-free and

overall survival in glioma (Lin et al. 2016; Lv et al. 2017; Wu et al. 2015; Zhao et al. 2018).

To conclude, this systematic review and meta-analysis shows that the presence of sGFAP is indicative of grade IV glioma, but the relative low sensitivity currently limits the usefulness as a biomarker for initial diagnosis. Additional studies are needed to determine the whether sGFAP can be detected in high grade gliomas without contrast enhancements, whether sGFAP monitoring is relevant during disease progression, and to determine the potential of GFAP isoforms and other IF proteins in body fluids as biomarkers for (the follow-up of) grade IV glioma.

Materials and Methods

Systematic Review

Collection of all biomedical literature on measurements of IFs in body fluids (serum, cerebral spinal fluid [CSF], urine, saliva) of glioma patients was systematically performed according to the Preferred Reporting Items for Systematic Reviews and Meta-Analyses (PRISMA) guidelines (Moher et al. 2009). The PubMed database was screened on April 12th 2020 for publications on IFs, glioma, and body fluids using a search string with Medical Subject Headings (MeSH) and Title/Abstract filters as listed in Supp. Table 1. The same search string was used again on March 24th 2021. All articles were independently assessed by two researchers (DMF and JVA) via the online web-tool Rayyan (Qatar Computing Research Institute) (Ouzzani et al. 2016). Reviews were also examined to identify additional relevant studies.

Primary outcomes of interest included the number of patients with detectable IF levels in serum, CSF and/or other body fluids, and mean or median levels of IFs in the serum, CSF and/or other body fluids of primary, non-treated glioma patients separated per glioma malignancy grade, as documented by the World Health Organization (Louis et al. 2016). Detectable levels were defined as values that surpassed the lower limit of detection (LLOD) as specified by the authors of the paper (Supp. Table 3). Prespecified inclusion criteria resulted in the selection of all studies of patients with non-treated glioma (WHO Grade I, II, III, and IV) that reported on the appropriate outcome data. Exclusion criteria were: patient age <18 years, case reports, animal studies, non-English reports, articles not available in full text, in vitro studies, and studies that did not provide comparative data on outcomes of interest or otherwise did not meet inclusion criteria.

Data extraction

Data on primary glioma patients in which IF levels in body fluids were determined, were used. Data for any outcome of interest was extracted from the text of included

studies. When the outcome measures were not reported in the text, the data points were extracted from the graphs using https://automeris.io/WebPlotDigitizer (Rohatgi 2020).

Meta-Analysis and Judgement of Bias and Applicability

The extracted data on GFAP protein levels in serum (sGFAP) of glioma patients separated by grade and in controls were further used for a meta-analysis. The 'quantile estimation' model by McGrath et al. (McGrath et al. 2020) was applied in RStudio (version 1.2.5042) (R Foundation for Statistical Computing, Vienna) (R Core Team 2013) and the outcome was subsequently applied in the metaphor package (Viechtbauer 2010). In brief, the sampling variance of effect sizes was estimated for all studies and meta-analysed using the inversed variance method and the random-effects model. The outcome measure was the average estimate of the median for sGFAP levels within glioma grades or controls and the average estimate of the difference of the median for sGFAP level differences between glioma grades and/or controls. Significance was defined as $P \leq 0.05$ with a 95% confidence interval, and was determined for each estimated median either to be significantly different than zero or significantly different between groups. Heterogeneity was assessed with the tau2 statistic (estimated variance of true effects) and the I2 statistic (percentage of variation across studies) with the aforementioned metaphor package. Robustness of results was judged with the QUADAS-2 tool, which consists of four domains concerning risk of bias and applicability to which a label of 'low risk', 'high risk', or 'unknown' was assigned for every included study by DMF and JVA (Whiting et al. 2011). Disagreement between the two investigators or lack of information resulted in an 'unknown' assessment. The funnel plot of the results and subsequent regression test for funnel plot asymmetry were generated using the metaphor package for RStudio (Viechtbauer 2010). Forest plots of sensitivity and specificity and SROC curves were plotted with the mada package for RStudio (Doebler and Holling 2015). Graphics were made with the ggplot2 package for RStudio and the Seaborn package in Jupyter notebook (Python) (Wickham 2016; Waskom et al. 2020).

Acknowledgments:

All authors reviewed and approved the manuscript before submission. We would like to thank Isabel Retel Helmrich for her valuable feedback concerning the data analysis. We would like to acknowledge the KWF for funding.

Author Contributions:

Conceptualisation, J.V.A, D.M.F, P.A.J.T.R and E.M.H.; methodology, D.M.F; formal analysis, D.M.F.; investigation, J.V.A and D.M.F; writing—original draft preparation,

J.V.A. and D.M.F; writing—review and editing, J.V.A., D.M.F, E.M.H and P.A.J.T.R; supervision, J.V.A., E.M.H. and P.A.J.T.R; funding acquisition, E.M.H. and P.A.J.T.R. All authors have read and agreed to the published version of the manuscript.

References

Aldape, Kenneth, Jeremy N Rich, Giles W Robinson, David H Rowitch, John H Sampson, Michael D Taylor, Paul Workman, and Richard J Gilbertson. 2019. "Statement Brain Tumours." *Nature Reviews Clinical Oncology* 16 (August). https://doi.org/10.1038/s41571-019-0177-5.

Baumgarten, Peter, Johanna Quick-Weller, Florian Gessler, Marlies Wagner, Julia Tichy, Marie Therese Forster, Christian Foerch, Volker Seifert, Michel Mittelbronn, and Christian Senft. 2018. "Pre- and Early Postoperative GFAP Serum Levels in Glioma and Brain Metastases." *Journal of Neuro-Oncology* 139 (3): 541–46. https://doi.org/10.1007/s11060-018-2898-1.

Becker, Annette, Basant Kumar Thakur, Joshua Mitchell Weiss, Han Sang Kim, Hector Peinado, and David Lyden. 2016. "Extracellular Vesicles in Cancer: Cell-to-Cell Mediators of Metastasis." *Cancer Cell* 30 (6): 836–48.

Bodegraven, Emma J. van, Jessy V. van Asperen, Pierre A.J. Robe, and Elly M. Hol. 2019. "Importance of GFAP Isoform-Specific Analyses in Astrocytoma." *Glia* 67 (8): 1417–33. https://doi.org/10.1002/glia.23594.

Bodegraven, Emma J. van, Jessy V. van Asperen, Jacqueline A. Sluijs, Coen B.J. van Deursen, Miriam E. van Strien, Oscar M.J.A. Stassen, Pierre A.J. Robe, and Elly M. Hol. 2019. "GFAP Alternative Splicing Regulates Glioma Cell-ECM Interaction in a DUSP4-Dependent Manner." *FASEB Journal : Official Publication of the Federation of American Societies for Experimental Biology* 33 (11): 12941–59. https://doi.org/10.1096/fj.201900916R.

Bossche, Wouter B L van den, Arnaud J P E Vincent, Cristina Teodosio, Jeroen Koets, Aladdin Taha, Anne Kleijn, Sandra de Bruin, et al. 2020. "Monocytes Carrying GFAP Detect Glioma, Brain Metastasis and Ischaemic Stroke, and Predict Glioblastoma Survival." *Brain Communications* 3 (1). https://doi.org/10.1093/braincomms/fcaa215.

Brommeland, T., L. Rosengren, S. Fridlund, R. Hennig, and V. Isaksen. 2007. "Serum Levels of Glial Fibrillary Acidic Protein Correlate to Tumour Volume of High-Grade Gliomas." *Acta Neurologica Scandinavica* 116 (6): 380–84. https://doi.org/10.1111/j.1600-0404.2007.00889.x.

Chung, Byung-min, Jeremy D Rotty, and Pierre A Coulombe. 2013. "Networking Galore : Intermediate Filaments and Cell Migration." *Current Opinion in Cell Biology* 25 (5): 600–612. https://doi.org/10.1016/j.ceb.2013.06.008.

Doebler, Philipp, and Heinz Holling. 2015. "Meta-Analysis of Diagnostic Accuracy with Mada." 2015. https://cran.r-project.org/package=mada.

Etienne-Manneville, Sandrine. 2018. "Cytoplasmic Intermediate Filaments in Cell Biology." *Annual Review of Cell and Developmental Biology* 34 (1): annurev-cellbio-100617-062534. https://doi.org/10.1146/annurev-cellbio-100617-062534.

Galbo, Phillip M., Michael J. Ciesielski, Sheila Figel, Orla Maguire, Jingxin Qiu, Laura Wiltsie, Hans Minderman, and Robert A. Fenstermaker. 2017. "Circulating CD9+/GFAP+/Survivin+ Exosomes in Malignant Glioma Patients Following Survivin Vaccination." *Oncotarget* 8 (70): 114722–35. https://doi.org/10.18632/oncotarget.21773.

Gállego Pérez-Larraya, Jaime, Sophie Paris, Ahmed Idbaih, Caroline Dehais, Florence Laigle-Donadey, Soledad Navarro, Laurent Capelle, et al. 2014. "Diagnostic and Prognostic Value of Preoperative Combined GFAP, IGFBP-2, and YKL-40 Plasma Levels in Patients with Glioblastoma." *Cancer* 120 (24): 3972–80. https://doi.org/10.1002/cncr.28949.

Hayakawa, T, K Morimoto, Y Ushio, T Mori, T Yoshimine, A Myoga, and H Mogami. 1980. "Levels of Astroprotein (an Astrocyte-Specific Cerebroprotein) in Cerebrospinal Fluid of Patients with Brain Tumors. An Attempt at Immunochemical Diagnosis of Gliomas." *Journal of Neurosurgery* 52 (2): 229–33. https://www.ncbi.nlm.nih.gov/pubmed/7351563.

Hepner, Adriana, Jason Porter, Felicia Hare, Syed Sameer Nasir, Henrik Zetterberg, Kaj Blennow, and Michael Gary Martin. 2019. "Serum Neurofilament Light, Glial Fibrillary Acidic Protein and Tau Are Possible Serum Biomarkers for Activity of Brain Metastases and Gliomas." *World Journal of Oncology* 10 (4–5): 169–75. https://doi.org/10.14740/wjon1228.

Hohmann, and Dehghani. 2019. "The Cytoskeleton- A Complex Interacting Meshwork." *Cells* 8 (4): 362. https://doi.org/10.3390/cells8040362.

Hol, Elly M., and Milos Pekny. 2015. "Glial Fibrillary Acidic Protein (GFAP) and the Astrocyte Intermediate Filament System in Diseases of the Central Nervous System." *Current Opinion in Cell Biology* 32: 121–30. https://doi.org/10.1016/j.ceb.2015.02.004.

Hu, Leland S, Andrea Hawkins-Daarud, Lujia Wang, Jing Li, and Kristin R Swanson. 2020. "Imaging of Intratumoral Heterogeneity in High-Grade Glioma." *Cancer Letters* 477: 97–106.

Husain, Hatim, William Savage, Stuart A Grossman, Xiaobu Ye, Peter C Burger, Allen Everett, Chetan Bettegowda, et al. 2012. "Pre- and Post-Operative Plasma Glial Fibrillary Acidic Protein Levels in Patients with Newly Diagnosed Gliomas." *Journal of Neuro-Oncology* 109 (1): 123–27. https://www.ncbi.nlm.nih.gov/pubmed/22492246.

Ilhan-Mutlu, Aysegul, Ludwig Wagner, Georg Widhalm, Adelheid Wöhrer, Sophie Bartsch, Thomas Czech, Harald Heinzl, et al. 2013. "Exploratory Investigation of Eight Circulating Plasma Markers in Brain Tumor Patients." *Neurosurgical Review* 36 (1): 45–56. https://doi.org/10.1007/s10143-012-0401-6.

Jung, C. S., C. Foerch, A. Schänzer, A. Heck, K. H. Plate, V. Seifert, H. Steinmetz, A. Raabe, and M. Sitzer. 2007. "Serum GFAP Is a Diagnostic Marker for Glioblastoma Multiforme." *Brain* 130 (12): 3336–41. https://doi.org/10.1093/brain/awm263.

Kao, Chen-Yuan, and Eleftherios T Papoutsakis. 2019. "Extracellular Vesicles: Exosomes, Microparticles, Their Parts, and Their Targets to Enable Their Biomanufacturing and Clinical Applications." *Current Opinion in Biotechnology* 60: 89–98.

Kiviniemi, Aida, Maria Gardberg, Janek Frantzén, Riitta Parkkola, Ville Vuorinen, Marko Pesola, and Heikki Minn. 2015. "Serum Levels of GFAP and EGFR in Primary and Recurrent High-Grade Gliomas: Correlation to Tumor Volume, Molecular Markers, and Progression-Free Survival." *Journal of Neuro-Oncology* 124 (2): 237–45. https://doi.org/10.1007/s11060-015-1829-7.

Koszewicz, Magdalena, Slawomir Michalak, Malgorzata Bilinska, Slawomir Budrewicz, Mikolaj Zaborowski, Krzysztof Slotwinski, Ryszard Podemski, and Maria Ejma. 2016. "Is Peripheral Paraneoplastic Neurological Syndrome Possible in Primary Brain Tumors?" *Brain and Behavior* 6 (6): e00465. https://www.ncbi.nlm.nih.gov/pubmed/27186442.

Lange, Ryan P., Allen Everett, Pratima Dulloor, Frederick K. Korley, Chetan Bettegowda, Cherie Blair, Stuart A. Grossman, and Matthias Holdhoff. 2014. "Evaluation of Eight Plasma Proteins as Candidate Blood-Based Biomarkers for Malignant Gliomas." *Cancer Investigation* 32 (8): 423–29. https://doi.org/10.3109/07357907.2014.933237.

Lewis, Jean, Ali A. Alattar, Johnny Akers, Bob S. Carter, Michael Heller, and Clark C. Chen. 2019. "A Pilot Proof-Of-Principle Analysis Demonstrating Dielectrophoresis (DEP) as a Glioblastoma Biomarker Platform." *Scientific Reports* 9 (1): 1–10. https://doi.org/10.1038/s41598-019-46311-8.

Lin, Lin, Guangzhi Wang, Jianguang Ming, Xiangqi Meng, Bo Han, Bo Sun, Jinquan Cai, and Chuanlu Jiang. 2016. "Analysis of Expression and Prognostic Significance of Vimentin and the Response to Temozolomide in Glioma Patients." *Tumor Biology* 37 (11): 15333–39. https://doi.org/10.1007/s13277-016-5462-7.

Liu, Mengyuan, Ruoyu Wang, Xuren Sun, Yuting Liu, Zhi Wang, Jin Yan, Xiangyu Kong, Shanshan Liang, Qiuge Liu, and Tong Zhao. 2020. "Prognostic Significance of PD-L1 Expression on Cell-surface Vimentin-positive Circulating Tumor Cells in Gastric Cancer Patients." *Molecular Oncology* 14 (4): 865–81.

Louis, David N., Arie Perry, Guido Reifenberger, Andreas von Deimling, Dominique Figarella-Branger, Webster K. Cavenee, Hiroko Ohgaki, Otmar D. Wiestler, Paul Kleihues, and David W. Ellison. 2016. "The 2016 World Health Organization Classification of Tumors of the Central Nervous System: A Summary." *Acta Neuropathologica* 131 (6): 803–20. https://doi.org/10.1007/s00401-016-1545-1.

Ludwig, Nicole, Andreas Keller, Sabrina Heisel, Petra Leidinger, Veronika Klein, Stefanie Rheinheimer, Claudia U Andres, et al. 2009. "Improving Seroreactivity-Based Detection of Glioma." *Neoplasia* 11 (12): 1383–89. https://doi.org/10.1593/neo.91018

Lv, Donglai, Lin Lu, Zongtao Hu, Zhenle Fei, Meiqin Liu, Lei Wei, and Jun Xu. 2017. "Nestin Expression Is Associated with Poor Clinicopathological Features and Prognosis in Glioma Patients: An Association Study and Meta-Analysis." *Molecular Neurobiology* 54 (1): 727–35. https://doi.org/10.1007/s12035-016-9689-5.

Lyubimova, N. V., Yu S. Timofeev, A. A. Mitrofanov, A. Kh Bekyashev, Z. A. Goncharova, and N. E. Kushlinskii. 2020a. "Glial Fibrillary Acidic Protein in the Diagnosis and Prognosis of Malignant Glial Tumors." *Bulletin of Experimental Biology and Medicine* 168 (4): 503–6. https://doi.org/10.1007/s10517-020-04741-9.

Lyubimova, N. V., M. G. Toms, E. E. Popova, Y. V. Bondarenko, V. B. Krat, and N. E. Kushlinskii. 2011a. "Neurospecific Proteins in the Serum of Patients with Brain Tumors." *Bulletin of Experimental Biology and Medicine* 150 (6): 732–34. https://doi.org/10.1007/s10517-011-1236-9.

Lyubimova, N V, Yu S Timofeev, A A Mitrofanov, A Kh Bekyashev, Z A Goncharova, and N E Kushlinskii. 2020b. "Glial Fibrillary Acidic Protein in the Diagnosis and Prognosis of Malignant Glial Tumors." *Bulletin of Experimental Biology and Medicine* 168: 503–6. https://doi.org/10.1007/s10517-020-04741-9

Lyubimova, N V, M G Toms, E E Popova, Y V Bondarenko, V B Krat, and N E Kushlinskii. 2011b. "Neurospecific Proteins in the Serum of Patients with Brain Tumors." *Bulletin of Experimental Biology and Medicine* 150 (6): 732–34. https://doi.org/10.1007/s10517-011-1236-9.

Mandrekar, Jayawant N. 2010. "Receiver Operating Characteristic Curve in Diagnostic Test Assessment." *Journal of Thoracic Oncology* 5 (9): 1315–16. https://doi.org/https://doi.org/10.1097/JTO.0b013e3181ec173d.

Mark, A Mittler, C Walters Beverly, and G Stopa Edward. 1996. "Observer Reliability in Histological Grading of Astrocytoma Stereotactic Biopsies." *Journal of Neurosurgery* 85 (6): 1091–94. https://doi.org/10.3171/jns.1996.85.6.1091.

McGrath, Sean, Hojoon Sohn, Russell Steele, and Andrea Benedetti. 2020. "Meta-Analysis of the Difference of Medians." *Biometrical Journal* 62 (1): 69–98. https://doi.org/10.1002/bimj.201900036.

Messing, Albee, and Michael Brenner. 2020. "GFAP at 50." *ASN Neuro* 12. https://doi.org/10.1177/1759091420949680.

Middeldorp, J., and E. M. Hol. 2011. "GFAP in Health and Disease." *Progress in Neurobiology* 93 (3): 421–43. https://doi.org/10.1016/j.pneurobio.2011.01.005.

Moher, D, A Liberati, J Tetzlaff, and D G Altman. 2009. "Preferred Reporting Items for Systematic Reviews and Meta-Analyses: The PRISMA Statement." *Bmj* 339: b2535. https://doi.org/10.1136/bmj.b2535.

Müller, Carolin, Johannes Holtschmidt, Martina Auer, Ellen Heitzer, Katrin Lamszus, Alexander Schulte, Jakob Matschke, et al. 2014. "Cancer: Hematogenous Dissemination of Glioblastoma Multiforme." *Science Translational Medicine* 6 (247): 1–10. https://doi.org/10.1126/scitranslmed.3009095.

Neagu, M R, R Y Huang, D A Reardon, and P Y Wen. 2015. "How Treatment Monitoring Is Influencing Treatment Decisions in Glioblastomas." *Curr Treat Options Neurol* 17 (4): 343. https://doi.org/10.1007/s11940-015-0343-8.

Ostrom, Quinn T, Gino Cioffi, Haley Gittleman, Nirav Patil, Kristin Waite, Carol Kruchko, Jill S Barnholtz-sloan, Case Comprehensive, and Case Western. 2019. "Neuro-Oncology CBTRUS Statistical Report : Primary Brain and Other Central Nervous System Tumors Diagnosed in The" 21: 1–100. https://doi.org/10.1093/neuonc/noz150.

Ouzzani, M, H Hammady, Z Fedorowicz, and A Elmagarmid. 2016. "Rayyan-a Web and Mobile App for Systematic Reviews." *Syst Rev* 5 (1): 210. https://doi.org/10.1186/s13643-016-0384-4.

Pascalis, Chiara De, Carlos Pérez-González, Shailaja Seetharaman, Batiste Boëda, Benoit Vianay, Mithila Burute, Cécile Leduc, Nicolas Borghi, Xavier Trepat, and Sandrine Etienne-Manneville. 2018. "Intermediate Filaments Control Collective Migration by Restricting Traction Forces and Sustaining Cell–Cell Contacts." *The Journal of Cell Biology* 217 (9), 3031-3044, jcb.201801162. https://doi.org/10.1083/jcb.201801162.

R Core Team. 2013. "R: A Language and Environment for Statistical Computing." Vienna, Austria: R Foundation for Statistical Computing. http://www.r-project.org/.

Ramos, Irene, Konstantinos Stamatakis, Clara L Oeste, and Dolores Pérez-Sala. 2020. "Vimentin as a Multifaceted Player and Potential Therapeutic Target in Viral Infections." *International Journal of Molecular Sciences* 21 (13): 4675.

Reitsma, J B, A S Glas, A W Rutjes, R J Scholten, P M Bossuyt, and A H Zwinderman. 2005. "Bivariate Analysis of Sensitivity and Specificity Produces Informative Summary Measures in Diagnostic Reviews." *J Clin Epidemiol* 58 (10): 982–90. https://doi.org/10.1016/j.jclinepi.2005.02.022.

Rohatgi, Ankit. n.d. "WebPlotDigitizer." Pacifica, California, USA. https://automeris.io/WebPlotDigitizer.

Ruutiainen, J, J Newcombe, A Salmi, D Dahl, and H Frey. 1981. "Measurement of Glial Fibrillary Acidic Protein (GFAP) and Anti-GFAP Antibodies by Solid-phase Radioimmunoassays." *Acta Neurologica Scandinavica* 63 (5): 297–305. https://doi.org/10.1111/j.1600-0404.1981.tb00783.x

Sartori, Maria Teresa, Alessandro Della Puppa, Andrea Ballin, Elena Campello, Claudia Maria Radu, Graziella Saggiorato, Domenico d'Avella, Renato Scienza, Giuseppe Cella, and Paolo Simioni. 2013. "Circulating Microparticles of Glial Origin and Tissue Factor Bearing in High-Grade Glioma: A Potential Prothrombotic Role." *Thrombosis and Haemostasis* 110 (2): 378–85. https://doi.org/10.1160/TH12-12-0957.

Schmid, Dominic, Uwe Warnken, Pauline Latzer, Dirk C Hoffmann, Judith Roth, Stefanie Kutschmann, Hannah Jaschonek, et al. 2021. "Diagnostic Biomarkers from Proteomic Characterization of Cerebrospinal Fluid in Patients with Brain Malignancies." *Journal of Neurochemistry* 158(2): 522-538. https://doi.org/https://doi.org/10.1111/jnc.15350.

Sharma, Pooja, Sarah Alsharif, Arwa Fallatah, and Byung Min Chung. 2019. "Intermediate Filaments as Effectors of Cancer Development and Metastasis: A Focus on Keratins, Vimentin, and Nestin." *Cells* 8 (5): 497. https://doi.org/10.3390/cells8050497.

Shemilt, M, A Boutin, F Lauzier, R Zarychanski, L Moore, L A McIntyre, L Nadeau, et al. 2019. "Prognostic Value of Glial Fibrillary Acidic Protein in Patients With Moderate and Severe Traumatic Brain Injury: A Systematic Review and Meta-Analysis." *Crit Care Med* 47 (6): e522–29. https://doi.org/10.1097/ccm.0000000000003728.

Shih, Chung Chih, Tzong Shiun Lee, Fon Yih Tsuang, Pei Lin Lin, Ya Jung Cheng, Hsiao Liang Cheng, and Chun Yu Wu. 2017. "Pretreatment Serum Lactate Level as a Prognostic Biomarker in Patients Undergoing Supratentorial Primary Brain Tumor Resection." *Oncotarget* 8 (38): 63715–23. https://doi.org/10.18632/oncotarget.18891.

Skalli, Omar, Ulrika Wilhelmsson, Charlotte Örndahl, Boglarka Fekete, Kristina Malmgren, Bertil

Rydenhag, and Milos Pekny. 2013. "Astrocytoma Grade IV (Glioblastoma Multiforme) Displays 3 Subtypes with Unique Expression Profiles of Intermediate Filament Proteins." *Human Pathology* 44 (10): 2081–88. https://doi.org/10.1016/j.humpath.2013.03.013.

Stassen, Oscar M.J.A., Emma J. van Bodegraven, Fabrizio Giuliani, Martina Moeton, Regina Kanski, Jacqueline A. Sluijs, Miriam E. van Strien, Willem Kamphuis, Pierre A.J. Robe, and Elly M. Hol. 2017. "GFAPδ/GFAPα Ratio Directs Astrocytoma Gene Expression towards a More Malignant Profile." *Oncotarget* 8 (50): 88104–21. https://doi.org/10.18632/oncotarget.21540.

Szymaś, J, S Morkowski, and F Tokarz. 1986. "Determination of the Glial Fibrillary Acidic Protein in Human Cerebrospinal Fluid and in Cyst Fluid of Brain Tumors." *Acta Neurochirurgica* 83 (3): 144–50. https://www.ncbi.nlm.nih.gov/pubmed/3812039.

The U.S. Food and Drug Administration. 2018. "FDA Authorizes Marketing of First Blood Test to Aid in the Evaluation of Concussion in Adults." 2018. https://www.fda.gov/news-events/press-announcements/fda-authorizes-marketing-first-blood-test-aid-evaluation-concussion-adults.

Tichy, Julia, Sabrina Spechtmeyer, Michel Mittelbronn, Elke Hattingen, Johannes Rieger, Christian Senft, and Christian Foerch. 2015. "Prospective Evaluation of Serum Glial Fibrillary Acidic Protein (GFAP) as a Diagnostic Marker for Glioblastoma." *Journal of Neuro-Oncology* 126 (2): 361–69. https://doi.org/10.1007/s11060-015-1978-8.

Urbanavičiūtė, Rūta, Kęstutis Skauminas, and Daina Skiriutė. 2020. "The Evaluation of AREG, MMP-2, CHI3L1, GFAP, and OPN Serum Combined Value in Astrocytic Glioma Patients' Diagnosis and Prognosis." *Brain Sciences* 10 (11): 872. https://doi.org/10.3390/brainsci10110872

Verhaak, Roel G.W., Katherine A. Hoadley, Elizabeth Purdom, Victoria Wang, Yuan Qi, Matthew D. Wilkerson, C. Ryan Miller, et al. 2010. "Integrated Genomic Analysis Identifies Clinically Relevant Subtypes of Glioblastoma Characterized by Abnormalities in PDGFRA, IDH1, EGFR, and NF1." *Cancer Cell* 17 (1): 98–110. https://doi.org/10.1016/j.ccr.2009.12.020.

Viechtbauer, Wolfgang. 2010. "Conducting Meta-Analyses in R with the Metafor Package." *Journal of Statistical Software* 36 (3): 1–48. https://doi.org/10.18637/jss.v036.i03

Vietheer, Julia-Mareen, Johannes Rieger, Marlies Wagner, Christian Senft, Julia Tichy, and Christian Foerch. 2017. "Serum Concentrations of Glial Fibrillary Acidic Protein (GFAP) Do Not Indicate Tumor Recurrence in Patients with Glioblastoma." *Journal of Neuro-Oncology* 135(1): 193-199. https://doi.org/10.1007/s11060-017-2565-y.

Waskom, Michael, Maoz Gelbart, Olga Botvinnik, Joel Ostblom, Paul Hobson, Saulius Lukauskas, and Thomas Brunner. 2020. "Mwaskom/Seaborn: V0.11.1." Zenodo. 2020. https://doi.org/http://doi.org/10.5281/zenodo.4379347.

Wei, Ping, Wei Zhang, Liu-Song Yang, Hai-Shi Zhang, Xiao-En Xu, Ying-Hua Jiang, Feng-Ping Huang, and Qian Shi. 2013. "Serum GFAP Autoantibody as an ELISA-Detectable Glioma Marker." *Tumour Biology : The Journal of the International Society for Oncodevelopmental Biology and Medicine* 34 (4): 2283–92. https://doi.org/10.1007/s13277-013-0770-7

Whiting, P F, A W Rutjes, M E Westwood, S Mallett, J J Deeks, J B Reitsma, M M Leeflang, J A Sterne, and P M Bossuyt. 2011. "QUADAS-2: A Revised Tool for the Quality Assessment of Diagnostic Accuracy Studies." *Ann Intern Med* 155 (8): 529–36. https://doi.org/10.7326/0003-4819-155-8-201110180-00009.

Wickham, Hadley. 2016. "Ggplot2: Elegant Graphics for Data Analysis." Springer. 2016. https://ggplot2.tidyverse.org.

Wu, Bin, Caixing Sun, Fang Feng, Minghua Ge, and Liang Xia. 2015. "Do Relevant Markers of Cancer Stem Cells CD133 and Nestin Indicate a Poor Prognosis in Glioma Patients? A Systematic Review and Meta-Analysis." *Journal of Experimental and Clinical Cancer Research* 34 (1). https://doi.org/10.1186/s13046-015-0163-4.

Yong, Raymund L, and Russell R Lonser. 2013. "Safety of Closed Brain Biopsy: Population-Based Studies Weigh In." *World Neurosurgery* 79 (1): 53–54. https://doi.org/10.1016/j.wneu.2012.05.016.

Zhao, Jiaxin, Liqiu Zhang, Xingli Dong, Lu Liu, Linman Huo, and Huirong Chen. 2018. "High Expression of Vimentin Is Associated with Progression and a Poor Outcome in Glioblastoma." *Applied Immunohistochemistry and Molecular Morphology* 26 (5): 337–44. https://doi.org/10.1097/PAI.0000000000000420.

Supplementary Data

Supplementary Figures

Supp. Fig. 1-3: A forest plot of the average estimated median GFAP levels in serum of grade III, II patients and controls, respectively, as meta-analysed with inverse variance and a random-effects model;

Supp. Fig. 4-6: A forest plot of average estimated median difference of sGFAP levels between grade IV patients and grade III/II/I patients, respectively, as meta-analysed with inverse variance and a random-effects model.

Supp. Fig. 7-9: A forest plot of average estimated median difference of sGFAP levels between grade III patients and grade II/I patients and controls, respectively, as meta-analysed with inverse variance and a random-effects model.

Supp. Fig. 10: A forest plot of average estimated median difference of sGFAP levels between grade I patients and controls as meta-analysed with inverse variance and a random-effects model.

Supplementary Tables

Supp. Table 1: Search strategy used to search the PubMed database on April 12th, 2020 and March 24th, 2021;

Supp. Table 2: An overview of the control group as described in the respective articles;

Supp. Table 3: An overview of the studies included in the meta-analysis and the methodological details of the assays used to detect sGFAP;

Supp. Table 4: Overview of all studies used for incidence of detection;

Supp. Table 5: An overview of all eligible studies for the level of GFAP in serum of grade I, II, and III patients.

Supp. Table 6: An overview of the judgments on bias and applicability as assessed with the QUADAS-2

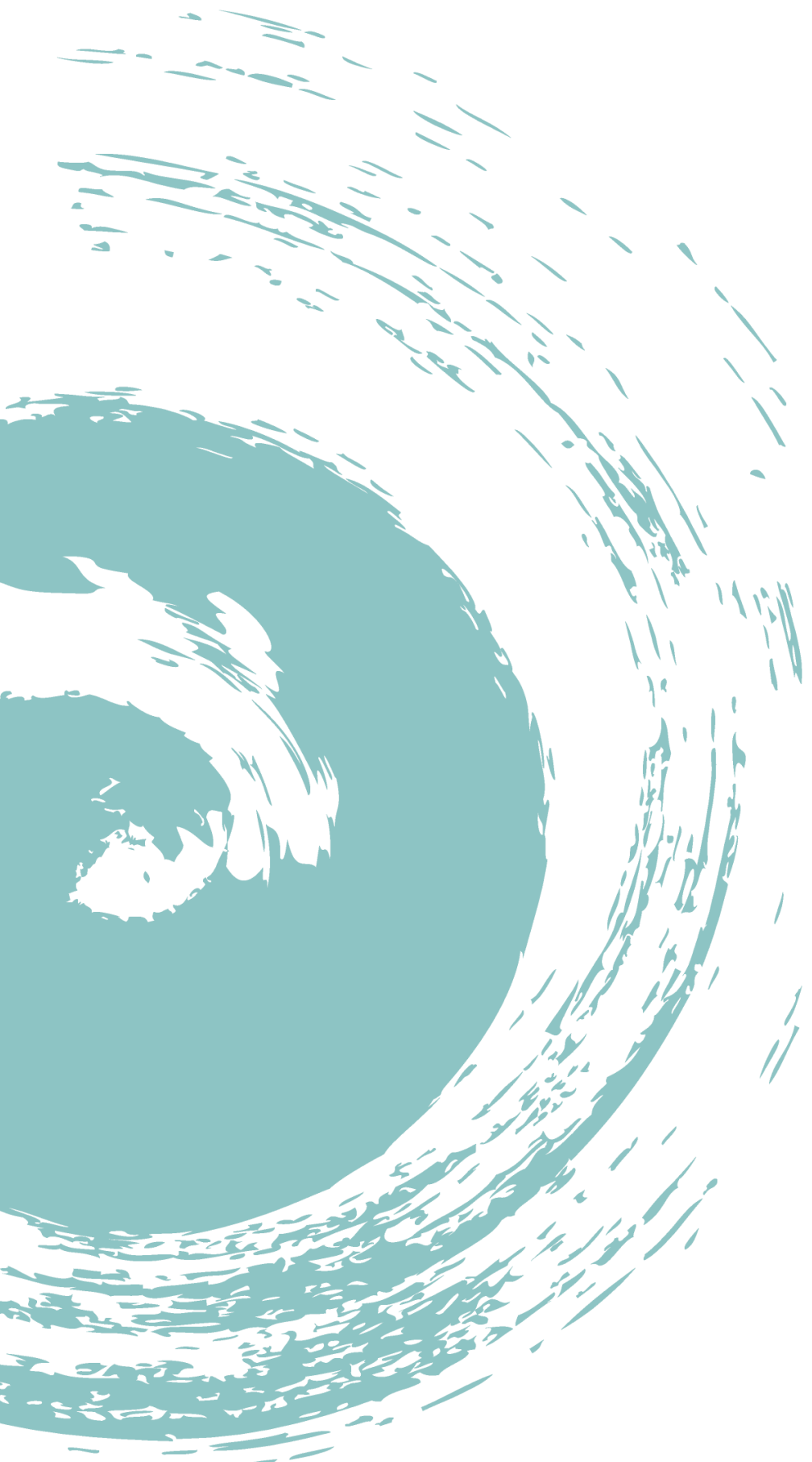

General discussion

The high invasiveness of glioma cells is a major challenge in effectively treating patients suffering from glioma. The invading cells escape therapeutical interventions and cause tumour recurrence elsewhere in the brain (Claes, Idema, and Wesseling 2007; Sahm et al. 2012; Cuddapah et al. 2014). This is one of the main causes of the bad prognosis (Ho et al. 2014). In the past years, there has been increasing attention for the role of intermediate filaments (IFs) in cell migration and invasion (Leduc and Etienne-Manneville 2015). IF proteins regulate cellular processes essential for cell migration, such as cell polarisation, cell adhesion, and actin dynamics (Ivaska et al. 2007; Chung, Rotty, and Coulombe 2013; Seetharaman and Etienne-Manneville 2020). In addition, the transition from immobile to migratory cells is often associated with changes in the IF network composition, for instance during wound healing (Gilles et al. 1999; Menko et al. 2014; Walker et al. 2018), breast cancer invasion (Cheung et al. 2013), and epithelial to mesenchymal transition (Thiery et al. 2009; Mendez, Kojima, and Goldman 2010; Sharma et al. 2019).

Glial fibrillary acidic protein (GFAP) is the IF protein that is most characteristic for glioma cells (van Bodegraven et al. 2019b). This thesis aims at better understanding the function and relevance of the GFAP protein in glioma cell invasion. A major starting point was the observation that glioma malignancy grade is associated with changes in the expression levels of GFAP alternative splice isoforms (Stassen et al. 2017). In addition, changing the ratio between splice isoforms GFAPδ and GFAPα is associated with altered expression of genes related to cell-extracellular matrix (ECM) interaction (Stassen et al. 2017). As diffuse gliomas are highly infiltrative, and cell-ECM interactions are an important component of cell invasion (Claes, Idema, and Wesseling 2007; Doyle and Yamada 2016), we hypothesised that GFAP splice variants are differentially involved in regulating cell invasion of glioma cells. In this last part of the thesis, I will re-evaluate this hypothesis which was formulated at the beginning of the PhD project. I will summarise and review the major findings of the different chapters and discuss open questions. Next, I will zoom in on the methodological approaches we used and discuss the strengths, weaknesses, and ongoing developments in the field. In the last section of the general discussion, the clinical applications and implications of the findings will be discussed, as well as considerations for future research. The general discussion will end with a conclusion and perspective on the role and regulation of GFAP in diffuse gliomas.

1. Fundamental insights into the role of GFAP in diffuse glioma
   1.1. GFAP regulates glioma cell invasion in an isoform-specific manner
   1.2. Manipulation of the GFAPδ/α-ratio, a functional role in proliferation?
   1.3. The protective role of GFAP in migration induced stress
   1.4. Unravelling the molecular mechanism downstream of GFAP
   1.5. The heterogeneous nature of GFAP and IF expression in gliomas
2. Methodological considerations
   2.1. Using CRISPR-Cas9 to regulate IF expression
   2.2. Glioma cell lines as experimental models for diffuse glioma
   2.3. Modelling glioma invasion
3. Clinical applications and considerations
   3.1. Investigating glioma invasion, why is it important?
   3.2 Relevance of GFAP as a diagnostic tool and therapeutical target.
4. Conclusion and future perspectives

1. Fundamental insights into the role of GFAP in diffuse glioma

1.1 GFAP regulates glioma cell invasion in an isoform-specific manner

Cell adhesion and force generation on the ECM are essential components of adhesion-driven forms of cellular translocation (De Pascalis and Etienne-Manneville 2017; Doyle and Yamada 2016; Yamada and Sixt 2019). Expression of ECM receptors at the cell surface allows a cell to bind to the substrate, creating a scaffold for a cell to generate a force with the actomyosin network, allowing the cell to pull itself forward (Blanchoin et al. 2014; Elosegui-Artola et al. 2016). In this thesis and earlier work from our lab (Moeton et al. 2014; Stassen et al. 2017), we consistently find that regulation of the expression levels of GFAP splice variants GFAPδ and GFAPα leads to adaptations of the cell that involve interaction with the ECM. In **Chapter 1** we have shown that dominance of GFAPδ in the cell, caused by depleting GFAPα with CRISPR-Cas9 technology, leads to an increased extracellular deposit of the ECM molecule laminin, an increased expression of integrins that facilitate binding to laminin, and altered cell-adhesion dynamics. Also, the actomyosin organisation and general morphology were different in these cells. These observations strongly suggest that the GFAPδ/α ratio leads to molecular alterations that equip the cell for cellular invasion.

In addition to cell adhesion, additional factors come into play when studying cell migration/ invasion within a three-dimensional (3D) tissue context. As discussed in **Chapter 2**, invasion into the brain parenchyma requires an additional adaptive response of cells, as tissues are densely packed with cell bodies, cell processes, and different compositions and organisations of ECM molecules (Yamada and Sixt 2019;

Van Helvert, Storm, and Friedl 2018). As introduced in the **Introduction**, glioma cell invasion typically occurs alongside pre-existing structures in the brain called Scherer's structures (Peiffer 1999; Cuddapah et al. 2014). The most likely explanation for this is that the aligned topology of cellular structures and ECM molecules of blood vessels, white matter tracts, and the subarachnoid space provide the path of least resistance (Cuddapah et al. 2014). As different factors come into play, molecular adaptations that drive rapid migration on flat surfaces do not always facilitate fast migration in 3D environments. A good example of this is a recent study in migrating fibroblast, where expression of vimentin accelerates migration on 2D surfaces but hampers migration speed when cells are migrating through confinement (Patteson, Pogoda, et al. 2019). Therefore, when studying invasion it is important to mimic the native environment of migrating cells. In this thesis, our main approach to this end was using *ex vivo* organotypic brain slice cultures as described in **Chapter 3**. In paragraph 2.3 of the General Discussion, the strengths and limitation of this model with be further discussed.

In line with our initial hypothesis, we indeed observed in **Chapter 4** that regulation of the GFAPδ/α-ratio leads to altered migratory behaviour of GFAPδ/α-high and GFAPδ/α-low cells. The GFAPδ/α-high cells, i.e. with a dominant expression of GFAPδ cells, had the most diffuse growth pattern in *ex vivo* organotypic brain slice cultures and *in vivo.* These cells also showed the most adaptations *in vitro* in **Chapter 1**. The diffuse character of the GFAPδ/α-high cells was linked to an increased percentage of motile cells that migrated with high persistence, mostly in the direction of the brain parenchyma. An unexpected finding, however, was that modulating the GFAPδ/α-ratio in the other direction also increased the number of invading cells, yet through different dynamics. GFAPδ/α-low cells, i.e. with a dominant expression of GFAPα, showed higher motility and increased cell speed, but cells migrated with lower migration persistence. The migration behaviours of the GFAPδ/α-high and low cells overlap with behaviour patterns observed in the 'invasive margin' and 'diffuse infiltration' margin of the glioma tumour, as described by Alieva et al. 2019. These two regions of the tumour were associated with slow but directed migration and fast but random migration respectively (Alieva et al. 2019). Also in a different study from Juliano et al. 2018, these two migration dynamics are described when comparing the motility of glioma cells (migrating in a 'super diffusion pattern', slow but persistent) and microglia (migrating in a 'simple random walk pattern', low persistence). The authors of this paper attribute the different migration modes to restricted versus non-restricted environments (Juliano et al. 2018). Together, it can be speculated that GFAPδ/α-high cells tend to migrate into the confined environment of the brain, whereas GFAPδ/α-low cells remain in the tumour core. The fact that the latter cell group has higher intrinsic mobility compared to controls, likely explains why still more GFAPδ/α-high cells invade the tissue.

The deformability of the nucleus is a rate-limiting factor when cells have to

navigate through narrow constrictions of the interstitial space in tissues (McGregor, Hsia, and Lammerding 2016). Cells with softer, easier deformable nuclei tend to be more successful in migrating through small pore sizes in comparison to cells with stiffer nuclei (Davidson et al. 2014; Harada et al. 2014). It is known from glial cells and other cell types that the IF network forms a cage around the nucleus (Dupin, Sakamoto, and Etienne-Manneville 2011; Patteson, Pogoda, et al. 2019; Patteson, Vahabikashi, et al. 2019), and that this nuclear cage affects the mechanical properties of the perinuclear area (Patteson, Pogoda, et al. 2019). In **Chapter 4**, we observed changes in the nuclear shape in GFAPδ/α-high cells. Therefore, in **Chapter 5** we originally aimed to investigate whether changes in the GFAPδ/α-ratio would affect the organisation and mechanical properties of the perinuclear cage, as this could be a complementary mechanism underlying the increased capacity of GFAPδ/α-high cells to infiltrate the brain parenchyma. To test this hypothesis, we made use of microfluidic migration chambers where the confined pores of the interstitial space are mimicked with PDMS pillars (Davidson et al. 2015; Denais et al. 2016). Although we observed that manipulating the GFAPδ/α-ratio had some effects on confined migration success rate and speed in the expected direction, the effects were minor and were not consistent between the GFAPδ/α-ratio modulated cell clones. We, therefore, concluded that deformability of the nucleus is not the main driving factor of the more diffuse growth patterns of the GFAPδ/α-high cells, and the increased invasiveness is more likely linked to the adapted cell-ECM interactions.

In **Chapter 5** we further explored the effects of regulating IF expression levels in glioma cells by investigating the effect of full depletion of GFAP or vimentin. Depletion of all GFAP isoforms did not significantly affect cell invasion in *ex vivo* organotypic brain slices, this confirms that the effects we observe in **Chapter 4** are dependent on the GFAPδ/α-ratio and not on general lower levels of GFAP. The absence of an effect of depleting vimentin was however somewhat surprising. Vimentin is typically seen as a pro-migration protein, and depletion of vimentin frequently leads to decreased migration or migratory speed on flat surfaces in many different types of cells (Mendez, Kojima, and Goldman 2010; Vuoriluoto et al. 2011; Chung, Rotty, and Coulombe 2013), including in glioma cells (Nowicki et al. 2019). In a 3D context, vimentin expression can however have the opposite effect on migration speed as depletion speeds up migration through confinement (Patteson, Pogoda, et al. 2019; Tudor et al. 2019). Thus, we expected a similar pattern in glioma cells lacking vimentin in the *ex vivo* organotypic brain slices, but we did not. One possible explanation for the lack of effect of vimentin depletion is that we use an assay where vimentin depleted cells are co-injected with control cells. Van Bodegraven et al discovered that loss of vimentin in glioma cells affects leader- but not follower cells (personal communication). During collective migration, groups of cells move in a collective manner allowing efficient distribution of forces between cells at the front (leader cells) and rear (follower cells) (Mayor and Etienne-Manneville 2016;

De Pascalis and Etienne-Manneville 2017). It is known that IFs contribute to collective migration modes of primary astrocytes, and are involved in the redistribution of forces in the migration front and rear (De Pascalis et al. 2018). Therefore it is likely that the effect of vimentin depletion is masked when vimentin expressing cells are still present.

1.2 Manipulation of the GFAPδ/α-ratio, a functional role in proliferation?

The go-or-grow hypothesis is a paradigm that states that there is a dichotomy between proliferation and invasion (Dhruv et al. 2013). Evidence for this hypothesis comes from the observation that glioma cells pause migration before entering mitosis (Farin et al. 2006) and from the fact that Ki67 labelling of proliferative cells is higher in the core of glioma tumour tissue in comparison to the rim (Dhruv et al. 2013). The go-or-grow hypothesis is relevant for glioma therapy, as therapeutical interventions that target invasion can have a negative impact on the outcome due to their effect on proliferation. An example of this is the effect of myosin IIA: depletion of myosin IIA in cells implanted in orthotopic xenografts leads to less cell invasion but to a higher mortality as the tumour mass more rapidly expands (Picariello et al. 2019).

Based on the effect of the GFAPδ/α-ratio on cell invasion (**Chapter 4)**, we hypothesised that the GFAPδ/α-ratio induces a shift in the go-or-grow paradigm and would therefore impact proliferation as well. Tumours of mice implanted with the first set of cell clones (CRISPR set A) indeed expanded at different rates: GFAPδ/α-low cells grew more rapidly whereas the diffusely growing GFAPδ/α-high cells expanded slower. To systematically investigate the proliferative index, we set up BrdU-assays of cells in the *ex vivo* organotypic brain slices (Fig. 1a) as described in **Chapter 3.** We indeed observed an opposite effect on proliferation in GFAPδ/α-high and low cells, similarly to what we observed *in vivo* (Fig. 1b). However, when we repeated these experiments with a second set of sgRNAs (CRISPR set B), we could not replicate these findings (Fig. 1b). Based on these results we conclude that the differences we observe in proliferation are most likely due to clonal differences. Nevertheless, both GFAPδ/α-high clones that we investigated have low proliferation indices, therefore it cannot be fully ruled out that a more invasive nature is associated with decreased proliferation, as was also observed in the myosin-IIA depletion study (Picariello et al. 2019).

We have also investigated the proliferative index of the CRISPR set A in 2D, namely in cells seeded on coverslips. Interestingly, the differences we observed in the *ex vivo* brain slices were not present when cells were plated on coverslips, although we have to stress that the incubation time with BrdU was different (2 hours versus 6 hours). This tells us that the proliferation index is context-dependent and is likely influenced by biochemical and mechanical factors present in the brain. This is in line with a study from Farin et al., that showed that cell divisions of transplanted glioma cells frequently

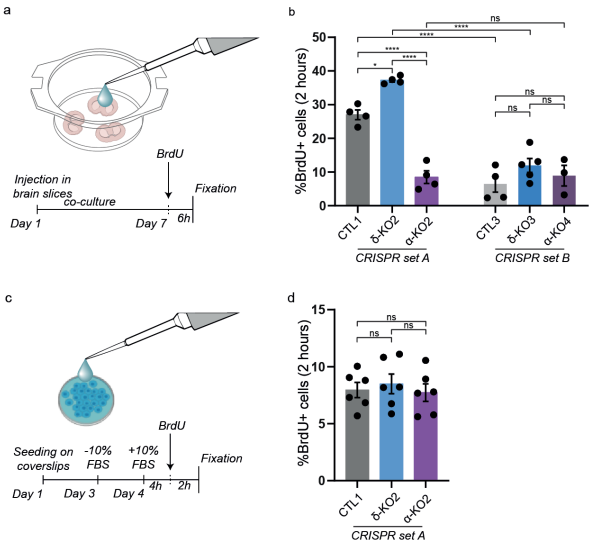

Figure 1. Determining the proliferative indices of GFAPδ/α modulated cells. (a) Schematic of the BrdU-assay in organotypic brain slices. H2B-mNeonGreen positive GFAP-modulated cells and controls were injected into the brain slices (Chapter 3, 4) and cultured for 1 week. BrdU was incubated during the last 6 hours of the culture period. (b) Quantification of the percentage of BrdU+ cells. GFAPδ/α ratio significantly altered proliferation in cells generated with CRISPR set A, but not B. n= 3 (α-KO4), n=4 (CTL1, CTL3, δ-KO2, α-KO2), and n=5 (δ-KO3) organotypic brain slices from independent experiments. (c) Schematic of the BrdU-assay of cells grown on PDL-coated coverslips (schematic generated with biorender.com). Cells were starved for 24 hours by depleting the medium of 10% FBS. BrdU was added to the medium 4 hours after supplementing the medium with 10% FBS and incubated for 2 hours. (d) Quantification of the percentage of BrdU+ cells. GFAPδ/α ratio had no significant effects on the proliferation of cells cultured on PDL-coated coverslips.

occur at cell division 'hot spots' near vascular branch points. The authors suggest that mitosis is triggered by local environmental cues (Farin et al. 2006). Whether these cues are mechanical or chemical of nature, and whether cells with different GFAPδ/α-ratios respond differently to these cues, remain open questions for further investigation.

1.3 The protective role of GFAP in migration induced stress.

We serendipitously discovered in **Chapter 5** another role of GFAP in protecting glioma cells against migration induced damage. Initially focussing on cell speed and success rate during confined migration, we observed that glioma cells without GFAP frequently presented a nuclear fragmentation phenotype, where the nucleus broke into smaller fragments. We observed that nuclear fragments were also present in *ex vivo* organotypic brain slices injected with GFAP-KO cells and that the fragmentation phenotype was associated with frequent nuclear envelope (NE)-ruptures and exchange between cytoplasm and nucleoplasm. Since there were no significant differences in frequency of

nuclear fragmentation between the GFAPδ/α-ratio modulated cells, we concluded that the phenotype is isoform independent and can most likely be attributed to features of the head or rod-domain of the protein. Nevertheless, it is still possible that prevention of the nuclear fragmentation phenotype is more dependent on GFAPα, simply because of the higher abundance of this isoform within the cell.

As discussed in **The Introduction**, GFAP can bind to Heat Shock Protein 27 (HSP27) and protein chaperone αB-crystallin (CRYAB) and has therefore been linked to the cellular stress response (Perng et al. 2006). The GFAP-vimentin network in astrocytes is also involved in protecting the cell from oxygen-glucose deprivation-induced cell death (De Pablo et al. 2013). It is therefore not surprising that GFAP also protects against other forms of stress, such as migration induced stress as described here. Recent studies associated loss of vimentin with more frequent cell death events and DNA damage in fibroblasts, macrophages, and carcinoma cells that migrated through confinements (Patteson, Vahabikashi, et al. 2019; Tudor et al. 2019; Stankevicins et al. 2019). In our experiments, the protective role of vimentin was less evident, although nuclear fragments were observed in *ex vivo* organotypic brain slices injected with vimentin-KO cells. In GFAP depleted cells, we saw that the vimentin network still formed a cage around the nucleus when cells are migrating through the confinement (Fig. 2a). Nuclear blebs are observed in regions without vimentin, whereas regions with high vimentin intensity are associated with nuclear indentations (Fig. 2a), confirming that vimentin affects nuclear morphology as we described in **Chapter 5**. It would be interesting to investigate how the loss of both proteins would affect the nuclear integrity during migration through confinement.

One thing that needs to be further explored, is why we could not fully replicate the phenotype in another glioma cell line. In the KT1937 line, a cell line that was directly isolated from a grade IV tumour, we observed more nuclear fragmentations in clonal control cells in comparison to the GFAP-KO cells. Interestingly, when investigating the GFAP network in the parental KT1937 line, we occasionally observed GFAP aggregates in cells that had migrated through confinement (Fig. 2b), something we did not observe in the parental U251 cell line (Fig. 2c). If the GFAP network of the KT1937 cell line is indeed more prone to aggregation, then this could explain the increased susceptibility to nuclear fragmentation of the control clone, as GFAP may not be able to execute its physiological function when sequestered in aggregates. Aggregation of GFAP is most typically associated with Alexander's disease, where the so-called Rosenthal fibres have major effects on the physiology of the cell (Hagemann 2022). Rosenthal fibres can sometimes also be observed in glioma, where they are mostly associated with low-grade tumours (Cillekens et al. 2000). It remains to be investigated how these aggregates occur and what the consequences are for the (migration induced) stress response of glioma cells.

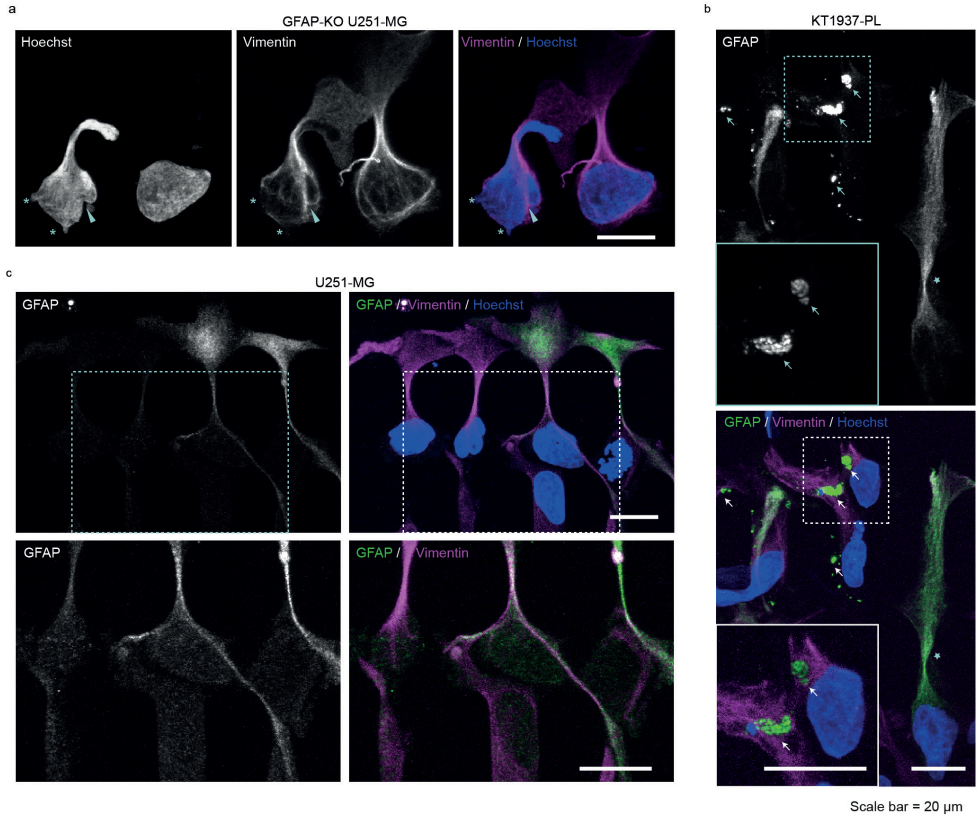

Figure 2. GFAP and vimentin organisation of cells in the confined migration microfluidic devices. (a) Example image of GFAP-KO U251-MG cells with a nucleus in the confined area (left nucleus) or before confinement (right nucleus). Vimentin forms a cage around the nucleus. The arrowhead indicates a region with a nuclear indentation and prominent vimentin filaments. The asterisks indicate nuclear blebs. Vimentin filaments are absent in these regions. (b) Example image of KT1937 cells in the confined migration microfluidic devices. The star shape indicates a cell with normal filamentous GFAP. The arrows indicate GFAP aggregates. (c) Example image of U251-MG cells in the confined migration microfluidic devices. The structure of GFAP appears soluble rather than filamentous (upper image). Soluble GFAP signal is detected in the nuclear area (lower image). Scale bar = 20 µm.

1.4 Unravelling the molecular mechanism downstream of GFAP

What are the molecular mechanisms underlying the GFAPδ/α-induced invasion patterns and the protective role of GFAP in migration induced stress? In **Chapter 1** and **Chapter 5** we have identified some pieces of the molecular puzzle. In **Chapter 1** we show that dual-specificity phosphatase 4 (DUSP4), also known as mitogen-activated protein kinase (MAPK) phosphatase 2, is strongly associated with the GFAPδ/α ratio and that the expression is essential for the molecular alterations observed in GFAPδ/α-high cells. In GFAPδ/α-high cells increased levels of phosphorylated c-Jun N-terminal kinase (JNK) are observed, which has also been reported in cells with GFAPδ overexpression

(Perng et al. 2008). As DUSP4 is typically known as a nuclear phosphatase, it has to be further investigated how these two molecules are linked together in the GFAPδ/α-high cells. In **Chapter 5** we show that loss of GFAP is associated with more frequent NE-ruptures during confined migration and with an increased background activity of caspase-3/7. We propose that entry of cytosolic nucleases underlies the nuclear fragmentation phenotype and promotes accidental cell death. Entry of cytosolic nucleases upon NE-rupture has been described before and contributes to genomic instability (Nader et al. 2021). Although the nucleases responsible for the fragmentation have not yet been identified, DNA Fragmentation Factor 45 is a good candidate due to the earlier established link with GFAP as a binding partner (Hanus, Kalinowska-Herok, and Widlak 2010).

To further unravel the molecular mechanisms downstream of GFAP, it is first necessary to better understand the organisation of GFAP within the cell and the regulation hereof. Although the IF network is often taken as a starting point when thinking about the functions of IF proteins, in principle there can be separate functions for IF proteins incorporated within a network or in soluble (unit length filaments/ short filaments) form. Whereas early studies showed that the soluble pool of vimentin is minimal in cells in culture (Blikstad and Lazarides 1983; Çolakoglu and Brown 2009; Soellner, Quinlan, and Franke 1985), a study by Murray and colleagues showed that this soluble fraction of vimentin can increase significantly depending on the rigidity of the substrate and can reach levels up to 67% solubility (Murray, Mendez, and Janmey 2014). In U251-MG cells, filamentous structures of GFAP, but also vimentin, are not always obvious (Fig. 2c). Solubility of GFAP may also be dependent on the expression of vimentin, as filamentous structures of GFAP were not observed in the vimentin-KO cells (Chapter 5, Supp. Fig. 1). As loss of the GFAP perinuclear cage in vimentin-KO cells did not lead to the same frequency in nuclear fragmentations in comparison to the GFAP-KOs, we hypothesise that the nuclear fragmentation phenotype is not fully dependent on the IF perinuclear cage, but at least partially to soluble/ cytosolic GFAP. The effect we observed on nuclear size, on the other hand, may still be reliant on filamentous GFAP in the perinuclear cage.

Also concerning the GFAPδ/α-dependent roles in glioma invasion, network versus soluble protein contribution remains to be determined. GFAPδ and GFAPα could differentially affect the ultrastructure of the IF network, thereby affecting cellular mechanics and potentially mechanobiology (van Bodegraven and Etienne-Manneville 2021). The ultrastructure of the IF network is dependent on the type of IF protein expressed, as became evident from cryoEM characterisation of astrocytes depleted from GFAP or vimentin, which show differences in density and compactness of the IF network (Lepekhin et al. 2001; Menet et al. 2001). Based on the assembly properties of GFAPα and GFAPδ, it is likely that the ratio of the two isoforms have an effect on

the ultrastructure of the IF network. Whereas GFAPα can self-assemble into filaments, GFAPδ does not have this capacity and can only be tolerated in the network in small amounts to avoid a network collapse (Nielsen and Jørgensen 2004; Moeton et al. 2016). Also the exchange dynamics of GFAPδ is slower compared to GFAPα (Moeton et al. 2016). Mechanical characterisation of *in situ* assembled polymers of IF proteins further shows that the tail-region is an important contributor to the strain stiffening behaviour of filaments, the phenomenon that the filament becomes stiffer when larger strains are applied (Block et al. 2015). In IF proteins desmin, vimentin, and keratin8/18 strain behaviour was absent in IF proteins lacking the tail-domain (Lin et al. 2010).

Alternative to differences in the IF network, another likely scenario is that distinct binding partners of GFAPα and GFAPδ underlie the downstream effects. The specific 41-42 amino acids of the C-terminus of the GFAP isoforms can lead to different protein-protein interactions in the tail region of the protein. It is known that GFAPδ has decreased affinity for other IF proteins and desmosomal proteins periplakin and envoplakin, but specifically binds to presenilin, a protein that is part of the γ-secretase complex (Nielsen and Jørgensen 2004). Additional screens for protein-protein interactions specific for the tail-region of the GFAP protein may help to further unravel the molecular mechanisms behind the phenotypes.

Lastly, although GFAP is mostly known as a cytosolic protein, there are indications that GFAP is present in the nucleus as well (Paulus and Roggendorf 1988). A predicted nuclear localisation signal is present both in the GFAP head domain, as well as in the GFAPα tail domain (Hobbs, Jacob, and Coulombe 2016). We have occasionally observed GFAP positivity in the nucleus of cells as well (Fig. 2c), although the aspecific binding of the primary antibody cannot be ruled out. The presence of GFAP in the nucleus would have implications for both the isoform-dependent and independent roles in invasion, as this would add another dimension to how GFAP can protect the nucleus from fragmentation or facilitate invasion. GFAPδ has been identified as a binding partner of transcription factor Sox2 (Senner, personal communication), direct interaction of the two proteins within the nucleus and the effect on transcription should be considered in future research.

1.5 The heterogeneous nature of GFAP and IF expression in gliomas

This thesis has largely focussed on the functional consequences of different GFAP protein compositions in the cell. However, an important question that remains is how endogenous expression levels of GFAP and other IF proteins are regulated. Initiation of invasion is often associated with changes in the IF network composition. Examples of this are the upregulation of keratin 14 in the invasive edge of breast cancer organoids (Cheung et al. 2013) and the enrichment of vimentin in cells protruding into the healing wound of lens epithelium (Menko et al. 2014). To investigate whether similar changes

in IF expression occur in glioma tissue, we performed an explorative study where we compared the IF expression levels in different parts of macroscopic grade IV tumours (Fig. 3a), using RNAseq data from the Ivy Glioblastoma Atlas Project (IGAP, https://glioblastoma.alleninstitute.org/). We indeed found that distinct regions of the tumour have significant differences in the expression levels of vimentin, GFAP, nestin, and lamin B2 (Fig. 3a). When comparing different regions, only vimentin was differentially expressed, with the most abundant expression in the infiltrating tumour region (Fig. 3b-d). This is in line with what is known about vimentin concerning epithelial to mesenchymal transition (Thiery et al. 2009; Mendez, Kojima, and Goldman 2010; Sharma et al. 2019) and what was observed in the healing lens epithelium (Menko et al. 2014). To further follow up on these results, we explored the protein expression levels of GFAP and vimentin in U3117-spheroids embedded in Matrigel (Fig. 3e). Here we also observed a clear enrichment of vimentin in the cells in the invasive margin (Fig. 3f,g). In comparison to vimentin, GFAP was more heterogeneously expressed throughout the tumour (Fig. 3f,g). Based on these findings, we have strong indications that localisation

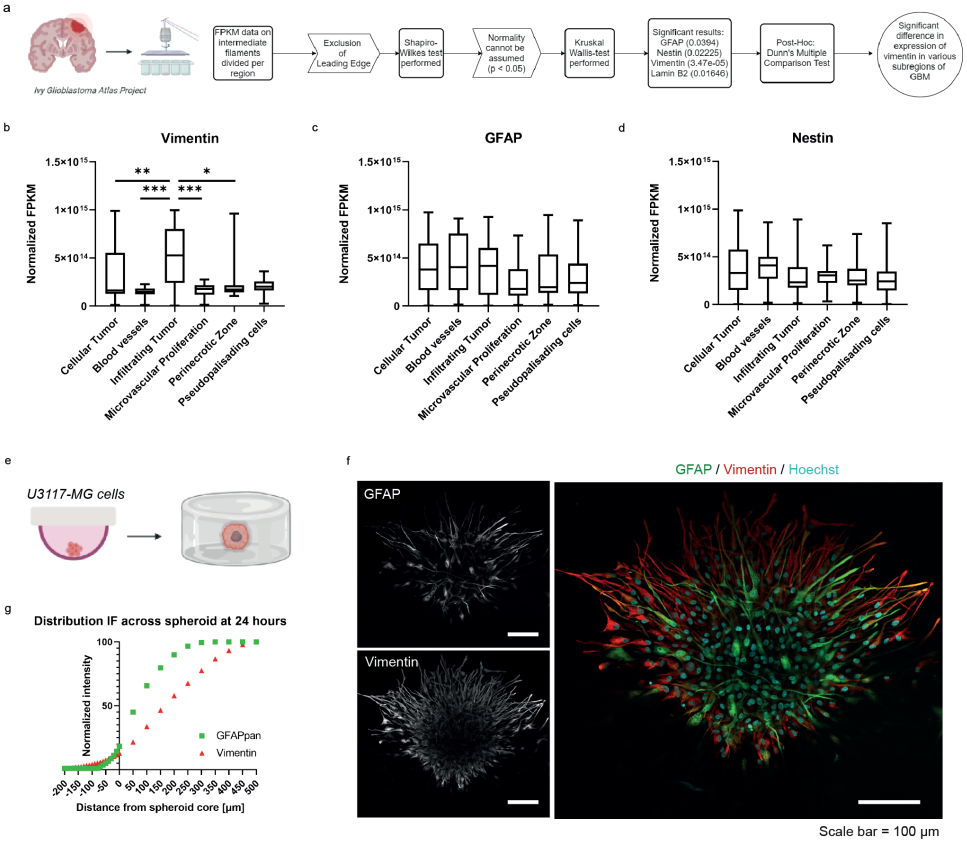

in the tumour drives the IF expression pattern. The observation that vimentin is mainly enriched in invading cells also has implications for the interpretation of the results from **Chapter 4**. As the integration of GFAPδ into the IF network of GFAPδ/α-high cells is dependent on vimentin (Nielsen and Jørgensen 2004), the phenotype we observe may be partially mediated through vimentin. The relation between vimentin and GFAPδ remains to be further investigated.

Another important question for future research is how GFAP isoforms are expressed in different regions of the tumour. Earlier studies performed by our group on tissue microarrays of grade IV glioma patients showed that tumour areas can contain regions with high and low GFAPδ/α ratio cells, indicating that there is high intratumoral heterogeneity (van Bodegraven, 2019a). Repeating this study on whole tumour sections would allow investigating whether GFAPδ/α ratio high and low populations are enriched in specific regions of the tumour. Particularly the GFAPδ/α ratio in hypoxic vs non-hypoxic areas should be examined. In **Chapter 4** we speculate that hypoxia may be a driving factor in the switch in GFAP alternative splicing. The hypoxic microenvironment is an important driver of glioma stem cell-like phenotypes (Colwell et al. 2017; Tejero et al. 2019) and has been linked to glioma aggressiveness and tumour invasiveness (Domènech et al. 2021; Wang et al. 2016; Huang et al. 2018). Recently it was discovered that hypoxia also drives an adult-to-foetal splicing transition through regulation muscle blind-like proteins (MBNL) (Voss et al. 2020), a splicing factor that also has predicted binding sites for GFAP (Paz et al. 2010, http://sfmap.technion.ac.il/). Given the enrichment of GFAPδ in the neurogenic niches of the brain (van den Berge et al. 2010; Roelofs et al. 2005), GFAPδ/α-high cells may represent a 'stem-cell-like', highly invasive population of glioma cells that are maintained within hypoxic niches of the tumour. The link between hypoxia and GFAP alternative splicing is thus a relevant lead to follow-up within the context of glioma biology.

<Figure 3. Intratumour heterogeneity of IF-expression (a) A schematic representation and the statistical pipeline for RNA-seq data obtained from the Ivy Glioblastoma Atlas Project (IGAP). FPKM normalised values of eight IFs from different microdissected anatomical regions of grade IV tumours were obtained from the web interface of the IGAP database (https://glioblastoma.alleninstitute.org/). 122 samples from 10 patients were included. Microdissected regions from the leading edge were excluded, as we expected contamination of the dataset with non-malignant cells based on the IF-expression levels. (b-d) Normalised FPKM values for Vimentin (b), GFAP (c) and Nestin (d). 'Blood vessels' stands for the hyperplastic blood vessels in the cellular tumour. Significance was determined using a Kruskal Wallis-test followed by Dunn's multiple comparisons test. (e) Schematic representation of the encapsulation of hanging drops derived from U3117-MG glioma cells in Matrigel. (f) Representative image of the distribution of GFAPpan and Vimentin in a 3117mg spheroid encapsulated in Matrigel fixated after 24 hours. (g) Normalised intensity of GFAP (green) and Vimentin (red) shown as distribution across the spheroid depicted in (f) 24 hours after encapsulation. X=0 refers to the rim of the core of the spheroid. All subsequent positive values refer to the leading edge of the spheroid and invaded cells, and negative values refer to the distribution of IFs within the core. Scale bar = 100 μm. All schematics are created with biorender.com. Figure is adapted from Master Thesis of Daria M. Fedorushkova, 2020.

2. Methodological considerations

In this thesis, we made use of glioma cell lines, genetic modification using Clustered Regularly Interspaces Short Palindromic Repeats (CRISPR)-Cas9, and invasion models to investigate the role of GFAP in glioma cell biology. In the next section of the general discussion, I will describe the strengths and weaknesses of the our experimental approaches.

2.1 Using CRISPR-Cas9 to regulate IF expression

The discovery of CRISPR-Cas9 has revolutionised the field of genome editing (Cong et al. 2013; Mali et al. 2013). Cas9 is a nuclease that is part of the adaptive immune system in bacteria and archaea. In combination with a single guide RNA (sgRNA), it recognises and cleaves complementary sequences that are adjacent to a protospacer adjacent motif (PAM) in the genome, providing a useful tool for specifically targeting genes of interest (Zhang, Wen, and Guo 2014). A common concern with the use of genome-editing tools is the risk of off-target effects. Off-target sequences in the genome that have high homology to the sgRNA used are at risk of being targeted by Cas9, leading to aspecific modifications of the genome (Doench et al. 2016). Although the predicted risk of off-target effects was taken into account in the selection of the sgRNAs used (Concordet and Haeussler 2018; Doench et al. 2016), we did not systematically test for off-target effects. However, as we use two different sets of sgRNAs in **Chapter 4**, we are confident that the effects we describe on cell invasion and migration persistence are not due to off-target effects. This is further strengthened by the fact that most of the results we found in **Chapter 1** and **Chapter 4** are replicated, albeit to a lesser extent, when the GFAPα transcript was silenced with the use of short hairpin RNAs (Moeton et al. 2014). In **Chapter 5** we have only used a single sgRNA to generate GFAP and Vim-KO cells, which is a limitation of this study. However, as the off-target scores of these sgRNAs were more beneficial, most likely as exons were targeted instead of introns, the changes that the effects we observe are due to off-target effects are lower.

Successful on-target nuclease activity of CRISPR-Cas9 leads to the generation of a double-strand break (DSB), which can be repaired by the DNA damage repair factors through nonhomologous end-joining (NHEJ) or homology-directed repair (HDR) (Zhang, Wen, and Guo 2014). In theory, the repair of DSB with NHEJ causes a single indel mutation leading to a frameshift, or a deletion of a predicted number of nucleotides between two adjacent sgRNA targets (Anzalone, Koblan, and Liu 2020). In practice, however, we have experienced that the mutations we created by using two sgRNA combinations were not always the mutations that we predicted. As an example, GFAPα-KO clones 3 and 4 had a shift of 10 nucleotides in the deleted region while using the same sgRNA combination (Chapter 4, Supp. Fig. 2). In addition,

we have detected cell lines in which a part of the deleted sequence was inverted and inserted back into the genome through HDR, and lines where a part of the plasmid was inserted into the deleted region. On-target mutagenesis after CRISPR-Cas9, like large deletions and complex genomic rearrangements, have been described in literature as well (Leibowitz et al. 2021; Kosicki, Tomberg, and Bradley 2018; Y. Lin et al. 2014), and this is important to consider in future studies where the IF network is targeted using CRISPR-Cas9 technology.

All in all, CRISPR-Cas9 is a useful tool to manipulate the IF network composition and GFAP isoform expression, but like all techniques, it has its limitations. The developments in the field of CRISPR-Cas9 technology are rapidly expanding (Anzalone, Koblan, and Liu 2020). More and more orthologs of natural occurring Cas9 nucleases are being discovered, each with its unique advantages (Gasiunas et al. 2020), and discovered nucleases are optimised to improve their efficiency (Kim et al. 2019). These alternatives to the more traditional Cas9 from *Streptococcus pyogenes* that was used in this thesis should be considered to improve the specificity or efficiency of targeting IF proteins or isoforms in the future. To regulate alternative splicing, an alternative approach is to use nucleases that target RNA instead of DNA, like the Cas13 family (Gootenberg et al. 2017; Konermann et al. 2018). Du and colleagues recently developed a system where Cas13d was coupled to splicing regulatory domains to regulate the splicing of the *SMN2* transcript (Du et al. 2020). A similar approach can be considered to regulate the splicing of the *GFAP* transcript to modify the GFAPδ/α ratio.

2.2 Glioma cell lines as experimental models for diffuse glioma

Most of the experiments described in this thesis have been performed in the U251-MG cell line. The U251-MG line originates from a 75-year old male glioma patient and was first published in 1968 (Pontén and Macintyre 1968). Since then, the cell line has been distributed to different laboratories around the world, making it one of the most commonly used experimental model for grade IV glioma to date (Li et al. 2017). There are some limitations to the use of the U251-MG cell line as a model for diffuse glioma. First of all, it is hypothesised that the long-term culture of these cells in serum has caused a loss of their 'stem cell-like' properties (Lee et al. 2006). In addition, important morphological features of grade IV glioma, like diffuse infiltration and microvascular proliferation, are not observed when these cells are injected into mouse models, and clinical characterisation of the original tumour is lacking (Xie et al. 2015). Therefore, within the field of neuro-oncology, there is a preference for the use of more recently established experimental models of patient-derived cells that have been cultured under serum-free conditions (Xie et al. 2015).

In this thesis, we have attempted to repeat the CRISPR-Cas9 experiments in

glioma experimental models from the Human Glioblastoma Cell Culture (HGCC) resource (www.hgcc.se), using the cell lines U3024-MG, U3088-MG and U3117-MG (Xie et al. 2015). Although we were successful in generating GFAPδ-KOs in the U3117-MG line, all other attempts to create GFAPδ-KOs and GFAPα-KOs were unsuccessful. In comparison to the U251-MG cells, we experienced lower survival rates of single cells after single-cell sorting and more difficulties in expanding single-cell clones into a large populations. This and the relatively low efficiency of creating large sequence deletions (+/- 870 nucleotides in GFAPα-KO) are most likely the explanations why were not able to repeat the CRISPR-Cas9 experiment in these cell lines. It has to be noted that we selected the three lines based on their earlier described non-infiltrative behaviour in *ex vivo* organotypic brain slices (Pencheva et al. 2017), as we wanted to test whether manipulating the GFAPδ/α-ratio would make these cells more invasive. Nevertheless, these attempts stress that certain experimental manipulations are more difficult in the newer experimental models of glioma, and show that we are still dependent on more robust cell models to answer certain biological questions.

2.3 Modelling glioma invasion

Traditional migration assays on flat rigid 2D surfaces do not mimic the cellular complexity and physiological and mechanical properties of the brain parenchyma in which glioma cells normally navigate (de Gooijer et al. 2018). As we found that regulation of GFAP expression affected cell-ECM interactions, we strived to use invasion models that closely mimic the cell- and ECM compositions of the brain. In **Chapter 3** we describe a protocol where we combine *ex vivo* organotypic slice cultures of mouse brains with whole-mount immunofluorescent imaging, to precisely visualise the 3D invasion patterns of glioma cells with confocal imaging. *Ex vivo* organotypic brain slices are commonly used in glioma research (Pencheva et al. 2017; De Boüard et al. 2002; Xu et al. 2016; S. Jung et al. 2002; Codega and Mellinghoff 2017), as they provide a more high throughput alternative to *in vivo* studies, whilst maintaining a relevant brain microenvironment (de Gooijer et al. 2018). The novel combination with whole-mount immunofluorescent staining allows high-resolution imaging of cells in the tumour core and the mouse brain tissue and is a successful strategy to systematically quantify the invasive capacities of glioma cells. Although *ex vivo* organotypic brain slices are a good model to study the invasive capacities of cells alongside existing structures of the brain, a limitation to the model is the viability of the mouse brain tissue. Native brain-resident cells lose viability throughout the culture period (Pencheva et al. 2017), making this model less suitable to study interactions between glioma and non-malignant brain cells. In **Chapter 4**, we, therefore, combine *ex vivo* organotypic brain slices with *in vivo* intravital microscopy. This *in vivo* model most closely resembles the native microenvironment of glioma cells, due to the functional vasculature and normal functioning cells (Margarido et al. 2020).

The intravital technique however has the disadvantage that highly specialised equipment and training is needed to perform these procedures. The combination of *ex vivo* brain slices and *in vivo* intravital imaging allowed us to quantify the invasive properties of multiple cell clones, and further diving into the short-term dynamics of a selection of them.

One disadvantage of both models is that human cells are studied in a murine context. For the *in vivo* studies, the use of human cells also means that immunocompromised mice have to be used (Okada, Vaeteewoottacharn, and Kariya 2019), therefore the native response of the immune system could not be investigated in **Chapter 4**. Cerebral organoid technologies can be used to study glioma cell invasion in a human tissue context (Joseph et al. 2021) and is increasingly applied in the last couple of years (Hubert et al. 2016; Linkous et al. 2019; Azzarelli 2020; Ogawa et al. 2018). An important limitation of this model is the lack of vascularisation of cerebral organoids, which limits the investigation of perivascular routes of invasion. The cerebral organoid field, however, is rapidly developing and vascularised organoids have been described (Mansour et al. 2018; Cakir et al. 2019). These vascularised organoids hold great potential for studying glioma invasion in the future.

At last, we combined *ex vivo* organotypic brain slice models with microfluidic devices that mimic tissue confinement in **Chapter 5**. Although these microfluidic devices are a simplification of the native conditions, they have the great benefit that the conditions are controllable and easily applicable for live-cell imaging studies (Davidson et al. 2015). A limitation, however, is the rigidity of the PDMS-pillars in the confined migration device. The brain parenchyma is one of the softest tissues in the body (Barnes, Przybyla, and Weaver 2017), therefore the PDMS confinements do not fully match the characteristics of tissue confinements in the brain. Nevertheless, as the nuclear fragmentation phenotype observed in these microfluidic devices was also observed in the *ex vivo* organotypic brain slices, we are confident that this phenotype is not an artefact of the microfluidic device confined migration model.

3. Clinical applications and considerations

Most of the thesis was focussed on fundamental questions regarding the role and relevance of GFAP in gliomas. In the last part of the thesis, I will focus more on the clinical questions and discuss the potential of GFAP as a diagnostic tool and a therapeutical target.

3.1 Investigating glioma invasion, why is it important?

The invasive characteristics of diffuse gliomas highly impact the malignancy of the disease (Claes, Idema, and Wesseling 2007). The formation of secondary tumours

is almost inevitable, and tumour recurrence contributes to the bad prognosis of the disease (Ho et al. 2014). Transcriptomic profiling and evolutionary branching of recurrent tumours suggest that relapse-associated clones already exist years before diagnosis (Wang et al. 2016). From a skeptical point of view, one can thus propose that studying the mechanisms behind glioma invasion is irrelevant concerning prolonging the life expectancy of a patient, as the therapeutical window to halt glioma invasion and avoid recurrence has long passed when the primary tumour is diagnosed. Although a better understanding of glioma invasion indeed might not lead to avoidance of tumour recurrence, there are still other reasons why studying glioma invasion is important. First and foremost, glioma invasion has a strong impact on the quality of life of patients. With the recent discovery that glioma cells can form functional synapses with neurons (Venkatesh et al. 2019; Venkataramani et al. 2019), it can be suggested that the cognitive deficits commonly associated with gliomas (Klein, Duffau, and De Witt Hamer 2012; van Kessel et al. 2017) are an indirect result of invaded glioma cells that disturb neuronal networks. Also, epileptic seizures can be potentially be explained by cell invasion (Venkataramani et al. 2020). Finding strategies to avoid glioma invasion may thus improve these clinical features of the disease, thereby positively impacting the quality of life. Second, a better understanding of the driving factors of glioma invasion may contribute to hampering the unwanted side-effects of current treatment strategies. As an example, an intravital imaging study from Alieva and colleagues showed that taking tumour biopsies can drive glioma invasion of the non-resected tumour cells. This stimulatory effect on migration is due to the inflammatory response induced by the biopsy and can be blocked by dexamethasone treatment (Alieva et al. 2017). Further investigation into pharmaceutical interventions or adjustment of surgical tools may help to avoid treatment-induced invasion in the future. Finally, hijacking glioma invasion can potentially be used as a treatment strategy. Jain and colleagues exploited the tendency of glioma cells to migrate along aligned fibres by inserting a nanofiber film in the vicinity of glioma cells in xenografted mice. Glioblastoma cells were found to migrate along these fibres into a hydrogel containing toxins, and this lead to a reduction in tumour volume (Jain et al. 2014). Altogether, these examples show that a better understanding about the causes, characteristics and consequences of glioma invasion is not only important from a fundamental point of view, but also from a clinical perspective.

3.2 Relevance of GFAP as a diagnostic tool and therapeutical target.

In **Chapter 6** we investigated the clinical relevance of alterations in the GFAP network by reviewing literature reporting on GFAP in body fluids of glioma patients. With a meta-analysis on all studies until April 2021 that measured the levels of serum GFAP (sGFAP) in samples of glioma patients of different grades and controls, we showed that the presence of sGFAP is specifically occurring in grade IV glioma patients, but

is not detected in all patients. Additional studies are needed to investigate whether the presence or levels sGFAP can be used as a diagnostic tool. It would be interesting to investigate whether sGFAP can be used to differentiate between high- and low-grade non-enhancing tumours. Non-enhancing tumours are typically associated with low-grade tumours, however, in 30-40% of the cases they turn out to be grade IV tumours, thereby leading to an underestimation of tumour aggressiveness (Hu et al. 2020). Also, the link between sGFAP levels and tumour volume is a promising lead to follow up on (Gállego Pérez-Larraya et al. 2014; Kiviniemi et al. 2015; Jung et al. 2007; Tichy et al. 2016). Thus, monitoring sGFAP levels in grade IV patients may prove to be relevant in the future.

An interesting direction for future studies is to investigate where the sGFAP is coming from and how it ends up in the blood circulation. For the source of sGFAP, the tumour cells themselves are the most likely candidates, however, it cannot be ruled out that reactive astrocytes are the source. An argument for the latter is the fact that sGFAP is also detected in patients with traumatic head injury (Shemilt et al. 2019). Assuming that glioma cells are the source of sGFAP, extracellular GFAP can be a result of necrosis or active secretion by tumour cells. In the systematic literature search performed in Chapter 6, we did identify studies that detected GFAP on the surface of microparticles and exosomes that were present in the blood of glioma patients (Sartori et al. 2013; Galbo et al. 2017), indicating that GFAP may also be expressed on the cell surface of glioma cells, similarly to cell surface expression of vimentin (Patteson et al. 2020). From a clinical point of view, surface expression of GFAP is an interesting phenomenon as it might pose a novel target for therapeutical interventions. Exploiting the surface-expression of IFs on tumour cells is not novel, as monoclonal antibodies against the ectodomain of vimentin (Pritumumab) are currently being applied in Phase I clinical trials (Babic et al. 2017), after demonstrating therapeutic benefit in patients with gliomas (Glassy and Hagiwara 2009). Also, nestin can be found on the surface of glioma stem cells (Jin et al. 2013). Exploiting cell surface expression of glioma-enriched IF proteins may be a novel strategy to locally deliver drugs to disseminated glioma cells.

4 Conclusion and future perspectives.

This thesis aimed to better understand the function and relevance of the GFAP protein in glioma biology. We have shown that GFAP plays a dual role in glioma cell invasion. First of all, we show that GFAP isoforms distinctively facilitate cell invasion into the brain parenchyma. In GFAPδ/α-high cells, increased dominance of GFAPδ leads to molecular alterations that equip cells to better infiltrate confined spaces using adhesion based migration modes. This includes 1) increased deposit of ECM proteins (laminin), 2) alterations in the expression of genes involved in ECM remodelling (MMPs and

A2M) and 3) alterations in the expression of genes that facilitate binding to the native and self-produced matrix (ITGA6, ITGA7, ITGB1). These molecular alterations lead to slow, but directional cell invasion into the brain parenchyma resulting in a diffuse growth pattern. A GFAPδ/α-low ratio on the other hand has the opposite effect on migration persistence. Cells with low GFAPδ/α ratios are highly motile, but migrate in a random fashion. In addition to facilitating specific forms of migration, GFAP protects the cell from migration induced nuclear and cellular damage in an isoform independent manner. On top of these functional roles of GFAP, we show that GFAP in serum is specifically elevated in grade IV patients, opening up avenues of research for GFAP as a serum biomarker.

The development and progression of diffuse gliomas are associated with many changes in the microenvironment of the brain parenchyma. The proliferating glioma mass, infiltrating immune cells, and the adaptive responses of the native non-malignant cells cause major changes in the chemical and physical characteristics of the affected brain region (Barnes, Przybyla, and Weaver 2017; Broekman et al. 2018). This is due to cytokine and chemokine release, but also due to cell compression, elevated fluid pressure and changes in the ECM composition (Barnes, Przybyla, and Weaver 2017; Broekman et al. 2018). Because of the mechanosensitive nature of the IF network (Gregor et al. 2014; Swift et al. 2013), we propose that the alterations in tissue mechanics affect the composition and organisation of the IF network in glioma cells. Additional factors, like hypoxia, or therapeutical interventions may further drive the altered expression levels of IF proteins and regulate alternative splicing of GFAP. We propose that these changes in IF protein composition help to adapt the glioma cell to the chemical- and or environmental needs of that specific environments and drive specific behaviours like cell invasion. Altogether, we propose that GFAP and other IF proteins play a major role in glioma cell-environment reciprocity, where environmental factors affect the composition and organisation of the IF network, and the IF network affects how a cell interacts with its environment (Fig. 4).

The role of GFAP and other IFs in cell-environment reciprocity is not only relevant for glioma, but also for normal brain development and other brain diseases. Expression and alternative splicing of GFAP and other IF proteins change throughout development within the different cell types (Middeldorp et al. 2010; Kirkcaldie and Dwyer 2017). As developmental programs are often hijacked in glioma (Neftel et al. 2019; Dirkse et al. 2019), a better understanding of the regulation and function of GFAP during normal brain development may also lead to relevant insights for glioma. Also, many neurological disorders are associated with changes in IF network composition, the best example being the overexpression of GFAP and vimentin in reactive gliosis (Hol and Pekny 2015). The role of IFs in cell-environment reciprocity likely plays a major role in these contexts as well.

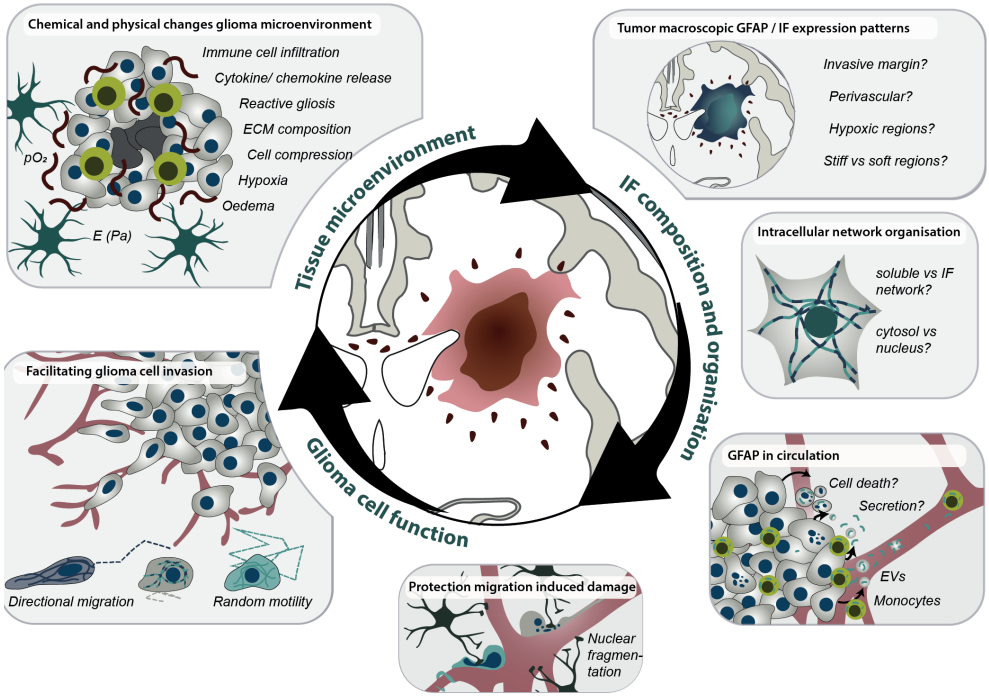

Figure 4. Intermediate filaments in the continuum of glioma cell-environment reciprocity. GFAPα or general GFAP is illustrated with lightblue, GFAPδ with darkblue. Abbreviations: ECM = extracellular matrix; E (Pa) = elastic modulus; EVs = extracellular vesicles; IF = intermediate filament; pO2 = tissue oxygen tension.

All in all, in our aim of getting a better grasp on GFAP in glioma, we discovered that GFAP is not only a marker to identify tumours of glial origin, but that it also plays a broad functional role in glioma behaviour, from regulating cell invasion to protecting the cell against migration inducted nuclear fragmentation.

References

Alieva, Maria, Verena Leidgens, Markus J. Riemenschneider, Christoph A. Klein, Peter Hau, and Jacco van Rheenen. 2019. "Intravital Imaging of Glioma Border Morphology Reveals Distinctive Cellular Dynamics and Contribution to Tumor Cell Invasion." *Scientific Reports* 9 (1): 1–11. https://doi.org/10.1038/s41598-019-38625-4.

Alieva, Maria, Andreia S. Margarido, Tamara Wieles, Erik R. Abels, Burcin Colak, Carla Boquetale, Herke Jan Noordmans, Tom J. Snijders, Marike L. Broekman, and Jacco van Rheenen. 2017. "Preventing Inflammation Inhibits Biopsy-Mediated Changes in Tumor Cell Behavior." *Scientific Reports* 7 (1): 7529. https://doi.org/10.1038/s41598-017-07660-4.

Anzalone, Andrew V., Luke W. Koblan, and David R. Liu. 2020. "Genome Editing with CRISPR–Cas Nucleases, Base Editors, Transposases and Prime Editors." *Nature Biotechnology* 38 (7): 824–44. https://doi.org/10.1038/s41587-020-0561-9.

Azzarelli, Roberta. 2020. "Organoid Models of Glioblastoma to Study Brain Tumor Stem Cells." *Frontiers in Cell and Developmental Biology* 8 (April): 1–9. https://doi.org/10.3389/fcell.2020.00220.

Babic, Ivan, Elmar Nurmemmedov, Venkata M. Yenugonda, Tiffany Juarez, Natsuko Nomura, Sandeep C. Pingle, Mark C. Glassy, and Santosh Kesari. 2017. "Pritumumab, the First Therapeutic Antibody for Glioma Patients." *Human Antibodies* 26 (2): 95–101. https://doi.org/10.3233/HAB-170326.

Barnes, J. Matthew, Laralynne Przybyla, and Valerie M. Weaver. 2017. "Tissue Mechanics Regulate Brain Development, Homeostasis and Disease." *Journal of Cell Science* 130 (1): 71–82. https://doi.org/10.1242/jcs.191742.

Berge, Simone A. van den, Jinte Middeldorp, C. Eleana Zhang, Maurice A. Curtis, Brian W. Leonard, Diego Mastroeni, Pieter Voorn, Wilma D.J. van de Berg, Inge Huitinga, and Elly M. Hol. 2010. "Longterm Quiescent Cells in the Aged Human Subventricular Neurogenic System Specifically Express GFAP-δ." *Aging Cell* 9 (3): 313–26. https://doi.org/10.1111/j.1474-9726.2010.00556.x.

Blanchoin, Laurent, Rajaa Boujemaa-Paterski, Cécile Sykes, and Julie Plastino. 2014. "Actin Dynamics, Architecture, and Mechanics in Cell Motility." *Physiological Reviews* 94 (1): 235–63. https://doi.org/10.1152/physrev.00018.2013.

Blikstad, I., and E. Lazarides. 1983. "Vimentin Filaments Are Assembled from a Soluble Precursor in Avian Erythroid Cells." *Journal of Cell Biology* 96 (6): 1803–8. https://doi.org/10.1083/jcb.96.6.1803.

Block, Johanna, Viktor Schroeder, Paul Pawelzyk, Norbert Willenbacher, and Sarah Köster. 2015. "Physical Properties of Cytoplasmic Intermediate Filaments." *Biochimica et Biophysica Acta* (*BBA) - Molecular Cell Research* 1853 (11): 3053–64. https://doi.org/10.1016/j.bbamcr.2015.05.009.

Bodegraven, Emma J. van. 2021. "Intermediate Filaments from Tissue Integrity to Single Molecule Mechanics." *Cells*, *10*(8), 1905. https://doi.org/10.3390/cells10081905

Bodegraven, Emma J. van. 2019a. "GFAP revisited - From biomarker to an isoform-specific function in glioma malignancy." PhD thesis. Utrecht University.

Bodegraven, Emma J. van, Jessy V. van Asperen, Pierre A.J. Robe, and Elly M. Hol. 2019b. "Importance of GFAP Isoform-Specific Analyses in Astrocytoma." *Glia* 67 (8): 1417–33. https://doi.org/10.1002/glia.23594.

Boüard, Sophie De, Christo Christov, Jean Sébastien Guillamo, Lina Kassar-Duchossoy, Stéphane Palfi, Caroline Leguerinel, Michel Masset, Odile Cohen-Hagenauer, Marc Peschanski, and Thierry Lefrançois. 2002. "Invasion of Human Glioma Biopsy Specimens in Cultures of Rodent Brain Slices: A Quantitative Analysis." *Journal of Neurosurgery* 97 (1): 169–76. https://doi.org/10.3171/jns.2002.97.1.0169.

Broekman, Marike L., Sybren L. N. Maas, Erik R. Abels, Thorsten R. Mempel, Anna M. Krichevsky, and Xandra O. Breakefield. 2018. "Multidimensional Communication in the Microenvirons of Glioblastoma." *Nature Reviews Neurology* 14 (8): 482-495. https://doi.org/10.1038/s41582-018-0025-8.

Cakir, Bilal, Yangfei Xiang, Yoshiaki Tanaka, Mehmet H. Kural, Maxime Parent, Young Jin Kang, Kayley Chapeton, et al. 2019. "Engineering of Human Brain Organoids with a Functional Vascular-like System." *Nature Methods* 16 (11): 1169–75. https://doi.org/10.1038/s41592-019-0586-5.

Cheung, Kevin J., Edward Gabrielson, Zena Werb, and Andrew J. Ewald. 2013. "Collective Invasion in Breast Cancer Requires a Conserved Basal Epithelial Program." *Cell* 155 (7): 1639–51. https://doi.org/10.1016/j.cell.2013.11.029.

Chung, Byung-min, Jeremy D Rotty, and Pierre A Coulombe. 2013. "Networking Galore : Intermediate Filaments and Cell Migration." *Current Opinion in Cell Biology* 25 (5): 600–612. https://doi.org/10.1016/j.ceb.2013.06.008.

Cillekens, J. M.J., J. A.M. Beliën, P. Van Der Valk, T. J.C. Faes, P. J. Van Diest, M. A.M. Broeckaert, J. H. Kralendonk, and W. Kamphorst. 2000. "A Histopathological Contribution to Supratentorial Glioma

Grading, Definition of Mixed Gliomas and Recognition of Low Grade Glioma with Rosenthal Fibers." *Journal of Neuro-Oncology* 46 (1): 23–43. https://doi.org/10.1023/A:1006496328729.

Claes, An, Albert J. Idema, and Pieter Wesseling. 2007. "Diffuse Glioma Growth: A Guerilla War." *Acta Neuropathologica* 114 (5): 443–58. https://doi.org/10.1007/s00401-007-0293-7.

Codega, Paolo, and Ingo K. Mellinghoff. 2017. "Dissecting Glioma Invasiveness in a 3D-Organotypic Model." *Trends in Molecular* Medicine 23(9), 776-777. https://doi.org/10.1016/j.molmed.2017.07.009.

Çolakoglu, Gülsen, and Anthony Brown. 2009. "Intermediate Filaments Exchange Subunits along Their Length and Elongate by End-to-End Annealing." *Journal of Cell Biology* 185 (5): 769–77. https://doi.org/10.1083/jcb.200809166.

Colwell, Nicole, Mioara Larion, Amber J. Giles, Ashlee N. Seldomridge, Saman Sizdahkhani, Mark R. Gilbert, and Deric M. Park. 2017. "Hypoxia in the Glioblastoma Microenvironment: Shaping the Phenotype of Cancer Stem-like Cells." *Neuro-Oncology* 19 (7): 887–96. https://doi.org/10.1093/neuonc/now258.

Concordet, Jean Paul, and Maximilian Haeussler. 2018. "CRISPOR: Intuitive Guide Selection for CRISPR/Cas9 Genome Editing Experiments and Screens." *Nucleic Acids Research* 46 (W1): W242–45. https://doi.org/10.1093/nar/gky354.

Cong, L., Ran, F.A., Cox, D., Lin, S., Barretto, R., Habib, N., Hsu, P.D., Wu, X., Jiang, W., Marraffini, L.A. 2013. "Multiplex Genome Engineering Using CRISPR/Cas Systems," *Science* 339(6121), 819-823. DOI: 10.1126/science.1231143

Cuddapah, Vishnu Anand, Stefanie Robel, Stacey Watkins, and Harald Sontheimer. 2014. "A Neurocentric Perspective on Glioma Invasion." *Nature Reviews. Neuroscience* 15 (7): 455–65. https://doi.org/10.1038/nrn3765.

Davidson, Patricia M., Celine Denais, Maya C. Bakshi, and Jan Lammerding. 2014. "Nuclear Deformability Constitutes a Rate-Limiting Step during Cell Migration in 3-D Environments." *Cellular and Molecular Bioengineering* 7 (3): 293–306. https://doi.org/10.1007/s12195-014-0342-y.

Davidson, Patricia M., Josiah Sliz, Philipp Isermann, Celine Denais, and Jan Lammerding. 2015. "Design of a Microfluidic Device to Quantify Dynamic Intra-Nuclear Deformation during Cell Migration through Confining Environments." *Integrative Biology* 7 (12): 1534–46. https://doi.org/10.1039/c5ib00200a.

Denais, Celine M., Rachel M. Gilbert, Philipp Isermann, Alexandra L. McGregor, Mariska Te Lindert, Bettina Weigelin, Patricia M. Davidson, Peter Friedl, Katarina Wolf, and Jan Lammerding. 2016. "Nuclear Envelope Rupture and Repair during Cancer Cell Migration." *Science* 352 (6283): 353–58. https://doi.org/10.1126/science.aad7297.

Dhruv, Harshil D., Wendy S. McDonough Winslow, Brock Armstrong, Serdar Tuncali, Jenny Eschbacher, Kerri Kislin, Joseph C. Loftus, Nhan L. Tran, and Michael E. Berens. 2013. "Reciprocal Activation of Transcription Factors Underlies the Dichotomy between Proliferation and Invasion of Glioma Cells." *PLoS ONE* 8 (8). https://doi.org/10.1371/journal.pone.0072134.

Dirkse, Anne, Anna Golebiewska, Thomas Buder, Petr V. Nazarov, Arnaud Muller, Suresh Poovathingal, Nicolaas H.C. Brons, et al. 2019. "Stem Cell-Associated Heterogeneity in Glioblastoma Results from Intrinsic Tumor Plasticity Shaped by the Microenvironment." *Nature Communications* 10 (1): 1–16. https://doi.org/10.1038/s41467-019-09853-z.

Doench, John G., Nicolo Fusi, Meagan Sullender, Mudra Hegde, Emma W. Vaimberg, Katherine F. Donovan, Ian Smith, et al. 2016. "Optimized SgRNA Design to Maximize Activity and Minimize Off-Target Effects of CRISPR-Cas9." *Nature Biotechnology* 34 (2): 184–91. https://doi.org/10.1038/nbt.3437.

Domènech, Marta, Ainhoa Hernández, Andrea Plaja, Eva Martínez-Balibrea, and Carmen Balañà. 2021. "Hypoxia: The Cornerstone of Glioblastoma." *International Journal of Molecular Sciences* 22 (22).

https://doi.org/10.3390/ijms222212608.

Doyle, Andrew D., and Kenneth M. Yamada. 2016. "Mechanosensing via Cell-Matrix Adhesions in 3D Microenvironments." *Experimental Cell Research* 343 (1): 60–66. https://doi.org/10.1016/j.yexcr.2015.10.033.

Du, Menghan, Nathaniel Jillette, Jacqueline Jufen Zhu, Sheng Li, and Albert Wu Cheng. 2020. "CRISPR Artificial Splicing Factors." *Nature Communications* 11 (1): 1–11. https://doi.org/10.1038/s41467-020-16806-4.

Dupin, Isabelle, Yasuhisa Sakamoto, and Sandrine Etienne-Manneville. 2011. "Cytoplasmic Intermediate Filaments Mediate Actin-Driven Positioning of the Nucleus." *Journal of Cell Science* 124 (6): 865–72. https://doi.org/10.1242/jcs.076356.

Elosegui-Artola, Alberto, Roger Oria, Yunfeng Chen, Anita Kosmalska, Carlos Pérez-González, Natalia Castro, Cheng Zhu, Xavier Trepat, and Pere Roca-Cusachs. 2016. "Mechanical Regulation of a Molecular Clutch Defines Force Transmission and Transduction in Response to Matrix Rigidity." *Nature Cell Biology* 18 (5): 540–48. https://doi.org/10.1038/ncb3336.

Farin A, Suzuki SO, Weiker M, Goldman JE, Bruce JN, Canoll P. 2006. "Transplanted Glioma Cells Migrate and Proliferate on Host Brain Vasculature: A Dynamic Analysis." *Glia*, *53*(8), 799-808.. https://doi.org/10.1002/glia

Galbo, Phillip M, Michael J Ciesielski, Sheila Figel, Orla Maguire, Jingxin Qiu, Laura Wiltsie, Hans Minderman, and Robert A Fenstermaker. 2017. "Circulating CD9+/GFAP+/Survivin+ Exosomes in Malignant Glioma Patients Following Survivin Vaccination." *Oncotarget* 8 (70): 114722–35. https://www.ncbi.nlm.nih.gov/pubmed/29383115.

Gállego Pérez-Larraya, Jaime, Sophie Paris, Ahmed Idbaih, Caroline Dehais, Florence Laigle-Donadey, Soledad Navarro, Laurent Capelle, et al. 2014. "Diagnostic and Prognostic Value of Preoperative Combined GFAP, IGFBP-2, and YKL-40 Plasma Levels in Patients with Glioblastoma." *Cancer* 120 (24): 3972–80. https://doi.org/10.1002/cncr.28949.

Gasiunas, Giedrius, Joshua K. Young, Tautvydas Karvelis, Darius Kazlauskas, Tomas Urbaitis, Monika Jasnauskaite, Mantvyda M. Grusyte, et al. 2020. "A Catalogue of Biochemically Diverse CRISPR-Cas9 Orthologs." *Nature Communications* 11 (1). https://doi.org/10.1038/s41467-020-19344-1.

Gilles, Christine, Myriam Polette, Jean Marie Zahm, Jean Marie Tournier, Laure Volders, Jean Michel Foidart, and Philippe Birembaut. 1999. "Vimentin Contributes to Human Mammary Epithelial Cell Migration." *Journal of Cell Science* 112 (24): 4615–25. https://doi.org/10.1242/jcs.112.24.4615.

Glassy, Mark C., and Hideaki Hagiwara. 2009. "Summary Analysis of the Pre-Clinical and Clinical Results of Brain Tumor Patients Treated with Pritumumab." *Human Antibodies* 18 (4): 127–37. https://doi.org/10.3233/HAB-2009-0209.

Gooijer, Mark C. de, Miriam Guillén Navarro, Rene Bernards, Thomas Wurdinger, and Olaf van Tellingen. 2018. "An Experimenter's Guide to Glioblastoma Invasion Pathways." *Trends in Molecular Medicine* 24 (9): 763–80. https://doi.org/10.1016/j.molmed.2018.07.003.

Gootenberg, Jonathan S., Omar O. Abudayyeh, Jeong Wook Lee, Patrick Essletzbichler, Aaron J. Dy, Julia Joung, Vanessa Verdine, et al. 2017. "Nucleic Acid Detection with CRISPR-Cas13a/C2c2." *Science* 356 (6336): 438–42. https://doi.org/10.1126/science.aam9321.

Gregor, Martin, Selma Osmanagic-Myers, Gerald Burgstaller, Michael Wolfram, Irmgard Fischer, Gernot Walko, Guenter P. Resch, Almut Jörgl, Harald Herrmann, and Gerhard Wiche. 2014. "Mechanosensing through Focal Adhesion-Anchored Intermediate Filaments." *FASEB Journal* 28 (2): 715–29. https://doi.org/10.1096/fj.13-231829.

Hagemann, Tracy L. 2022. "Alexander Disease: Models, Mechanisms, and Medicine." *Current Opinion in Neurobiology* 72: 140–47. https://doi.org/10.1016/j.conb.2021.10.002.

Hanus, Jakub, Magdalena Kalinowska-Herok, and Piotr Widlak. 2010. "Identification of Novel Putative

Regulators of the Major Apoptotic Nuclease DNA Fragmentation Factor." *Acta Biochimica Polonica* 57 (4): 521–27. https://doi.org/10.18388/abp.2010_2438.

Harada, Takamasa, Joe Swift, Jerome Irianto, Jae-won Shin, Kyle R Spinler, Avathamsa Athirasala, Rocky Diegmiller, P C Dave P Dingal, Irena L Ivanovska, and Dennis E Discher. 2014. "But Softness Can Limit Survival" 204 (5): 669–82. https://doi.org/10.1083/jcb.201308029.

Helvert, Sjoerd Van, Cornelis Storm, and Peter Friedl. 2018. "Mechanoreciprocity in Cell Migration." *Nature Cell Biology* 20 (1): 8–20. https://doi.org/10.1038/s41556-017-0012-0.

Ho, Vincent K.Y., Jaap C. Reijneveld, Roelien H. Enting, Henri P. Bienfait, Pierre Robe, Brigitta G. Baumert, and Otto Visser. 2014. "Changing Incidence and Improved Survival of Gliomas." *European Journal of Cancer* 50 (13): 2309–18. https://doi.org/10.1016/j.ejca.2014.05.019.

Hobbs, Ryan P., Justin T. Jacob, and Pierre A. Coulombe. 2016. "Keratins Are Going Nuclear." *Developmental Cell* 38 (3): 227–33. https://doi.org/10.1016/j.devcel.2016.07.022.

Hol, Elly M., and Milos Pekny. 2015. "Glial Fibrillary Acidic Protein (GFAP) and the Astrocyte Intermediate Filament System in Diseases of the Central Nervous System." *Current Opinion in Cell Biology* 32: 121–30. https://doi.org/10.1016/j.ceb.2015.02.004.

Hu, Leland S, Andrea Hawkins-Daarud, Lujia Wang, Jing Li, and Kristin R Swanson. 2020. "Imaging of Intratumoral Heterogeneity in High-Grade Glioma." *Cancer Letters* 477: 97–106. https://doi.org/10.1016/j.canlet.2020.02.025

Huang, Weiyi, Xiaopeng Ding, Hanbing Ye, Jingying Wang, Junfei Shao, and Tao Huang. 2018. "Hypoxia Enhances the Migration and Invasion of Human Glioblastoma U87 Cells through PI3K/Akt/MTOR/HIF-1α Pathway." *NeuroReport* 29 (18): 1578–85. https://doi.org/10.1097/WNR.0000000000001156.

Hubert, Christopher G., Maricruz Rivera, Lisa C. Spangler, Qiulian Wu, Stephen C. Mack, Briana C. Prager, Marta Couce, Roger E. McLendon, Andrew E. Sloan, and Jeremy N. Rich. 2016. "A Three-Dimensional Organoid Culture System Derived from Human Glioblastomas Recapitulates the Hypoxic Gradients and Cancer Stem Cell Heterogeneity of Tumors Found in Vivo." *Cancer Research* 76 (8): 2465–77. https://doi.org/10.1158/0008-5472.CAN-15-2402.

Ivaska, Johanna, Hanna Mari Pallari, Jonna Nevo, and John E. Eriksson. 2007. "Novel Functions of Vimentin in Cell Adhesion, Migration, and Signaling." *Experimental Cell Research* 313 (10): 2050–62. https://doi.org/10.1016/j.yexcr.2007.03.040.

Jain, Anjana, Martha Betancur, Gaurangkumar D. Patel, Chandra M. Valmikinathan, Vivek J. Mukhatyar, Ajit Vakharia, S. Balakrishna Pai, Barunashish Brahma, Tobey J. MacDonald, and Ravi V. Bellamkonda. 2014. "Guiding Intracortical Brain Tumour Cells to an Extracortical Cytotoxic Hydrogel Using Aligned Polymeric Nanofibres." *Nature Materials* 13 (3): 308–16. https://doi.org/10.1038/nmat3878.

Jin, Xiong, Xun Jin, Ji Eun Jung, Samuel Beck, and Hyunggee Kim. 2013. "Cell Surface Nestin Is a Biomarker for Glioma Stem Cells." *Biochemical and Biophysical Research Communications* 433 (4): 496–501. https://doi.org/10.1016/j.bbrc.2013.03.021.

Joseph, Justin V., Mathilde S. Blaavand, Thomas Daubon, Frank AE Kruyt, and Martin K. Thomsen. 2021. "Three-Dimensional Culture Models to Study Glioblastoma — Current Trends and Future Perspectives." *Current Opinion in Pharmacology* 61: 91–97. https://doi.org/10.1016/j.coph.2021.08.019.

Juliano, Joseph, Orlando Gil, Andrea Hawkins-Daarud, Sonal Noticewala, Russell C. Rockne, Jill Gallaher, Susan Christine Massey, et al. 2018. "Comparative Dynamics of Microglial and Glioma Cell Motility at the Infiltrative Margin of Brain Tumours." *Journal of the Royal Society Interface* 15 (139). https://doi.org/10.1098/rsif.2017.0582.

Jung, C. S., C. Foerch, A. Schänzer, A. Heck, K. H. Plate, V. Seifert, H. Steinmetz, A. Raabe, and M. Sitzer. 2007. "Serum GFAP Is a Diagnostic Marker for Glioblastoma Multiforme." *Brain* 130 (12): 3336–41. https://doi.org/10.1093/brain/awm263.

Jung, Shin, Hyun Woo Kim, Je Hyuk Lee, Sam Suk Kang, Hyang Hwa Rhu, Young Il Jeong, Soo Yeon Yang, et al. 2002. "Brain Tumor Invasion Model System Using Organotypic Brain-Slice Culture as an Alternative to in Vivo Model." *Journal of Cancer Research and Clinical Oncology* 128 (9): 469–76. https://doi.org/10.1007/s00432-002-0366-x.

Kessel, Emma van, Anniek E. Baumfalk, Martine J.E. van Zandvoort, Pierre A. Robe, and Tom J. Snijders. 2017. "Tumor-Related Neurocognitive Dysfunction in Patients with Diffuse Glioma: A Systematic Review of Neurocognitive Functioning Prior to Anti-Tumor Treatment." *Journal of Neuro-Oncology* 134 (1): 9–18. https://doi.org/10.1007/s11060-017-2503-z.

Kim, Daesik, Kevin Luk, Scot A. Wolfe, and Jin Soo Kim. 2019. "Evaluating and Enhancing Target Specificity of Gene-Editing Nucleases and Deaminases." *Annual Review of Biochemistry* 88: 191–220. https://doi.org/10.1146/annurev-biochem-013118-111730.

Kirkcaldie, Matthew T.K., and Samuel T. Dwyer. 2017. "The Third Wave: Intermediate Filaments in the Maturing Nervous System." *Molecular and Cellular Neuroscience* 84, 68-76. https://doi.org/10.1016/j.mcn.2017.05.010.

Kiviniemi, Aida, Maria Gardberg, Janek Frantzén, Riitta Parkkola, Ville Vuorinen, Marko Pesola, and Heikki Minn. 2015. "Serum Levels of GFAP and EGFR in Primary and Recurrent High-Grade Gliomas: Correlation to Tumor Volume, Molecular Markers, and Progression-Free Survival." *Journal of Neuro-Oncology* 124 (2): 237–45. https://doi.org/10.1007/s11060-015-1829-7.

Klein, Martin, Hugues Duffau, and Philip C. De Witt Hamer. 2012. "Cognition and Resective Surgery for Diffuse Infiltrative Glioma: An Overview." *Journal of Neuro-Oncology* 108 (2): 309–18. https://doi.org/10.1007/s11060-012-0811-x.

Konermann, Silvana, Peter Lotfy, Nicholas J. Brideau, Jennifer Oki, Maxim N. Shokhirev, and Patrick D. Hsu. 2018. "Transcriptome Engineering with RNA-Targeting Type VI-D CRISPR Effectors." *Cell* 173 (3): 665-676.e14. https://doi.org/10.1016/j.cell.2018.02.033.

Kosicki, Michael, Kärt Tomberg, and Allan Bradley. 2018. "Repair of Double-Strand Breaks Induced by CRISPR–Cas9 Leads to Large Deletions and Complex Rearrangements." *Nature Biotechnology* 36 (8). https://doi.org/10.1038/nbt.4192.

Leduc, Cécile, and Sandrine Etienne-Manneville. 2015. "Intermediate Filaments in Cell Migration and Invasion: The Unusual Suspects." *Current Opinion in Cell Biology* 32: 102–12. https://doi.org/10.1016/j.ceb.2015.01.005.

Lee, Jeongwu, Svetlana Kotliarova, Yuri Kotliarov, Aiguo Li, Qin Su, Nicholas M. Donin, Sandra Pastorino, et al. 2006. "Tumor Stem Cells Derived from Glioblastomas Cultured in BFGF and EGF More Closely Mirror the Phenotype and Genotype of Primary Tumors than Do Serum-Cultured Cell Lines." *Cancer Cell* 9 (5): 391–403. https://doi.org/10.1016/j.ccr.2006.03.030.

Leibowitz, Mitchell L., Stamatis Papathanasiou, Phillip A. Doerfler, Logan J. Blaine, Lili Sun, Yu Yao, Cheng Zhong Zhang, Mitchell J. Weiss, and David Pellman. 2021. "Chromothripsis as an On-Target Consequence of CRISPR–Cas9 Genome Editing." *Nature Genetics* 53 (6): 895–905. https://doi.org/10.1038/s41588-021-00838-7.

Lepekhin, Eugene A., Camilla Eliasson, Claes Henric Berthold, Vladimir Berezin, Elisabeth Bock, and Milos Pekny. 2001. "Intermediate Filaments Regulate Astrocyte Motility." *Journal of Neurochemistry* 79 (3): 617–25. https://doi.org/10.1046/j.1471-4159.2001.00595.x.

Li, Hezhen, Bingxi Lei, Wei Xiang, Hai Wang, Wenfeng Feng, Yawei Liu, and Songtao Qi. 2017. "Differences in Protein Expression between the U251 and U87 Cell Lines." *Turkish Neurosurgery* 27 (6): 894–903. https://doi.org/10.5137/1019-5149.JTN.17746-16.1.

Lin, Yanni, Thomas J. Cradick, Matthew T. Brown, Harshavardhan Deshmukh, Piyush Ranjan, Neha Sarode, Brian M. Wile, Paula M. Vertino, Frank J. Stewart, and Gang Bao. 2014. "CRISPR/Cas9 Systems Have off-Target Activity with Insertions or Deletions between Target DNA and Guide RNA Sequences." *Nucleic Acids Research* 42 (11): 7473–85. https://doi.org/10.1093/nar/gku402.

Lin, Yi Chia, Norman Y. Yao, Chase P. Broedersz, Harald Herrmann, Fred C. MacKintosh, and David A. Weitz. 2010. "Origins of Elasticity in Intermediate Filament Networks." *Physical Review Letters* 104 (5): 1–4. https://doi.org/10.1103/PhysRevLett.104.058101.

Linkous, Amanda, Demosthenes Balamatsias, Matija Snuderl, Lincoln Edwards, Ken Miyaguchi, Teresa Milner, Batsheva Reich, et al. 2019. "Modeling Patient-Derived Glioblastoma with Cerebral Organoids." *Cell Reports* 26 (12): 3203-3211.e5. https://doi.org/10.1016/j.celrep.2019.02.063.

Mali, Prashant, Luhan Yang, Kevin M. Esvelt, John Aach, Marc Guell, James E. DiCarlo, Julie E. Norville, and George M. Church. 2013. "RNA-Guided Human Genome Engineering via Cas9." *Science* 339 (6121): 823–26. https://doi.org/10.1126/science.1232033.

Mansour, Abed Alfatah, J. Tiago Gonçalves, Cooper W. Bloyd, Hao Li, Sarah Fernandes, Daphne Quang, Stephen Johnston, Sarah L. Parylak, Xin Jin, and Fred H. Gage. 2018. "An in Vivo Model of Functional and Vascularized Human Brain Organoids." *Nature Biotechnology* 36 (5): 432–41. https://doi.org/10.1038/nbt.4127.

Margarido, Andreia S., Laura Bornes, Claire Vennin, and Jacco van Rheenen. 2020. "Cellular Plasticity during Metastasis: New Insights Provided by Intravital Microscopy." *Cold Spring Harbor Perspectives in Medicine* 10 (11): 1–21. https://doi.org/10.1101/cshperspect.a037267.

Mayor, Roberto, and Sandrine Etienne-Manneville. 2016. "The Front and Rear of Collective Cell Migration." *Nature Reviews Molecular Cell Biology* 17 (2): 97–109. https://doi.org/10.1038/nrm.2015.14.

McGregor, Alexandra Lynn, Chieh Ren Hsia, and Jan Lammerding. 2016. "Squish and Squeeze - the Nucleus as a Physical Barrier during Migration in Confined Environments." *Current Opinion in Cell Biology* 40: 32–40. https://doi.org/10.1016/j.ceb.2016.01.011.

Mendez, Melissa G, Shin-Ichiro Kojima, and Robert D Goldman. 2010. "Vimentin Induces Changes in Cell Shape, Motility, and Adhesion during the Epithelial to Mesenchymal Transition." *FASEB Journal : Official Publication of the Federation of American Societies for Experimental Biology* 24 (6): 1838–51. https://doi.org/10.1096/fj.09-151639.

Menet, Véronique, Minerva Giménez Y Ribotta, Norbert Chauvet, Marie Jeanne Drian, Julie Lannoy, Emma Colucci-Guyon, and Alain Privat. 2001. "Inactivation of the Glial Fibrillary Acidic Protein Gene, but Not That of Vimentin, Improves Neuronal Survival and Neurite Growth by Modifying Adhesion Molecule Expression." *Journal of Neuroscience* 21 (16): 6147–58. https://doi.org/10.1523/jneurosci.21-16-06147.2001.

Menko, A. S., B. M. Bleaken, A. A. Libowitz, L. Zhang, M. A. Stepp, and J. L. Walker. 2014. "A Central Role for Vimentin in Regulating Repair Function during Healing of the Lens Epithelium." *Molecular Biology of the Cell* 25 (6): 776–90. https://doi.org/10.1091/mbc.E12-12-0900.

Middeldorp, Jinte, Karin Boer, Jacqueline A. Sluijs, Lidia De Filippis, Férechté Encha-Razavi, Angelo L. Vescovi, Dick F. Swaab, Eleonora Aronica, and Elly M. Hol. 2010. "GFAPδ in Radial Glia and Subventricular Zone Progenitors in the Developing Human Cortex." *Development* 137 (2): 313–21. https://doi.org/10.1242/dev.041632.

Moeton, Martina, Regina Kanski, Oscar M J A Stassen, Jacqueline A. Sluijs, Dirk Geerts, Paula Van Tijn, Gerhard Wiche, Miriam E. Van Strien, and Elly M. Hol. 2014. "Silencing GFAP Isoforms in Astrocytoma Cells Disturbs Laminin-Dependent Motility and Cell Adhesion." *FASEB Journal* 28 (7): 2942–54. https://doi.org/10.1096/fj.13-245837.

Moeton, Martina, Oscar M J A Stassen, Jacqueline A. Sluijs, Vincent W N van der Meer, Liselot J. Kluivers, Hedde van Hoorn, Thomas Schmidt, Eric A J Reits, Miriam E. van Strien, and Elly M. Hol. 2016. "GFAP Isoforms Control Intermediate Filament Network Dynamics, Cell Morphology, and Focal Adhesions." *Cellular and Molecular Life Sciences* 73 (21): 4101–20. https://doi.org/10.1007/s00018-016-2239-5.

Murray, Maria E., Melissa G. Mendez, and Paul A. Janmey. 2014. "Substrate Stiffness Regulates Solubility of Cellular Vimentin." *Molecular Biology of the Cell* 25 (1): 87–94. https://doi.org/10.1091/mbc.E13-

06-0326.

Nader, Guilherme Pedreira de Freitas, Sonia Agüera-Gonzalez, Fiona Routet, Matthieu Gratia, Mathieu Maurin, Valeria Cancila, Clotilde Cadart, et al. 2021. "Compromised Nuclear Envelope Integrity Drives TREX1-Dependent DNA Damage and Tumor Cell Invasion." *Cell* 184 (20): 5230-5246.e22. https://doi.org/10.1016/j.cell.2021.08.035.

Neftel, C., J. Laffy, Mariella G. Filbin, Toshiro Hara, Marni E. Shore, Gilbert J. Rahme, Alyssa R. Richman, et al. 2019. "An Integrative Model of Cellular States, Plasticity, and Genetics for Glioblastoma." *Cell* 178 (4): 835-849.e21. https://doi.org/10.1016/j.cell.2019.06.024.

Nielsen, Anders Lade, and Arne Lund Jørgensen. 2004. "Self-Assembly of the Cytoskeletal Glial Fibrillary Acidic Protein Is Inhibited by an Isoform-Specific C Terminus." *Journal of Biological Chemistry* 279 (40): 41537–45. https://doi.org/10.1074/jbc.M406601200.

Nowicki, Michal O., Josie L. Hayes, E. Antonio Chiocca, and Sean E. Lawler. 2019. "Proteomic Analysis Implicates Vimentin in Glioblastoma Cell Migration." *Cancers* 11 (4). https://doi.org/10.3390/cancers11040466.

Ogawa, Junko, Gerald M. Pao, Maxim N. Shokhirev, and Inder M. Verma. 2018. "Glioblastoma Model Using Human Cerebral Organoids." *Cell Reports* 23 (4): 1220–29. https://doi.org/10.1016/j.celrep.2018.03.105.

Okada, Vaeteewoottacharn, and Kariya. 2019. "Application of Highly Immunocompromised Mice for the Establishment of Patient-Derived Xenograft (PDX) Models." *Cells* 8 (8): 889. https://doi.org/10.3390/cells8080889.

Pablo, Yolanda De, Michael Nilsson, Marcela Pekna, and Milos Pekny. 2013. "Intermediate Filaments Are Important for Astrocyte Response to Oxidative Stress Induced by Oxygen-Glucose Deprivation and Reperfusion." *Histochemistry and Cell Biology* 140 (1): 81–91. https://doi.org/10.1007/s00418-013-1110-0.

Pascalis, Chiara De, and Sandrine Etienne-Manneville. 2017. "Single and Collective Cell Migration: The Mechanics of Adhesions." *Molecular Biology of the Cell* 28 (14): 1833–46. https://doi.org/10.1091/mbc.E17-03-0134.

Pascalis, Chiara De, Carlos Pérez-González, Shailaja Seetharaman, Batiste Boëda, Benoit Vianay, Mithila Burute, Cécile Leduc, Nicolas Borghi, Xavier Trepat, and Sandrine Etienne-Manneville. 2018. "Intermediate Filaments Control Collective Migration by Restricting Traction Forces and Sustaining Cell–Cell Contacts." *The Journal of Cell Biology* 217 (9): 3031-3044. ttps://doi.org/10.1083/jcb.201801162.

Patteson, Alison E., Katarzyna Pogoda, Fitzroy J. Byfield, Kalpana Mandal, Zofia Ostrowska-Podhorodecka, Elisabeth E. Charrier, Peter A. Galie, et al. 2019. "Loss of Vimentin Enhances Cell Motility through Small Confining Spaces." *Small* 15 (50), 1903180: 1–10. https://doi.org/10.1002/smll.201903180.

Patteson, Alison E., Amir Vahabikashi, Robert D. Goldman, and Paul A. Janmey. 2020. "Mechanical and Non-Mechanical Functions of Filamentous and Non-Filamentous Vimentin." *BioEssays* 42 (11): 1–12. https://doi.org/10.1002/bies.202000078.

Patteson, Alison E., Amir Vahabikashi, Katarzyna Pogoda, Stephen A. Adam, Kalpana Mandal, Mark Kittisopikul, Suganya Sivagurunathan, Anne Goldman, Robert D. Goldman, and Paul A. Janmey. 2019. "Vimentin Protects Cells against Nuclear Rupture and DNA Damage during Migration." *The Journal of Cell Biology* 218 (12): 4079-4092. https://doi.org/10.1083/jcb.201902046.

Paulus, Werner, and Wolfgang Roggendorf. 1988. "Vimentin and Glial Fibrillary Acidic Protein Are Codistributed in the Same Intermediate Filament System of Malignant Glioma Cells in Vivo - A Double-Labeling Immunoelectron-Microscopical Study." *Virchows Archiv B* 56 (1): 67–70. https://doi.org/10.1007/BF02890003.

Paz, Inbal, Martin Akerman, Iris Dror, Idit Kosti, and Yael Mandel-Gutfreund. 2010. "SFmap: A Web

Server for Motif Analysis and Prediction of Splicing Factor Binding Sites." *Nucleic Acids Research* 38 (SUPPL. 2): 1–5. https://doi.org/10.1093/nar/gkq444.

Peiffer, Jürgen. 1999. "Hans-Joachim Scherer (1906-1945), Pioneer in Glioma Research." *Brain Pathology* 9 (2): 241–45. https://doi.org/10.1111/j.1750-3639.1999.tb00222.x.

Pencheva, Nora, Mark C. de Gooijer, Daniel J. Vis, Lodewyk F.A. Wessels, Tom Würdinger, Olaf van Tellingen, and René Bernards. 2017. "Identification of a Druggable Pathway Controlling Glioblastoma Invasiveness." *Cell Reports* 20 (1): 48–60. https://doi.org/10.1016/j.celrep.2017.06.036.

Perng, M, Shu-Fang Wen,Terry Gibbon, Jinte Middeldorp, Jacqueline Sluijs, and and Roy A. Quinlan* Elly M. Hol. 2008. "Glial Fibrillary Acidic Protein Filaments Can Tolerate the Incorporation of Assembly-Compromised GFAP-, but with Consequences for Filament Organization and αB-Crystallin Association." *Molecular Biology of the Cell* 82 (4): 327–31. https://doi.org/10.1091/mbc.E08.

Perng, Ming Der, Mu Su, Shu Fang Wen, Rong Li, Terry Gibbon, Alan R. Prescott, Michael Brenner, and Roy A. Quinlan. 2006. "The Alexander Disease-Causing Glial Fibrillary Acidic Protein Mutant, R416W, Accumulates into Rosenthal Fibers by a Pathway That Involves Filament Aggregation and the Association of AB-Crystallin and HSP27." *American Journal of Human Genetics* 79 (2): 197–213. https://doi.org/10.1086/504411.

Picariello, Hannah S., Rajappa S. Kenchappa, Vandana Rai, James F. Crish, Athanassios Dovas, Katarzyna Pogoda, Mariah McMahon, et al. 2019. "Myosin IIA Suppresses Glioblastoma Development in a Mechanically Sensitive Manner." *Proceedings of the National Academy of Sciences of the United States of America* 116 (31): 15550–59. https://doi.org/10.1073/pnas.1902847116.

Pontén, J., and E. H. Macintyre. 1968. "Long Term Culture of Normal and Neoplastic Human Glia." *Acta Pathologica et Microbiologica Scandinavica* 74 (4): 465–86. https://doi.org/10.1111/j.1699-0463.1968.tb03502.x.

Roelofs, Reinko F., David F. Fischer, Simone H. Houtman, Jacqueline A. Sluijs, Wendy Van Haren, Fred W. Van Leeuwen, and Elly M. Hol. 2005. "Adult Human Subventricular, Subgranular, and Subpial Zones Contain Astrocytes with a Specialized Intermediate Filament Cytoskeleton." *Glia* 52 (4): 289–300. https://doi.org/10.1002/glia.20243.

Sahm, Felix, David Capper, Astrid Jeibmann, Antje Habel, Werner Paulus, Dirk Troost, and Andreas Von Deimling. 2012. "Addressing Diffuse Glioma as a Systemic Brain Disease with Single-Cell Analysis." *Archives of Neurology* 69 (4): 523–26. https://doi.org/10.1001/archneurol.2011.2910.

Sartori, Maria Teresa, Alessandro Della Puppa, Andrea Ballin, Elena Campello, Claudia Maria Radu, Graziella Saggiorato, Domenico d'Avella, Renato Scienza, Giuseppe Cella, and Paolo Simioni. 2013. "Circulating Microparticles of Glial Origin and Tissue Factor Bearing in High-Grade Glioma: A Potential Prothrombotic Role." *Thrombosis and Haemostasis* 110 (2): 378–85. https://doi.org/10.1160/TH12-12-0957.

Seetharaman, Shailaja, and Sandrine Etienne-Manneville. 2020. "Cytoskeletal Crosstalk in Cell Migration." *Trends in Cell Biology* 30 (9): 720–35. https://doi.org/10.1016/j.tcb.2020.06.004.

Sharma, Pooja, Sarah Alsharif, Arwa Fallatah, and Byung Min Chung. 2019. "Intermediate Filaments as Effectors of Cancer Development and Metastasis: A Focus on Keratins, Vimentin, and Nestin." *Cells* 8 (5): 497. https://doi.org/10.3390/cells8050497.

Shemilt, M, A Boutin, F Lauzier, R Zarychanski, L Moore, L A McIntyre, L Nadeau, et al. 2019. "Prognostic Value of Glial Fibrillary Acidic Protein in Patients With Moderate and Severe Traumatic Brain Injury: A Systematic Review and Meta-Analysis." *Crit Care Med* 47 (6): e522–29. https://doi.org/10.1097/ccm.0000000000003728.

Soellner, P., R. A. Quinlan, and W. W. Franke. 1985. "Identification of a Distinct Soluble Subunit of an Intermediate Filament Protein: Tetrameric Vimentin from Living Cells." *Proceedings of the National Academy of Sciences of the United States of America* 82 (23): 7929–33. https://doi.org/10.1073/

pnas.82.23.7929.

Stankevicins, Luiza Da Cunha, Marta Urbanska, Daniel AD. Flormann, Emmanuel Terriac, Zahra Mostajeran, Annica K.B. Gad, Fang Cheng, John E. Eriksson, and Franziska Lautenschläger. 2019. "Vimentin Provides the Mechanical Resilience Required for Amoeboid Migration and Protection of the Nucleus." *BioRxiv*, 720946. https://doi.org/10.1101/720946.

Stassen, Oscar M.J.A., Emma J. van Bodegraven, Fabrizio Giuliani, Martina Moeton, Regina Kanski, Jacqueline A. Sluijs, Miriam E. van Strien, Willem Kamphuis, Pierre A.J. Robe, and Elly M. Hol. 2017. "GFAPδ/GFAPα Ratio Directs Astrocytoma Gene Expression towards a More Malignant Profile." *Oncotarget* 8 (50): 88104–21. https://doi.org/10.18632/oncotarget.21540.

Swift, Joe, Irena L. Ivanovska, Amnon Buxboim, Takamasa Harada, P. C.Dave P. Dingal, Joel Pinter, J. David Pajerowski, et al. 2013. "Nuclear Lamin-A Scales with Tissue Stiffness and Enhances Matrix-Directed Differentiation." *Science* 341 (6149). https://doi.org/10.1126/science.1240104.

Tejero, Rut, Yong Huang, Igor Katsyv, Michael Kluge, Jung Yi Lin, Jessica Tome-Garcia, Nicolas Daviaud, et al. 2019. "Gene Signatures of Quiescent Glioblastoma Cells Reveal Mesenchymal Shift and Interactions with Niche Microenvironment." *EBioMedicine* 42: 252–69. https://doi.org/10.1016/j.ebiom.2019.03.064.

Thiery, Jean Paul, Hervé Acloque, Ruby Y.J. Huang, and M. Angela Nieto. 2009. "Epithelial-Mesenchymal Transitions in Development and Disease." *Cell* 139 (5): 871–90. https://doi.org/10.1016/j.cell.2009.11.007.

Tichy, Julia, Sabrina Spechtmeyer, Michel Mittelbronn, Elke Hattingen, Johannes Rieger, Christian Senft, and Christian Foerch. 2016. "Prospective Evaluation of Serum Glial Fibrillary Acidic Protein (GFAP) as a Diagnostic Marker for Glioblastoma." *Journal of Neuro-Oncology* 126 (2): 361–69. https://www.ncbi.nlm.nih.gov/pubmed/26518540.

Tudor, Sara M., Lavenus, Sandrine B., and Logue, Jeremy S. 2019. "A Flexible Network of Vimentin Intermediate Filaments Promotes the Migration of Amoeboid Cancer Cells through Confined Environments. *bio*R*xiv*, 788810. https://doi.org/https://doi.org/10.1101/788810.

Venkataramani, Varun, Dimitar Ivanov Tanev, Thomas Kuner, Wolfgang Wick, and Frank Winkler. 2020. "Synaptic Input to Brain Tumors: Clinical Implications." *Neuro-Oncology* 23(1): 23-33. https://doi.org/10.1093/neuonc/noaa158.

Venkataramani, Varun, Dimitar Ivanov Tanev, Christopher Strahle, Alexander Studier-Fischer, Laura Fankhauser, Tobias Kessler, Christoph Körber, et al. 2019. "Glutamatergic Synaptic Input to Glioma Cells Drives Brain Tumour Progression." *Nature* 573 (7775): 532–38. https://doi.org/10.1038/s41586-019-1564-x.

Venkatesh, Humsa S., Wade Morishita, Anna C. Geraghty, Dana Silverbush, Shawn M. Gillespie, Marlene Arzt, Lydia T. Tam, et al. 2019. "Electrical and Synaptic Integration of Glioma into Neural Circuits." *Nature* 573 (7775): 539–45. https://doi.org/10.1038/s41586-019-1563-y.

Voss, Dillon M., Anthony Sloan, Raffaella Spina, Heather M. Ames, and Eli E. Bar. 2020. "The Alternative Splicing Factor, MBNL1, Inhibits Glioblastoma Tumor Initiation and Progression by Reducing Hypoxia-Induced Stemness." *Cancer Research* 80 (21): 4681–92. https://doi.org/10.1158/0008-5472.can-20-1233.

Vuoriluoto, K., H. Haugen, S. Kiviluoto, J. P. Mpindi, J. Nevo, C. Gjerdrum, C. Tiron, J. B. Lorens, and J. Ivaska. 2011. "Vimentin Regulates EMT Induction by Slug and Oncogenic H-Ras and Migration by Governing Axl Expression in Breast Cancer." *Oncogene* 30 (12): 1436–48. https://doi.org/10.1038/onc.2010.509.

Walker, J. L., B. M. Bleaken, A. R. Romisher, A. A. Alnwibit, and A. S. Menko. 2018. "In Wound Repair Vimentin Mediates the Transition of Mesenchymal Leader Cells to a Myofibroblast Phenotype." *Molecular Biology of the Cell* 29 (13): 1555–70. https://doi.org/10.1091/mbc.E17-06-0364.

Wang, Jiguang, Emanuela Cazzato, Erik Ladewig, Veronique Frattini, Daniel I.S. Rosenbloom, Sakellarios Zairis, Francesco Abate, et al. 2016. "Clonal Evolution of Glioblastoma under Therapy." *Nature Genetics* 48 (7): 768–76. https://doi.org/10.1038/ng.3590.

Wang, Ying, Tao Liu, Ning Yang, Shuo Xu, Xingang Li, and Donghai Wang. 2016. "Hypoxia and Macrophages Promote Glioblastoma Invasion by the CCL4-CCR5 Axis." *Oncology Reports* 36 (6): 3522–28. https://doi.org/10.3892/or.2016.5171.

Xie, Yuan, Tobias Bergström, Yiwen Jiang, Patrik Johansson, Voichita Dana Marinescu, Nanna Lindberg, Anna Segerman, et al. 2015. "The Human Glioblastoma Cell Culture Resource: Validated Cell Models Representing All Molecular Subtypes." *EBioMedicine* 2 (10): 1351–63. https://doi.org/10.1016/j.ebiom.2015.08.026.

Xu, W. L., Y. Wang, J. Wu, and G. Y. Li. 2016. "Quantitative Analysis of U251MG Human Glioma Cells Invasion in Organotypic Brain Slice Co-Cultures." *European Review for Medical and Pharmacological Sciences* 20 (11): 2221–29.

Yamada, Kenneth M., and Michael Sixt. 2019. "Mechanisms of 3D Cell Migration." *Nature Reviews Molecular Cell Biology*, no. Box 1. https://doi.org/10.1038/s41580-019-0172-9.

Zhang, Feng, Yan Wen, and Xiong Guo. 2014. "CRISPR/Cas9 for Genome Editing: Progress, Implications and Challenges." *Human Molecular Genetics* 23 (R1): 40–46. https://doi.org/10.1093/hmg/ddu125.

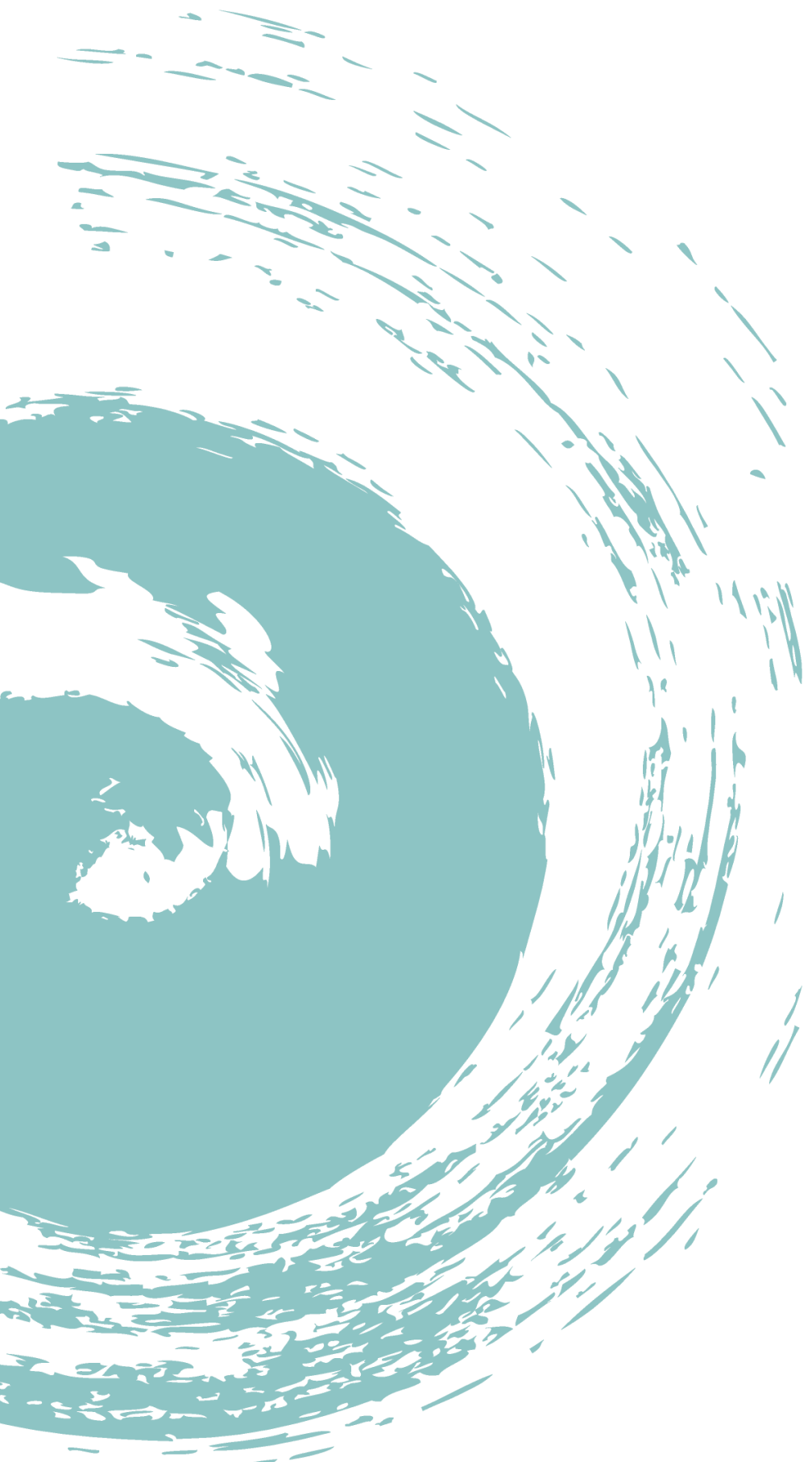

Addendum

Nederlandse samenvatting

Gliomen zijn een vorm van hersentumoren die ontstaan uit de gliacellen in het brein. Gliacellen in gezonde hersenen hebben een belangrijke rol in het in stand houden van homeostase van neurotransmitters, ionen en water, in het mogelijk maken van communicatie tussen zenuwcellen, en zijn het de stamcellen in de hersenen. Wanneer er echter een opeenstapeling van mutaties ontstaat in deze gliacellen, kunnen ze ongeremd gaan delen waardoor er een tumor begint te groeien. In het geval van gliomen zijn dit altijd kwaadaardige tumoren. Bij de meest ernstige en ook meest voorkomende vorm van glioom, ook wel glioblastoom genoemd, hebben patiënten na de initiële diagnose een gemiddelde levensduur van slechts 15 maanden. De behandeling die momenteel wordt toegepast, bestaande uit chirurgische verwijdering van de tumor in combinatie met radio- en chemotherapie, is niet in staat om de ziekte te genezen. Een van de onderliggende oorzaken van de maligniteit van de ziekte is het invasieve karakter van de tumor. Uitzaaiingen naar andere organen komen zelden voor, maar daarentegen groeien glioomcellen wel het omliggende gezonde weefsel in, waardoor ze ontsnappen aan de therapie en er nieuwe tumoren kunnen ontstaan elders in het brein. Deze ingroei kan ook aanleiding geven tot verstoorde hersenfuncties, zoals epilepsie of cognitieve problemen.

In dit proefschrift heb ik geprobeerd beter in kaart te brengen welke componenten van de cel een rol spelen bij de ingroei/ invasie van glioomcellen. We hebben ons hierbij gericht op een onderdeel van het skelet van de cel wat zowel in gliacellen als in glioomcellen zit, namelijk 'glial fibrillary acidic protein' (zuur gliaal fibrillair eiwit) oftewel GFAP. GFAP-eiwitten vormen langdradige filamenten in de cel en zijn betrokken bij vele processen. Het GFAP-eiwit zelf is opgebouwd uit een 'hoofd-', 'staaf-' en 'staart'-domein, oftewel het begin, midden en uiteinde van het eiwit. Er bestaan verschillende varianten van GFAP omdat er in het transcript, de blauwdruk van het eiwit, meerdere alternatieven staan voor het staartdomein. Tijdens het proces met de naam 'alternatieve splicing' reguleert de cel welke van deze uiteindes gekozen wordt. De standaard variant is GFAPα en dit is de meest voorkomende vorm van GFAP in het brein. Echter, in gebieden van de hersenen waar stamcellen zich bevinden, vind je vaker GFAP met een ander uiteinde: GFAPδ. In eerder onderzoek is ontdekt dat de balans tussen GFAPδ en GFAPα verschilt in tumoren van patiënten met hooggradige gliomen (glioblastomen) en die met laaggradige gliomen. Het doel van dit proefschrift was om te bestuderen hoe deze moleculaire verandering het gedrag van de glioomcel beïnvloedt. Onze hypothese hierbij was dat veel aanwezigheid van GFAPδ t.o.v. GFAPα, zoals in hooggradige gliomen, zou bijdragen aan het invasieve karakter van de cel.

In **Hoofdstuk 1** hebben we de veranderende samenstelling van GFAPδ en GFAPα, zoals we dat zien bij patiënten, nagebootst in een kweekbakje. Hierbij hebben

we gebruik gemaakt van de CRISPR-Cas9 technologie, een methode waarmee je heel specifiek in het DNA van de cel kunt knippen. Door het gedeelte met informatie over het staartdomein van GFAPα of GFAPδ te verwijderen uit het genoom, hebben we de cel geforceerd om slechts één van de twee varianten tot expressie te brengen. We hebben ontdekt dat cellen met overwegend GFAPα of GFAPδ op moleculair niveau van elkaar verschillen. GFAPδ-dominante cellen ondergingen meerdere veranderingen die ervoor zorgden dat de cel zich beter in zijn omgeving kon bewegen. De cellen veranderden van vorm, produceerden meer extracellulaire matrix (een ondergrond voor de cel om zich overheen te trekken), en brachten meer 'integrines' tot expressie (eiwitten die aan extracellulaire matrix kunnen binden). We hebben 'Dual phosphatase specifc protein' (DUSP4, tweevoudig specifieke fosfatase 4, een eiwit dat correleert met maligniteit van gliomen) ontdekt als een centrale speler die ten grondslag ligt aan vele van deze moleculaire veranderingen.

In **Hoofdstuk 2** hebben we onderzocht hoe de eiwitfamilie waar GFAP een onderdeel van is, de zogenaamde intermediaire filamenten (IFen), in andere weefsels betrokken is bij migratie en invasie. We hebben dit gedaan door een overzicht te geven van de literatuur op dit gebied aan de hand van een review. In het eerste deel staat mechanowisselwerking ('mechanoreciprocity') centraal. We beschrijven hier hoe de samenstelling van IFen beïnvloed wordt door de fysieke eigenschappen van de omgeving, en hoe IFen zelf de omgeving beïnvloeden. In het tweede deel van de review beschrijven we wat er momenteel bekend is over hoe IFen het proces van celmigratie beïnvloeden, met daarbij een focus op complexere migratie in weefsels. Als laatste bespreken we recente ontdekkingen over de betrokkenheid van IFen bij mechanoweerstand ('mechanoresilience'). Recente onderzoeken laten zien dat IFen de cel beschermen tegen de mechanische stress waar een cel aan wordt blootgesteld tijdens migratie. We sluiten het review af met een hypothese dat de samenstelling van IFen door de cel kan worden veranderd om zich aan te passen aan de omgeving, zodat de cel zich op die manier kan klaarmaken voor bijvoorbeeld migratie en invasie.

Om ingroei en invasie van glioomcellen te kunnen bestuderen, zijn er modellen nodig die de normale omstandigheden waaraan de glioomcel wordt blootgesteld goed kunnen nabootsen. In **Hoofdstuk 3** hebben we zo'n een model beschreven . We hebben hiervoor gebruik gemaakt van plakjes weefsel van muizenhersenen. Glioomcellen die in deze plakjes worden aangebracht, maken gebruik van de buitenkant van bloedvaten om zich voort te bewegen, zoals ze dit ook in patiënten doen. In het hoofdstuk beschrijven we hoe deze migratie langs bloedvaten met hoge resolutie in kaart kan worden gebracht en kan worden gekwantificeerd. Ook beschrijven we een methode om te bepalen hoeveel glioomceldelingen er in dit model plaatsvinden.

In **Hoofdstuk 4** passen we de hersenplakjesmethode toe om te bepalen hoe

verschillende GFAP-samenstellingen de invasie van glioomcellen beïnvloeden. We vonden hier dat de tumoren van de cellen met aangepaste GFAP-samenstellingen er anders uitzagen. GFAPδ-dominante cellen zorgden voor diffuse tumoren, waarbij de verschillende cellen ver van elkaar vandaan waren gegroeid. We vonden dat meer GFAPδ-dominante cellen het muizenhersenweefsel infiltreerden, wat in lijn der verwachting was met wat we op basis van hoofdstuk 1 hadden voorspeld. Bij de GFAPα-dominante cellen vonden we echter onverwacht ook meer geïnfiltreerde cellen in het hersenweefsel, maar deze tumoren vertoonden niet het diffuse patroon wat we bij de GFAPδ-dominante cellen zagen. Om de verschillende groeipatronen beter te begrijpen, hebben we vervolgens de cellen geïmplanteerd in levende muizen en met microscopie de bewegingspatronen van de cellen gevolgd. We vonden hier inderdaad een verschil in bewegingspatronen tussen de cellen met verschillende GFAP-samenstellingen. GFAPα-dominante cellen bewegen meer en sneller, maar in willekeurige richting. GFAPδ-dominante cellen daarentegen zijn langzamer dan de GFAPα-dominante cellen, maar bewegen grotendeels in dezelfde richting. Dit laat dus zien dat de samenstelling van GFAP in glioomcellen invloed heeft op de groeipatronen van de tumor.

In **Hoofdstuk 5** bestuderen we wat er gebeurt als de cel helemaal geen GFAP meer heeft. Om dit te onderzoeken hebben we weer gebruik gemaakt van CRISPR-Cas9. In dit geval hebben we echter niet een stukje van de blauwdruk verwijderd, maar zorgen we ervoor dat de gehele blauwdruk van GFAP onleesbaar wordt. Met behulp van deze experimenten hebben we nog een aanvullende rol van GFAP tijdens ingroei ontdekt, en laten we zien dat GFAP bescherming biedt tegen door migratie veroorzaakte schade. Tijdens invasie moeten cellen zich soms in allerlei bochten wringen om door de nauwe ruimtes in het brein heen te komen. Met name de celkern, het grootste organel in de cel, moet soms worden vervormd om passage door nauwe ruimtes mogelijk te maken. Om dit vervormen van de celkern tijdens invasie na te bootsen, hebben we gebruik gemaakt van microfluidica waarbij cellen zich door microscopisch kleine pilaartjes moeten bewegen. We ontdekten dat celkernen van glioomcellen zonder GFAP soms in stukjes uiteenvallen wanneer ze door vernauwingen heen bewegen. De membraan van de celkern gaat ook vaker kapot, waardoor er uitwisseling kan plaatsvinden van enzymen in het cellichaam en in de celkern. We verwachten dat de afwezigheid van GFAP de kans vergroot dat er schadelijke enzymen de celkern binnendringen nadat de integriteit van het celkernmembraan door migratie is aangetast.

In **Hoofdstuk 6** bestuderen we of GFAP ook gebruikt kan worden als biomarker voor gliomen. GFAP is in gezonde condities niet aanwezig in bloedserum, maar kan door pathologische situaties in de circulatie terecht komen. Meerdere studies hebben onderzocht of GFAP in het serum van glioompatiënten te detecteren is. Met behulp van een meta-analyse hebben we al deze studies geïdentificeerd en de resultaten gecombineerd. De gecombineerde studies laten zien dat GFAP verhoogd is in het serum

van patiënten met een glioblastoom ten opzichte van zowel de gezonde controlegroep als van patiënten met een laaggradig glioom. Daarnaast vonden we in de literatuur aanwijzingen dat GFAP bij patiënten met een glioblastoom ook vaker gevonden wordt in andere lichaamsvloeistoffen, zoals cerebraal spinaal vloeistof, en ook in immuuncellen en membraanblaasjes in het bloed. Deze studies geven aan dat gliomen geassocieerd zijn met veranderende GFAP concentraties in lichaamsvloeistoffen. Echter zijn meer studies nodig om de relevantie van serum GFAP als biomarker en de toepasbaarheid hiervan vast te stellen.

De algemene conclusie van het proefschrift is dat GFAP een veelzijdige rol speelt in de biologie en pathologie van gliomen. We hebben gezien dat verschillende varianten van GFAP de invasie van glioomcellen reguleren en hiermee de groeipatronen van de tumor kunnen beïnvloeden. Ten tweede zien we dat GFAP tijdens weefselinvasie de cel beschermt tegen de schadelijke effecten die migratie door vernauwingen met zich mee kunnen brengen. Als laatste zien we dat GFAP specifiek gevonden wordt in het bloedserum van patiënten met een glioblastoom, maar niet in patiënten met een laaggradig glioom. Toekomstig onderzoek zal moeten uitwijzen hoe de varianten van GFAP verschillend tot expressie komen in de verschillende patiëntengroepen en hoe het in het bloed terechtkomt. De ontwikkeling en progressie van tumoren gaat gepaard met vele veranderingen in het aangedane weefsel. Dit wordt veroorzaakt door de druk die de groeiende tumor op het omringende weefsel uitoefent, door activatie van het immuunsysteem en door dysregulatie van zuurstof- en vloeistofhuishouding. We verwachten dat de glioomcel zich adapteert aan de veranderende omgeving, onder andere door de samenstelling van GFAP en andere IFen in de cel aan te passen. Dit kan vervolgens een verandering in het gedrag van de glioomcel teweeg brengen, en op deze manier tumorinvasie en -progressie bevorderen. Vervolgonderzoek zal deze hypothese moeten testen en verder in kaart moeten brengen welke moleculaire mechanismen hieraan ten grondslag liggen.

Al met al hebben we in dit proefschrift gepoogd om beter grip te krijgen op de rol en relevantie van GFAP in gliomen. We hebben ontdekt dat GFAP een brede functie heeft bij het gedrag van glioomcellen; van het reguleren van tumorcelinvasie tot het beschermen van de cel tegen celkernfragmentatie.

Dankwoord

Een van de eerste dingen die ik heb geleerd toen ik begon aan mijn PhD, is dat je boekje maar draait om één ding: het dankwoord. Gelukkig heb ik voor dit stuk geen tekort aan inspiratie, ik ben zeer dankbaar voor alle personen om mij heen die ervoor hebben gezorgd dat ik met veel plezier terugkijk op mijn PhD-tijd.

Allereerst zou dit proefschrift uiteraard niet tot stand zijn gekomen zonder de begeleiding van mijn geweldige promotoren. **Prof. dr. Hol**, beste **Elly**, hartelijk dank voor je mentorschap de afgelopen jaren. Ik ben je zeer dankbaar voor de vrijheid die ik bij je heb gekregen om zelf invulling te geven aan het project, met daarbij de benodigde sturing op momenten dat het nodig was. Ondanks je drukke agenda maakte je altijd tijd vrij om te praten over onderzoek of carrièrestappen, stimuleerde je me om na te denken over de toekomst en gaf je me een podium waar nodig. Ook je oog voor de sociale cohesie binnen de groep heb ik altijd zeer gewaardeerd, dit maakt waarom het Hol-lab zo'n fijne plek is om te werken. Ook gaat mijn dank uit naar **prof. dr. Robe**. Beste **Pierre**, ik kijk met veel plezier terug op onze meetings waarbij we ons konden verwonderen over exploderende nuclei. Je klinische en moleculaire kennis heeft mij veel geholpen om sturing te geven binnen mijn onderzoek en je stimulerende woorden maakten dat ik altijd weer met veel motivatie verderging met nieuwe experimenten.

Ten tweede bedank ik graag de leden van de beoordelingscommissie. **Prof. dr. Schiffelers**, **prof. dr Koenderink**, **prof. dr. Akhmanova**, **prof. dr. Boxem** en **dr. Broekman**, dank voor de tijd die jullie hebben genomen om mijn proefschrift te lezen en te beoordelen. Ik kijk uit naar de wetenschappelijke discussie die zal volgen tijdens mijn verdediging.

Emma, ik had me geen betere start van mijn PhD kunnen wensen dan de samenwerking met jou. Door ons gezamenlijke CRISPR-project zat ik gelijk helemaal in het onderwerp en werd ik snel besmet met je enthousiasme over het eiwit GFAP. Het blijft onvoorstelbaar dat we uiteindelijk maar iets langer dan een jaar hebben samengewerkt, ik heb in deze tijd superveel van je geleerd over het doen van onderzoek, het schrijven van papers en het afronden van een proefschrift. Ik kijk met veel plezier terug op ons gezamenlijk lab-werk, onze vele brainstorm-momentjes en natuurlijk de nerd-disco tijdens de Gordon Conferentie in Italië. Na je vertrek moest ik andere mensen vermoeien met mijn enthousiasme over GFAP, maar gelukkig hebben we ook toen je in Parijs zat nog met enige regelmaat de draad weer op kunnen pakken. Het is zo tof dat je nu weer terug bent in het Hol-lab om met de Veni-beurs je eigen onderzoek verder te ontwikkelen!

Amber en **Katherine**, mijn lieve paranimfen, we zijn ongeveer tegelijkertijd aan de uitdaging genaamd 'promoveren' begonnen en ik ben ontzettend blij dat jullie aan mijn zijde staan aan het einde van het traject. **Amber**, ik zie jou een beetje als de astrocyt van de groep: met warme persoonlijkheid en aanstekelijke enthousiasme zorg je voor homeostase binnen de groep. Als ik mijn werk presenteerde tijdens labmeetings, kon ik altijd rekenen op nuttige input van jou. Ik ben blij dat we deze jaren samen hebben kunnen lachen en klagen, met als hoogtepunt het labuitje wat we samen hebben georganiseerd naar Giethoorn. **Katherine**, ik vind het zo tof hoe jij hebt bewezen dat je prima een moleculair onderzoek kan doen terwijl je daarvoor amper een pipet hebt aangeraakt. Ondanks je bizar drukke schema met labwerk en nachtdiensten, kon ik altijd bij je terecht met vragen over protocollen, primaire KT-lijnen of gewoon om te kletsen. Om je te vinden hoefde ik alleen maar op het geluid van Radio 1 (of de naam Jasper) af te gaan. Het is zo gaaf dat je harde werk is beloond met een opleidingsplek tot KNO-arts!

Jacqueline, zonder jouw hulp was ik nog een jaar extra bezig geweest met het afronden van mijn proefschrift. Ontzettend bedankt voor al je hulp bij kleuringen, celkweek en vooral alle Western Blots (niemand krijgt zulke strakke bandjes zoals jij). Je bent een ontzettend fijne collega om mee samen te werken en de kalme, constante factor in de groep. **Roland**, ik denk met veel plezier terug aan onze FACS-sessies waarbij we onder werktijd konden kletsen over wat ons op dat moment dan ook bezig hield. Het was erg leuk om samen 'op te groeien' op de afdeling, ik eerst als master-student en jij als net afgestudeerde. Ik heb bewondering voor de manier waarop je omging met de persoonlijke omstandigheden die het werk lastiger maakten.

Jinte, bedankt voor al je fijne input tijdens de werkbesprekingen en voor je advies bij carrièrekeuzes. Het was erg inspirerend om te praten over je eigen carrière en ik ben erg benieuwd hoe je jouw eigen lab in Rijswijk gaat ontwikkelen. **Vanessa**, dankjewel voor al je adviezen bij het zoeken naar een postdoc. Ik vind het erg leuk en toevallig dat ik nu in dezelfde stad terechtkom waar jij je postdoc hebt gedaan. **Marjolein**, al hebben we tijdens je PhD-tijd weinig samen gewerkt, ik heb erg genoten van onze samenwerking bij Speerpunt Brein. Dankjewel dat je me hebt geïntroduceerd in de wonderlijke wereld van het UMC Utrecht. Je strakke organisatieskills waren bij je PhD-project al duidelijk, en heb ik bij het overnemen van je werkzaamheden zeer gewaardeerd. **Bart**, jij tilde PhD-filmpjes naar een hoger niveau. Ik verwacht nog steeds je naam over een aantal jaar bij de aftiteling van een arthouse film te zien. Bedankt voor de leuke samenwerking bij het maken bij het filmpje voor Emma. **Paul**, ik had nog nooit van croquet gehoord totdat je de gangen van de afdeling onveilig maakte met dit spel. Bedankt voor alle gekke competities en sociale lab-activiteiten die je initieerde. **Yuije**, I still think back

and laugh about the time you were eating durum candy in the office next to me, and made me think there was a gas leak in the building. Thankfully most other candies and food you brought were delicious. **Sophietje**, bedankt voor al je oprechte interesse en enthousiasme. Het was superfijn om zoveel input op mijn project te krijgen, zeker aan het begin. **Tamar**, nadat je de bench tegenover mij had verlaten, had ik gelukkig nog een PBS fles met je portret (gemaakt door Paul) om me aan jou te herinneren. Bedankt voor alle gezelligheid op het lab. **Ketharini**, thank you for being such an uplifting person in the lab, let's repeat our catch-up dinner soon. **Isadora**, it was so nice to have a little reunion in your hometown a couple of years back, thanks for showing me around in Rio.

Christiaan, mijn lab-buurman. Elke keer als je het elektrofysiologie hok besloot te verlaten en ons simpele zielen in het DNA-lab kwam vergezellen was het weer gezelligheid. Ik heb veel moeten lachen om je droge humor, mijn boterhammen met kaas zijn nooit meer hetzelfde sinds ik je favoriete nummer heb gehoord. **Lianne**, ik ken weinig mensen die zo sportief zijn als jij, ik ben blij dat het je af en toe is gelukt om het Hol-lab ook in beweging te krijgen. Ik ben nog steeds trots op de overwinning met de kanowedstrijd. Bedankt voor al je leuke initiatieven na werktijd! **Claudia**, I love how much I learned about axelotls, beatles and plants from you. I find your openness and positivity very admiring. **Marloes**, ik ben altijd onder de indruk van hoe makkelijk onderzoek doen jou lijkt af te gaan. Bedankt voor alle leuke momenten op en buiten het lab. **Werner**, ik ken niemand die zo enthousiast en overtuigend over onderzoek kan praten als jij, GFAP-onderzoek is in goede handen bij jou. Ik ben blij dat we samen nog het EuroIF congres in Limburg hebben kunnen bezoeken. **Anna** en **Tiziana**, volgens mij gaat de afdeling nog vele leuke borrels tegemoet als ik af kan gaan op de eerste paar die jullie hebben georganiseerd. Ik had graag wat langer met jullie samengewerkt buiten het digitale tijdperk. **Saskia, Gijsje, Hans, Soufyan, Lois** en **Charlotte** bedankt voor de leuke tijden die we hebben gehad in het Hol-lab!

Coen, **Dasha** en **Loïs**, wat heb ik geluk gehad met drie gemotiveerde studenten zoals jullie. **Coen**, naast je bijdrage aan dit proefschrift met de data die je hebt verzameld, wil ik je ook bedanken voor je strakke organisatieskills. Daar kon ik als eerstejaars PhD-student nog veel van leren. **Dasha**, dank voor je onuitputtelijke bron van enthousiasme en inzet. Ik heb zelden zo'n harde werker ontmoet als jij en ben supertrots op de dingen die je voor elkaar hebt gekregen in de coronatijd. Ik hoop dat je je skills als arts-onderzoeker in de toekomst weer kunt gaan inzetten voor glioblastoma-onderzoek. **Loïs**, je goed ontwikkelde labskills waren een geschenk aan het einde van mijn PhD. Ik ben je zeer dankbaar voor alle experimenten die je van mij hebt overgenomen en de kundigheid waarmee je deze hebt afgerond.

Ook gaat mijn dank uit naar de overige mensen van de afdeling Translational Neuroscience. **Prof. dr. Burbach**, beste **Peter**, bedankt dat je als afdelingshoofd zorgde voor een open atmosfeer en saamhorigheid tussen de verschillende onderzoeksgroepen, dit maakte de afdeling voor mij een hele prettige werkplek, zowel tijdens mijn master als tijdens mijn PhD. Ik denk met plezier terug aan de practica waarbij ik je heb geholpen, met elk jaar weer alle prachtige kunstwerken van Golgi-kleuringen van de studenten waarbij een dendriet steevast werd aangewezen als axon. Niet lang geleden gaf je het stokje over aan prof. dr. Hol en **prof. dr. Pasterkamp**. Beste **Jeroen**, al heb ik je rol als afdelingshoofd gedeeld met Elly maar kort mogen meemaken, ik heb wel van dichtbij kunnen zien hoe je lijntjes legt binnen het ziekenhuis als voorzitter van het Speerpunt Brein. Ik heb in de korte tijd als programmamanager ontzettend veel geleerd en wil je bedanken voor je steun en begeleiding in deze periode. Mijn dank gaat ook uit naar de rest van het managementteam en naar het secretariaat: **Joke, Remi, Roger, Krista, Vicki, Rianne, Ria** en **Sandra**, dank voor al jullie hulp gedurende de jaren. Dit proefschrift had ook niet tot stand kunnen komen zonder het geweldige werk van de analisten van de afdeling. Bij jullie kon ik altijd terecht met vragen over microscopen (**Youri**), cellen (**Keith**), muizen (**Christiaan, Nicky**), analyses (**Danny**), reagentia (**Marina, Leo, Henk**) en overige zaken (**Desiree, Jos, Mieneke, Mark, Erwin**). Helden van het onderwijs-team, beste **Geert, Mirjam, Maartje** en **Rahul**, dank dat jullie mij een aantal maanden hebben opgenomen en wegwijs hebben gemaakt in de wereld van het onderwijs. Ook al was het maar een korte tijd, ik heb ontzettend veel geleerd van jullie en genoten van de samenwerking. **Geert**, ook dank voor al je begeleiding bij het PhD-platform, ik waardeer je inzet om de studenten van de ECN-track met elkaar te verbinden.

Team Coffee from room 5.201, dear **Mateja**, **Paul** and **Marleen**. Although the name of our Whatsapp-group was poorly chosen as we barely touched the thousand coffee machines in our room, I am still grateful for the times we shared in the office and all the desired distractions in between experiments. **Mateja**, you were my go to person for experimental help outside of the Hol-lab, thank you for all your help looking up plasmids in the Pasterkamp-lab, introducing me to lentivirus pregnancy tests and for all other advice I got from you. More importantly I valued the time we spend outside of the lab, you and Roman (and now Maéva!) make such wonderful hosts and I really enjoyed the dinners, coffees and board game nights. **Paul**, as you were the most constant factor in our office pre-corona times due to your computer-bound PhD, your absence was really missed the last two years. Luckily you still returned every now and then so we could catch up. Thank you for all the interesting conversations we had in our office, due to all the things I learned from you about philosophers and philosophy, I think I earn the title 'Doctor of Philosophy' a little more. **Marleen**, I am happy that Remi decided

to place another desk in our oddly shaped office and that the desk was filled by you. Thank you for your uplifting spirit in the office and for the bike rides together to the Moskeeplein. How nice that we were neighbours for two weeks!

Valeria, my PhD-platform buddy, you always make me think about the way we do research and how this could be improved. Thank you for the inspiring conversations, nice hangouts in the park, dinners and walks, but also for your help with statistics. **Daniëlle**, you were the social driving force of the department, thank you for all your efforts in organising ugly sweater contests, drinks and what not. **Jacques**, thank you for introducing me to the world of zouk. Also to all the other PhD-students, postdocs and PIs of the department, **Andreia, Anna, Astrid, Danai, Daniëlle V, Divya, Emma, Eljo, Evelien, Fabien, Frank, Ilia, Ioannis, Janna, Jelle, Karlijn, Laura, Laurens, Lieke, Lill Eva, Louisa, Mark, Marieke, Marta, Nefeli, Onur, Özge, Oxana, Pavol, Ramona, Renata, Rianne, Rogier, Suzanne, Svetlana, Tijana, Vamshi and Veronne**, thank you for all the fun and science during lab outings, (alternative) drinks, ONWAR retreats, summer schools, and other social activities.

Half of the work presented in my thesis would not have been possible without the help of collaborators. **Rebeca**, I am happy that you were my partner in crime for the GFAP invasion project. Our journey together was a bit of a rollercoaster as we experienced success and failure together during the project. I enjoyed the time we worked together in the lab at the NKI (cursing the FACS machine) and our writing days working on the manuscript. You are so much fun to work with, I hope that we can find a way to work together again in the future. **Claire**, even though we mostly have seen each other through Zoom, I learned a lot from you and I am super happy that you became involved in the project. Thank you for all your input and advice during the project and the great feedback on the manuscript. **Prof. dr. van Rheenen**, dear **Jacco**, thank you for the great collaboration during the GFAP isoform project and for the guidance in bringing the project to a successful end.

Prof.dr. Lammerding, dear **Jan**, thank you for hosting me in your lab at Cornell University and for teaching me many different ways to torture cells. The visit to Ithaca was one of the highlights of my PhD, and this was largely due to the way I was welcomed to the lab by you and the lab members. I really appreciate all the scientific input I got from you during and after the stay and I hope we can keep collaborating in the future. Also to the members of the Lammerding-lab, particularly **Pragya, Jeremy, Melanie, Jeremiah** and **Tylor**, thank you for teaching me new techniques and for introducing me to the delicious ice-creams of the Dairy Bar.

Before I started my PhD, I had two amazing mentors who taught me all about pipetting, cloning, cell culture and in general how to perform science, and helped me with tricks that I continued to use during my PhD. **Kati** and **Robert**, thank you both for your guidance, patience and for the fun times in the lab during my master internships.

Natuurlijk zijn er ook een heleboel mensen buiten de werkvloer die ik zou willen bedanken, te beginnen met mijn vrienden. **Marloes**, die Teletubbietrui die je 24 jaar geleden aantrok op een maandag in september was de beste kledingkeuze ooit! Al zijn we in onze verdere school- en carrièrekeuzes daarna compleet de andere kant op gegaan, ik ben blij dat onze vriendschap nog altijd als vanouds blijft. Bedankt voor alle leuke avonturen, reisjes, uitjes, kaasplanken en wijntjes. Die laatste twee schijnen ze ook in Lyon te hebben, moeten we eens uitproberen. **Rozemarijn** en **Lotte**, al zien we elkaar inmiddels maar een paar keer per jaar, elke keer is het weer alsof we weer terug zijn in de aula van het Vincent van Gogh. Hopelijk blijven we onze traditie van Songfestival kijken, TT-nacht bezoeken, elkaar opzoeken in het buitenland en kerstdinertjes organiseren, voortzetten. **Joyce, Aletta** en **Nina**, aka **JAN**. Wie had ooit gedacht dat een van ons nog verder zou gaan met de lesstof van 'weefsels' van biomedische wetenschappen? Gelukkig gaan onze gesprekken inmiddels al lang niet meer over vakken van BMW. Bedankt voor alle leuke GT-avonden (toch een beter concept dan margarita en nacho-avonden), borrels en gezelligheid de afgelopen jaren. Ik ben blij dat ons gecancelde reisje naar Namibië binnenkort toch eindelijk kan plaatsvinden, leg de barbecue-aubergines maar vast klaar! Lieve JC Dynamique, lieve **Dianne, Elianne, Jacintha, Lisa, Maud, Rosanne, Sharon B** en **Sharon C**. Tijdens mijn PhD waren de dinsdagavonden standaard geblokt in mijn agenda voor etentjes met jullie. Gelukkig is de kwaliteit van de etentjes sinds de verlepte pasta pesto's aan het begin van onze club-etentijd flink omhoog gegaan. Ik ga onze standaard avondjes en random koffiemomentjes in Utrecht heel erg missen, maar voor clubweekenden en Lowlands ben ik zeker nog van de partij. Dank voor jullie vriendschap, steun en gezelligheid de afgelopen jaren!

Alanya, wat ben ik blij dat we niet alleen in San Francisco, maar ook in Utrecht vlak bij elkaar bleken te wonen. Dankjewel voor alle leuke wandelingetjes en terrasjes waarin we herinneringen uit SF op konden ophalen. **Jamie**, mijn favoriete Brabander van de van Bijnkershoeklaan! Bedankt voor alle superlieve kaartjes en leuke Maarseveenseplas chill-momentjes, bij jou voelt het altijd alsof ik op vakantie ben. **Renate**, al wonen we straks toch niet in dezelfde stad, ik hoop dat we snel elkaar kunnen opzoeken om te boulderen of plantjes te verpotten. **Rianne**, het is zo fijn dat we na al die jaren nog steeds contact houden en dat ik op de hoogte blijf van jullie lieve gezinnetje. Bedankt voor alle leuke bijkletsmomentjes. **Sjanne** en **Daan**, ik vind het zo cool dat jullie het avontuur gaan opzoeken aan de andere kant van de wereld! Bedankt voor de leuke uitjes tijdens de

saaie coronatijd, ik kijk uit naar het volgende huiskamerfeestjes zodra we allemaal weer terug zijn in Nederland. **Marloes** en **Merel**, mijn knappe nichtjes, wat zijn we altijd toch lief voor elkaar hè? Ik ben blij dat we ondanks de afstand elkaar nog blijven opzoeken, bedankt voor jullie gekke humor.

Lieve **pap** en **mam**, waar moet ik beginnen met jullie te bedanken. Jullie zijn de basis van alles, mijn veilige thuishaven. Bedankt dat jullie altijd je best deden om écht te begrijpen waar ik me nu al die tijd mee bezig hield, meedachten over keuzes die ik moest maken en enthousiasme toonden over de stappen die ik nam. Bedankt voor jullie onvoorwaardelijke steun en dat ik altijd op jullie terug kan vallen. De consequentie van dit laatste is wel dat het huis nu alweer volstaat met de spullen van een van jullie dochters, maar we beloven: er is snel ruimte weer ruimte voor de vouwwagen. Lieve **Geeske**, **Hella** en **Leonie**, wat heb ik een geluk dat ik drie oudere zussen heb die mij inspireren en waarbij ik kan afkijken hoe je het leven aanpakt. **Geeske**, wat bewonder ik je bold choices en je ondernemerschap. Dank dat ik altijd bij je terecht kan met vragen over carrièredilemma's, sollicitatiebrieven en grafisch design keuzes, maar vooral bedankt dat de deur in Twello altijd openstaat. **Hella**, mijn wetenschappelijke voorbeeld en avonturiers zus! Je onbegrensde en onbevreesde manier van leven is een bron van inspiratie. Bedankt voor alle bijzondere plekken op de wereld die jij me hebt laten zien. **Leonie**, ik ken niemand die zo'n groot hart heeft als jij. Bedankt voor al je zorgzaamheid en oprechtheid, maar ook voor alle keren dat je me de slappe lach hebt bezorgd met onze inside jokes. **Jan-Heiko**, **Sipko** en **Jorn**, mijn schoonbroertjes, jullie hebben ieder een unieke humor waar ik iedere keer weer om dubbel lig. Ik hoop dat we nog vele Dokter Denkers samen zullen oplossen. Jorn, bedankt ook voor je hulp bij mijn cover. **Owen** en **Merle**, mijn lieve neefje en nichtje, wat ben ik trots om jullie te zien opgroeien tot de personen die jullie zijn. Bedankt voor de vreugde die jullie mij brengen. Aan mijn schoonfamilie, **Frens, Petra, Astrid**, **Bram** en de nieuwste familieaanwinst **Roosmarijn**, bedankt dat jullie mij hebben verwelkomd en opgenomen in de familie en dat de deur altijd open staat. Jullie doorzettingsvermogen en daadkracht is voor mij een grote inspiratiebron.

Lieve **Jasper**, mijn mede-avonturier in het leven. Woorden schieten tekort om te beschrijven hoeveel je voor mij betekent. Bedankt dat ik mijn enthousiasme bij je kwijt kon over de meest nerdy dingen en dat ik bij je kon klagen over de cellen die niet meewerkten en experimenten die mislukken. Bedankt voor je onvoorwaardelijke steun, liefde, geduld en voor alle vrolijkheid die je in mijn leven brengt. Wat ben ik blij dat je aan mijn zijde staat bij ons volgende avontuur in Lyon.

About the author

By Katherine Tan and Amber Berdenis van Berlekom

Jessy van Asperen grew up in Zwiggelte, a small village in Drenthe, with three sisters. She attended secondary school at CS Vincent van Gogh in Assen. After obtaining her VWO diploma in 2011, she decided to go to Utrecht to study biomedical sciences, which she finished with a thesis on the role of the Central Amygdala in drug addiction under supervision of dr. H.M.B. Lesscher and prof. dr. L.J.M.J. Vanderschuren. Her interest in neuroscience was sparked, and she was admitted to the master Neuroscience and Cognition in Utrecht in 2014. She worked on the role of Semaphorin 6A in axon guidance during her first master internship, under the supervision of dr. K. Rehberg and prof. dr. R.J. Pasterkamp, but her interest for glial cells originated from her second master internship, where she characterized human iPSC derived astrocytes in 3D cultures in the lab of dr. E.M. Ullian under supervision of dr. R. Krencik at the University of California, San Francisco. Her excellent performances resulted in several publications, and a Cum Laude graduation. In 2017 she started a PhD in the Hollab under supervision of prof. dr. E.M. Hol and prof. dr. P.A.J. Robe. The projects started with a fruitful collaboration with dr. E.M. van Bodegraven. As a part of her PhD project, Jessy visited the lab of prof. dr. J. Lammerding at Cornell University in 2019. Her research on the different isoforms of GFAP in glioma resulted in this PhD thesis. Besides her excellent and versatile skills in the laboratory, Jessy is a loyal and social person with whom colleagues enjoy to work and participate in extracurricular activities. While finishing her thesis, she worked as an interim junior program manager at the strategic program brain, and junior educational personnel at the department of Translational Neuroscience of the UMC Utrecht. Going abroad keeps attracting Jessy, with a bachelor exchange to Melbourne Australia, a master research project in San Francisco US, a research exchange during her PhD in Ithaca US, and also many travels, of which the most recent to Chili and Argentina with her partner. Her academic career continues with another adventure across the border with a post-doc in Lyon, where she will investigate the dynamics of neurofilaments in zebrafish in the lab of dr. P. Bomont at Institute NeuroMyoGène.

List of publications

Rebeca Uceda-Castro*, **Jessy V. van Asperen***, Claire Vennin, Jacqueline A. Sluijs, Emma J. van Bodegraven, Andreia S. Margarido, Pierre A.J.T Robe, Jacco van Rheenen*, Elly M. Hol*. 2022. "GFAP splice variants fine-tune glioma cell invasion and tumour dynamics by modulating migration persistence". *Scientific reports*, 12(1): 1-14.

Jessy V. van Asperen*, Daria M. Fedorushkova*, Pierre A.J.T. Robe*, Elly M. Hol*. 2022. "Investigation of glial fibrillary acidic protein (GFAP) in body fluids as a potential biomarker for glioma: a systematic review and meta-analysis". *Biomarkers*, 27(1): 1-12.

Emma J. van Bodegraven, **Jessy V. van Asperen**, Jacqueline A. Sluijs, Coen B.J. van Deursen, Miriam E. van Strien, Oscar M.J.A. Stassen, Pierre A.J.T. Robe, Elly M. Hol. 2019. "GFAP alternative splicing regulates glioma cell–ECM interaction in a DUSP4-dependent manner. *The FASEB Journal*, 33(11): 12941-12959.

Emma J. van Bodegraven, **Jessy V. van Asperen**, Pierre A.J.T. Robe, Elly M. Hol. 2019. "Importance of GFAP isoform-specific analyses in astrocytoma". *Glia*, 67(8): 1417-1433.

Robert Krencik, Kyounghee Seo, **Jessy V. van Asperen**, Nupur Basu, Caroline Cvetkovic, Saba Barlas, Robert Chen, Connor Ludwig, Chao Wang, Michael E.Ward, Li Gan, Philip J.Horner, David H.Rowitch, Erik M. Ullian. 2017. "Systematic three-dimensional coculture rapidly recapitulates interactions between human neurons and astrocytes". *Stem Cell Reports*, 9(6): 1745-1753

Robert Krencik, **Jessy V. van Asperen**, Erik M. Ullian. 2017. "Human astrocytes are distinct contributors to the complexity of synaptic function". *Brain research bulletin*, 129: 66-73.

Morten T. Venø, Susanne T. Venø, Kati Rehberg, **Jessy V. van Asperen**, Bettina H. Clausen, Ida E. Holm, R. Jeroen Pasterkamp, Bente Finsen, Jørgen Kjems. 2017. "Cortical morphogenesis during embryonic development is regulated by miR-34c and miR-204". *Frontiers in Molecular Neuroscience*, 10, 31.

*These authors contributed equally

ISBN 978-90-393-7467-2